DOCTOR OF PHILOSOPHY

The functional characterisation of potential oncogenic roles of the human germ line genes PRDM9 and TEX19

Alharthi, Fahad

Award date:
2020

Awarding institution:
Bangor University

PRIFYSGOL
BANGOR
UNIVERSITY

The functional characterisation of potential oncogenic roles of the human germ line genes *PRDM9* and *TEX19*

Ph.D. Thesis
2020

Fahad Eidhah Alharthi

Declaration and Consent

Details of the Work

I hereby agree to deposit the following item in the digital repository maintained by Bangor University and/or in any other repository authorized for use by Bangor University.

Author Name: Fahad Eidhah H Alharthi

Title: The functional characterisation of potential oncogenic roles of the human germ line genes *PRDM9* and *TEX19*.

Supervisor/Department: DR. Ramsay McFarlan

Funding body (if any): Taif University, (Saudi Government).

Qualification/Degree obtained: PhD

This item is a product of my own research endeavours and is covered by the agreement below in which the item is referred to as "the Work". It is identical in content to that deposited in the Library, subject to point 4 below.

Non-exclusive Rights

Rights granted to the digital repository through this agreement are entirely non-exclusive. I am free to publish the Work in its present version or future versions elsewhere.

I agree that Bangor University may electronically store, copy or translate the Work to any approved medium or format for the purpose of future preservation and accessibility. Bangor University is not under any obligation to reproduce or display the Work in the same formats or resolutions in which it was originally deposited.

Bangor University Digital Repository

I understand that work deposited in the digital repository will be accessible to a wide variety of people and institutions, including automated agents and search engines via the World Wide Web.

I understand that once the Work is deposited, the item and its metadata may be incorporated into public access catalogues or services, national databases of electronic theses and dissertations such as the British Library's EThOS or any service provided by the National Library of Wales.

I understand that the Work may be made available via the National Library of Wales Online Electronic Theses Service under the declared terms and conditions of use (http://www.llgc.org.uk/index.php?id=4676). I agree that as part of this service the National Library of Wales may electronically store, copy or convert the Work to any approved medium or format for the purpose of future preservation and accessibility. The National Library of Wales is not under any obligation to reproduce or display the Work in the same formats or resolutions in which it was originally deposited.

Statement 1:
This work has not previously been accepted in substance for any degree and is not being concurrently submitted in candidature for any degree unless as agreed by the University for approved dual awards.

Signed …….. (candidate)
Date ……..

Statement 2:
This thesis is the result of my own investigations, except where otherwise stated. Where correction services have been used, the extent and nature of the correction is clearly marked in a footnote(s).
All other sources are acknowledged by footnotes and/or a bibliography.

Signed ……. (candidate)
Date …….
Statement 3:
I hereby give consent for my thesis, if accepted, to be available for photocopying, for inter-library loan and for electronic storage (subject to any constraints as defined in statement 4), and for the title and summary to be made available to outside organisations.

Signed ……. (candidate)
Date …….
NB: Candidates on whose behalf a bar on access has been approved by the Academic Registry should use the following version of **Statement 3:**
Statement 3 (bar):
I hereby give consent for my thesis, if accepted, to be available for photocopying, for inter-library loans and for electronic storage (subject to any constraints as defined in statement 4), after expiry of a bar on access.

Signed …… (candidate)
Date ……

Statement 4:

Choose **one** of the following options

a) I agree to deposit an electronic copy of my thesis (the Work) in the Bangor University (BU) Institutional Digital Repository, the British Library ETHOS system, and/or in any other repository authorized for use by Bangor University and where necessary have gained the required permissions for the use of third party material.	
b) I agree to deposit an electronic copy of my thesis (the Work) in the Bangor University (BU) Institutional Digital Repository, the British Library ETHOS system, and/or in any other repository authorized for use by Bangor University when the approved **bar on access** has been lifted.	
c) I agree to submit my thesis (the Work) electronically via Bangor University's e-submission system, however I **opt-out** of the electronic deposit to the Bangor University (BU) Institutional Digital Repository, the British Library ETHOS system, and/or in any other repository authorized for use by Bangor University, due to lack of permissions for use of third party material.	

Options B should only be used if a bar on access has been approved by the University.

In addition to the above I also agree to the following:

1. That I am the author or have the authority of the author(s) to make this agreement and do hereby give Bangor University the right to make available the Work in the way described above.

2. That the electronic copy of the Work deposited in the digital repository and covered by this agreement, is identical in content to the paper copy of the Work deposited in the Bangor University Library, subject to point 4 below.

3. That I have exercised reasonable care to ensure that the Work is original and, to the best of my knowledge, does not breach any laws – including those relating to defamation, libel and copyright.

4. That I have, in instances where the intellectual property of other authors or copyright holders is included in the Work, and where appropriate, gained explicit permission for the inclusion of that material in the Work, and in the electronic form of the Work as accessed through the open access digital repository, *or* that I have identified and removed that material for which adequate and appropriate permission has not been obtained and which will be inaccessible via the digital repository.

5. That Bangor University does not hold any obligation to take legal action on behalf of the Depositor, or other rights holders, in the event of a breach of intellectual property rights, or any other right, in the material deposited.

6. That I will indemnify and keep indemnified Bangor University and the National Library of Wales from and against any loss, liability, claim or damage, including without limitation any related legal fees and court costs (on a full indemnity bases), related to any breach by myself of any term of this agreement.

Signature: ……

Date : …….

Abstract

Cancer cells acquire a number of abnormal epigenetic and / or genetic properties. These enable cancer cells to grow, spread and escape the action of therapeutic and immunologic targeting. An important feature of many cancers is the re-activation of a set of genes which are normally expressed during distinct development stages. These genes include the germline genes. Cancer Testis Antigen (CTA) genes are normally expressed in male germ cells in the adult testes and variety of cancer cells. Understanding this group of genes has great significance in cancer biology. This research is aimed at investigation of the functions of two germ specific CTA genes, namely *PRDM9* and *TEX19*, both of which are activated in several kinds of tumours.

PRDM9 has histone methyltransferase activity to coordinate meiotic recombination hotspot activation. Activity the murine orthologue of human PRDM9, Meisetz, has been described as a meiotic recombination activator which is also involved in regulation of transcription for other meiosis specific genes. This current research indicates that *PRDM9* can affect cancer cell proliferation and may transcriptionally regulate other germline genes in cancer cells.

TEX19 functions in the germ line to mediate an array of process. TEX19 has recently been demonstrated to be an oncogenic driver with potential role in self-renewal and proliferation of cancer cells. This current research confirmed that TEX19 depletion affects proliferation of cancer cells. Also, it was found that siRNA depletion of TEX19 caused considerable decrease in histone H3K9Ac, showing a potential contribution of TEX19 to epigenetic regulation of chromatin and / or chromosomal dynamics. Finally, we found that TEX19 might control L1-ORF1p, which is a protein encoded by LINE-1 that is needed for retro-transposition. This feature shows both commonalties and distinctions to the reported activities of murine Tex19.1. This might reflect fundamental species differences, or specific *TEX19* functions in cancer cells. We put forward a model in which we propose TEX19 functions in oncogenesis as a nucleic acid mimetic.

Acknowledgements

I begin by offering thank to (ALLAH) for all things that He always assist me with in every endeavour that I take. In this research, He gave me confidence, motivation patience and the will to complete this work.

On achieving this task, I would like to present Special thanks and appreciation to my Supervisor Dr. Ramsay McFarlane for the encouragement, guidance, and enthusiasm during my laboratory work as well as write up phase. I have learned considerable things from him. I would like to extend my deepest thanks to Dr. Jane Wakeman, Dr. Natalia Gomez-Escobar and Dr. Ellen Vernon for encouraging me with their worthy suggestions during this project.

There are no words to describe the huge of my thanks to my father for his prayers for me during my studies, I am always proud of you. Endless thanks go of course to the warmest and biggest heart in the world, my mother, for the endless love and care she has given me since I was child. I would like to thank from the bottom of my heart my brothers Khaled, Omar, Saad, Abdullah and my sisters for encouraging and inspiring me to do the best I can do. I am grateful also to my wife Shuruq, for her unconditional love and constant encouragement, motivation and patience. I can not forget to express huge thanks to my little son Khaled; to him (I love how your smile brightens up my life).

I would also extend my appreciation to all my research colleagues in the McFarlane laboratory, I am grateful for their assistance, provided a very friendly environment and sharing the research knowledge. I would also like to thank all my friends for providing their support during my journey. Special thanks must go to my best friend Hussam Althagafi for helping me get through the difficult times during my study.

Last but not least, I would like to thank the Saudi Arabian government for giving chances for Saudi students to fulfil their dreams. A special thank goes to Taif University for guidance and support.

Abbreviations

°C	Degrees Centigrade
µg	Microgram
µL	Microliter
3'	Three prime end of DNA
5'	Five prime end of DNA
βACT	Beta Actin
AFP	Alpha-fetoprotein
ALT	alternative lengthening of telomere
amp	Ampicillin
BCA	Bicinchoninic acid
BLAST	Basic Local Alignment Search Tool
BLM	Bloom syndrome protein
bp	Base pair
BTB	Blood-testis barrier
BRCA1	Breast cancer susceptibility 1
BRCA2	Breast cancer susceptibility 2
cDNA	Complementary DNA
ChIP	Chromatin Immunoprecipitation
CNS	Central nervous system
CO	Crossover
CpG	-Cytosine-phosphate-guanine-
Cq	Quantification cycle
CTA	Cancer testis antigen
CT	Cancer-testis
D-loop	Disassociation loop
dH2O	Distilled water
dHJ	Double-Holliday junction
DMC1	Disrupted meiotic cDNA1
DMEM	Dulbecco's Modified Eagle Medium
DMSO	Dimethyl sulfoxide
DNA	Deoxyribonucleic acid

DNMT	DNA methyltransferase
DSB	Double-strand break
E. coli	*Escherichia coli*
ECL	Enhanced chemiluminescence
ES/ESC	Embryonic stem cells
F	Forward
EST	Expressed sequence tag
FBS	Foetal bovine serum
g	Gram
G0	Quiescent phase
G1	Gap-1 phase
G2	Gap-2 phase
G418	Geneticin
GAPDH	Glyceraldehyde 3-phosphate dehydrogenase
GOI	gene of interest
GP73	Golgi protein 73
HATs	Histone acetylransferases
HA tag	Human influenza hemagglutinin
Hela	Henrietta Lacks
HCC	Hepatocellular carcinoma
HCT116	Colon carcinoma
HDACs	Histone deacetylases
HKMTs	Histone lysine methyltransferases
HMTs	Histone methyltransferases
HR	Homologous recombination
kb	Kilobase
KDa	Kilodalton
KRAB	Kruppel-association box
L	Litter
LB	Luria bertani
LINEs	Long-interspersed nucleotide elements

M-PER	Mammalian protein extraction reagent
MAGE	melanoma-associated antigens
MAGE-A	Melanoma antigen family A
MRN	MRE11–RAD50–NBS1
mRNA	Messenger RNA
MW	Molecular weight
ml	Milliliter
N-terminal	Amino-terminal domain
NCBI	National Centre for Biotechnology Information
NCO	Non-crossover
ng	Nanogram
nM	Nanomolar
non X-CT	Non chromosome cancer testis genes
NY-ESO-1	New York oesophageal squamous cell carcinoma-1
OCT4	Octamer-binding transcription factor 4
ORF	Open reading frame
PBS	phosphate buffered saline
PCR	polymerase chain reaction
PRMTs	Protein arginine methyltransferases
PRDM9	PR domain zinc finger protein 9
PSA	Prostate-specific antigen
PTMs	Post translation modifications
PVDF	polyvinylidene difluoride
R	Reverse
r.p.m	Rotation per minute
RNA	Ribonucleic acid
RT-PCR	Reverse transcription PCR
S	Synthesis-phase
SAM	S-Adenosylmethionine
SC	Synaptonemal complex
SDS	Sodium dodecyl sulphate
SDS-PAGE	Sodium dodecyl sulphate polyacrylamide gel electrophoresis
SDSA	Synthesis-dependent strand annealing

siRNA	Small interfering RNA
SMC1β	Structural Maintenance of Chromosomes 1β
SNV	single nucleotide variation
SOC	Super Optimal broth with Catabolite repression
ssDNA	Single strand DNA
SSX-2	The synovial sarcoma X member 2
STAG3	Stromal Antigen 3
SW480	Colon adenocarcinoma
TAA	Tumour associated antigens
TBE	Tris-borate-EDTA
TBS	Tris buffered saline
TE	Transposable Element
TEX19	Testis expressed 19
TRE	tetracycline responsive element
Tris	Tris (hydroxymethyl) aminomethane
TS	Testis-specific
TSGs	Tumour suppressor genes
V	Volt
WB	Western blot
WCE	Whole cell extract
X-CT	X- chromosome cancer testis genes

List of Contents

List of figures

Chapter 1

Chapter 3

Chapter 4

Chapter 5

Chapter 6

List of Tables

Chapter 2

Chapter 4

Chapter 1

Introduction

Introduction

1.1 Cancer

1.1.1 Cancer overview

Cancer is both a leading cause of death and a major impediment to life expectancy across the globe (Jemal et al., 2011; Bray et al., 2018). Evaluations from the World Health Organization (WHO) in 2015 found cancer to be the first or second cause of death before age 70 in 91 out of 172 countries; it was ranked third or fourth in 22 countries (Bray et al., 2018).

Cancer is broadly defined as a disease caused by aberrant cell division leading to tumours (Cavallo et al., 2011). Uncontrolled cell division in benign tumours can transform them into malignant tumours (Aly, 2012). Cancer cells proliferate rapidly and aggressively due to the inhibition of natural cell cycle regulatory mechanisms (Jayashree et al., 2015). Cancerous diseases are classified one of two ways; based on the organ of origin, as in prostate, lung, or breast cancer, or tissue origin, as in sarcoma in supportive tissues and muscles, carcinoma in the epithelium, myeloma in plasma cells inside the bone marrow, and leukaemia in white blood cells (Siegel et al., 2012).

Malignant tumour cells can migrate to other organs of the body via the lymphatic or vascular systems, a process called metastasis, where they seed and form secondary tumours (Figure 1.1) (Fridman et al., 2014). Cancer is thought to emerge as a result of an accumulation of epigenetic or genetic modifications leading to mutations or chromosomal abnormalities (Wodarz & Zauber, 2015; Roy et al., 2017). Such alterations often involve DNA repair, cellular metabolism, chromosome segregation, and DNA duplications; also, mistakes in chromosome segregation or DNA repair can change cellular ploidy (Soto et al., 2017). In addition to biological factors driving cancer incidence and death rate, other features such as lifestyle, geographical location, and economic status have also been implicated, although all these factors are not mutually exclusive (Bray et al., 2018).

Global statistics for 2018 indicate a 9.6 million cancer death rate with 18.1 million newly diagnosed cancer cases in that year. In both sexes, lung cancer is the most commonly diagnosed, followed by cancer of the prostate or breast, colon or rectum, stomach, liver, and other organs. Lung cancer accounts for 18.4% of all cancer deaths (Bray et al., 2018). Twenty million cancer cases are expected by 2025 based on global epidemic evaluations (Bray, 2014).

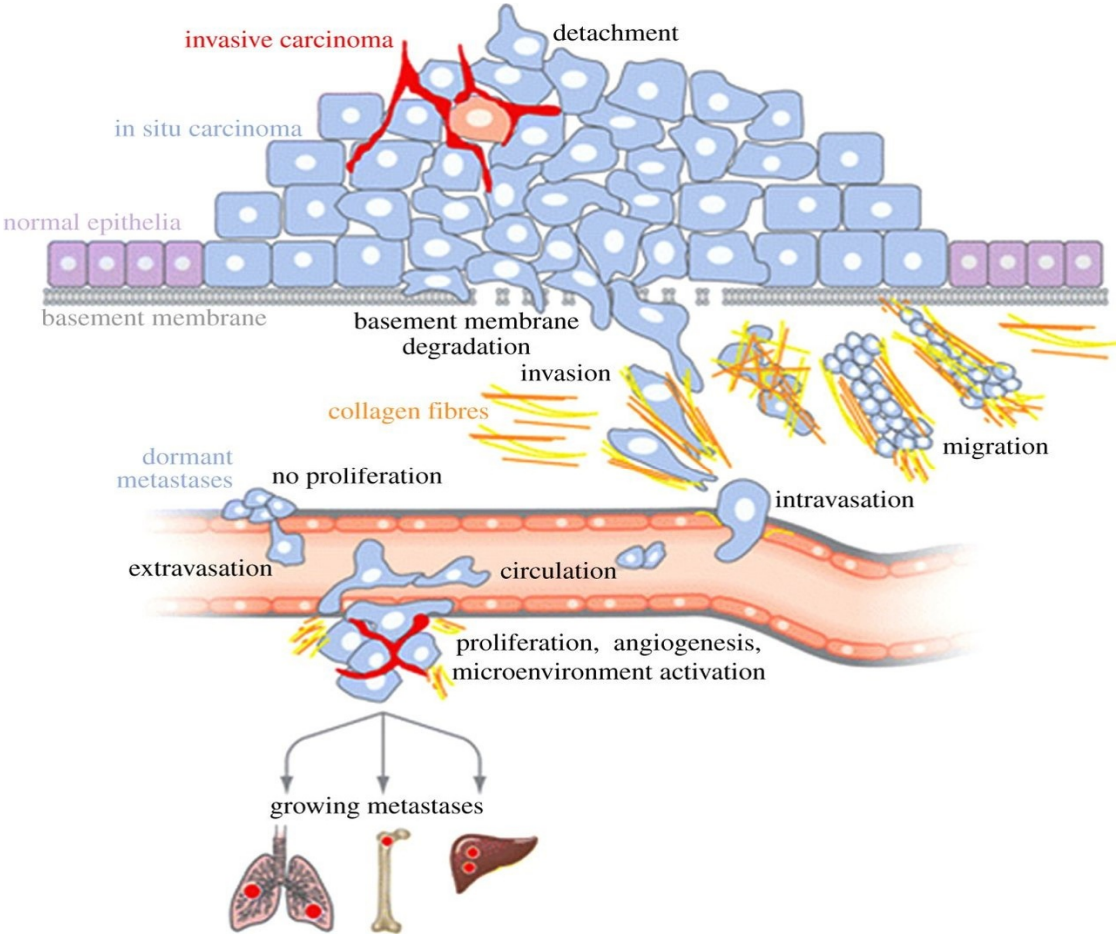

Figure 1.1 Phases of metastatic cancer. Primary tumours invade the basement membrane, specifically epithelial tissues, resulting in a loss of supporter junctions. Cells then move into the invasion process. Once cells enter the circulatory system, they can produce new cancers in different microenvironments (Taken from Djamgoz et al., 2014).

1.1.2 Types and causes of cancer

While determining the causes of a specific incidence of cancer remains challenging, some external factors such as chemical or radiation exposure (Barnes et al., 2018), smoking, or heavy alcohol consumption have been shown to increase cancer risk (Roswall et al., 2015). Environment, lifestyle and obesity have also been linked to cancer (Steele et al., 2017). Biological agents such as Hepatitis B or C viruses can also cause cancer in humans (Ringehan et al., 2017). Papillomavirus infection was specified as a significant risk factor for squamous cell carcinoma of the head and neck (Agalliu et al., 2016). A recent study found that alcohol is an important risk factor for several cancer types including cancer of the breast, liver, oropharynx and mouth (Hirko et al., 2016; Buykx et al., 2015). In addition, global alcohol consumption-related deaths increased from 3.6% in 2002 to 5.5% in 2012 of all cancer cases (Praud et al., 2016).

Cancers are partly attributed to molecular changes at the epigenetic and genetic levels that interfere with patterns of gene expression, effects of which include changes to levels of regulatory proteins or RNAs (Roy et al., 2017). For breast, prostate and colon cancers, genetic causes are thought to account for from 30% to 40% of an individual's risk (Wu et al., 2018). Epigenetic changes are thought to happen early in the development of tumours (Toiyama et al., 2014); in particular, genomic DNA hypomethylation occurs repetitive regions that affect gene activation. A loss of genome stability caused by activated or inactivated epigenetic regulatory proteins may also occur upon deregulation of epigenetic machinery (Hatzimichael et al., 2013).

1.1.3 Cancer Biomarkers

Early detection of cancer can decrease the risk of death. A cancer biomarker refers to any structure, process or substance that can be detected in the body that indicates the presence of cancer. Such biomarkers may be uncovered via examination of biomolecules such as nucleic acids (RNA or DNA), peptides or proteins, or other biochemical abnormalities. Biological factors suggesting the presence of cancer include transcriptional changes, post-translational modifications, and mutations in

somatic or germline cells (Henry & Hayes, 2012; Goossens et al., 2015; D'Andrea et al., 2017).

Prostate-specific antigen (PSA) is a commonly assayed cancer biomarker for prostate cancer. This biomarker is used to screen patients, determine their stage of cancer, and evaluate their potential response to therapy (Fabris et al., 2016). Alpha-fetoprotein (AFP) is a significant biomarker long used to reveal hepatocellular carcinoma (HCC) (Lai et al., 2012; Lou et al., 2017). A transmembrane protein known as Golgi protein 73 (GP73) located in the Golgi complex is frequently found in patients with liver abnormalities (Lou et al., 2017).

In addition to revealing early stages of cancer, cancer biomarkers also help determine treatment protocols for patients, distinguish between malignant and benign tumours, and recognize individual tumour types. For at-risk individuals, compulsory screening for cancer biomarkers could decrease overall cancer morbidity rates greatly (Burstein et al., 2011; Wu &Qu, 2015).

1.1.4 Hallmarks of cancer

Although the biology of cancer is extremely complex, important common features have been revealed over the last decade. Complications can be decreased through the identification of certain cancer hallmarks (special and complementary abilities) that promote tumour growth and malignant tumour invasion. These factors shape an organizing structure for understanding the diversity of these diseases (Wang et al., 2015). In 2000, Weinberg and Hanahan (2000) suggested six cancer hallmarks which indicate a transformation from normal to cancerous cells; they are as follows:

(1) Self-sufficient growth is enabled.
(2) Growth suppressors are evaded; that is, cancer cell division occurs due to the loss of growth inhibitory signals.
(3) Programmed cell death is evaded; that is, cancer cells avert the apoptosis that is fundamental for the expulsion of damaged cells.
(4) Angiogenesis is stimulated to provide tumours with the nutrients and oxygen necessary for survival.
(5) Cells carry out unlimited replication following the evasion of cell death that is supposed to occur when cells reach a certain density.
(6) Tumours invade tissue and expand to other organs in a process known as metastasis.

Hanahan and Weinberg added four more hallmarks of cancer in 2011: deregulation and reprogramming of energy metabolising pathways, immune system evasion, genomic instability leading to mutation, and tumour-promoting inflammation (Hanahan & Weinberg, 2011) (Figure1.2).

Sonnenschein and Soto (2013) proposed that cancer was not simply an uncontrolled proliferation event but involved altered signalling regulation by cancer cells. These researchers thus described cancer as an evolving, multifactorial process in a particular tissue (Sonnenschein & Soto, 2013).

Based on sequence methodologies, mRNA splice factors have also been linked to the development and metastasis of cancer (Oltean & Bates, 2014). RNA splicing contributes to the development of disease by modifying RNA transcripts implicated in cancer hallmark processes (Urbanski et al., 2018); specifically wherein splicing alterations are promoted or restricted by mutations near or within splice sites leading to aberrant splicing of genes that code for tumour suppressors (Dvinge et al., 2016).

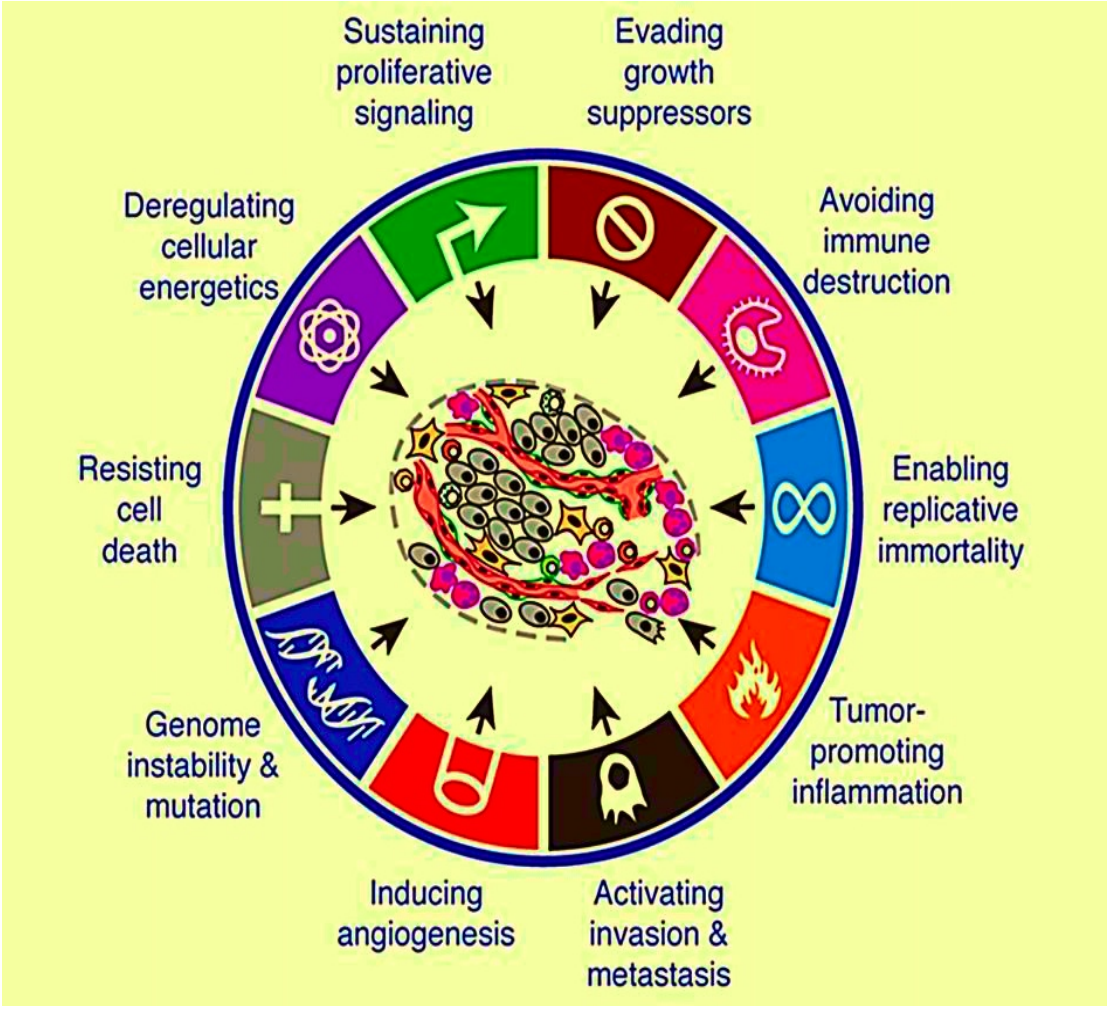

Figure 1.2 Hallmarks of cancer. Hallmarks that indicate cancer cell immortality as illustrated by Hanahan and Weinberg (2011).

1.1.5 Treatment for cancer

Cancer often goes undiagnosed until it is at an advanced stage when cancerous cells transform into metastatic cells and symptoms of tumour growth become visible. Any delay in diagnosis can have a negative impact on the efficacy of cancer therapy (Richards et al., 2017; Wardle et al., 2015). Conventional cancer therapies include radiation therapy, surgery, chemotherapy or some combination thereof (Meretoja et al., 2017; Shamsi & Islamian, 2017). One of the most frequently used therapeutic pathways is radiation, or radiotherapy, which uses gamma rays and X-rays to shrink

tumours. Radiotherapy can treat even early phase tumours (Wang et al., 2019), but it also affects normal tissue surrounding the tumour and causes unpleasant side effects such as nausea, skin irritation, fatigue and hair loss (De Ryck et al., 2015; Brown, Kirkbride & Marshall, 2015).

Surgical intervention is another effective therapy for removing solid tumours, and normal tissue around the lesion is usually removed as well to ensure all cancerous tissue has been excised. Despite this, however, tumours can return (Aly, 2012; Aris & Barrio, 2015). Chemotherapy attacks cancer cells directly to inhibit or reverse tumour growth or effect tumour cell death (Florea & Büsselberg, 2011). These therapies can prevent cell division, inhibit DNA repair and interrupt DNA synthesis to prevent cell growth and division. These therapies also affect normal cells, also, leading to side effects such as hair loss, nosebleeds, stomach ache, fatigue, anorexia, anaemia, and vomiting (Kreamer, 2014).

A relatively new avenue in cancer treatment is immunotherapy. This modality uses B-cells, T-cells and natural killer cells to target and destroy cancer cells (Harris & Drake, 2013; Thor, Straten & Garrido, 2016). In many cases, the patient's immune system alone is unable to eradicate cancer cells because tumours develop immune evasion mechanisms. Immune system therapeutics have been developed to enable the immune system to override oncogenic inhibition (Medina & Adams, 2016; Aly, 2012).

1.2 Tumorigenesis

In healthy cells, growth and differentiation are strictly regulated by well controlled mechanisms. An absence of cell proliferation control is a hallmark of cancerous cells. Oncogenes, genomic stability genes and tumour suppressor genes are often implicated in initiating tumourigenesis. These genes are critical to repairing damaged DNA and are also involved in chromosomal segregation and recombination (Negrini, Gorgoulis & Halazonetis, 2010; Hanahan & Weinberg, 2011; Ferguson et al., 2015).

1.2.1 Oncogenes

Proto-oncogenes are genes that regulate cell development by promoting cell division and prohibiting cell differentiation or death. Mutations in these genes often transform them into oncogenes that stimulate the evolution of cancer. Such mutations may increase the transcription levels of proteins or facilitate chromosomal translocations; these genes often work in combination with other oncogenes (Whitehurst, 2014; Roy et al., 2017). Oncogenes code proteins involved in a range of cellular process including apoptosis, induction of transcription factors, chromatin remodelling, production of hormone receptors, and growth regulation (Croce, 2008; Bagci & Kurtgöz, 2015). An example of oncogenes is the RAS family of gene. In humans, the four RAS proteins NRAS, HRAS, KRAS4A and KRAS4B coded by the three *RAS* genes participate in the coordination of cell signalling, and cell development and survival. Mutations in *Ras* oncogenes have been linked to roughly 30% of all cancer types (Pylayeva-Gupta, Grabocka & Bar-Sagi, 2011; Croce, 2008).

Viral oncogenes are able to initiate and guide the growth of cancer types arising from viral infections. Viral oncogenes can insert promoters into the DNA of the host and can transform proto-oncogenes into oncogenes, such as transcription factors (Santiago-Ortiz & Schaffer, 2016). Enhanced expression of transcription factors can modify the expression patterns of oncogenes or tumour suppressor genes (Ranzani et al., 2013). For example, in humans, the human papillomavirus (HPV) has been linked with many benign tumours such as warts and human herpesvirus 4 (EBV). EBNA-1 is a trans-activator of viral and host genes and has also been implicated in oncogenesis (Kang & Kieff, 2015; Rödel et al., 2018).

1.2.2 Tumour suppressor genes

Tumour suppressor genes (TSGs) are those that protect healthy cells from becoming cancerous. Mutations in TSGs can lead to the development of cancer (Llinas-Arias & Esteller, 2017). TSGs are important for controlling the cell cycle and apoptosis. Loss of function in these genes can cause disruptions to cell cycle control and lead to uncontrolled cell proliferation, a hallmark of cancer (Weinberg, 2013).

TP53 is an important tumour suppressor gene reported to fight cancer cells. P53 pathway of cell migration and tumour suppression is based on transcriptional regulation (Muller & Vousden, 2013; Stracquadanio et al., 2016). P53 inhibits cell cycle progression and controls apoptosis, and somatic genetic alterations in the *TP53* gene have been detected in more than 50% of all cancer genomes (Stracquadanio et al., 2016; Kandoth et al., 2013). Reduced or inhibited P53 activity is a frequent precursor of metastasis (Parrales & Iwakuma, 2015).

1.2.3 Genome Stability Genes

The maintenance of genome stability is also important for healthy cells (Yao & Dai, 2014). Biological changes that bring about genomic instability include point mutations and chromosomal rearrangements (He et al., 2018; Ferguson et al., 2015). Changes in DNA sequences and epigenetic alterations cause genomic instability via chromatin assembly changes, DNA methylation and histone modifications (Choi & Lee, 2013; Katto & Mahlknecht, 2011).

Genome stability genes are primarily responsible for repairing DNA damage that occurs upon exposure to mutagens or during DNA replication (Negrini, Gorgoulis & Halazonetis, 2010; Chian et al., 2018). Genome stability genes also participate in meiotic recombination. Genome stability genes have been implicated in breast cancer, most notably *BRCA1* and *BRCA2*; these genes assist with DNA repair and are also active in ovarian cancers (Trego et al., 2016). During oncogenesis, changes to other genes in combination with mutations in genome stability genes can result in tumour development (Janssen & Medema, 2013).

1.3 Cancer/Testis Antigens

1.3.1 Cancer/Testis Antigens Overview

The first CTA gene, melanoma antigen-1 *MAGE-A1*, was isolated in melanoma patients in the early 1990s (van der Bruggen et al., 1991). Old and Chen were the first to use the term cancer testis antigen (CTA) for this type of tumour-associated antigen (TAA), due to their limited presence in somatic tissues (de Carvalho et al., 2012). CTAs are protein antigens only normally present in male germ cells in the adult testes and not in healthy somatic cells (Li et al., 2017; Whitehurst, 2014; Yang et al., 2015).

Cancer testis (CT) genes are widely expressed at different levels that vary by tumour. Generally, CT genes are minimally expressed in leukaemia and lymphoma, and pancreatic and colon cancers. They are strongly expressed, however, in melanomas and ovarian and lung cancers (Caballero & Chen, 2009). Techniques used to examine CTA gene expression in cancerous cells and testes include post-genomics informatics technologies and cDNA oligonucleotides analyses (Lawrence et al., 2014; Wang et al., 2016).

Immune privilege is an important adaptive process to conserve particular tissues from the harmful impact of immune responses. In mammals, immunoprivileged tissues include the testes, the eyes and the brain (Caspi & Stein-Streilein, 2014). These tissues have the ability to accept immunogenic antigens. The aim of the immunoprivileged nature of specific tissues is to curb an expanded immune response that could damage the biological functions of the tissues (Chen, Deng & Han, 2016). In the testes specifically, the immune system is blocked from affecting germ cells by preventing their reaction to the immune system (Bhushan et al., 2016; Chen, Deng & Han, 2016). The isolation of late phases of germ cells from the immune system via the blood–testes barrier (BTB) is generally believed to be an important mechanism of the immune privilege of the testis. The tight junctions between adjacent Sertoli cells that shape the BTB in germ cells. The BTB helps to drive the CTAs to be immunogenic when produced in cancers (Hirohashi et al., 2016; Morgan et al., 2013).

1.3.2 Cancer-Testis Antigens Gene Classification

Based on large data set (https://www.ncbi.nlm.nih.gov/gene), such as the CT database (http://www.cta.lncc.br), the human genome has been postulated to contain approximately 277 CT genes classified in to 44 gene families (Gordeeva, 2018). CTA genes can be classified based on their chromosomal location. First, X-CTA genes are found on the X chromosome and are generally expressed in the placenta and the testis spermatogonial genes. *XAGE-2, XAGE-3, MAGE-8, MAGE-A10* and *NY-ESO-1* are recognized examples of X-CT genes (see Figure 1.3). X-CTA genes are generally in large paralogue families accounting for more than 50% of all CTA genes (Caballero & Chen, 2009; Kalejs & Erenpreisa, 2005; Rajagopalan et al., 2011; Stevenson et al., 2007). Second are the non-X-CTA genes, which are located on the autosomes. Most non-X-CTAs perform roles in spermatogenesis and fertilization during the meiosis phase and or post-meiotitic phase. *CP-1, SPAG9* and *SPO11* are examples of non-X-CT genes (Almeida et al., 2008; Caballero & Chen, 2009; Suri et al., 2015).

CTA genes can be further categorised into several groups according to their expression profile. Firstly, testis-restricted CTA genes are expressed only in the testis, placenta and at least one cancer type. Secondly, testis-brain-restricted CTA genes are expressed in the central nervous system (CNS), adult testis and at least one cancer type. Thirdly, testis-selective CTA genes are expressed in the testis, two somatic tissue types and one or more cancer types. Fourthly, testis-brain-selective CTA genes are expressed in the testis, CNS tissue, no more than two normal tissue types and one or more cancer types (Hofmann et al., 2008).

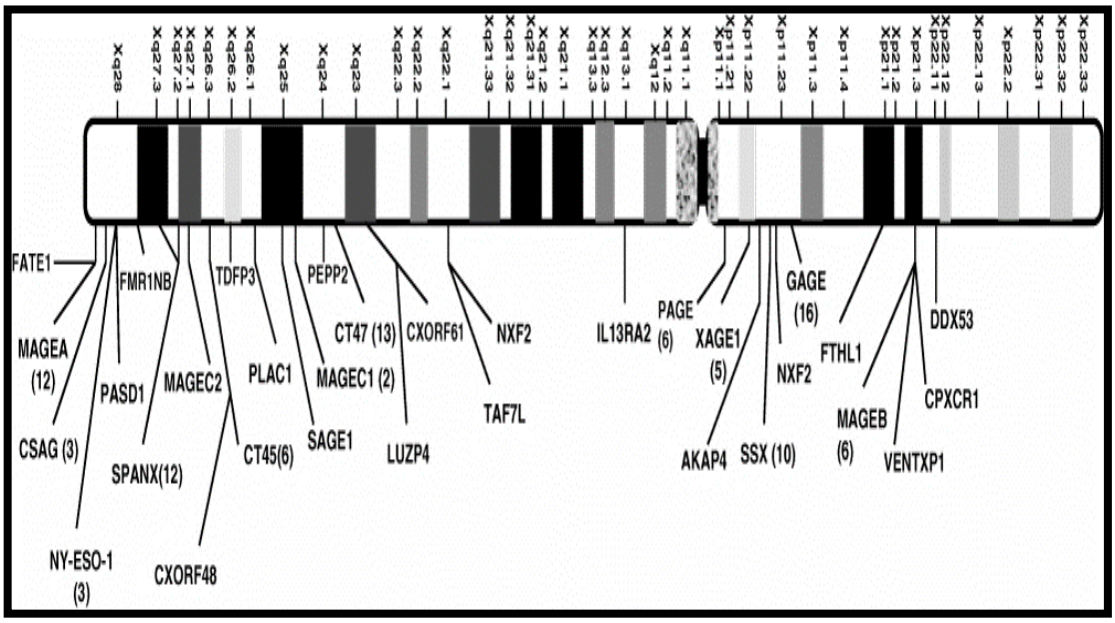

Figure 1.3 Examples of X-CT genes on the X chromosome. Diverse families of CTA genes are seen on the X chromosome (Caballero & Chen, 2009).

1.3.3 Cancer/Testis Antigens Gene Expression

Generally, most X-CTA family members are specifically expressed in mitotically active spermatogonia cells of the testes, although several are also expressed in placental cells. Non-X-CTA genes are expressed in the nearly late phases of germ cells differentiation (Stevenson et al., 2007). The examination of messenger RNA for CTA genes has also shown limited expression in non-germ line tissues. One postulated defining feature of CTA genes is that in non-germline tissues they are transcribed at less than 1% of their expression level in the normal testis (Caballero & Chen, 2009; Hemminger et al., 2014).

Generally, epithelial cancers, including bladder, prostate and breast cancer, have moderate CTA gene expression. Some studies have shown that CTA genes have a tendency to be co-expressed in similarly positive tumours. The expression of CTA genes usually appears raised in subsequent clinical phases, depending on the stage of the tumour (reviewed in Caballero & Chen, 2009). In bladder cancer, for example, *NY-ESO* is usually down-regulated, with no detectable expression in Stage 1 tumours, but 23% of Stage 2 tumours appear to exhibit expression (Kurashige et al., 2001). In

terms of cancer prognostics, the protein levels of CTAs have been examined in various cancer and normal tissues. For instance, *SCP-1, NY-ESO-1* and *MAGE-A* proteins have been assessed in several cancer tissues, and it was found that patients with these proteins in their tumours produced antibodies against these CTAs (reviewed in Caballero & Chen, 2009). CTA gene expression studies have shown different results in cases of cancer prognostics. In glioblastoma patients, some CTA genes (*CTCFL, XAGE3* and *OIP5*) were examined, and the results showed that the survival period of *OIP5* expressing patients was better than that of *OIP5* non-expressing, negative patients (Freitas et al., 2013). In other research, it was found that positive *MAGEA1* expression, particularly at the time of diagnosis, could possibly predict distant metastasis in osteosarcoma patients (Zou et al., 2012).

Abnormal production of PRDM-family proteins is usually related to cancer development, especially in colorectal cancer, leukaemia, breast cancer and cervical cancer (Hohenauer & Moore, 2012). In the PRDM family, only PRDM9 is considered to be a meiosis-specific protein. RT-PCR analysis found the expression of *PRDM9* in various cancer types, including breast cancer, colon cancer, ovarian cancer, leukaemia and melanoma (Feichtinger et al., 2012).

1.3.4 CTAs in cancer cells

When meiotic and other germ line genes are activated during oncogenesis, they are thought to guide both maintenance and support functions associated cancerous states across a range of cancer types (Simpson et al., 2005; Rousseaux et al., 2013; Whitehurst, 2014; McFarlane et al., 2015).

Cancerous cells and germ cells have certain characteristics in common. Tumourigenesis is linked to the stimulation of germ line genes found in cancerous cells (Rousseaux et al., 2013; McFarlane et al., 2015; Garcia-Soto et al., 2017). Several studies have implicated CTA genes in the initiation and progression of cancer, suggesting that activation of CTA genes in tumours may underlie critical aspects of cancer. Figure 1.4 shows instances of CTA genes and their suggested cancerous properties.

Some CT genes have been directly associated with the growth and development of cancer cells. SSX2 is a DNA binding protein that regulates chromatin structure. Knockdown of the SSX2 gene in melanoma cancer cells significantly decreases cellular proliferation (Gjerstorff et al., 2015). MAGE proteins promote the survival of cancer cells via interaction with p53, as it was found that depletion of *MAGE-A* gene expression enhances p53 recruitment to target promoters. It has also been suggested that MAGE-A interacts with the p53 DNA binding domain to block its transcriptional activity (Marcar, et al, 2015, Schooten, et al, 2018).

GAGE members from the CT antigen family, which include PAGE and GAGE proteins, prevent certain types of cancer cells from entering apoptotic pathways. Depletion of PAGE4 was found to encourage cell death and negatively affect tumour growth (Kulkarni et al., 2016). GAGE-7 curbs apoptosis in response to different types of apoptotic stimulation (Kao et al., 2014).

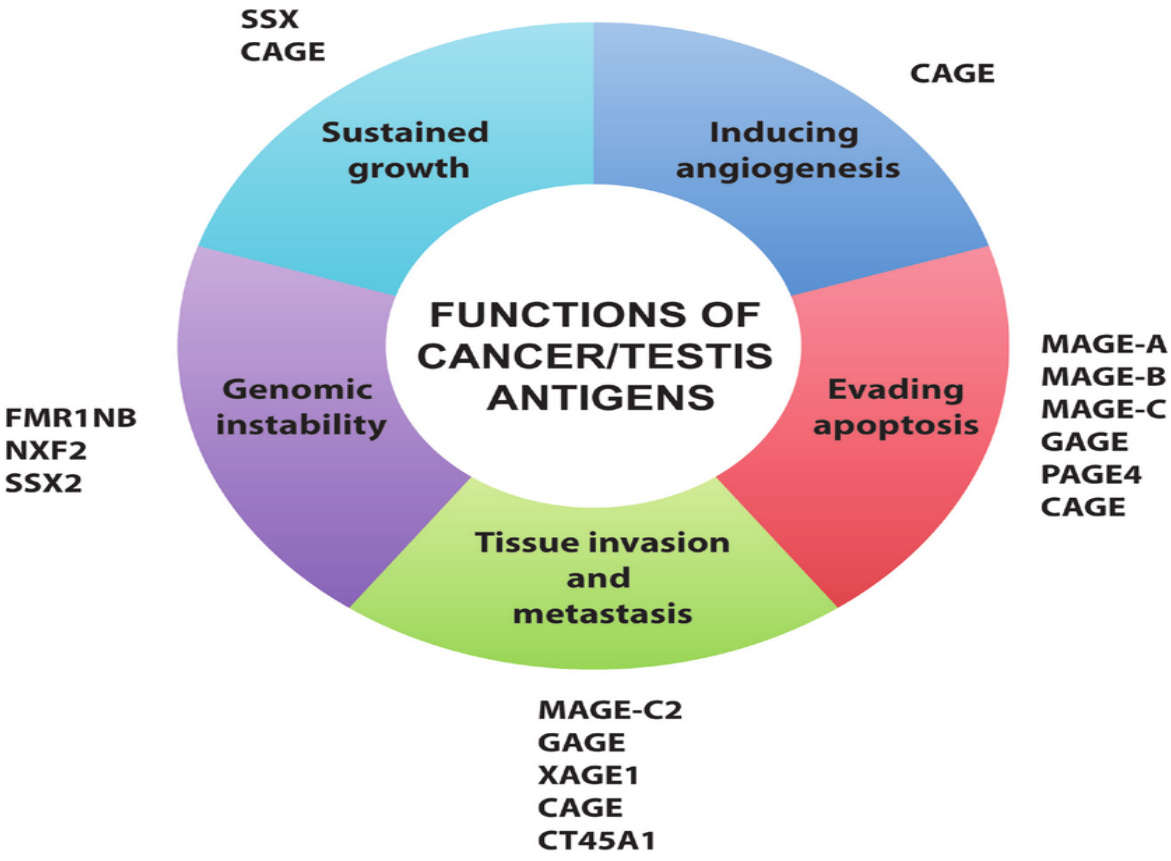

Figure 1.4 Oncogenic roles of CTAs. This diagram shows the functions of several CTA genes in conferring important tumour characteristics (Taken from Gjerstorff et al., 2015).

1.3.5 CTA genes in Immunotherapy

Immunotherapy is an important tool in cancer treatment. In general, cancer immunotherapy is categorized into two main groups, passive and active immunotherapy (Kazemi, 2016).

Active immunotherapy includes vaccines, while passive immunotherapy uses adoptive cell treatments or monoclonal antibodies (Lynch, 2016). CTAs are regarded as important targets in immunotherapy treatment (Fratta et al., 2011).

1.3.5.1 CTAs in active immunotherapy

Active immunotherapy stimulates the immune system to respond antagonistically to cancer or other harmful diseases. A non-explicit reaction can be induced in the immune system by agents such as cytokines. Other active immunotherapies provoke the immune system with therapeutic vaccines. The immune system is trained to detect and eradicate cancer cells by reacting to antigens on their surface (Baxter, 2014). Therapeutic vaccines using CTAs like NY-ESO-1 and MAGE-A3 have been tested in melanoma cancer patients, as these are known to influence tumour nodule regression (Caballero & Chen, 2009). The CTA SP17 vaccination has been confirmed in in *vivo* trials in mammals suffering from ovarian cancer (Chiriva et al., 2010). Genes from the *MAGE* group are highly expressed in many different tumours, including lung, melanoma, colon, ovarian, breast and multiple myeloma cancers. Developing and improving vaccines that target this group of genes may help prevent the incidence of several malignant tumours (Zhu et al., 2016).

1.3.5.2 CTAs in passive immunotherapy

In the field of passive immunotherapy, immune constituents or external antibodies are employed to trigger the immune response (Baxter, 2014). Genetic engineering of lymphocyte T-cells has helped control tumours in patients with metastatic cancer. The main task of adoptive immunotherapy is to isolate lymphocyte T-cells from patients (Yang & Rosenherg, 2016), culture these cells, and cultivate them in *vitro* to express specific tumour antigens. Then, the cells are reinfused back into the patient to fight tumour cells (Bonini & Mondino, 2015). Genetically engineered T-cells have shown promise in targeting CTA antigens. Hunder et al. (2008) employed autologous CD4+

T cell therapy against the CTA NY-ESO-1 in patients suffering from melanoma metastases. CD4+ T cells were removed from the patient, isolated and cultured in vitro, and then reimplanted. Two months after reinfusion, tests demonstrated a lack of nodal and pulmonary tumours, and after two years, tests found no signs of cancer in the patient (Hunder et al., 2008).

1.4 Epigenetic modification

The term 'epigenetic' refers to heritable changes in gene expression unrelated to the sequencing of DNA nucleotides (Hatzimichael & Crook, 2013; Saleem et al., 2015). Epimutations may be able to control genomic instability by silencing tumour inhibition genes or activating oncogenes, either freely or in combination with genetic mutations (Sharma et al., 2010). Epigenetic mechanisms appear significantly involved in controlling CTA gene expression in both tumour and normal cells (Videtic Paska and Hudler, 2015). Modification of histones and DNA methylation are epigenetic changes that can affect gene expression (Hatzimichael & Crook, 2013).

1.4.1 Chromatin structure

Chromatin was the first basic unit of the cell recognized to be present in different organisational levels. Chromatin refers to a mass of genetic material containing histone proteins and DNA (Li & Zhang, 2012; Nikolov & Taddei, 2016; Shen et al., 2017). The primary component of chromatin is the nucleosome; nucleosomes contain a histone octamer that contains two of each of the four core histones, H2A, H2B, H3 and H4. This structure is enclosed by around 147 base pairs of DNA, with between 20 and 80 bp of linker DNA connecting the nucleosomes. Linker DNA is also bound to another histone, H1, and this association results in a highly compact chromatin structure in the nucleus (Margueron &Reinberg, 2010; Li & Zhang, 2012). There are two main types of chromatin, heterochromatin and euchromatin. Heterochromatin contains H3K27 trimethylation and associates with transcriptionally silent locations. Chromatin changes affect various DNA processes, including gene transcription (Simon & Kingston, 2009; Machida et al., 2018). Euchromatin is found in active transcription regions, where DNA is exposed to allow the binding of transcription

machinery. Histones undergo significant post-translational modifications (PTM) to provide modularity within the nucleosome core. PTMs include acetylation, phosphorylation, ubiquitylation and methylation (Schon et al., 2018; Speranzini et al., 2016) (Figure 1.5).

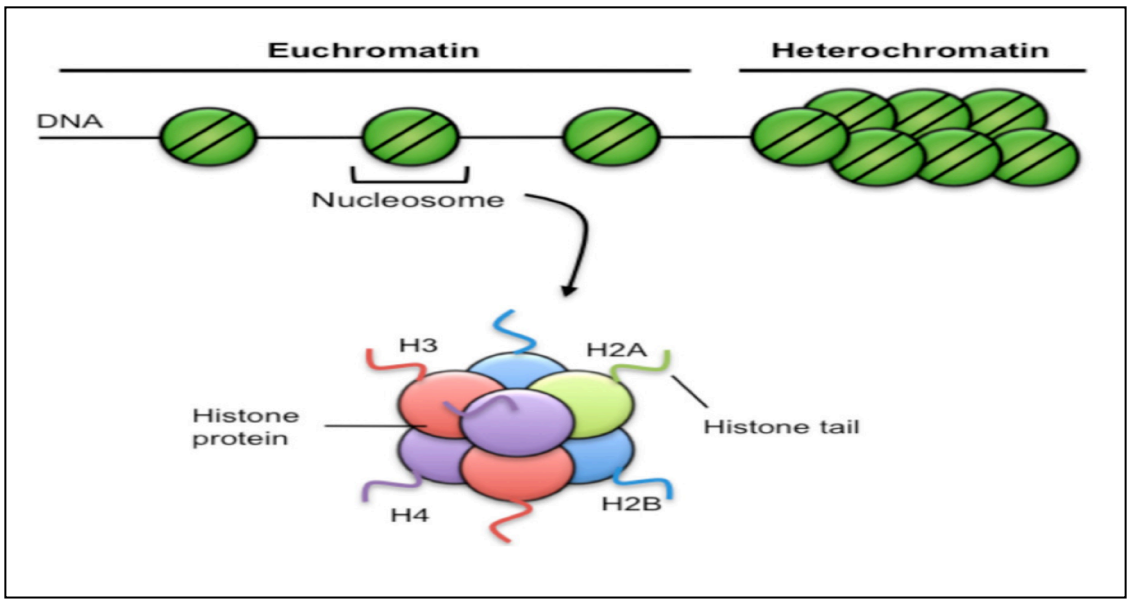

Figure 1.5 Formation of euchromatin and heterochromatin.
Euchromatin is an open chromatin structure able to accommodate gene transcription. Conversely, heterochromatin is compressed, as evidenced by a rise in nucleosome heterochromatin density, and prevents gene transcription (Adapted from Russ et al., 2012).

1.4.2 Acetylation of histones

Post-translational acetylation is enabled by conserved lysines at the N-terminals of all four core histones. Histone acetylation was the first post-translational histone modification found to be associated with gene regulation (Wang, Allis & Chi, 2007). Acetylated histones are frequently associated with transcriptionally active gene promoters.

Histone acetylation is regulated by two families of enzymes, histone deacetylases (HDACs) and histone acetyl transferases (HATs) (Figure 1.6). Histone modifying

enzymes enable rapid genetic responses to cellular needs (Bannister & Kouzarides, 2011). ε-N-acetyl lysine is generated via transference of an acetyl group to the ε-amino group of a lysine residue via HATs, which utilize acetyl coenzyme A (acetyl CoA) as a co-factor (Yin et al., 2017). HATs create an opening between nucleosomes and histones, enabling the binding of transcription factors followed by DNA transcription. Conversely, HDACs detach acetyl groups from histones that subsequently regain their positive charge, allowing fundamental interactions with negatively charged DNA, compaction facilitating chromatin condensation to prevent transcription (Ho & Crabtree, 2010; Li & Shogren-Knaak, 2008). Acetylation is the predominant histone modification, with a host of probable acetylation sites, including H3K9, H3K18, H3K14 and H4K8 (Kouzarides, 2007).

The two main categories of HATs, type A and type B, are classified based on their functions and probable source. A-type HATs are thought to catalyse acetylation and assist with gene transcription. Indeed, HAT motif A domains include binding locations for acetyl-CoA are common to proteins categorised as having HAT activity. B-type HATs catalyse acetylation phases related to the transport of newly created histones from the cytoplasm to the nucleus for binding to target DNA (Chrun, Modolo & Daniel, 2017). HDACs are considered transcriptional repressors, as the elimination of acetyl groups coincides with HDAC gene silencing (Bannister & Kouzarides, 2011). Over-expression of HDAC genes has been implicated in many cancers, and HDAC inhibitors are often used in conjunction with chemotherapeutic agents in cancer therapy (Kouraklis & Theocharis, 2002).

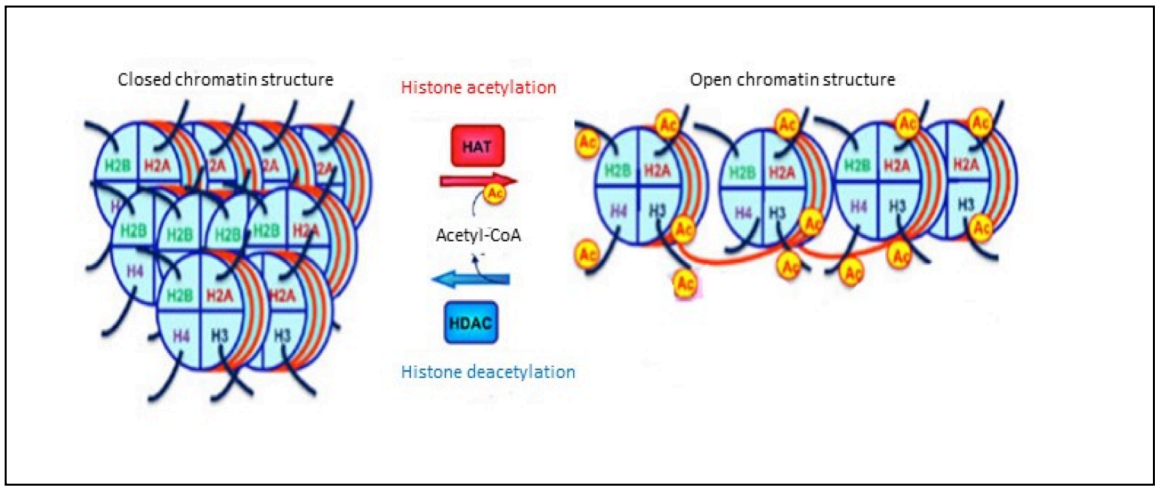

Figure 1.6 Histone acetylation and deacetylation. Histone acetyltransferases (HATs) add acetyl groups (Ac) to histone tails, creating openings in the nucleosome to facilitate the binding of transcription factors. Histone deacetylases (HDACs) remove the acetyl groups from the histone tails, allowing chromatin recondensation (adpted from Koprinarova, et al., 2016).

1.4.3 Methylation of histones

Histone methylation occurs at lysine and arginine residues, both of which are found in the histones H1, H2A, H2B, H3, and H4. Each residue can be methylated in several ways, depending on its genomic site and methylation level (Fuchs et al., 2006). Histone methylation has been associated with different types of DNA transcriptional regulation (Sims Iii & Reinberg, 2009).

Protein arginine methyltransferases (PRMTs) and histone lysine methyltransferases (HKMTs) build the histone methyltransferases (HMTs) structure that catalyse histone methylation. These enzymes add a methyl group (-CH3) from S-adenosylmethionine to specific target residues (Greer & Shi, 2012). Methylation of the ε-amino group of lysine can take different forms, such mono- (me), di- (me2) or tri- (me3) methylation and arginine residues can be mono- or tri-methylated (Bannister & Kouzarides, 2011). Methyl groups added to arginine or lysine can be removed by histone demethylase (HDM) enzymes (Dimitrova, Turberfield & Klose, 2015).

Histone methylation controls transcription-level gene expression and inhibits or stimulates gene expression depending on the methylation status of a particular lysine residue. Widely researched histone lysine methylation sites include H3K9, H3K4, H3K36, H3K27 and H3K79 (Gong & Miller, 2017). H3K9me2/3, H3K27me3, H3K4me1, H2K20me1/me2 and H4K20me3 are associated with heterochromatin and transcriptional silencing, whilst H3K36me3 and H3K4me2/3 are associated with euchromatin and transcriptional activation (Sims Iii & Reinberg, 2009).

1.4.4 DNA Methylation

DNA methylation has also been found to facilitate histone modification regulation (Du et al., 2015). In addition, it has been associated with genomic imprinting (Girardot, Feil & Llères, 2013) and X-chromosome inactivation (Lee & Bartolomei, 2013). During DNA methylation, DNA methyltransferases (DNMTs) catalyse the covalent addition of a methyl group to the 5' position of the cytosine base of CpG dinucleotides (Ballestar, 2011; Jones, 2012).

Tumour suppressor genes and DNA repair genes are silenced in cancer cells via hypermethylation of promoter regions and hypomethylation of non-promoter regions in their genomes (Akhavan-Niaki & Samadani 2013). Hypermethylation may also lead to genome instability and the disruption of DNA repair mechanisms and cell cycle and apoptosis regulation, which can lead to tumourigenesis (Wu & Bekaii-Saab, 2012). There is an association between hyper- and hypomethylation of CpG island promoter regions and the initiation and progression of cancer (Ballestar, 2011). Fratta et al. (2011) reported that a majority of cancer testis antigen (CTA) genes are subject to methylation in normal somatic cells, but that hypomethylation (demethylation) during spermatogenesis results in their activation.

1.5 Phases of cell division

The term cell cycle refers to the interval of time between every mitotic division (Kronja & Orr-Weaver, 2011). There are two main phases of the mitotic cell cycle. These are interphase and M phase. Interphase is further categorized into three organized stages: G1 phase (Gap 1), S phase (DNA synthesis) and G2 phase (Gap 2) as shown in Figure 1.7. Replication of DNA occurs during the S phase. On the other hand, M phase refers to the stage when the cell undergoes the mitotic division. G1 and G2 refer to the two gaps which occur prior to S phase and following the M phase. Cells grow during the interphase and fully replicate their DNA. During the G2 phase, the cell prepare for the division to form two daughter cells (Strahm & Capra, 2005, Kronja & Orr-Weaver, 2011). Besides these, non-dividing cells exist outside the cell cycle in a state termed G0 (Behl & Ziegler, 2014). As M phase spans a comparatively shorter period, majority of the cells spend most of the time of their life in interphase (Kronja & Orr-Weaver, 2011).

1.5.1 Mitotic cell division

The majority of healthy cells and cancer cells duplicate via mitotic division. Mitosis is a type of cell division through which a parent cell with diploid number of chromosomes divides to generate a pair of daughter cells with the same number of chromosomes as that of parent cell. This division normally takes place in somatic tissue for growth, tissue repair and homeostasis (Silkworth & Cimini, 2012). Replication of DNA occurs once in the S-phase of mitosis after which chromosomes segregate to generate two daughter cells. On the basis of chromosomal organisation and behaviour, the process of mitosis is further divided into a number of phases namely prophase, prometaphase, metaphase, anaphase, telophase and cytokinesis. Condensation of chromosomes initiates during the prophase stage. Replicated chromosomes appear thicker, shorter and can be viewed easily. Moreover, centrosomes duplicate and travel to opposite poles of the cell and initiation of assembly of mitotic (Silkworth & Cimini, 2012). In higher eukaryotes, prometaphase involves breakage of nuclear envelope. Also, chromosomes bind to the mitotic spindle

microtubules through a structure referred to as the kinetochore. During the metaphase stage, the chromosomes arrange themselves at the equator of the cell.

This arrangement occurs on the metaphase plate in the middle of the space between the opposite poles of the cell. Paired kinetochores are linked to the spindle microtubules. Anaphase involves separation of the paired sister chromatids and their synchronized movement towards opposite poles. This requires the cohesion between sister chromatids to be disrupt in a highly orchestrated fashion. During telophase, chromosomes reach at the opposite poles followed by their decondensation. A new nuclear envelop surrounds each one of the daughter nuclei. In cytokinesis the cytoplasm divides leading to formation of two daughter cells with same number of chromosomes as that of parent cell (Walczak et al., 2010).

1.5.2 Meiotic cell division

Two copies of every chromosome (homologues) are present in non-reproductive cells. One member of the homologous pair has been received from maternal lineage and the other from paternal lineage (Villeneuve & Hillers, 2001; Clift & Marston, 2011). Haploid sex cells or gametes are produced from diploid progenitor cells only in ovaries and testes.

During sexual reproduction, fusion of two gametes take place through fertilisation to make a zygote. During gametogenesis, it is important that the number of chromosomes should be decreased to half to assume the diploid state is restored upon gamete fusion. The stage is restored upon gametes fusion. The gametogenic nuclear division is termed as meiosis (Petronczki, Siomos & Nasmyth, 2003; Zickler & Kleckner, 2015).

The process of meiotic division is divided into two divisions namely reductional division (meiosis I) and equational division (meiosis II) (Gerton & Hawley, 2005; Lichten & de Massy, 2011) (Figure1.8).

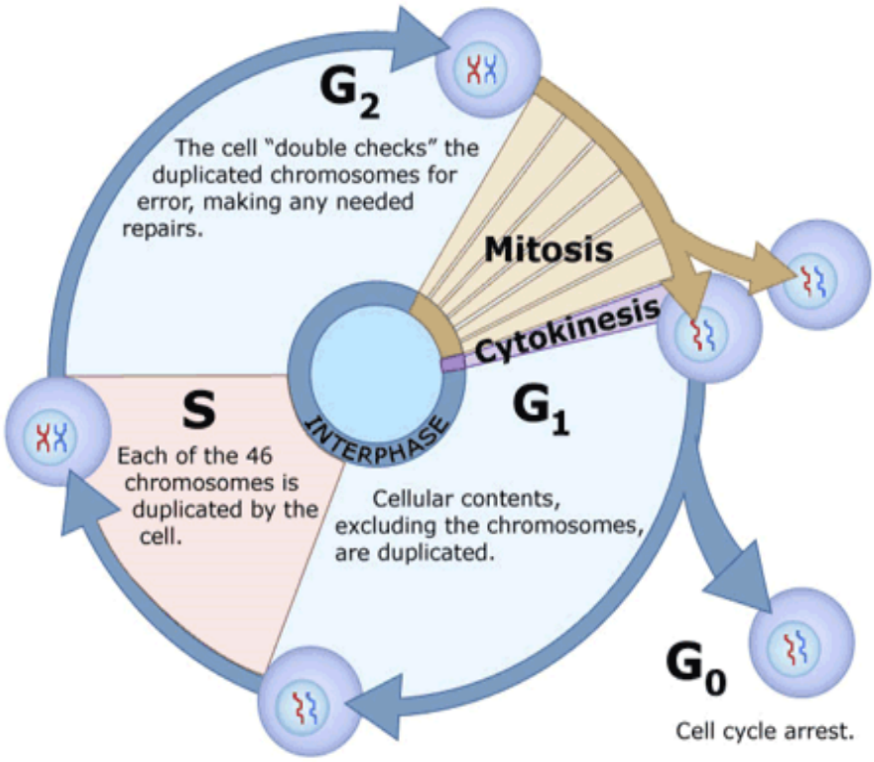

Figure 1.7 Schematic diagram showing different stages of cell cycle.
Different stages of mitotic cell cycle. These stages are referred to G1, S, G2 and M phase. The size of cell increases during interphase. DNA is synthesized during S phase so that the genome is duplicated prior to division. Cells growth stop during M phase which involves an organized process of division. G0 refers to the phase during which cell exists outside the cell cycle (Taken from Virtual Genetics Education Centre).

1.5.2.1 The first meiotic division, Meiosis I

Meiosis occurs in two successive chromosome segregation events meiosis I and II which follow just one round of DNA replication. There are four distinct phases in first meiotic division. These are prophase I, metaphase I, anaphase I and telophase I. During pre-meiotic stage of meiosis, chromosomal duplication takes place for doubling the sister chromatid pairs before meiotic division. After pre –meiotic DNA replication sister chromatids remain linked via a meiosis-specific cohesin complex. Accordingly, every set of chromosomes is formed of a pair of identical sister

chromatids (Lee & Amon, 2001). Prophase I is important phase that involves several special steps that include pairing of homologous chromosomes, synapsis and the formation of DNA double-strand break (DSB). For that reason, prophase I is further subdivided into five progressive steps namely leptotene, zygotene, pachytene, diplotene and diakinesis. This classification is based on chromosomal morphology and the formation of links between homologous chromosomes during stage of synapsis (Klutstein & Cooper, 2014).

Leptotene involves condensation of duplicated sister chromatids. Thereby, the chromosomes appear thicker and shorter. This is followed by zygotene phase, when homologous chromosomes pair and initiate formation of a structure termed the synaptonemal complex (SC). Formation of this structure is known as synapsis. Accordingly, a chromosomal pair is composed of four chromatids and one chromosome comes from each parent. At this stage, an homologous chromosomal pair is called bivalent. In pachytene, Synapsis gets completed and chromosomal pairs are more strongly connected through the SC and structures known as chiasmata (Youds & Boulton, 2011).

Chiasmata refers to the physical connection between homologous chromosome DNA molecules during meiotic division (Hirose, et al, 2011). Chiasmata resolution involves crossing over between the homologous chromosome as well as DNA exchange within bivalents (Youds & Boulton, 2011). Crossing over generates formation of a novel combination of the genetic material in the gametes which is major evolutionary driver. During diplotene, detachment of homologous chromosomes is started in a process termed as desynapsis. Yet, these pairs sustain their link at chiasmata and sister chromatid cohesion until the anaphase I stage. Dissociation of the SC gets completed during the final stage of prophase I (in the diakinesis sub stage). During this stage, condensation of chromosomes continues and the meiosis I spindle is formed (Tsai & McKee, 2011). Spindle fibres continue to form during metaphase I which also involves alignment of the bivalents in a double row. Monopolar orientation of the sister kinetochores is ensures a reductional division in meiosis I. Because of this, the paternal and maternal chromosomes get correctly segregated at opposite poles of the cell (Hirose, et al, 2011). Sister chromatid cohesion along the arms of chromosome gets resolved during anaphase I. However, these sister chromatids sustain their connection at centromeres till the initiation of anaphase II. Moreover, homologous chromosomes are pulled apart by the microtubules such that one set reaches one pole

and the other on opposite pole of the cell (Lee & Amon, 2001). Nuclear membrane develops during the telophase I. This membrane envelops the segregating chromosomes thereby forming two distinct nuclei. Nuclei thus formed contain half number of chromosomes as compared to the parent cell. For that reason, first meiotic division is termed as reductional division (Villeneuve & Hillers, 2001).

1.5.2.2 The second meiotic division, Meiosis II

The second meiotic division is similar to the mitotic division, as the number of chromosomes is not reduced. It is therefore an equational division. Upon initiation of meiosis II, every daughter nucleus is already in the haploid state. Moreover, every chromosome is constituted of two chromatids linked at the centromere. Meiosis II is responsible for segregation of these chromatids (Page & Hawley, 2003). This division is shorter as compared to first meiotic division. Still, it is divided into four stages namely prophase II, metaphase II, anaphase II and telophase II. There is no additional DNA replication between meiosis I and II (Wassmann, 2013). Prophase II involves condensation of chromosomes and break down of the nuclear membrane. During metaphase II, every chromosome comprising of two chromatids gets aligned on the cell equator with the help of spindle fibres. This is followed by bi-polar separation of centromeres of every sister pair during anaphase II. At this stage, one chromatid starts to travel to opposite end of the cells by helping of spindle fibres (Tsai & McKee, 2011). By the end of meiosis II division, division of cytoplasm takes place during telophase II resulting in division of the original cell into four daughter cells which possess half number of chromosomes, every cell contains a unique genotype (Page & Hawley, 2004). In this division, sister kinetochores are linked to microtubules from opposite poles (Dudas, Ahmad & Gregan, 2011).

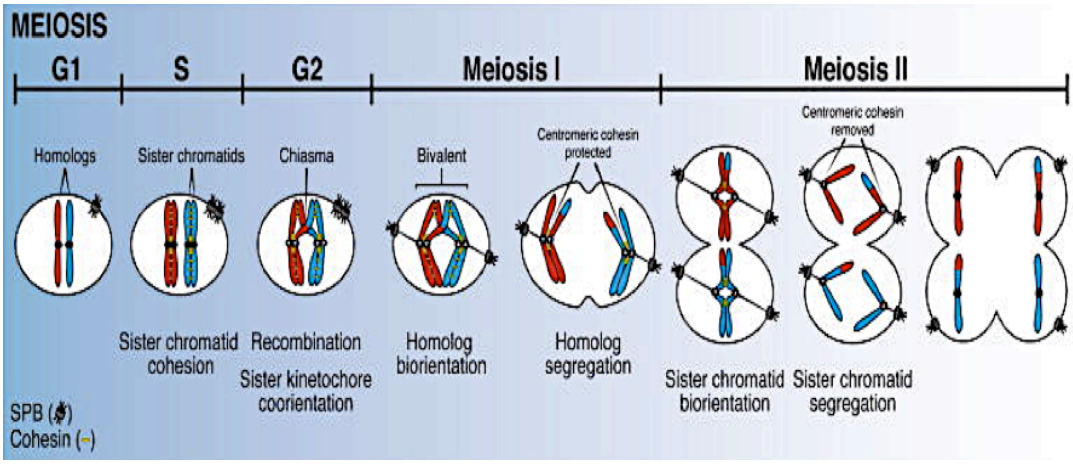

Figure 1.8 Phases of meiosis.

Meiotic division involves the process of DNA replication which takes place during S phase. After this, two nuclear divisions occur (meiosis I and meiosis II). Before undergoing the first meiotic division, every chromatid of the non-homologous chromosomes connects through cohesin complexes (shown in yellow). Homologous chromosomes pair with one another followed by inter homologous recombination to result in formation of chiasmata. Centromeres of homologous chromosomes attach with the microtubules arising from spindle poles (SPB). In eukaryotes, this structure is called centrosome. During metaphase I, homologous pairs of chromosomes arrange themselves on the metaphase plate. The conjoined homologues (bivalents) then get segregated to opposite poles of the cell. This occurs in anaphase I during which chiasmata are resolved. During telophase, the production of two daughter cells takes place. During metaphase II chromosomes are arranged on the metaphase plate. Anaphase II involves separation of sister chromatids. Segregation of chromosomes gets completed in the telophase II resulting in formation of four haploid cells having half the main number of chromosomes. In order to promote segregation of homologous chromosomes, cohesin at the arms of chromosomes are cleaved during meiosis I. However, the cohesin present on centromeres (sister kinetochores) are protected thereby keeping the sister chromatids linked to one another. The centromeric cohesin present between sister kinetochores is removed during anaphase II thereby allowing sister chromatids to separate and migrate to opposite poles (Miller, Amon & Ünal, 2013).

1.5.2.3 Meiotic Homologous Recombination (HR)

Inter-homologue recombination (HR) is crucial aspect of meiotic prophase I. It also considered as the main source of exchange of genetic information allowing formation of novel allelic combinations in the population. Besides this, HR also functions to maintain genome stability, which has been found to be linked with numerous disorders of humans (Segurel, 2013). Two different outcomes for meiotic HR can occur, namely crossover (CO) and non-crossover (NCO). During meiosis I division, one crossover event is necessarily needed for formation of each bivalent (Baudat et al., 2013; Kowalczykkowski, 2015).

The process of meiotic recombination is aimed at forming inter-homologue linkages that allow the reductional division in coordination with the monopolarity of sister centromeres. Crossover recombination also has major a contribution to creating genetically distinct gametes. These processes are therefore crucial for genetic biological diversity. It has been established that recombination does not take place at random positions in the genome. It is concentrated in certain parts of genome termed hotspots. A protein, PRDM9, has been identified, which is capable of activating hotspots in mammals, and hence regulates the place of action for several meiotic recombination initiation genes (Baudat, Imai & De Massy, 2013; Baker, et al, 2014). SPO11, in complex with another factor, *TOPOVIBL,* mediates the formation of the DNA double-strand breaks (DSBs) that enable the meiotic HR to initiate (Yamada & Ohta, 2013). SPO11-*TOPOVIBL* mediates the breakage of both DNA strands which it does by acting as dimer. Subsequently the MRN (MRE11-RAD50-NBS1) complex of proteins remove this dimer from the DNA through endonucleolytic cleavage (Lam & Keeney, 2015). Further DSB resection in the 5' to 3' direction, at a distance from the DSB, is considered to be brought about by the BLM (Bloom syndrome protein) and the nuclease Exol. On the other hand, resection from 3' to 5' direction towards DSB end from a position adjacent to the DSB is brought about by MRE11 endonucleases (Shibata et al., 2014). This end processing results in single-stranded DNA (ssDNA) with a free 3' end at each side of the DSB (Figure 1.9) (de Massy, 2013).

The ssDNA-binding protein, replication protein A (RPA) links RAD51 to ssDNA by preventing secondary structures forming on ssDNA prior RAD51 loading. Invasion of strands into homologous chromosomes is initiated by loading of the recombinases DMC1 and RAD51 to develop nucleoprotein filaments on the 3' ssDNA (Holthausen, Wyman & Kanaar, 2010; Ranjha, Howard & Cejka, 2018). RAD51 and DMC1, mediate inter –homologue duplex strand invasion creating a dissociation loop (D-loop) (Dray et al., 2011; So et al., 2017). Creation of RAD51 nucleoprotein filaments also involves several other factors like the PALB2 protein and the breast and ovarian cancer-related proteins BRCA1 and BRCA2 (O'Donovan and Livingston, 2010; Feng & Jasin, 2017).

Double Holiday junctions (dHJs) can be subsequently created as consequence of ssDNA invasion and linking to another complementary strand. Alternatively, a synthesis dependent strand annealing (SDSA) pathway can occur in which the D-loop is unwound and the expanded invading strand is able to re-anneal with the different end of the DSB. Moreover, DNA synthesis acts on the reannealed strand like a template to finish the repair. The SDSA pathway can only undergo non-crossover events, which makes it less likely to generate chromosomal rearrangements (Heyer et al., 2010). If SDSA is not used, the extended D-loop can capture the DSB's other side, which is known as a second-end capture. This model can generate a double Holiday Junction (dHJ) between the chromatids of opposing Homologues both opposing parts (Szostak et al., 1983). This seems to be the D-loop extension's most important product for meiosis (Bzymek et al., 2010). The dHJ can be dissolved by the BTRR complex, which includes BLM–TOPO3a–RMI1–RMI2 (Raynard, Bussen & Sung et al., 2006; Karow et al., 2000) which results in the detachment of the sister chromatids without crossing over. If the dHJ is not able to be dissolved (for example, when the BLM is absent), then it can be cleaved either through the endonuclease Mus81/Eme1 complex (Boddy et al., 2001) or by GEN1 (Chan & West, 2015) in a model known as dHJ resolution, which appears in both crossovers and non-crossovers (Constantinou et al., 2002), as seen in Figure 1.9.

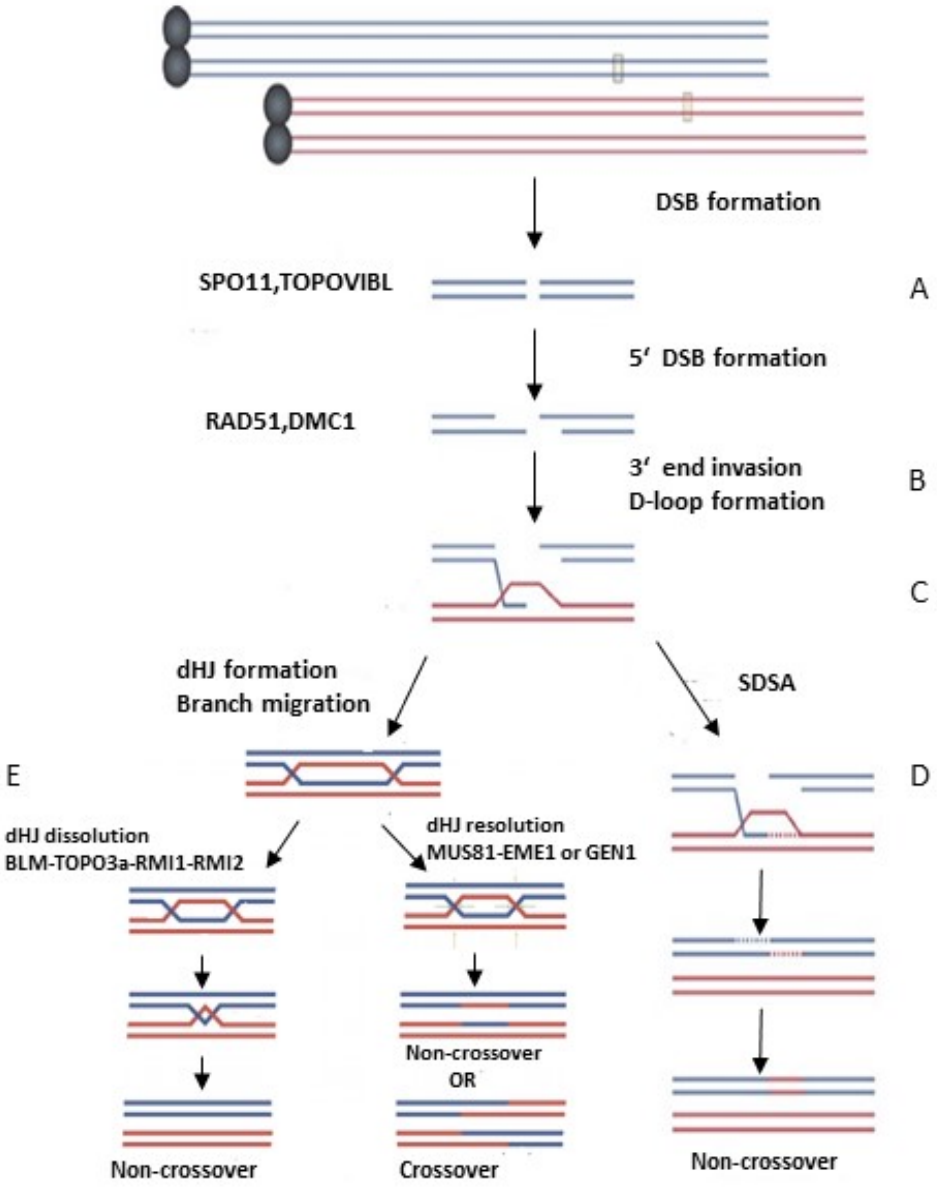

Figure 1.9 Schematic diagram of meiotic recombination occurring through DSB pathway.

Diagram shows models for the two main recombination pathways. (A) Formation of DSB occurs when both strands of the DNA are cleaved by the SPO11- *TOPOVIBL* complex. This cleavage occurs resulting in SPO11 covalently attached to the 5' ends of the DNA. After this, SPO11 is removed by the MRN protein complex resulting in generation of 3' single strand DNA (ssDNA) overhangs. (B) A D-loop is initiated when a single 3' end overhang invades other homologue. (C) Synthesis of DNA occurs after this and for this purpose; other homologue is utilized as a template. (D) Dissociation of the D-loop and invasion of the opposite end of original strand may lead to non-crossover. This mechanism is called synthesis dependent strand annealing (SDSA) and can result in gene conversion. (E) In the case of dHJ dissolution, BLM and TOPO3a encourage branch migration to invade DNA strands, which may result in a catenate that is detected by TOPO3a, RMI1, and RMI2 together. A dHJ can then be dissolved without crossovers. DNA strands can be cleaved either by the Mus81/Eme1 complex or GEN1 in the case of dHJ resolution. Further, the broken strands can be re-joined on the detached sister chromatids. Indeed, dHJ resolutions can result in the generation of crossover and non-crossover events. Adapted from (Handel & Schimenti, 2010 ; Wechsler et al., 2011).

1.5.2.4 Meiotic Recombination gene in cancer

Emerging evidence is demonstrating that cancer chromosome biology has a relationship with meiotic chromosome regulator genes (McFarlane & Wakeman, 2017; Feichtinger & McFarlane, 2019). The involvement of numerous meiotic recombination genes in different stages of tumour development, persistence and spread has been identified. A variety of cancers show expression and potential function of different meiotic recombination genes, such as *SPO11* (Koslowski et al., 2002), *HORMAD1* (Chen et al., 2005) *SYCP3* (Modarressi et al., 2004), *SYCP1* (Tureci et al., 1998). More detailed examples are given below.

An oncogenic chromosome event is known as Alternative Lengthening of Telomeres (ALT) after each round of DNA replication in somatic cells, the ends of linear chromosomes (telomeres) become short. This shorting helps to control and monitor cell division via many mechanisms, like stimulation of p53 and activation of the DNA-damage checkpoint (Di et al., 2003). Therefore, the change of healthy human cells to become cancer cell demands maintenance of telomeres, which can be via reactivation of telomerase, the enzyme needed telomere extending or via a (ALT) (Henson et al., 2002). The ALT pathway can work by a recombination-mediated technique in the absence of telomerase-mediated elongation, and telomeres behave as broken chromosome ends. This requires RAD51 to mediate strand invasion from an uncapped telomere into a non-sister telomere and allow the invading end to work like a substrate for DNA replication (Dilley et al, 2016). This event can guide tumour formation and permit proliferative tumour cell activity and possibly contribute to tumour cell evolution (Venkatesan et al., 2017). MND1-HOP2, two meiotic specific proteins are essential for ALT to remain active. MND1-HOP2 function to bias ALT recombination toward an interhomologue route rather than toward inter-sister chromatid repair (Cho et al., 2014).

The synaptonemal complex (SC) is a meiosis-specific, proteinaceous, zipper-like structure. It participates in synapsis of homologous chromosomes in prophase I of meiosis. The SC plays an important role in the crossover formation. SC is built up by two axial structures created along the centre of the homologous chromosomes that include SCP2 and SCP3 proteins; the central elements include SYCE1-3 and TEX12,

along with transverse filaments of SCP1 protein that binds the lateral with central elements (Nielsen & Gjerstorff, 2016). SYCP3 is believed to be part of an essential section of the SC lateral elements (outer linear structures of the SC). The meiosis-specific SC protein SYCP3 can act oncogenically by weakening or damaging recombination by obstructing the action of the tumour suppressor recombination organiser BRCA2. Also, the production of SYCP3 in cancer cells guides ploidy changes and can be considered an important example of a meiotic chromosome regulator that affects chromosomal segregation in the case of cancer cells (Hosoya et al., 2011).

HORMA domain proteins, including HORMAD1, perform many functions during meiotic recombination, such as helping form the SC, homologue alignment promotion, and ensuring all DSBs are repaired. HORMAD1 is thought to ensure correct DSB processing, leading to meiotic homologous recombination during meiosis I by arranging several meiosis-specific elements, including HOP2–MND1 (Tsubouchi & Roeder, 2002; Chen et al., 2004). Watkins et al. (2015) demonstrated a recombination-associated role for HORMAD1 in cancer cells. They assumed that the abnormal expression of HORMAD1 may damage the regular homologous recombination repair pathway operated by the recombinase RAD51, which can result in the choice of an ill-defined alternative DSB repair pathway. HORMAD1 expression exists in many tumours, including breast, bladder, lung, endometrial, and colon tumours (Aung et al., 2006; Watkins et al., 2015). Indeed, additional researchers have reported the involvement of HORMAD1 in the regulation of oncogenic recombination mechanisms and therapeutic resistance (Gao et al., 2018; Nichols et al., 2018). The expression of HORMAD1 is related to weak prognoses and leads to genotoxic (involving irradiation), especially in lung adenocarcinomas (Nichols et al., 2018; Gao et al., 2018). HORMAD1 may promote the effective resectioning of DSBs, which may allow the repair of therapeutically induced DNA damage.

1.6 Transposable elements

Transposons are mobile genetic fragments that can "jump" or transpose from one locus to another in the genome (MacLennan et al., 2017; Sotero-Caio et al., 2017) and can engender genetic alterations. Transposases catalyse this process (Beck et al., 2011; Burns, 2017). Many genome sequence studies have suggested that transposable elements (TEs) and their remnants constitute a substantial part of the eukaryotic genome. Indeed, many different genomic rearrangements like insertion, deletion, and translocation occur through transposition (Dewannieux & Heidmann, 2013; Bourque et al., 2018).

Transposable elements are categorized into two classes. Class I comprises retro-transposons that utilize RNA transcription mechanisms to copy and paste themselves to another site. Class II transposons are DNA transposons that excise themselves from the donor site and re-integrate at another site (Wicker, et al., 2007; Bourque et al., 2018). Although 5% of the human genome is made up of class II transposons, these transposons are not thought to be active. Conversely, approximately 45% of the human genome is made up of class I transposons, which are divided into groups depending on whether they possess long terminal repeats (LTRs) or not (non-LTRs). Additionally, there are two types of non-LTRs, short-interspersed nucleotide elements (SINEs), and long-interspersed nucleotide elements (LINEs) (Dewannieux & Heidmann, 2013).

LTRs include human endogenous retroviruses (HERVs), which are flanked by LTRs and bear a significant structural resemblance to other retroviruses. Some researchers have proposed that acquisition of HERVs occurred through infection of germline cells by ancient retroviruses that later evolved and were assimilated into the genome, pointing to basic retroviral genes like *Pol*, *Gag* and *Pro* found in HERVs (Dewannieux & Heidmann, 2013; Bourque et al., 2018). TEs are active in several kinds of cancer, as evidenced by mRNA and protein analyses (Burns, 2017).

1.7 PRDM9

PRDM9 has previously been identified as meiotic CT gene (Feichtinger et al., 2012). PR domain-containing protein 9 (PRDM9) facilitates meiotic recombination regulation by binding to meiotic recombination hotspots in humans and mice, and it is called Meisetz in mice (Baudat et al., 2010; Paigen & Petkov, 2018). The PRDM protein family contains 17 members in humans and 16 in mice. According to Parvanov et al. (2010), there are three functional domains in PRDM9. The first is an N-terminal Kruppel-association box (KRAB) domain that can promote protein-protein interactions and inhibit transcription by attaching to a tethered DNA binding domain. The second is a PR/SET domain (Meisetz) at the centre of the protein that engages in histone methyl transferase activity resulting in tri-methylation of H3K4 and H3K36 (Hayashi et al., 2005) and related changes to chromatin structure. Finally, the terminal C2H2 zinc-finger domain is the primary DNA binding domain (Figure 1.10).

According to Hayashi et al. (2005), *PRDM9* is only transcribed in germline cells and primarily engages in histone methyltransferase activity via the PR/SET domain. In mice, *Prdm9* trimethylates the fourth lysine of histone H3 (H3K4). Research has also reported increased mono-, di- and tri-methylation of H3K4 attributed to this protein (Wu, al., 2013; Eram, al., 2014). Trimethylation of the lysine 36 of H3 (H3K36) by this protein has also been reported (Eram et al., 2014). PRDM9 can methylate other core histones H2A, H2B and H4, but does so to a lesser degree than for H3 methylation (Xiaoying et al., 2014).

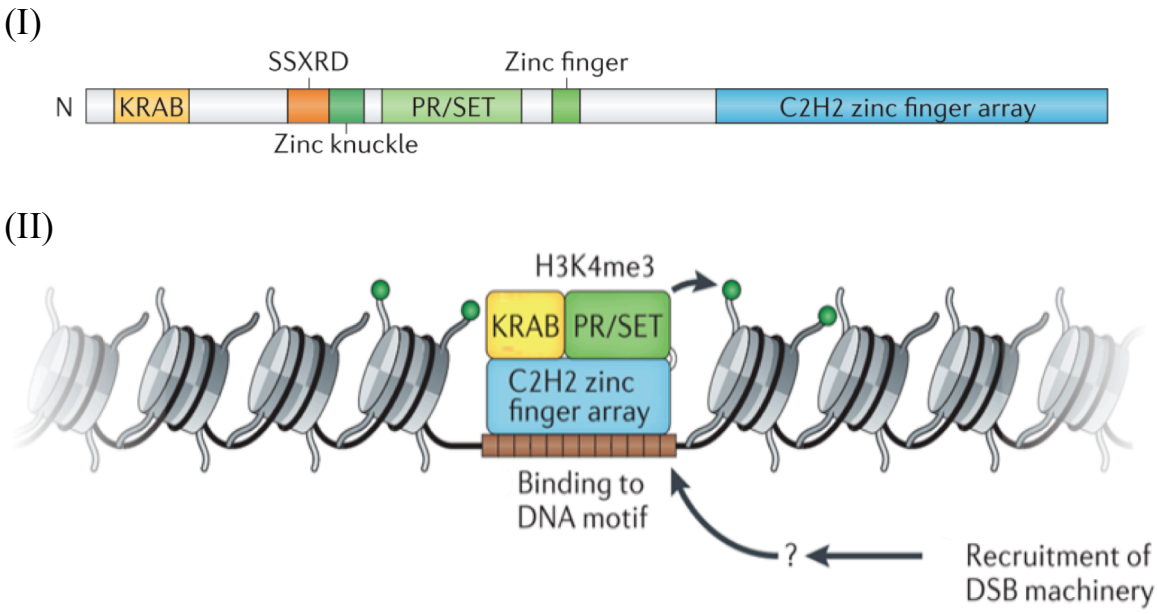

Figure 1.10 Model of PRDM9 structure and meiotic DSB localisation mechanism. (I) The PR domain-containing protein 9 (PRDM9) is a histone methyltransferase made up of three core domains, a KRAB domain including a synovial sarcoma X breakpoint region (SSXRD), a PR/SET domain that engages in histone methyltransferase activity, and a zinc finger (C2H2) domain. (II) Suggested mechanism of PRDM9 attachment to the meiotic hotspot DNA motif via the C2H2 domain. Once bound to DNA, the PR/SET domain conducts H3K4me3 on adjacent nucleosomes. The KRAB motif is theorized to enable interaction with other proteins, which may facilitate recruitment of DSB machinery, encompassing the SPO11 protein (Adapted from Baudat and Frédéric, 2013).

According to a study in mice, the *Prdm9*/Meisetz gene is expressed in the initial phases of meiotic division. Disruption of this gene results in hybrid sterility in male and female mice due to extreme deficiencies in the DSB repair pathway, the ineffective pairing of homologues, and an inability to formulate sex-specific characteristics (Hayashi et al., 2005). Five distinct tandem repeats have been identified through gene sequencing performed on 20 mouse strains. These repeats enable binding to different DNA sites (Parvanov et al., 2010). Testis-specific *Rik* gene (termed as *Morc2b*) expression is impaired in *Prdm9-/-* mice, suggesting that Prdm9 (Meisetz) can engage in transcriptional r regulation of meiotic genes (Hayashi et al., 2005).

Human *PRDM9* was identified as a CTA gene by Feichtinger et al., (2012) using two different identification protocols. In the first, genes previously reported to demonstrate meiosis-specific expression were manually analysed. In the second, a bioinformatic screen involving several steps was carried out. A total of 744 mouse meiosis-specific genes were identified, followed by the assignment of human orthologues of these genes. Genes excluded were those not present in cancer expressed sequence tag (EST) libraries and non-testis EST libraries for normal somatic tissues. Selected genes were analysed with RT-PCR, and expression patterns were cross-referenced to a meta-analysis of cancer microarray data collected from patients. *PRDM9* was found to be a type of meiCT gene only expressed in the testis (in normal tissues) and different types of cancer cell lines/tissues.

1.8 TEX19

The first identification of the mammalian *TEX19* gene was in mouse germ cells, and orthologues thereof are only found in mammals (Kuntz et al., 2008). Duplication of *TEX19* orthologues has been reported in rodents; these animals have a paralogue pair of genes called *Tex19.1* and *Tex19.2*. The human genome contains only a single *TEX19* gene. Murine *Tex19.1* and *Tex19.2* are located on chromosome 11, and the human *TEX19* gene is located on chromosome 17. Both *TEX19* and *Tex19.1* have been positionally associated with other genes like *Sectm1*, *UTS2R* and *CD7*. The orientation of *TEX19* relative to the centromere is similar in humans and rodents,

space also occupied by *UTS2R*. It can thus be surmised that human *TEX19* is more closely related to murine *Tex19.1* than *Tex19.2*, base on these chromosomal features as shown in Figure 1.11 (Kuntz et al., 2008).

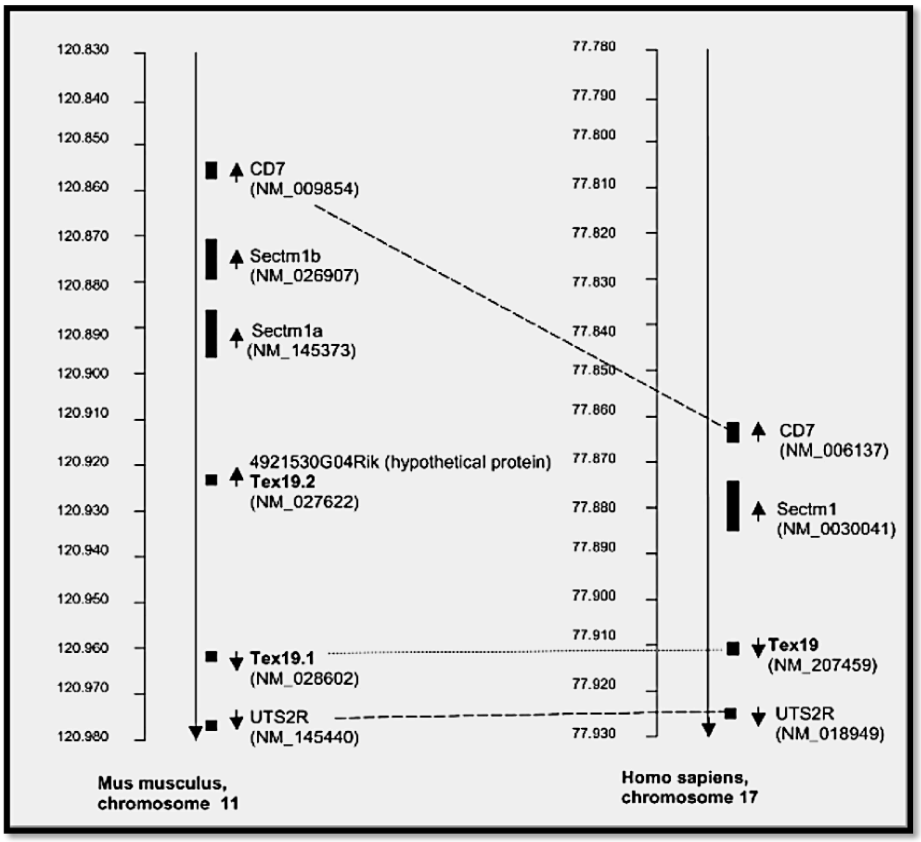

Figure 1.11 Schematic of chromosomal context of murine and human *TEX19* orthologues *Tex19.1*and *Tex19.2* are located on mouse chromosome 11, and *TEX19* is located on human chromosome 17 (Kuntz et al., 2008).

Expression of *Tex19.1* and *Tex19.2* paralogues varies in mice. Expression of *Tex19.2* has not been found during early embryogenesis, but has been detected in the male somatic gonad lineage and in female germ cells (Tarabay et al., 2013). Conversely, expression of *Tex19.1* has been identified in early embryos as well as pluripotent stem cells (Kuntz et al., 2008). Expression of *Tex19.1* occurs in a similar manner to that of the stem cell determinant gene *Oct4*, and *Tex19.1* expression is decreased during embryonic stem cell differentiation (Zhong et al., 2016); possibly indicating that *Tex19.1* is involved in the regulation of self-renewal and stem cell pluripotency.

Preliminary analysis of *TEX19* expression in humans revealed that it is orthologous to the *Tex19.1* gene, and its expression has also been found in human embryonic stem cells (ESCs). Spermatogonia germ line cells are found in the seminiferous tubules of the testis and contain the Tex19.1 protein, strongly suggesting that this protein is involved in germ line cell processes (Öllinger et al., 2008; Tarabay et al., 2013). Loss of Tex19.1 has also been shown to cause delays in embryonic development, suggesting a possible role in embryogenesis or placental function (Yang et al., 2010; Reichmann et al., 2013). *Tex19.1* is likely involved in meiotic cell division, as *Tex19.1* deletion creates disorders in the meiotic synapses of chromosomes during spermatogenesis (Yang et al., 2010). Consistent with embryonic delays in the mutant, deletion of *Tex19.1* has also been reported to cause placental defects in female mice and infertility in males (Crichton et al., 2017). Thus, the presence of *Tex19.1* might be essential for spermatogenesis in males and proper placental development in females (Crichton et al., 2017; Öllinger et al., 2008). In the early stages of spermatogenesis, deletion of *Tex19.1* results in alterations to the expression of chromatid cohesion genes that support meiotic recombination, such as *Rec8* and *Smc1β* and so *Tex19.1* might have an indirect role on meiosis (Öllinger et al., 2008).

Other studies have reported that *Tex19.1* regulates TEs. Expression of long interspersed nuclear elements (LINE-1) RNA in the placenta is enhanced by *Tex19.1* deletion and might cause placental dysfunction (Reichmann et al., 2013). Regulation of *Tex19.1* may control TEs and maintain the balance of the genome (Reichmann et al., 2013). *Sectm1*, genomically adjacent to *TEX19*, is also involved in retro-transposon regulation (Bianchetti et al., 2015), suggesting a possible functional relation between these genes.

Tex19.1 regulation of TEs has been demonstrated. Tex19.1 can interact directly with L1-ORF1p, an L1-encoded protein crucial for retro-transposition. Tex19.1 contributes to controlling ORF1p by stimulating protein polyubiquitylation, thus limiting LINE-1 mobilization. This is thought to be mediated by Tex19.1 stimulating interaction between ORF1p and the Ubr2 ubiquitin of ligase (Figure 1.12). The absence of *Tex19.1* has been shown to increase levels of L1-ORF1p and amplify L1 mobilization in mouse pluripotent embryonic stem cells. These data indicate that *de novo* retro-transposition during the pluripotent phase of the germline cycle is inhibited by Tex19.1 and underscore the significance of post-translational regulation of L1 retrotransposon-encoded proteins in sustaining mammalian trans-generational genome stability (MacLennan et al., 2017).

Planells-Palop et al. (2017) demonstrated that depletion of TEX19 in cancer cell lines reduces cell proliferation and self-renewal. These researchers conducted RNA sequencing on total polyA-RNA taken from SW480 cells treated with *TEX19* siRNA and untreated cells. Their findings indicated that at least of 80 different gene transcripts were considerably altered (up-/down regulated) in the presence of *TEX19* siRNA. Levels of *TEX19* mRNA decreased, and levels of *PIWIL1* mRNA increased. These results recapitulated the RT-PCR findings of Feichtinger et al. (2012). Amongst the 80 affected genes, *RAD21L1* and *SEPT12* are recognised as CT genes suggesting TEX19 regulates at least some meiotic genes (Feichtinger et al., 2012). Additional analysis revealed that transcript levels of several genes linked to cancer cell proliferation were altered when TEX19 was depleted, suggesting an important role for *TEX19* in regulating oncogenic proliferation via a transcriptional regulation pathway (Planells-Palop et al., 2017).

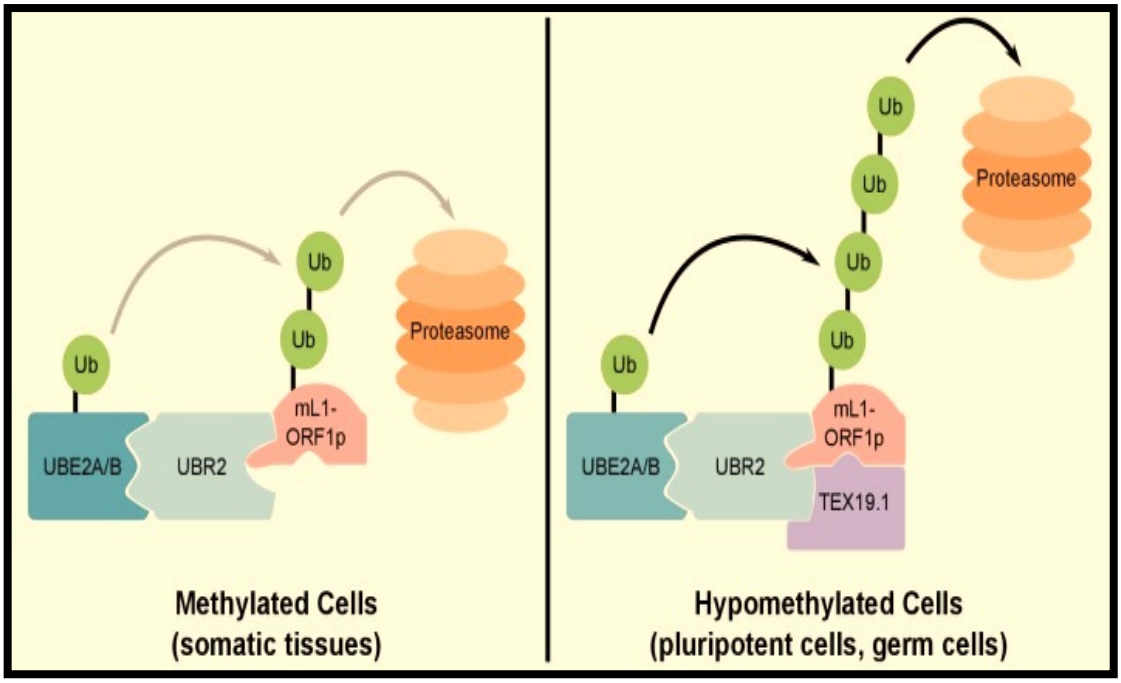

Figure 1.12 Model demonstrating proposed activities of Tex19.1 in mice. The E3 ubiquitin RING domain ligates UBR2 to its cognate E2 ubiquitin, conjugating UBE2A/B that works in concert with mL1-ORF1p to encourage ubiquitylation and proteasome-dependent protein turnover in methylated somatic cells. Tex19.1, found in hypomethylated germ line cells and pluripotent cells, interacts with Ubr2 and mL1-ORF1p to additionally enhance polyubiquitylation and proteasome-dependent mL1-ORF1p turnover. Specifically, the mechanism employed by Tex19.1 inhibits Ubr2 activity (Reichmann et al., 2017) (Taken from MacLennan et al., 2017).

TEX19 was found to be a cancer-selective CT gene demonstrating normal expression in the testis and thymus and abnormal expression in certain cancer cell lines. Although, expression of *TEX19* was originally reported in the thymus, this is thought to be related to age-related tissue atrophy, the *TEX19* gene was later shown to be only be expressed in the testis of healthy adults (Feichtinger et al., 2012; McFarlane group unpublished). qRT-PCR/RT-PCR assessment reported that 60% of bladder tumours demonstrated *TEX19* expression (Zhong et al., 2015). High levels of the TEX19 protein have been found in both high and low grade tumours in addition to bladder cancer cell lines (Zhong et al., 2015). These findings suggest that *TEX19* might be a promising biomarker in the diagnosis and prognosis of certain cancers (Zhong et al., 2016; Feichtinger et al., 2012).

1.9 Project aims

The overarching aims are to determine whether meiotic regulators function to control chromosome dynamics in cancer. The *PRDM9* gene was hypothesised to control the expression of several meiosis gene in cancer cells (Feichtinger et al., 2012). Therefore, one of the main aim of this research is to investigate whether overexpression/low expression of *PRDM9* in cancer cells might influence/decrease the expression of other genes.

Additionally, we aim to study the role of TEX19 in cancer cells. We wish to confirm that reduction of TEX19 alters cancer cell proliferation, and investigate if TEX19 depletion can influence any histone modifications, as unpublished work from the McFarlane group has indicated a role for TEX19 in epigenetic regulation in cancer cells. Finally, we wished to determine whether the murine Tex19.1 functional regulation of LINE-1 ORF1 protein is also apparent for human TEX19 in cancer cells, and if so, is this a universal feature of an TEX19 expressing cancer cells.

Chapter 2
Materials and Methods

2. Materials and Methods

2.1 Human cell culture

2.1.1 Cell culture growth

The cancer cell lines used in this study are shown in table 2.1 and were grown in an appropriate media (Table 2.1) completed with foetal bovine serum (FBS) (Invitrogen: GIBCO 10270). The cells were then cultured in a protected humidified incubator at 37°C with 5% CO_2 and regularly checked for mycoplasma contamination using a mycoplasma PCR detection kit (Sigma Aldrich, #MP0035).

Table 2.1 Cell lines used in this study and growth conditions

Cell line names	Origin	Culture Media conditions	CO_2
SW480	Human colon adenocarcinoma	Dulbecco's modified Eagle's medium (DMEM) + GLUTAMAXTM (Invitrogen,GIBCO 61965) supplemented with 10% FBS	5%
HeLa Tet-On® 3G	Stably transfected Human cervical cancer with pCMV-Tet3G vector (McFarlane lab).	Dulbecco's modified Eagle's medium (DMEM) + GLUTAMAXTM (Invitrogen, GIBCO 61965) + 10% Tet System Approved FBS	5%
HCT116	Human colon carcinoma	McCoy's 5A medium + GLUTAMAXTM (Invitrogen; 36600) + 10% FBS	5%
HCT116 Tet-On® 3G	Stably transfected Human colon carcinoma with pCMV-Tet3G vector (McFarlane lab).	McCoy's 5A medium + GLUTAMAXTM (Invitrogen; 36600) + 10% FBS	5%
H460	Large cell lung carcinoma	RPMI 1640 + GLUTAMAXTM supplemented with 10% FBS and 2 mM sodium pyruvate	5%

2.1.2 Thawing frozen cells

Cell vials were taken from a liquid nitrogen tank and was directly submerged in a water bath at 37°C. The cells were thawed by gentle mixing for approximately 40-60 seconds. Subsequently, the cell suspensions were removed from the cryovials, placed in 5 mL of prewarmed medium in a falcon tube and extracted by centrifugation at 100 xg for 5 minutes. The medium was then removed using an aspiration pipette and the cells were re-suspended in 10 mL of fresh medium. After that, the cells were mixed well, divided into T75 flasks and incubated as listed in Table 2.1. The cells were checked every day until they reached the desired confluence.

2.1.3 Harvesting and freezing cultured cells

When the cells reached approximately 80% confluence they were harvested and either frozen or split. The culture media was removed using a sterilised aspiration pipette. The cells were washed once with 3 mL 1x Phosphate – buffered saline (Invitrogen, 14190-094) to remove any remaining FBS, trypsinised with 1 mL of 1x trypsin-EDTA (Invitrogen, GIBCO 1370163) and incubated for 3 minutes to allow the cells to detach from the flask. An additional 5 mL of pre-warmed complete media was used to prevent further trypsinisation

A TC20 automated cell counter (Bio-Rad, cat #145-0102) was used to count the number of cells, which were then centrifuged at 100 xg for 5 minutes. The supernatant was carefully removed with a sterilised aspiration pipette. At this point it was possible to transfer the cells into two new flasks (thus dividing them) or preparing them for storage. To store the cells, cell pellets were resuspended in 1 mL of chilled freezing medium (90% FBS mixed with 10% of dimethyl sulfoxide [Sigma –Aldrich, D8418]). The cells were then immediately transferred to a 2 mL cryotube and placed in a CoolCell LX Freezing Container at -80°C for 24-48 hours and then placed for long-term storage in liquid nitrogen.

2.1.4 Cell counting

In this study, a TC20 automated cell counter (Bio- Rad, cat #145-0102), which is designed to count the number of cells in 1 mL of PBS and illustrate the percentage of viable cells, was used to count the cells. The cell pellet was suspended in 1 mL PBS and the resulting 10 µL of cells were quickly and gently mixed with 10 µL of 0.4% trypan blue. Subsequently, 10 µL of the total mixture was transferred to a Bio-Rad counting slide (Bio-Rad cat # 145-0011).

2.2 siRNA (small interfering RNA)

The cell lines used in this experiment determined the number of cells and particular media used. For HCT116 and H460, 1.5 x 10^5 cells were used, while for SW480 2.0 x 10^5 cells were used. The cells were seeded into 6-well plates and incubated to obtain approximately 50–60% confluence. The transfection mix was prepared using 10 nM siRNA (Qiagen) with 6 µL Hiperfect reagent (Qiagen, 301705) until 100 µL free serum medium was obtained; the transfection mixture was then mixed in a vortex machine. The transfection mixture was incubated at least for 25 minutes at room temperature to ensure that it was mixed well. The siRNA mixture was then dropped into the culture and the plates were carefully shaken to allow the siRNA to mix uniformly. Finally, the plates were incubated under normal growth conditions. In this experiment, a new treatment was prepared each day and each treatment was used for three days (Table 2.2).

On the day of harvest, the cells were collected to extract protein and RNA in order to examine the mRNA depletion, mainly by quantitative reverse transcription PCR (RT-qPCR) and western blot. Untreated cells and the negative control siRNA were used as controls, in addition to the target gene treatment.

Table 2.2 The sequences of siRNA used for genes knockdown

Gene	siRNA Name	Source	Target sequencing
PRDM9	Hs _PRDM9_ 7 Hs_ PRDM9_ 8 Hs_ PRDM9_10	Qiagen; SI04299890 Qiagen; SI04338747 Qiagen; SI05105590	5'-CCACACAGCCGTAATGACAAA-3' 5'-GTGGACAAGGTTTCAGTGTTA-3' 5'-GAAGAGAAATGTAAGATTCTA-3'
TEX19	Hs _*TEX19*_ 7	Qiagen: Hs_FLJ35767_7	5'-TTCAACATGGAGATCAGCTAA-3'
NI (Non-Interferece siRNA)	Negative Control siRNA	Qiagen: 1022076	----------

2.3 Total RNA extraction and cDNA construction

An RNeasy Plus Mini Kit (Qiagen, #74136) was used according to the manufactuer's instruction to extract total RNA. The cells were washed in 1x PBS to remove any residue of trypsinisation and then the PBS was removed.

RTL plus buffer was used to lyse the cells and to reveal inoperative RNase activity. Based on the number of cells, different amounts of the buffer were used (350 µL for less than 5×10^6 cells; approximately 600 µL for more than 10^7 cells). A gDNA eliminator spin column was used to remove any genomic DNA at this stage. The lysate was then transferred to a separate RNeasy spin column and the protocol buffer was used to isolate the RNA.

A NanoDrop 2000 was used to determine the concentration and quality of the RNA. The first strand of cDNA was synthesised using the superscript III First Strand Synthesis System (Thermo Fisher Scientific, #1808-051). 1- 2 µg of RNA were used with the reverser transciptase reactions, in accordance with the manufacturer's instructions. RNase H treatment after cDNA synthesis was also used with all samples to degrade residual RNA. The final cDNA obtained was diluted a 1:5 ratio with DNase/RNase-free water and quality was assessed using RT-PCR and *β ACT* primers.

2.4 Polymerase chain reaction

2.4.1 Qualitative RT-PCR

RT-PCR was amplified using 25 µL of MyTaq Red (Bioline, #BIO-25043). As per the manufacturer's instructions, each individual tube contained 0.5 µL each of primer, 1x MyTaq Red and RNase-free water (REF P119) and 1 µL of cDNA. The PCR amplification started with initial denaturation at 95°C for 1 minute, then denaturing at the same temperature for 35–40 cycles.

The denatured mixture was annealed at a temperature for 15 seconds and the extension was prepared for 30 seconds/kb. The annealing temperature was chosen specifically for the set of primers designed for the reaction (as listed in Table 2.3). The final step in this stage was elongation at 72°C for 5 minutes.

For all PCR products, a 0.8-1.5 % agarose gel (sigma, # A9539) prepared with 7 µL peqGreen dye (Peqlab, #37-5000). The gels were run at approximately 100 V for 1 hour in TBE buffer (Alpha Laboratories, #EL0080) and visualised using the Bio-Rad ChemiDoc XRS imaging system. During this study, 5 µL of DNA markers (100 bp [NEB, #N0467] or 50bp [NEB, #N0556]) was used to guide size assessment.

2.4.2 Primers design for RT-PCR

The gene sequences used were selected from the Database of the National Center for Biotechnology Information (NCBI, http://www.ncbi.nlm.nih.gov/). Two sets of primers (reverse and forward) were designed using Primer3 software (available at http://www.Genome.wi.mit.edu/cgi-bin/ Primer/Primer3www.cgi). This software was also used to check the length and annealing temperature of each sequence, which prevented the formation of primer dimers as much as possible. The chosen primers were synthesised using Eurofins MWG Operon (available at http://www.Eurofinsgenomics.EU/). RNase-free water was used to dilute the primers to a concentration of 10 pmol so that they were ready to use in PCR reactions.

Table 2.3 The sequences for RT-PCR primers used in this study and the expected size in base pair

Gene	Primer	Primer Sequence	Product Size (bp)	Annealing Temp. °C
βACT	F	5'- TGCTATCCCTGTACGCCTCT-3'	553	58
	R	5'- T CGTCATACTCCTGCTTGCTG -3'		
PRDM9	F	5'-CAGGCTCAGAAACCAGTGTC-3'	655	60
	R	5'-GTTCCTGGCCGTATTCATCC-3'		
TEX19	F	5'- GTGCCCACATGAACAGAGAC-3'	345	60.5
	R	5'- GACATGCCCTCTTCCTCATAC-3'		
TEX19	F	5'- GCTTCAACATGGAGATCAGC-3'	386	58.4
	R	5'- GAAGCTCCTCAAATCTCCAG-3'		
GAGE1	F	5'- TAGACCAAGGCGCTATGTAC -3'	245	58.4
	R	5'- CATCAGGACCATCTTCACAC -3'		
SSX2	F	5'- CAGAGATCCAAAAGGCC -3'	407	58.4
	R	5'- CTCGTGAATCTTCTCAGAGG -3'		
REC8	F	5'- GTTGGTGAAGCGCGAATACC -3'	488	60.5
	R	5'- GGAACTTCAGGAGGGATCTC -3'		
MAGEA1	F	5'- CCCACTACCATCAACTTCAC -3'	676	58.4
	R	5'- CTCTTGCACTGACCTTGATC -3'		
MORC1	F	5'- CAGGAGCTGTGCAATGATGT -3'	455	58.4
	R	5'- CATTGCCCCAGAGAGATTTC -3'		
MORC2	F	5'- TGACCTGCCTCTTCCTGTCT -3'	776	58.4
	R	5'- GAACATGCCATCCAGATCCC -3'		
PRDM1	F	5'-CAGTGCCTTCTCCTTTACCG-3'	768	60.5
	R	5'-ATGTCATCCTCCACGTCCTC-3'		
PRDM6	F	5'-GCACCTGGATTGGACCTTTC-3'	384	60.5
	R	5'-CTTGTCTGCACATGGCTTCC-3'		
PRDM4	F	5'-GGGGACAGGTCATGTAGATG-3'	384	60.5
	R	5'-TGTCCCTGGGTAGGAAGATG-3'		
STRA8	F	5'-TGGCAGGTTCTGAATAAGGC3'	723	58.4
	R	5'-GAAGCTTGCCACATCAAAGG-3'		
SYCE1	F	5'- CTGCTCAAGGAAGAGAAGCT -3'	318	60.5
	R	5'- CTCTTCCTCTTGTGTGCTCT -3'		
SYCE2	F	5'- CTTCTCCTCTCTGGACTCAA -3'	339	60.5
	R	5'- CATCTGAGTCTTAGGCTCTG -3'		
SYCP1	F	5'- GGTCAGCAGAAAGCAAGCAA -3'	645	60.5
	R	5'- GGCAGATGTCCACAGATAGT -3'		
SYCP3	F	5'- GTCTTCTGCAGGAGTAGTTG -3'	509	58.4
	R	5'- CACTTGCTATCTCTTGCTGC -3'		
NUT	F	5'-CACCACCAGTTGCTCAACTG-3'	623	60
	R	5'-CTCCTTCACAGCTTCTGGTG-3'		
ODF4	F	5'-GACAAGATGGGAGACTGCTG-3'	602	60.5
	R	5'- GGTGTCTGTGATCGTCTGTG 3'		

SEPT12	F	5'- CTGCAGCTGCATTCACTGAC -3'	608	60.5
	R	5'- CGGATAAGCAGGTCTCTCAG -3'		
TDRD12	F	5'-GAGCTAAAGTGCTGGTGCAG-3'	641	60.5
	R	5'- CTGAGGTCACCGACAATACC -3'		
MAGEB5	F	5'- CCTCCACTGAGAGTTCATGC -3'	655	60.5
	R	5'- CTTGGGCTCTCTTCCTCATC -3'		
L1 ORF1	F	5'- TCC TCA CCA GCA ACA GAAC -3'	207	60
	R	5'- TTT CAG CTC CAT CAG CTCC -3'		
PRDM7	F	5'- CTTCATTGACAGCTGTGCTG -3'	755	60.5
	R	5'- AGTTCCTGGCCATACTCATC -3'		
PRDM11	F	5'- AAAGCTTCCAGCAAGTGGAC -3'	680	60.5
	R	5'- TACATCCCCCTCATCAAAGC -3'		
HORMAD1	F	5'- GCCCAGGATCTACACAGTTA -3'	684	60.5
	R	5'- CCATTCGTTCTCTCTCAGTG -3'		
HORMAD2	F	5'- GAGAGCTCTTATGGAGAACG-3'	707	60.5
	R	5'- CTGGAGCACTCAGAACTTTG-3'		

2.4.3 Quantitative Real-time PCR

Go Taq qPCR Master Mix (Promega, #A6001) was used to initiate the qRT-PCR reaction in a Bio-Rad CFX96 Real-Time PCR Detection System C100 thermal cycler in a Hard-Shell 96-well plate (Bio-Rad, #9655). Each individual sample was tripled to obtain a final amount of 20 µL.

Every reaction mixture consisted of 1X qPCR Master Mix and primers were obtained at a final concentration of 0.2 µM and 2 µL of diluted cDNA. The studied sequences were amplified with an initial denaturation hold at 95°C for 10 minutes, 40 cycles at 60°C for 30 seconds and finally at 72°C for 10 seconds (the elongation stage). A melt curve study was considered after the 40 cycles of reaction were complete.

Bio-Rad CFX Manager 3.0 software was used to examine the primers' specificity and efficiency as well as to evaluate gene expression and the cycle threshold. Commercial primers (Qiagen, QuantiTech Primer Assay) and designed q-PCR primers were used in this study, as shown in the primer list presented in Tables 2.4

Table 2.4 List of RT-qPCR primers

Gene	Assay Name	Cat.number
β ACT	Hs_ACTB _1_SG	Qiagen; QT00095431
GAPDH	Hs_GAPDH _2_SG	Qiagen; QT0192646
PRDM9	Hs_PRDM9_1_SG	Qiagen; QT01023631
TEX19	Hs_TEX19_1_SG	Qiagen; QT00033047
MAGEA1	Hs_MAGEA1_1_SG	Qiagen; QT00012320

Non-commercial primers

Gene	Primer	Primer Sequence
ORF1	F	5'-AAACCAAGGCTCGAGAACTACGT-3'
	R	5'-CATTGCTGATACCCTTTCTTCCA-3'

2.5 Protein Extraction

2.5.1 Whole-cell lysate

The cell pellets suspended in 1x PBS were transferred to a sterilised Eppendorf tube and spun at 4,000 g at 4°C for 2 minutes. The supernatant was then carefully removed using an aspiration pipette, leaving just the pellet. M-PER lysis buffer (Thermo Fisher Scientific, #78503) was used to lyse the whole cell. M-PER reagent was used because of the pellets' weight (15 µL of M-PER buffer/1 µg pellet).

According to the manufacturer's instructions, M-PER buffer was complemented with Phosphatase Inhibitor Cocktail and Halt Protease Inhibitor Cocktail (Thermo Fisher Scientific, #78420 and #87785, respectively). The tube containing the whole cell suspension was shaken for 10 minutes at room temperature and then spun at 4°C at 14,000 xg for 15 minutes. The protein concentration was quantified using a Nanodrop (Thermo Fisher Scientific) and a BCA Protein Assay Kit (Thermo Fisher Scientific, #23227), as standard.

2.5.2 Histone extraction lysate

In this study, the Histone Extraction Kit (Abcam, #ab113476) was used as a selective method to extract histone proteins. In the first step, pellets were harvested using a cold centrifuge at 4°C and 1000 r.p.m for 4 minutes. Subsequently, the cells were re-suspended in 1X pre-lysis buffer (approximately 10^7 cells/mL) and lysed on ice for approximately 10 minutes, stirring occasionally. The mixture was subjected to cold centrifugation at 4°C and 10,000 r.p.m for 90 seconds. The supernatant was removed immediately and the cells were re-suspended using lysis buffer (approximately 180 µL/10^7 cells); the tube was then incubated on ice for approximately 30–35 minutes. The mixture was centrifuged at 4°C and 12,000 r.p.m for 6 minutes, the supernatant (including acid-soluble proteins) was transferred to a new sterilised Eppendorf tube and 0.3 mL of Balance-DTT buffer was immediately added to 1 mL of supernatant. The protein concentration was then quantified using a NanoDrop (Thermo Fisher Scientific) and a BCA Protein Assay Kit (Thermo Fisher Scientific, #23227).

2.6 Western Blot

Nearly 30 µg of extracted protein was used in each individual well for western blot analysis. The protein samples were prepared by adding a suitable amount of 4x LDS sample loading dye (Invitrogen, #NP0007) and 10x Reducing agent (Invitrogen, #NP0004), supplemented with sterile RNA-free water to obtain a total volume of 15 µL. Each blended sample was boiled at nearly 70°C for 12 minutes. The first lane of the gel was loaded with a Precision Plus Protein Dual Color Standard protein ladder (Bio-Rad, #1610374).

All prepared samples were loaded on NuPAGE Novex 4-12% Bis-Tris (Thermo Fisher Scientific, #NP0322) in buffer consisting of NuPAGE MOPS SDS (Thermo Fisher Scientific, #NP0001) at 103 V for 65 minutes. The proteins were then transferred to a nitrocellulose membrane (Amersham, Lot num: A10043101) by using Trans-blot® TurboTM RTA Mini PVDF transfer Kit (Bio-Rad cat# 1704272) that was prepared in a semi dry transfer programme device (Trans-Blot® TurboTM Biorad; # 1704150) at 2.5 A for 7 minutes. The transfer mixture consisted of 600 mL of distilled water, 200 mL 100% absolute ethanol and 200 mL of 5x transfer buffer

(Bio-Rad, #10026938). This mixture was shaken well at room temperature for 20 minutes. The transferred membrane was incubated at room temperature for at least 1 hour in milk solution (10% fat-free milk in 1x PBS and 0.5% Tween-20 [Sigma-Aldrich, #P1379]). The primary antibody was then diluted with blocking buffer to a suitable concentration and incubated with the transferred membrane at 4°C overnight on a shaker (Table 2.5).

The membrane was washed in washing solution (0.5% Tween mixed with 1x PBS) for 10 minutes three times at room temperature with gentle shaking, then incubated in the milk solution with corresponding secondary antibodies at room temperature for 1 hour with careful shaking. The membrane was then washed for 10 minutes three times at room temperature to remove any unbound antibodies. The secondary antibodies used in this study are illustrated in Table 2.6

Different ECL were used as to detect the signals: Chemiluminescent Peroxidase Substrate-3 from (Sigma-Aldrich; #CPS3100-1KT) or Pierce ECL Plus substrate from (ThermoFisher Scientific; #32132). Finally, the membrane was exposed to X-ray film (Thermo Fisher Scientific; #34091) in a dark room for a favourable time of exposureor photographed with a ChemiDoc XRS+ Imaging System digital camera (Bio-Rad #1708265). The ImageLabTM software 4.1 programme was chosen for visualisation. However, blocking buffer from abcam (Ab126587) and washing solution from Thermo Fisher (28358) were used for histone methylation western blotting.

Table 2.5 The primary antibodies used for the western blot analyses and their dilutions

Primary Antibody	Host	Source	Dilution	CAT#
Anti-PRDM9	Rabbit	Abcam	1:1000	Ab85654
Anti-PRDM9	Rabbit	Abcam	1:1000	Ab101013
Anti-TEX19	Sheep	R&D	1:250	AF6319
Anti-LINE-1 ORF1p	Mouse	Merck Millipore	1:250	MABC1152
Anti-H3K4 (mono) methyl	Rabbit	Cell Signalling	1:1000	9732S
Anti-H3K4 (di) methyl	Rabbit	Abcam	1:5000	Ab32356

Anti-H3K4 (tri) methyl	Rabbit	Abcam	1:5000	Ab8580
Anti-H3k9(Tri) methyl	Mouse	GeneTEX	1:1000	Gtx50900
Anti-H3K18 Ac	Rabbit	Cell Signalling	1:1000	13998s
Anti-GAPDH	Mouse	Santa Cruz	1:3000	SC-365062
Anti –Total H3	Mouse	Abcam	1:1000	Ab10799
Anti-H3K9 AC	Mouse	Abcam	1:500	Ab12179
Anti-H3K36me3	Rabbit	Cell Signalling	1:1000	9763
Anti-H3K4me3	Rabbit	Cell Signalling	1:1000	9727

Table 2.6 The secondary antibodies used for the western blot analyses and their dilutions

Secondary Antibody	**Species reactivity**	**Source**	**Dilution**	**CAT#**
Anti-Mouse	Mouse	Cell Signalling	1:3000	7076
Anti-Rabbit	Rabbit	Cell Signalling	1:3000	7074
Anti-Sheep	Sheep	R&D	1:20000	HAF016
Anti- Mouse DyLight	Mouse	Thermo Scientific	1:5000	SA234709
Anti-Rabbit DyLight	Rabbit	Abcam	1:5000	Ab216777

2.7 Proliferation curve preparation

Cells were grown in 6-well plates at particular concentrations based on the cell line (10^5 cells/mL for HCT116 and $2x10^5$ cells/mL for SW480 cells); the final volume was 2 mL/well. Treatment with non-interfering RNA/siRNA was conducted daily to traeats cells, as mentioned in Section 2.2. Throughout this study, all experiments were carried out in triplicate and the morphology of cells were recorded daily. Trypan blue (Invitrogen, 15250-061) and a TC20 automated cell counter (Bio-Rad, #1450102) were used to count cells after trypsinisation and as the basis for designing the curve.

2.8 The cloning of Flag N terminal and c- myc into pTRE-3G Vector

2.8.1 Primers design and PCR amplification

The full open reading frame of *PRDM9* was obtained from the NCBI. *PRDM9* was cloned into pGEM then it was used as a template. Amplification of template (*PRDM9)* was carried out using primers including tags, N-FLAG, C-Myc and restriction site (Table 2.7) *PRDM9* cDNA included with N-FLAG, C-Myc tags then were cloned into pTRE-3G. *Bam*HI and *Nhe*I were used as restriction enzyme in cloning.

The PCR conditions start with pre-cycling melting for 30 seconds at 98°C, 35 cycles of denaturing for 10 seconds at 98°C and at annealing temperature (60–65°C) for 30 seconds. The extension stage lasted for 30 seconds at 72°C/kb and a final extension process was conducted for 10 minutes at 72°C. To check, 5 µL of the PCR reaction was run on 1% agarose gel.

Table 2.7 Primer sequences used for cloning and their expected size

Gene	Primer	Primer Sequence	Product Size (bp)	Annealing Temp °C
PRDM9 ***-****NFLAG*	F	5'TTCGCTAGCATGTACAAAGACGATGACGACAA GATGAGCCCT 3'	2658	58
	R	5' GAAGGATCCTTACTCATCCTCCCTGCAGA 3'		60
PRDM9 ***-*** *C MYC*	F	5' TCCGCTAGCATGAGCCCTGAAAAGTCCCAAGA 3'	2658	58
	R	5'GAAGGATCCTTACAGGTCCTCCTCGAAGATCAG CTTCTGCTCCTC 3'		58

2.8.2 Purification and DNA digestion

The PCR reactions were prepared at a total final volume of 50 µL. Twenty-five µL of PCR products were mixed with 5 µL of blue loading dye (NEB, B7021S) and run on 1% agarose gel, after which particular bands were chosen for purification. Nucleospin Gel and PCR Clean-up (MACHEREY-NAGEL, #740609-250) were used to purify the PCR products. Nearly 25 µL of the purified PCR product was digested using 5 µL

of CutSmart TM Buffer (Bioline, B7204S) buffer, 1 µL of restriction enzyme and 18 µL of distilled water to obtain a final volume of 50 µL. Then samples were incubated at 37°C for approximately 2 hours followed by run on a 1% agarose gel.

2.8.3 Ligation and transformation

The N-FLAG:PRDM9 and C-myc:PRDM9 was ligated in pTRE-3G plasmid individually. The concentration of the inserted DNA and plasmid was measured using NanoDrop (ND_1000). The ligation mixture consisted of 50 ng of vector mixed with the detected molar ratio of the insert, 1 µL of T4 DNA ligase (Promega, M180A) and 1 µL of 10x ligase buffer (Promega, C126B). At final stage, 20 µL of ddH2O (Sigma, W4502) was added to the DNA ligation mixture.

The ligation mixture was carefully mixed, and short spun then incubated at 4°C overnight. Transformation was carried out by preparing a vial of NEB 10-beta competent *E. coli* (BioLabs, C3019H) and placing it on ice for approximately 10 minutes to thaw. In accordance with the manufacturer's instructions, 5 µl of ligation mixture was added to *Escherichia coli* (BioLabs, C3019H) and chilled for 30 minutes on ice with gentle flicking; it was heat shocked in a 42°C water bath for 30 seconds and then samples were chilled on ice again for 5 minutes. 950 µL of Super Optimal broth with Catabolite repression (SOC) was added to the mixture, which was incubated at 37°C and shaken vigorously at 250 r.p.m for 1 hour. Samples were plated on LB agar petri dishes containing 100 mg/mL ampicillin (Sigma, A9518) and all plates were incubated at 37°C overnight.

To complete this stage, serial dilutions of transformation reaction prepared and the samples were plated on LB agar petri plates containing 100 mg/mL ampicillin (Sigma, A9518). All plates were then transferred for overnight incubation at 37°C (Table 2.8).

Table 2.8 Reagent to prepare LB and LB agar media for *E. coli* growth

Media	Amount
Luria Broth (LB)	
NaCl	10 g
Yeast extract	5 g
Tryptone	10 g
Water	up to 1 litre
For LB agar plates	
Agar	10 g
Water	up to 1 litre

2.8.4 Colony screening

Sterilised micropipette tips were used to pick up several colonies from the overnight plates after transformation. Each individual colony was rinsed with 20 µL water. The PCR reaction was carried out using an internal primer to detect the presence of *PRDM9* in the chosen colonies. The PCR reaction mixture consisted of 5 µL of a colony mixed with 0.5 µL of each primer, 12.5 µL of 2x MyTaq redMax, and 6.5 µL of distilled water. The rest of the water/colony mixtures, including the positive PCR colonies, were inocubated overnight at 37°C in 5 mL of LB liquid medium has 100 mg/mL ampicillin.

2.8.5 Plasmid isolation from *E. coli*

A mini preparation was performed using approximately 5 mL of *E. coli* overnight culture and 100 mg/mL ampicillin. A QIAprep Spin Miniprep Kit (250) (Qiagen, 27106) was used to extract plasmids from the bacterial culture according to the manufacturer's instructions. Cells were harvested from the culture by centrifuging it at 4°C and 4,000 xg for 10 minutes. P1 buffer was used to resuspend the pellet, which

was then moved to a fresh clean sterilize Eppendorf tube. 250 µL of P2 buffer was added followed by 350 µL of N3 buffer. The tubes were centrifuged for approximately 10 minutes at 13,000 xg. The supernatant was then moved to a spin tube and centrifuged for 1 minute at 13,000 xg. 750 µL of PE washing buffer was added, the columns were spun once more for 1 minute at 13,000 xg and the supernatant wash was aspirated. The columns were centrifuged once more to remove any remaining washing buffer. Finally, the samples were eluted using 50 µL of elution buffer. The purified plasmid sample was digested by the detected restriction enzymes to confirm that the correct strand was cloned and the cloned genes were sequenced to determine that they were the correct orientation and to check for any mutations.

2.8.6 *E. coli* glycerol stock

Based on the positive PCR results, the residual LB/colony mixture (approximately 17 µL) was moved to a 50 mL tube containing 10 mL of a mixture of the LB medium with sufficient antibiotic. The tube was incubated overnight at 37°C with vigorous shaking. The following day, 1 mL of the bacteria culture was mixed with approximately 200 µL of sterile glycerol in a new cryovial and mixed in a vortex machine for short while. The following data was recorded: cloned ID, plasmid name, bacteria strain, cloning site and date on the vial, and the tube was placed in a -80°C freezer for long-term storage.

2.9 Establishing of a double Tet-On 3G stable cell line

2.9.1 Puromycin selection

The HCT116 cell line was grown in 6-well plates containing a specific medium (see Table 2.1) with 100 µg/mL of G418. Approximately seven doses of puromycin were added to the plate each day to determine the smallest dose of puromycin required to kill all cells within 4 to 5 days. 4 µg/mL was chosen as the minimum dose for colony selection.

2.9.2 Creating of double stable HCT116 Tet-On 3G stable cell line

HCT116 Tet-On 3G cell lines were grown in a 6-well plate until they reached confluence level. It was prepared to evolve double stable HCT116 Tet-On 3G cell lines including *N-FLAG:PRDM9* and *C-myc:PRDM9*. 2 µg sample of recombinant vector pTRE3G including PRDM9 was then transfected in each well in addition to 100 ng of linear puromycin as a selection marker (20:1 ratio), with help of Xfect transfection mixture (Clontech, #PT5003-2) regarding to the protocol provided with manufacturer. After 2 days the confluent cells were transferred to 10 cm dishes and cultured for a further 2 days. Media, including 4 µg/mL puromycin and 100 µg/mL of Geneticin, were then added to the dishes and refreshed every 4 days. After 6–8 days each healthy single colony was picked and transferred to a 24-well plate. The cells were cultured with a suitable concentration of selective antibiotics (G418 and puromycin). The confluent cells were divided into 3 wells of a 6-well plate and transferred to T75 flasks when they became confluent. Some samples were screened and the rest were frozen in liquid nitrogen.

2.9.3 Examination of a double stable HCT116 Tet-On 3G stable cell line

Gene induction was checked using doxycycline (Sigma, D9891-5G) for each colony. In this experiment, each clone was cultured in a 10 cm dish and 1 µg/mL of doxycycline was used on positive plates. The negative control was cultured but no doxycycline was added. The cells were incubated in a protected humidified incubator for 48 hours at 37°C in 5% CO2; they were then harvested and their RNA was extracted and used for RT-PCR and qRT-PCR to determine whether or not the expression of *PRDM9* had been induced.

2.9.4 Sequencing PCR results

Samples of 500 ng/μL of DNA were sent for sequencing and mixed with sterile water in ready-labelled tubes. This plasmid was sequenced with primers designed by Eurofins Company to prove that the PRDM9 cDNA with tags was correctly cloned in the right orientation without mutations. The BLAST was used to check the sequencing results. These results were blasted and aligned with the corresponding genes.

Chapter 3

Functional analysis and potential roles of PRDM9 in cancer cells

3. Functional analysis and potential roles of PRDM9 in cancer cells

3.1 Introduction

Around 19 transcription activators are encoded by the PRDM family. A SET domain is present in these activators and histone methyltransferase activity has proven to be a characteristic feature of this domain. This domain is followed by numerous motifs of a zinc finger and these motifs promote protein-RNA, protein-DNA and protein-protein interactions. It is interesting to note that oncogenic properties are demonstrated by PRDM family members. It has been established that alterations in several members of this family are linked to development of cancer (Sorrentino et al., 2018).

The role of the PRDM9 in regulation of transcription has long been established. An orthologue of PRDM9 in mice is Meisetz has proven to be a histone methyltransferase. It is essentially involved in prophase I progression during initial stages of meiosis I prophase. Researchers have detected *Meisetz* transcripts only in germ cells of female foetal gonads and postnatal testis during meiosis I (Hayashi et al., 2005). According to Hayashi et al. (2005), damage to the *Meistz* gene in mice results in sterility in both genders due to impaired meiotic double-stranded break (DSB) repair mechanism, impaired sex body production and disturbance in pairing of homologous chromosomes. The role of Meisetz as a transcriptional activator during meiotic division has also been confirmed. Meisetz also controls the expression of *Morc2b* (testis specific *RIK* gene). Expression of human *PRDM9* has been detected in numerous cancer cell lines and its absence in healthy cells; however, testis germ cells are the exception (Feichtinger et al., 2012). It has been proposed that the *PRDM9* gene can serve as a promising CT gene biomarker and it can be utilized in several areas of cancer therapy, including immunotherapy and/or cancer vaccination.

A characteristic feature of cancer is over proliferation of cells which involves disruption of the cell signalling system responsible for controlling the cell cycle. With the passage of time, cancer cells proliferate in an unchecked manner and escape the process of programmed cell death. Researchers have identified that expression of CTA genes is correlated with the rate of proliferation of cancerous cells. For example,

Maxfield and colleagues (2015) demonstrated the effect of expression of CTA genes on the viability of cancerous cells. Similarly, Lajmi et al. (2015) reported that proliferation rate and viability of melanoma cells is negatively affected by the disturbed expression of *MAGEC2*. According to Wang et al. (2016) increased expression of the *MAGE-A1* gene may induce the oncogenic process and this augments the division of multiple myeloma cells. Conversely, reduced expression causes reduction in proliferation of melanoma cells.

It has been demonstrated through studies that binding of PRDM9 with certain motifs of DNA facilitate trimethylation of histones at lysine K4 and K36 (H3K4me3 and H3K36me3) through methyltransferases activity which is brought about by PR/SET domain. As a consequence, during meiosis proteins required to initiate DSBs are recruited close to its binding site. It can therefore be stated that the sites for meiotic recombination is determined by the PRDM9 protein in addition to its transcription activator role. The histone methyltransferase action of PRDM9, which has been shown *in vitro,* has also been demonstrated *in vivo*. For this purpose, H3K4me3 and H3K36me3 was enriched at recombination hotspots determined by the PRDM9 protein (Powers et al., 2016). Yamada et al., (2017) have discovered that distribution genomic of PRDM9 dependent H3K4me3 is strongly correlated with H3K36me3. Also, the greatest degree of enrichment is noticed at the nucleosomes present adjacent to the site of PRDM9 binding.

The goal of this chapter was to study PRDM9 biological activity in various cancer cells. We aimed to address whether PRDM9 can influence cancer cell survival. RT-PCR was utilized to study whether overexpression of *PRDM9* in cancer cells could alter the expression of different genes which might influence the oncogenic characteristics of the cells.

3.2 Results

3.2.1 Knockdown of PRDM9 in SW480 cells

PRDM9 mRNA knockdown was performed in a SW480 cell line utilising various small interfering RNA. Four different siRNAs (the Qiagen Company) were used to deplete the *PRDM9* gene transcripts. As there is considerable homology between *PRDM7* and *PRDM9* sequences, siRNAs were used to specifically target and effect *PRDM9* transcripts. The negative control was non-interfering RNAs. All siRNAs were transferred into cultures for 3 days, then RNA was extracted from all the cultures. qRT - PCR was used to detect the mRNA of *PRDM9* and measure efficiency of depletion. The data in Figure 3.1 show that the cells cultured with siRNA7 and siRNA10 presented obvious alteration in *PRDM9* mRNA levels relative to the non-interfering siRNA (Ni) control.

3.2.2 Examination of protein levels following PRDM9 siRNA treatment in SW480 cells

Western blotting was used to assess the levels of the PRDM9 protein following the treatment of the siRNAs. siRNAs were utilized for 3 days, then cells were harvested and protein extracted.

An anti –PRDM9 polyclonal antibody (Abcam-ab85654) was utilized to identify PRDM9 protein levels. Extract from untreated cells, as well as the non-interference controls presented band at nearly 103 kDa using the anti-PRDM9 antibody. Data presented a clear depletion of the PRDM9 protein level when siRNA 7 and 10 were used, which is consistent with the qRT – PCR analysis (Figure 3.2). GAPDH analysis was carried out in this study to examine the quality of loading.

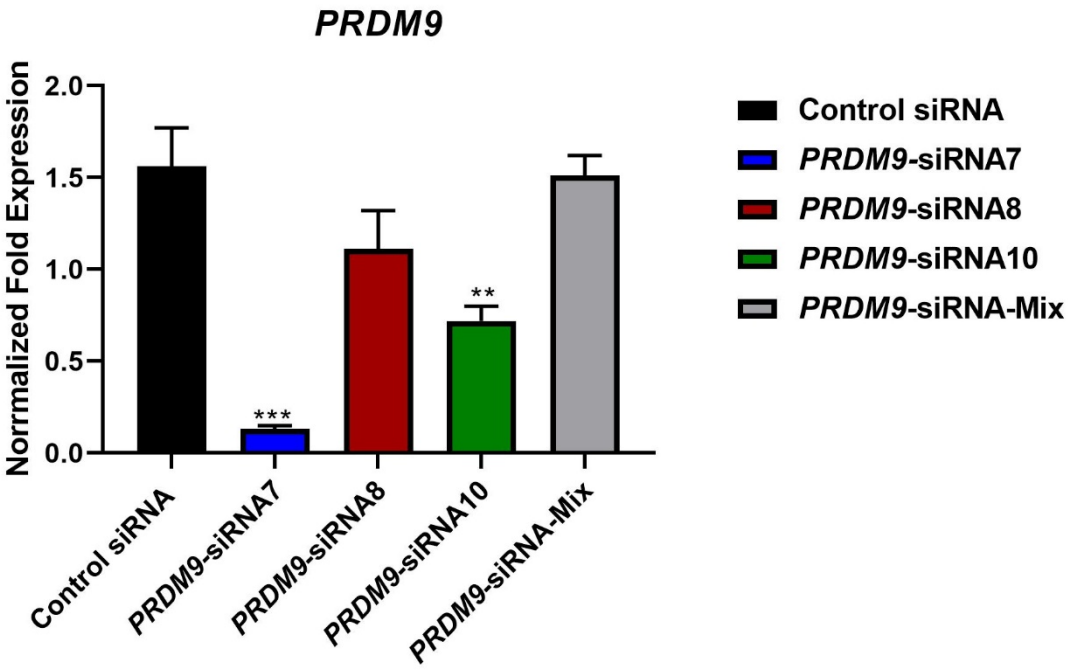

Figure 3.1 qRT-PCR showing the mRNA levels of *PRDM9* after siRNA treatment in SW480 cells. 4 different siRNAs were utilized 7, 8, 10 and combination of two siRNAs (8 and 10) to deplete PRDM9 in the SW480 cell line. The bar chart displays the mRNA levels of *PRDM9*. The *PRDM9* mRNA data were normalised to the qRT-PCR data of two genes, *GAPDH* and *βACT*. P values presented significant changes when siRNA7 and siRNA10 were utilised compared to the non-interference (** P value < 0.01 and *** P value < 0.001).

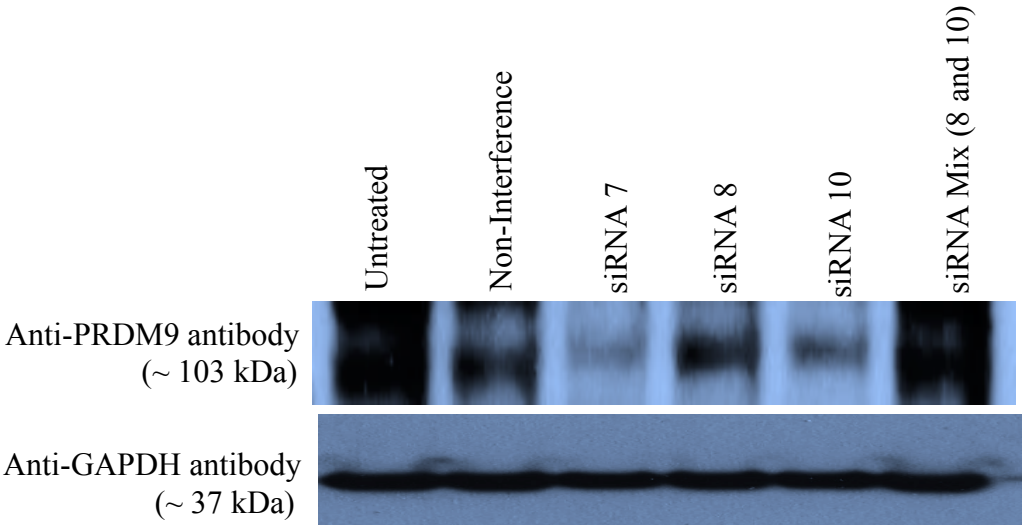

Figure 3.2 Western blot technique illustrating the amount of PRDM9 protein following siRNA treatment in SW480 cells. To deplete PRDM9 in the SW480 cell line 4 siRNA treatments were utilized; 7, 8, 10 and siRNAs 8 and 10 combined (8 and 10 mix) . Depletion, indicated by relative reduction in intensity of 103 kDa band, was observed in siRNA 7 and siRNA 10, a slight effect, compared to both the untreated cells and non-interference siRNA. GAPDH detection was employed as a loading control.

3.2.3 Impact of PRDM9 depletion on SW480 cell proliferation

A study of the alterations of cell proliferation was carried out. siRNA 7 was used for 7 days in addition to untreated cells and non-interference (as controls) to examine the impact of PRDM9 depletion. Every day, we harvested cells and the total number of cells was documented (Figure 3.3.I). The qRT-PCR technique was carried out to examine the ability of *PRDM9* mRNA depletion in siRNA7 cultures, as illustrated in Figure 3.3.II. siRNA treats caused a decrease in proliferation and total cell counts.

3.2.4 Knockdown of PRDM9 in HCT116 cells

An attempt to knockdown *PRDM9* mRNAwas carried out using 4 types of *PRDM9* siRNAs in an HCT116 cell line. Gene expression of *PRDM9* was examined utilizing qRT-PCR to detect whether *PRDM9* mRNA decreased following siRNA knockdown after 3 days of treatment in various types of siRNAs. The qRT-PCR data displayed notable knockdown of *PRDM9* mRNA in the HCT116 cells. The depletion was detected in siRNAs 7 relative to non-interference (Figure 3.4). The *PRDM9* qRT-PCR data were normalised to *GAPDH* and *βACT*.

3.2.5 Examination of protein levels following siRNA treatment in HCT116 cells

Examination of the alterations of the PRDM9 protein following the treatment of siRNA was done using western blotting. siRNAs were used for 3 days then we harvested cells and whole cell lysates were collected. A new batch of anti-PRDM9 (Abcam-ab85654) antibody was used to identify the PRDM9 protein level. Untreated cells as well as the non-interference siRNA presented an obvious band in nearly 103 kDa utilizing the anti-PRDM9 antibody. The data showed clear depletion of PRDM9 protein level when siRNA 7 was used (Figure 3.5). GAPDH was used in this study as a positive loading control.

I)

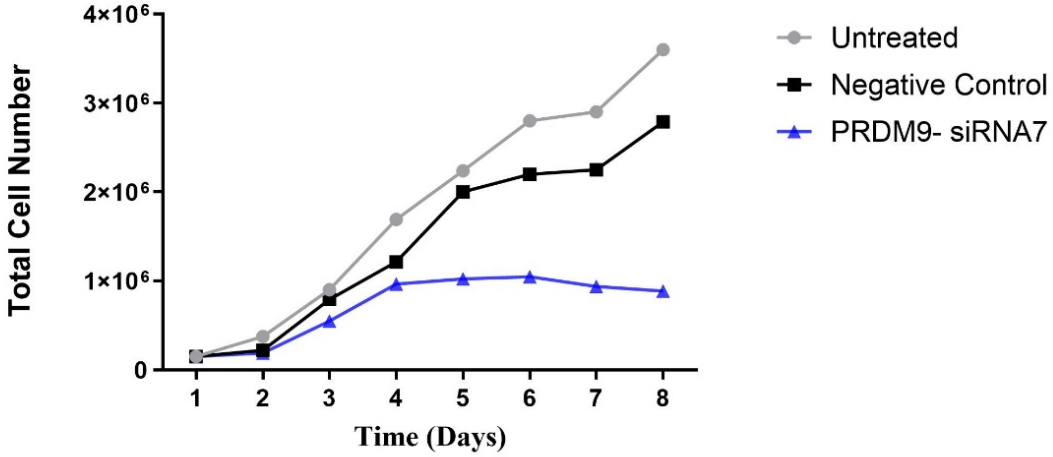

II)

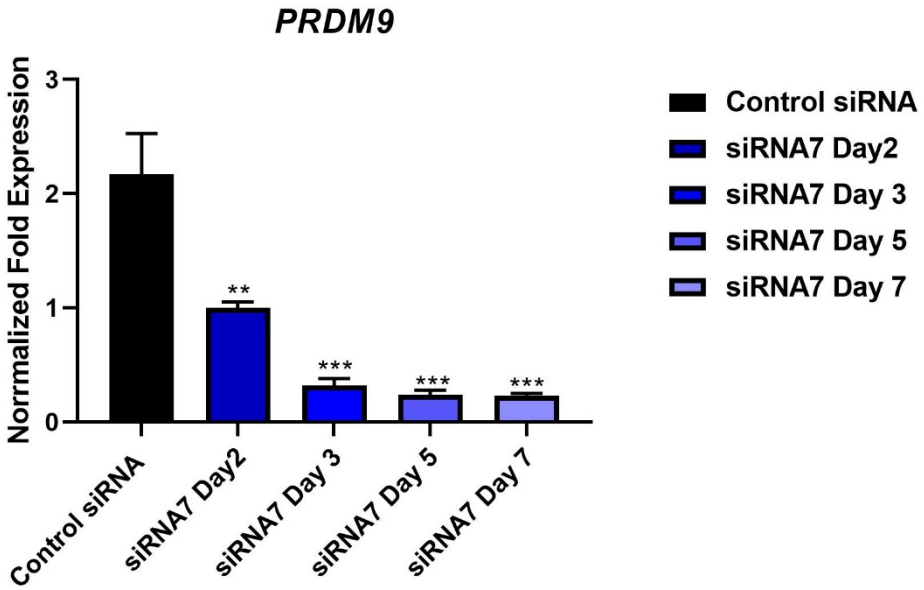

Figure 3.3 Cell proliferation curve of SW480 cells constructed utilising PRDM9 siRNAs 7 for 7 days. I) The curve displays cell counts of treatment for 7 days. Notable changes in the cell counts were detected comparing untreated cells as well as non-interference siRNA. II) The efficiency of depletion of PRDM9 was assessed utilising qRT-PCR (** P value < 0.01 and *** P value < 0.001).

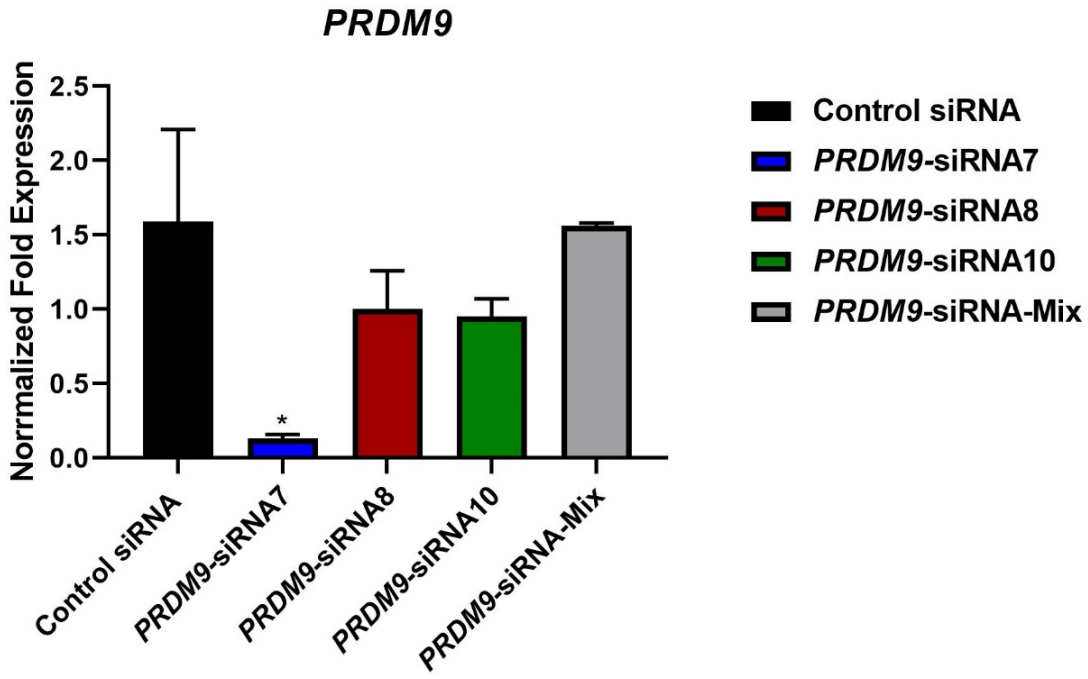

Figure 3.4 qRT-PCR analysis of *PRDM9* mRNA levels after siRNA treatment in HCT116 cells. 4 different siRNAs were utilized 7, 8, 10 and combination of two siRNAs (8 and 10) to deplete PRDM9 in the HCT116 cell line. The data display the *PRDM9* mRNA levels. The *PRDM9* data were normalised to the qRT-PCR data of two genes *GAPDH* and *βACT*. P values presented noticeable changes when siRNA7 was utilised, relative to the non-interference (* P value < 0.05).

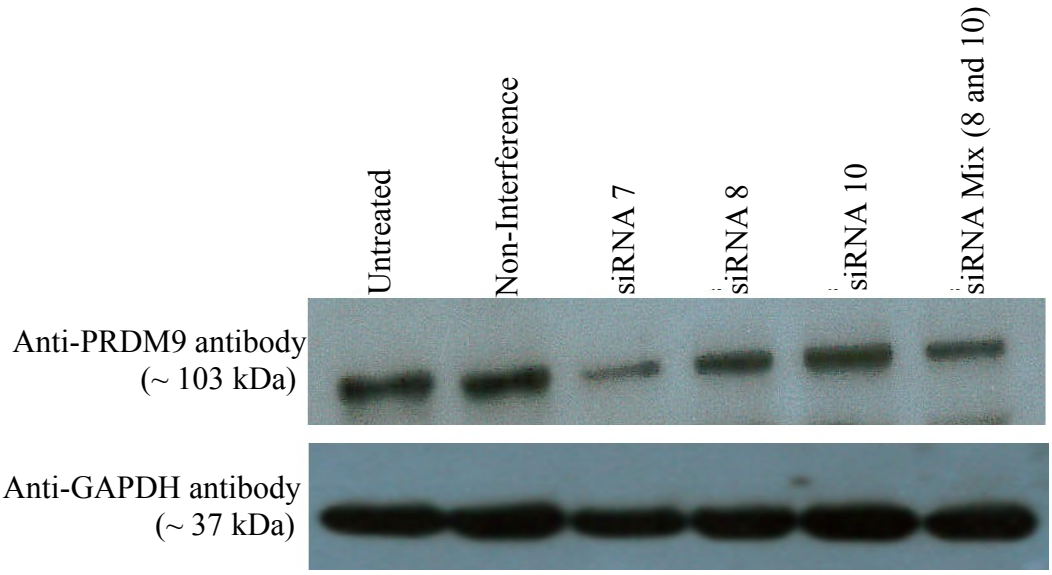

Figure 3.5 Western blot showing the amount of PRDM9 protein following siRNA treatment in HCT116 cells. Different siRNAs were utilized 7, 8, 10 and combination of two siRNAs (8 and 10) to deplete PRDM9 in the HCT116 cell line. Depletion was observed in cultures treated with siRNA 7 (at the size of roughly 103 kDa) compared to both the untreated cells and non-interference. GAPDH was utilized in this study as a positive loading control.

3.2.6 Examination of the validity of the expression of *PRDM9* created clones

Integration of *PRDM9* into HeLa Tet-On 3G cells was previously prepared in the McFarlane group (Ahmad Almatrafi, PhD thesis, 2014). The HeLa Tet-On 3G cell line permits a gene of interest to be induced using doxycycline. This was carried out to establish a double stable cell line involving pTRE3G:PRDM9 vector as well as the transactivator protein of Tet-On which allow the regulation of *PRDM9* expression using doxycycline. Two clones (A and B) were constructed to investigate *PRDM9* function.

RT-PCR and qRT-PCR were used to examine the induction of *PRDM9* in clone A and clone B. A colony that had pTRE3G (the vector) was considered a negative control. Separately, each clone (A and B) was cultured in the presence of 1 μg/ml doxycycline (activating transcription). The same number of cells were cultured in absence of doxycycline. Cells were harvested and the total RNA was isolated to synthesise cDNA to examine *PRDM9* expression in the absence and the presence of doxycycline. *βACT* expression was used to test the quality of the synthesised cDNA (Figure 3.6). cDNA from testis was considered a positive control for this experiment to examine the expression of *PRDM9*.

qRT -PCR was carried out for further analysis to measure the expression of *PRDM9* in clones A and B following addition of doxycycline. RT-PCR analysis illustrated an observed expression of *PRDM9* in clone A as well as clone B after treatment of the cells with 1 μg/ml doxycycline, while there was no expression of *PRDM9* in the untreated cultures. The *PRDM9* results were controlled to the qRT -PCR data of two reference genes *GAPDH* and *βACT.* qRT -PCR corresponded to the conventional RT -PCR data, and it showed significant induction of *PRDM9* after 24 hours of culture treatment; however, no expression of *PRDM9* was detected in the absence of doxycycline.

I)

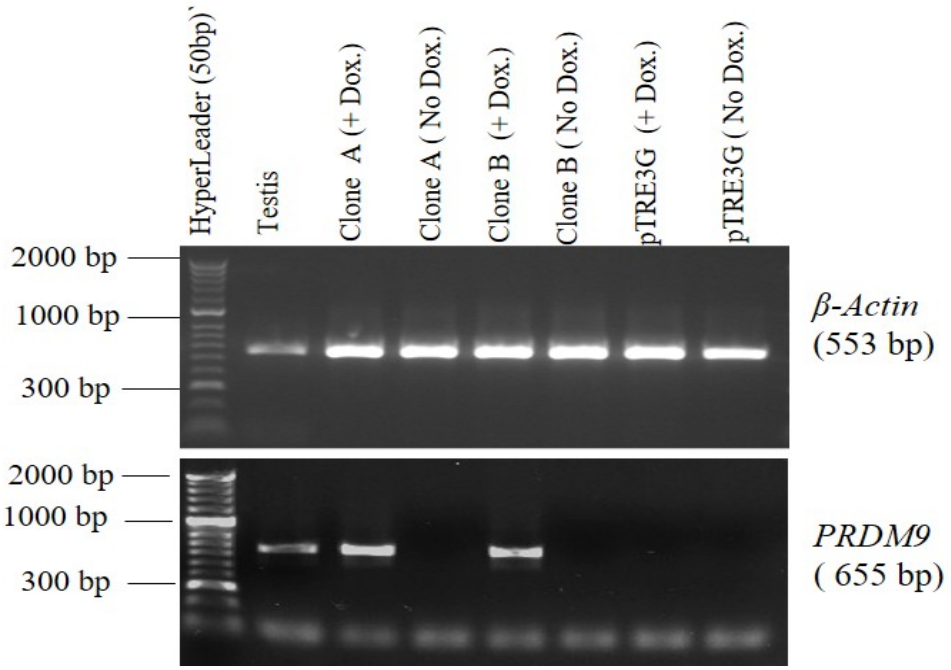

II)

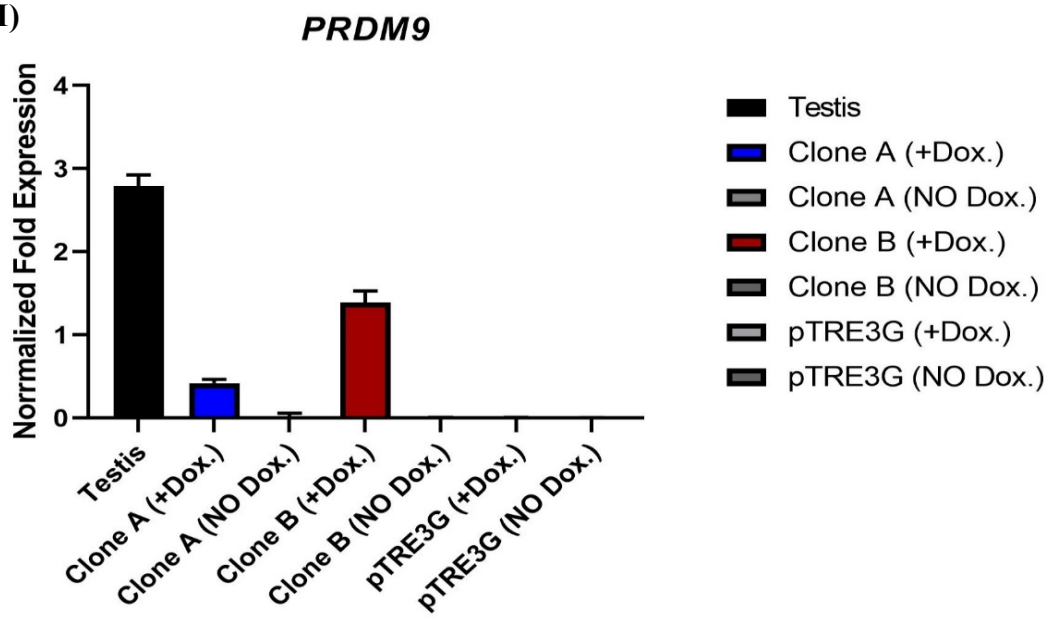

Figure 3.6 Analysis of expression of *PRDM9* in 2 independent clones. I) RT-PCR data illustrate the expression of *PRDM9* in the presence and absence of doxycycline. The agarose gel shows expression of *βACT* as a positive control for examination of the quality of the cDNA. A pTRE3G clone is presented as a negative control, while the testis is presented as a positive control for *PRDM9* expression. II) qRT-PCR analysis shows the mRNA levels of *PRDM9* for each clone after addition of doxycycline treatments in a HeLa Tet-On 3G cell. The *PRDM9* data were relative to the qRT -PCR data of 2 references genes, *GAPDH* and *βACT.*

3.2.7 PRDM9 could serves as a transcriptional activator

Van der Bruggene and co-workers (1991) discovered the melanoma-associated antigens known as MAGE. These antigens are members of the CTA family (van der Bruggen et al., 1991; Xiao & Chen, 2004). Around 55 members are present in the MAGE family, and these have been grouped into two sub-families, namely MAGE-I and MAGE-II. MAGE-I contains MAGE-A, MAGE-B and MAGE-C sub-group. MAGE-D sub group has been placed in the MAGE-II sub-family (Sang et al., 2011; Zajac et al., 2017). MAGE-A antigens have proven to be strictly tumour-specific. There are 12 members of the MAGE-A group (MAGE-A1 to MAGE-A12), and these are found in numerous tumour tissues including those of bladder carcinoma, breast cancer, and lung cancer (Zajac et al., 2017).

Here, we used RT-PCR and qRT-PCR analysis to examine weather high expression of *PRDM9* can influence expression of *MAGEA1* (Figure 3.7 and Figure 3.8). We extracted RNA from two independent *PRDM9* expressing clones (A and B). Each clone was harvested from a culture that was treated either in the presence or absence of 1 μg/ml doxycycline for 1 day. cDNA was then produced from each clone.

The results, presented in Figure 3.7, show slightly increased *MAGEA1* expression especially in clone B after the overexpression of *PRDM9.* qRT -PCR was utilized to quantify *MAGEA1* mRNA levels following overexpression of *PRDM9* (Figure 3.8.I). *MAGEA1* mRNAs showed a high level of expression after doxycycline induction, specifically in clone B, which was correlated to the mRNA levels of *PRDM9* (Figure 3.8.II). In light of these data, PRDM9 may have the ability, as transcription activator, to activate *MAGEA1* expression.

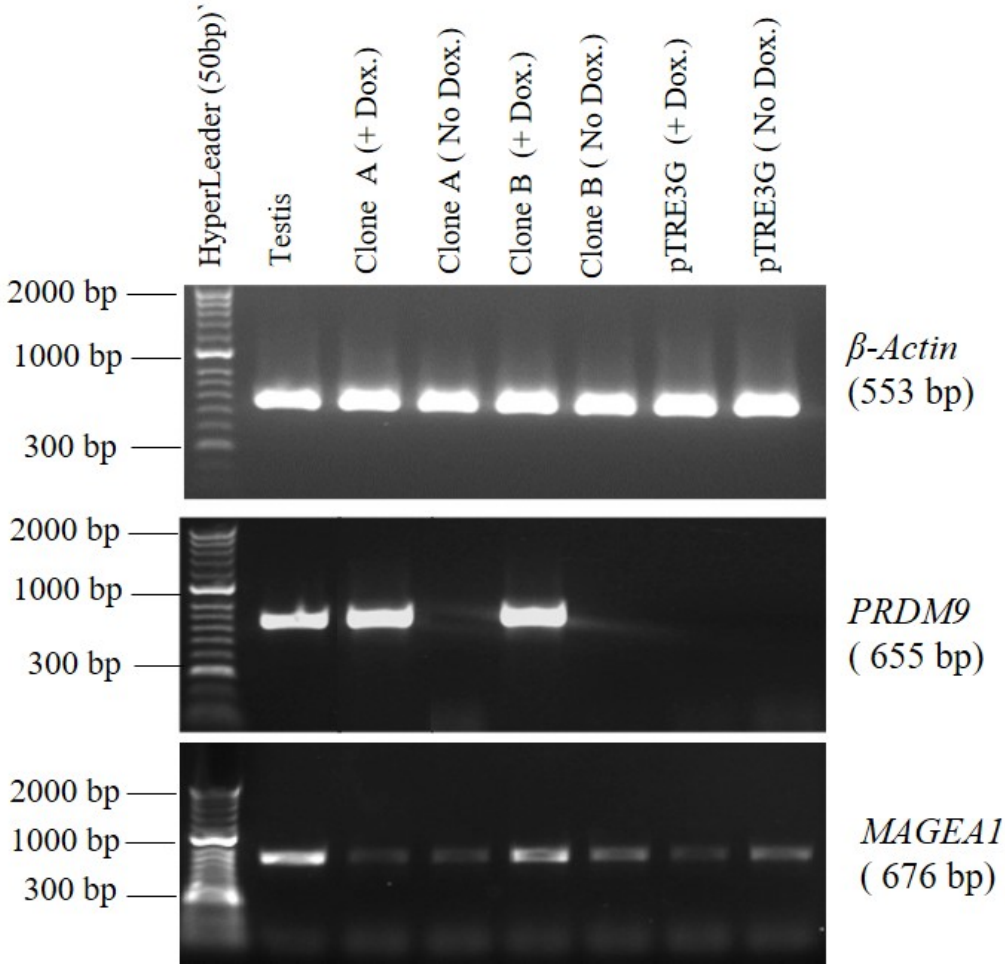

Figure 3.7 RT-PCR analysis displays *MAGEA1* gene expression following the induction of *PRDM9* in HeLa Tet-On 3G cells. The quality of the cDNA was examined by checking *βACT* mRNA. Clear expression of *PRDM9* was detected following doxycycline induction in both clones (A as well as B); while in the absence of doxycycline no expression of *PRDM9* was detected. A pTRE3G clone was considered a negative control, while the testis is presented to examine *MAGEA1* and *PRDM9* expression. *MAGEA1* expression was seen after doxycycline induction, which was correlated to *PRDM9* expression. 1% agarose gel prepared with pic green was used to detect the PCR products.

I)

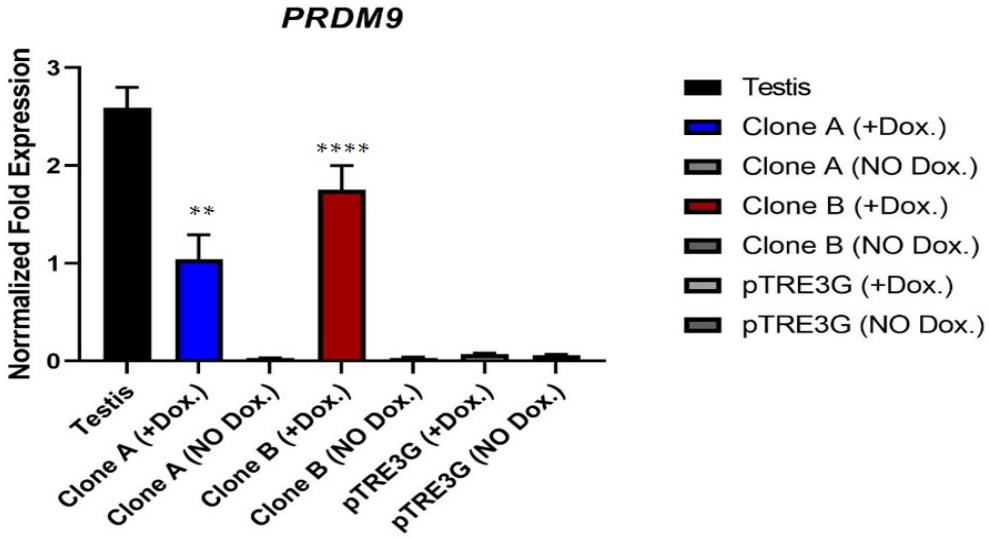

II)

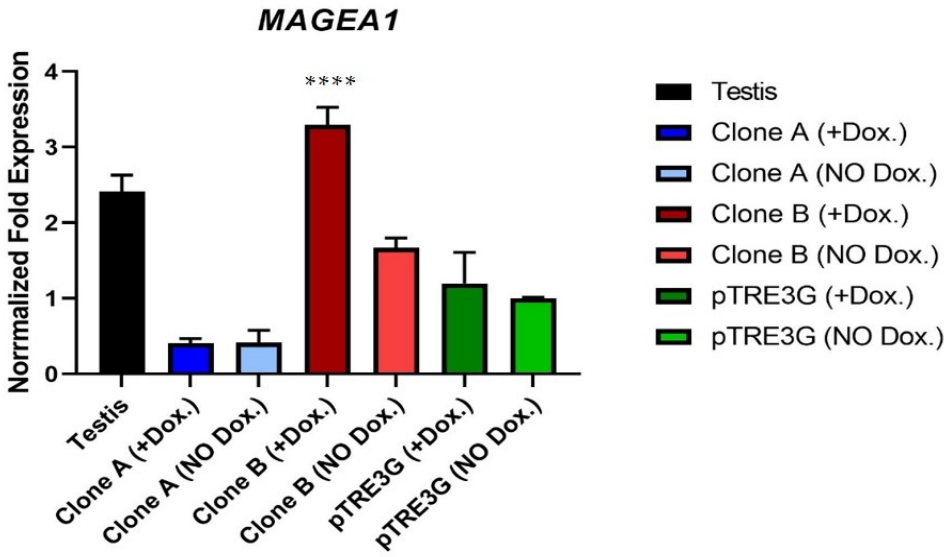

Figure 3.8 qRT-PCR analysis of the mRNA levels of *PRDM9* and *MAGEA1* for each clone in the presence of doxycycline treatments in HeLa Tet-On 3G. I) The bar chart displays the levels of *PRDM9* mRNA in the presence of doxycycline treatments in both clones (A as well as B). P values presented significant changes in presence of doxycycline in both clones (A and B), relative to the presence of doxycycline in (pTRE3G) (** P value < 0.01 and **** P value < 0.0001). II) Data displays the *MAGEA1* mRNA levels in the presence of doxycycline treatments in both clones (A as well as B). P values presented significant changes in presence of doxycycline in (B), relative to the presence of doxycycline in (pTRE3G) (**** P value < 0.0001). The *PRDM9* and *MAGEA1* data were normalised to the qRT -PCR data of two genes, *GAPDH* and *βACT*.

3.2.8 The impact of overexpression of *PRDM9* on *MORK* genes

In the mouse, Hayashi and co-workers (2005) recognised that *PRDM9* was involved in the regulation expression of some genes, including *Morc2b* (Hayashi et al., 2005). Here, we tried to answer whether the overexpression of human *PRDM9* changes the expression of human *MORC* genes. RT-PCR analysis was used to examine the impact of *PRDM9* high expression in the *MORC* genes (*MORC1*, *MORC2* and *MORC3*). Data, presented in Figure 3.9, show that *MORC1* has no expression following *PRDM9* overexpression. On the other hand, *MORC2* and *MORC3* presented expression either in uninduced or induced HeLa Tet-On 3G Cells with pTRE3G presented identical results for these genes. These data need additional investigation using qRT-PCR.

3.2.9 The impact of overexpression of *PRDM9* on several genes of the *PRDM* group

RT-PCR analysis was utilised to examine the link between *PRDM9* expression and several *PRDM* genes. cDNAs were created individually from each clone (A, B and pTRE3G) following treatment with doxycycline. Data, presented in Figure 3.10, show an increase of *PRDM1* expression in Clone A after 24 and 48 hours of doxycycline treatment. In the case of the *PRDM7* gene, there is a clear induction following *PRDM9* induction. *PRDM6* and *PRDM4* genes display no apparent alterations in expression following induction of *PRDM9*.

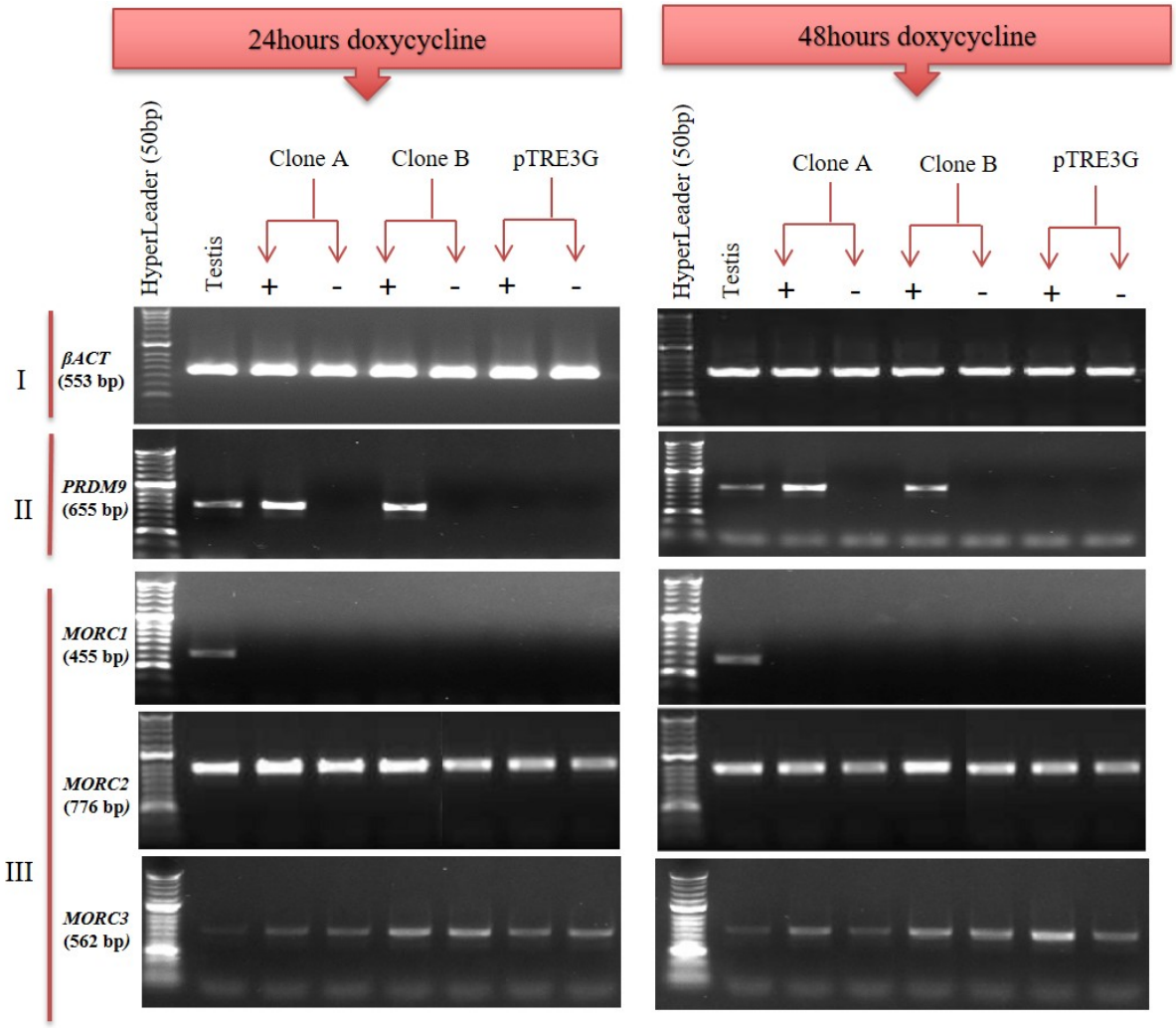

Figure 3.9 RT-PCR analyses display *MORC* gene expression following the induction of *PRDM9* expression in HeLa Tet-On 3G cells. I) The quality of the cDNA was examined by checking *βACT* mRNA. II) Clear expression of *PRDM9* was seen in the presence of doxycycline in both clones (A and B), while in the absence of doxycycline *PRDM9* did not show any expression. A pTRE3G clone is presented as negative control while the testis is presented to examine the *PRDM9* expression. III) The *MORC1* gene displayed no expression following induced expression of *PRDM9* while *MORC2* and *MORC3* displayed expression in induced and uninduced *PRDM9* cells.1% agarose gel prepared with a pic-green was used to detect the PCR products.

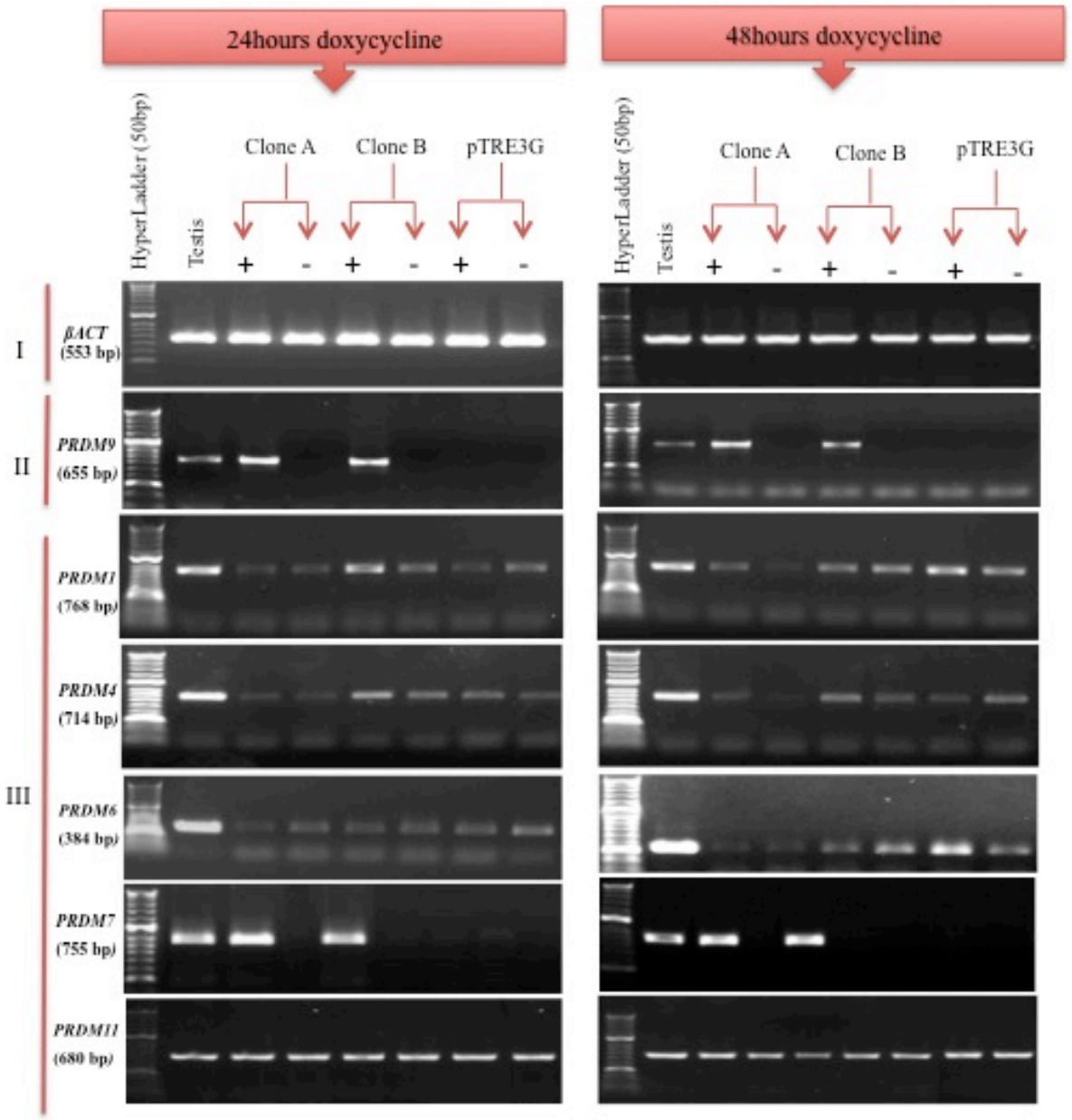

Figure 3.10 RT-PCR analyses display *PRDM* genes expression following the induction of *PRDM9* expression in HeLa Tet-On 3G cells. I) The quality of the cDNA was examined by checking *βACT* mRNA. II) Clear expression of *PRDM9* was seen in the presence of doxycycline in both clones (A and B), while in the absence of doxycycline *PRDM9* did not show any expression. A pTRE3G clone is presented as negative control while the testis is presented to examine the *PRDM9* expression. III) The *PRDM* genes examined in this study displayed expression in both presence and absence of doxycycline. *PRDM7* expression was identical to the *PRDM9* gene. 1% agarose gel prepared with a pic-green was used to detect the PCR products.

3.2.10 The impact of overexpression of *PRDM9* on synaptonemal complex genes

The synaptonemal complex (SC) is a key structure which forms on chromosomes in meiosis. Some meiosis genes have the ability to encode function, which participates in the structure of the SC, for example, *SYCP1*, *SYCP3*, *SYCE1* and *SYCE2*. It has been suggested that *PRDM9* expression may coordinate different meiosis genes. In this study, we used RT-PCR with primers related to SC genes (Figure 3.11). The data indicate that there was no change of the examined SC genes with overexpression of *PRDM9*.

3.2.11 The impact of overexpression of *PRDM9* on other meiosis-specific genes

Expression of other meiosis-specific genes were examined to detect whether *PRDM9* overexpression may be able to influence their expression. In this study, the *HORMAD1* gene demonstrated expression in clone A, clone B and in the negative control. *HORMAD2*, *STRA8* and *SSX2* displayed expression with PCR products at the expected size only on the positive control (testis), while no expression was detected in either cell lines following *PRDM9* overexpression. *REC8* and *GAGE1* showed expression in Clone B treated with doxycycline and faint expression in pTRE3G was also detected (Figure 3.12).

Several potential cancer/testis-restricted genes were examined following overexpression of *PRDM9*. *NUT*, *ODF4*, *TDRD12* and *SEPT12* displayed no expression either in the presence or absence of doxycycline treatment, while clear expression was detected in all these groups of genes in the positive control (testis) (Figure 3.13).

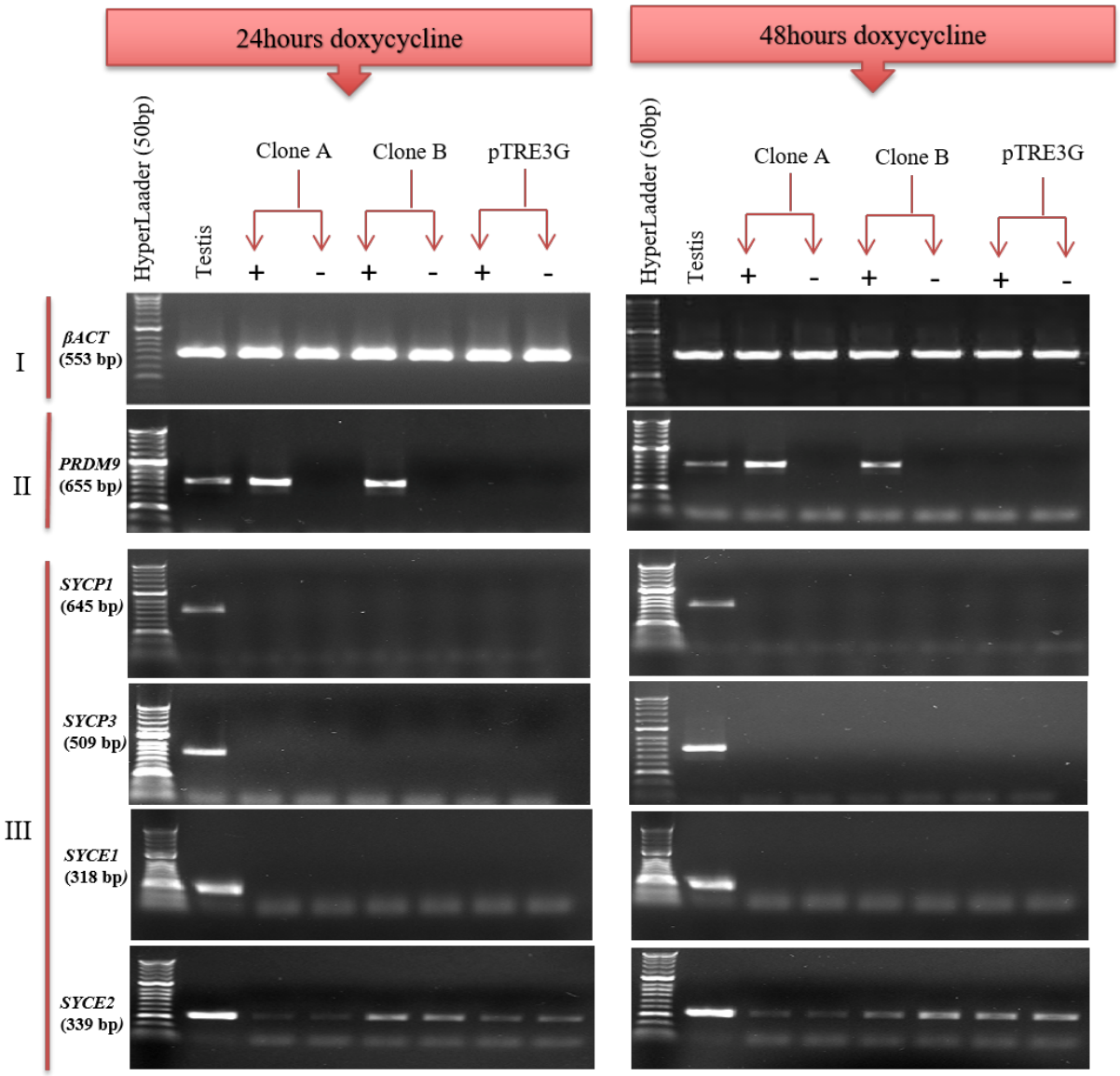

Figure 3.11 RT-PCR technique displays some synaptonemal complex gene expression following the induction of *PRDM9* expression in HeLa Tet-On 3G cells. I) The quality of the cDNA was examined by checking *βACT* mRNA. II) Clear expression of *PRDM9* was seen in the presence of doxycycline in both clones (A and B), while in the absence of doxycycline *PRDM9* did not show any expression. A pTRE3G clone is presented as negative control while the testis is presented to examine the *PRDM9* expression. III) *SYCP1*, *SYCP3* and *SYCE1* displayed no expression following induced expression of *PRDM9*. *SYCE2* displayed expression in both induced and uninduced *PRDM9* genes and in the negative control as well. 1% agarose gel prepared with a pic-green was used to detect the PCR products.

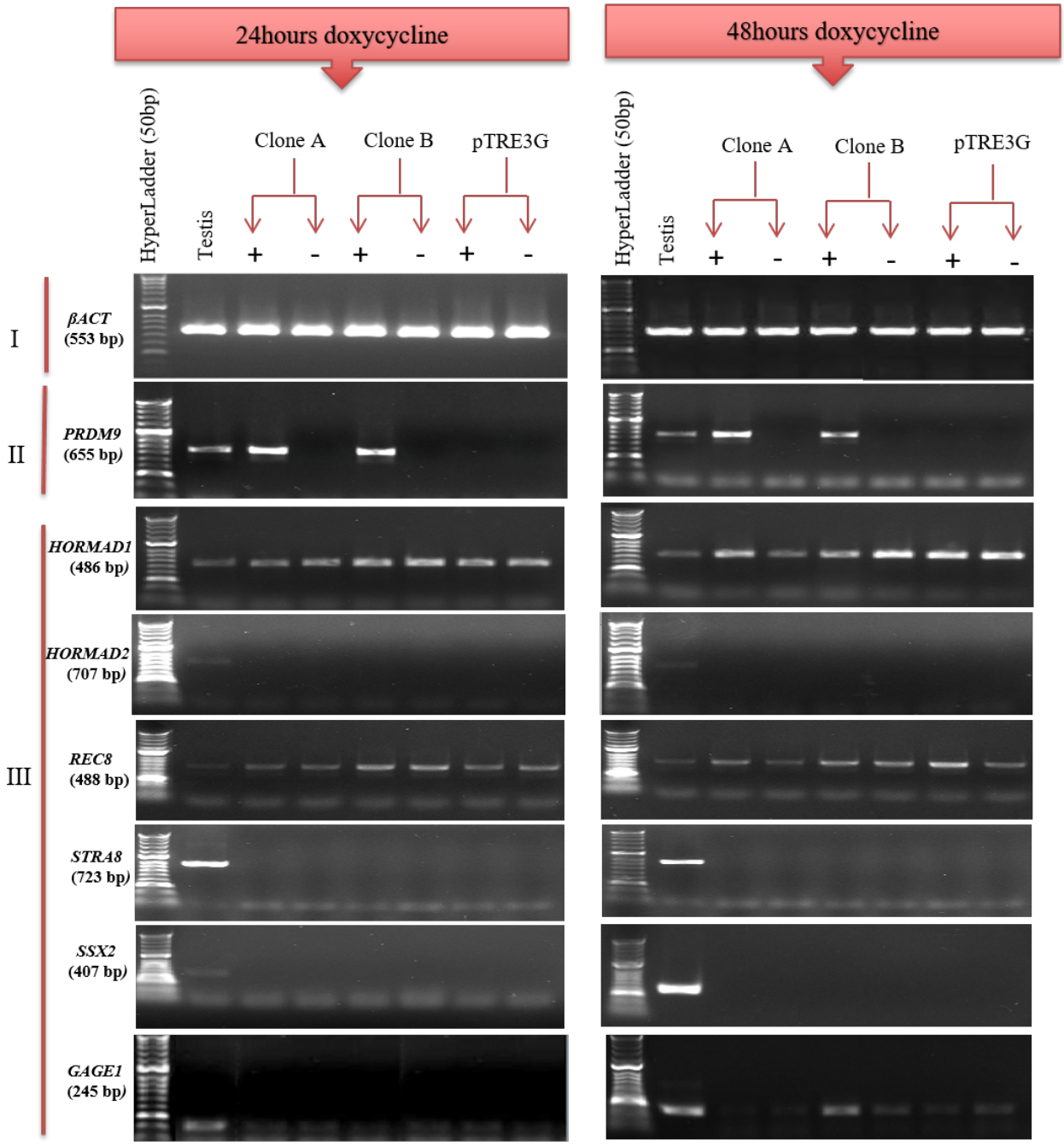

Figure 3.12 RT-PCR technique displays some meiosis /specific gene expression following the induction of *PRDM9* expression in HeLa Tet-On 3G cells. I) The quality of the cDNA was examined by checking *βACT* mRNA. II) Clear expression of *PRDM9* was seen in the presence of doxycycline in both clones (A and B), while in the absence of doxycycline *PRDM9* did not show any expression. A pTRE3G clone is presented as negative control while the testis is presented to examine the *PRDM9* expression. III) *HORMAD2*, *STRA8* and *SSX2* displayed expression only in the positive control (testis). No expression of these genes appeared either in presence or in non-presence of doxycycline. *REC8* and *GAGE1* showed expression in Clone B treated with doxycycline, and faint expression in pTRE3G was detected.

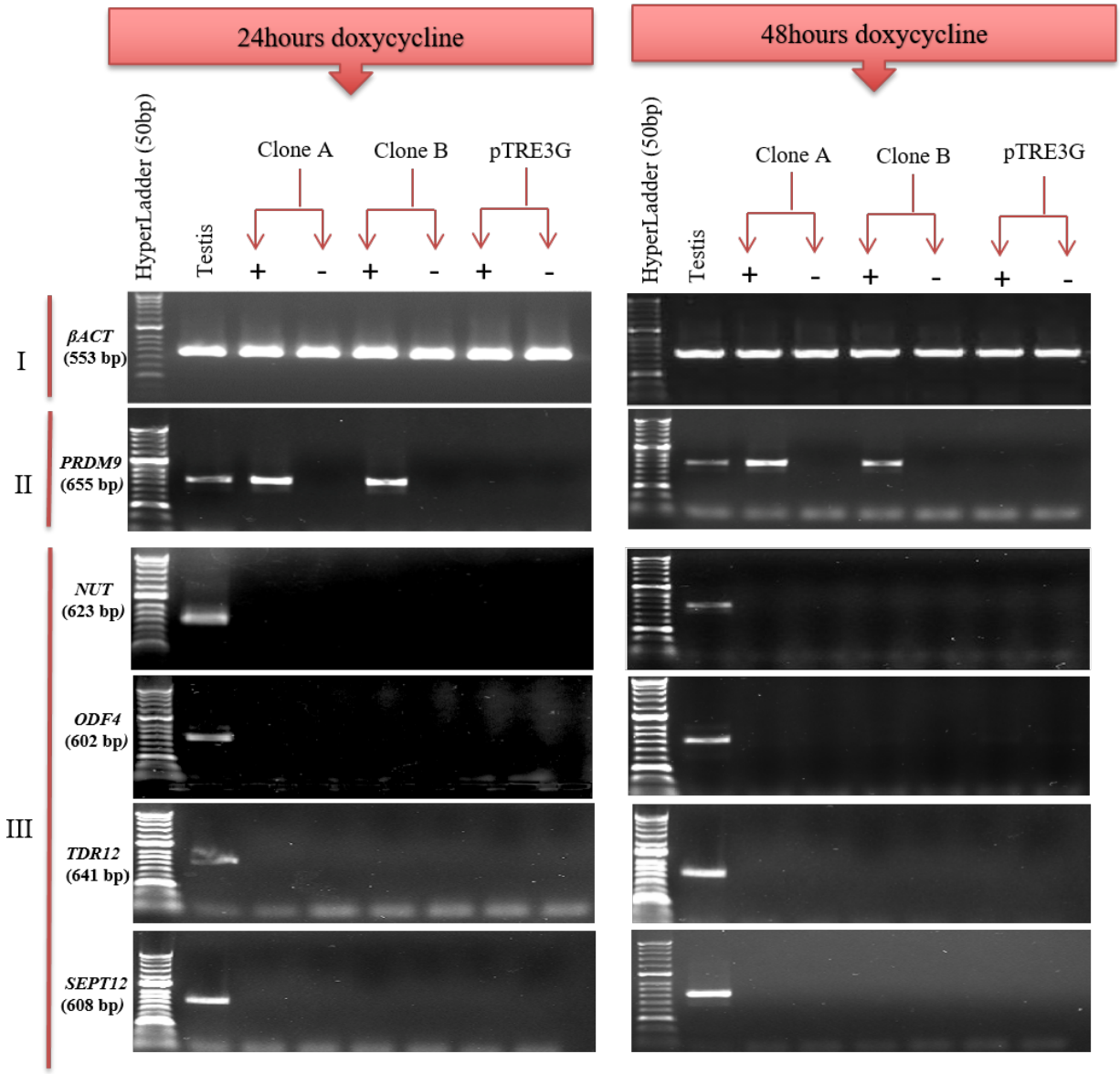

Figure 3.13 RT-PCR technique displays some meiosis-specific gene expression following the induction of *PRDM9* expression in HeLa Tet-On 3G cells. I) The quality of the cDNA was examined by checking *βACT* mRNA. II) Clear expression of *PRDM9* was seen in the presence of doxycycline in both clones (A and B), while in the absence of doxycycline *PRDM9* did not show any expression. A pTRE3G clone is presented as negative control while the testis is presented to examine the *PRDM9* expression. III) *NUT*, *ODF4*, *TDRD12* and *SEPT12* displayed no expression either in presence or in non- presence of doxycycline treatment, while clear expression was detected in all these examined genes in the positive control (testis).

3.2.12 Examination of H3K4me3 and H3K36me3 activity of PRDM9

PRDM9 histone methyltransferase activity has been reported (Eram et al., 2014; Powers et al., 2016). Wu and his colleagues found that PRDM9 has the ability to catalyse H3K4me3 (Wu et al., 2013). This finding is related to the activity of transcription (Schneider et al., 2004), the beginning of recombination hotspots and repair of DNA (Wurtele & Verreault, 2006).

In this study, HeLa Tet-On cell were cultured, and expression of *PRDM9* was induced for 24-48 hours in the presence of doxycycline in each culture independently. We then extracted lysates of cells to examine the levels of H3K4me3 and H3K36me3, as displayed in Figure 3.14. No difference in the proteins levels appeared relating to H3K4 and H3K36 associated with the alterations in expression of *PRDM9*. The data shown in Figure 3.14 are a distinct attempt using several antibodies and different processes.

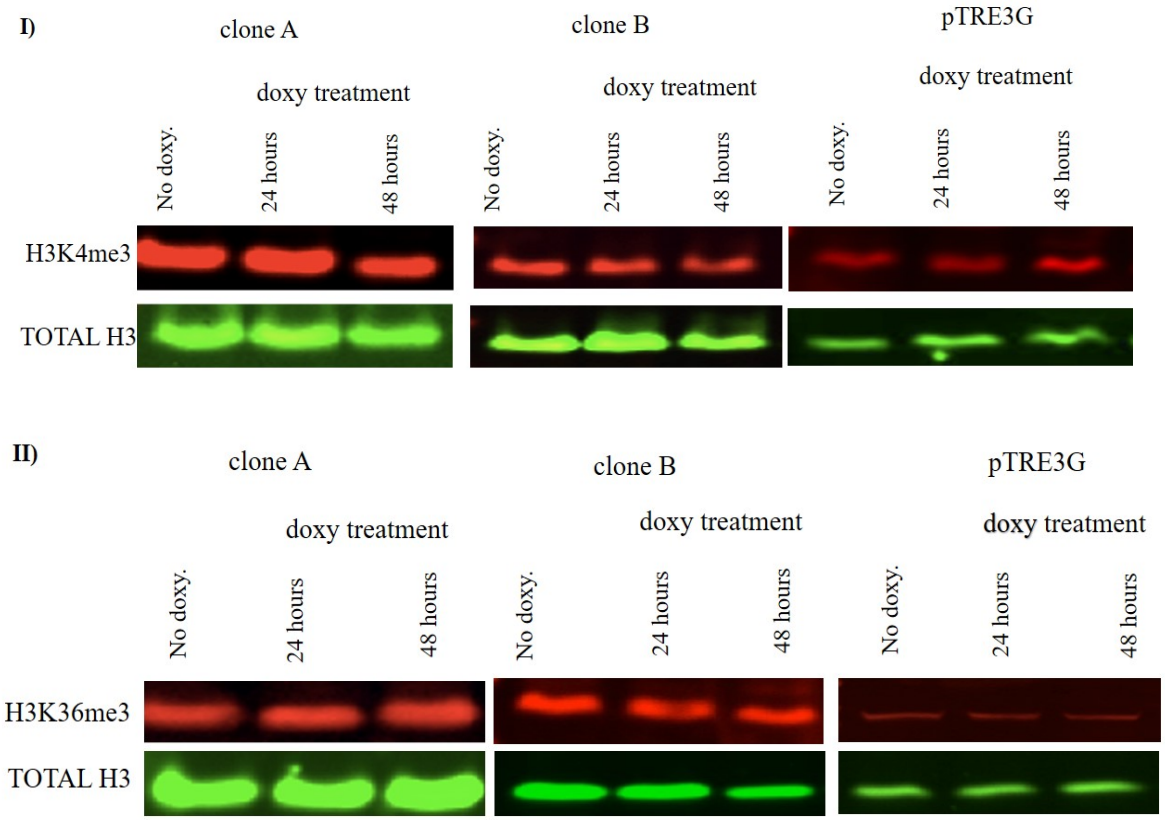

Figure 3.14 Immunoblotting displays H3K4me3 and H3K36me3 HeLa Tet-On 3G cells in overexpression of *PRDM9*. Individually, clones A, B and pTRE3G were cultured in the presence of doxycycline for 24 - 48 hours. One culture for each clone has not been induced and is consider as a negative control to examine induction by doxycycline. I) Immunoblot displays levels of the H3K4me3. II) Immunoblot displays levels of the H3K36me3. The anti - H3 antibody was used as a loading control.

3.2.13 Mutations found in the *PRDM9* sequence in established clones

The lack of any apparent increase in histone H3 methylation following PRDM9 induction led us to question the validity of the *PRDM9* clones. This research demonstrated that the integrated *PRDM9* sequence used in this study (clones A and B) carry a pair of point mutations relative to the reported human *PRDM9* sequence. These mutations involve substitution of a base pair in two codons which altered the sequence of amino acids. One mutation changed the 2008 base resulting in alteration of the 670 amino acid i.e. glycine is changed to arginine. The other mutation replaced the 2042 base of the coding sequence leading to alteration of the 681 amino acid, i.e. threonine is changed to serine as shown in Figure 3.15.

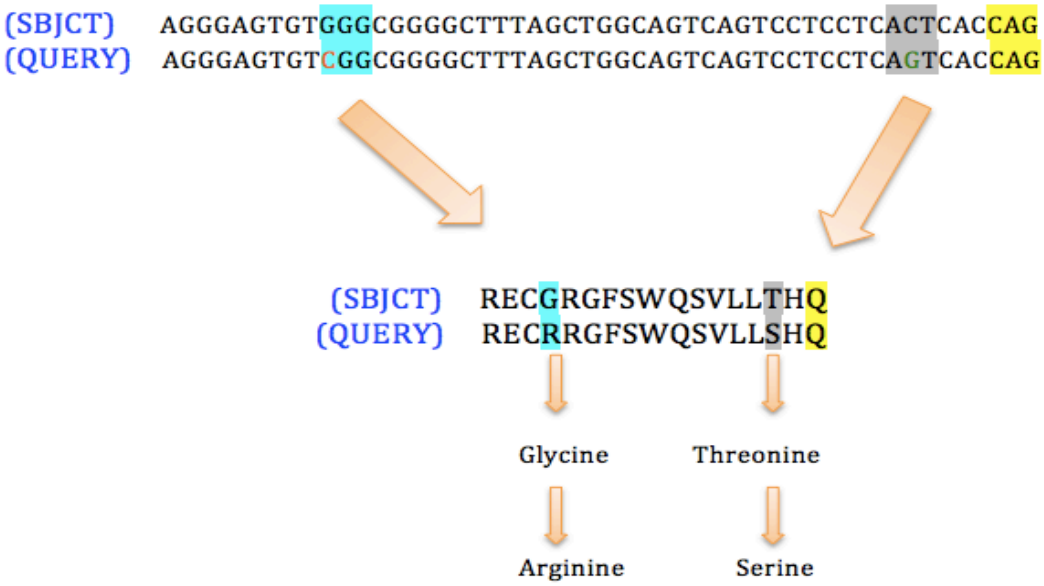

Figure 3.15 Diagram shows 2 mutations in the *PRDM9* sequence. The template that was established previously for clone A and clone B has 2 points of mutation.

3.3 Discussion

3.3.1 PRDM9 protein analysis and influence of PRDM9 knockdown in SW480 growth

Aberrant production of members of the PRDM family has been detected in several kinds of cancers like colorectal cancer, cervical cancer, breast cancer and leukaemia. Moreover, production of these proteins has been found to be associated with development of cancer (Hohenauer and Moore, 2012; Mzoughi, et al, 2016). Among all family members, it is only the PRDM9 which is meiosis-specific although the PRDM7 paralogue is also meiosis-specific but it is not known to be functional active and has established role in determining sites of meiotic recombination hotspots (Myers et al., 2010; Eram et al., 2014). The *PRDM9* gene has been reported to be a CT gene whose abnormal activation is detected in several tumours like melanoma, ovarian cancer, colon cancer and breast cancer (Feichtinger et al., 2012). In healthy as well as cancerous cells, *PRDM* genes play role in regulation of cellular proliferation (Hohenauer and Moore, 2012; Fog et al., 2012). For instance, *PRDM1* which is also called *BLIMP1*, is responsible for controlling cellular viability and proliferation by serving as a transcriptional activator which regulates expression of *TP53* (Yan et al., 2007). Development of germ cell lineage has been reported to essentially involve the coexpression of *PRDM1* and *PRDM14* (Di Zzzo et al., 2013).

Fumasoni et al., (2007) reported that a primate-specific gene, namely *PRDM7* evolved from duplication of the *PRDM9*. According to Hayashi et al. (2005), substantial homology exists between *PRDM7* and *PRDM9*. Proteins encoded by the PR domains of these two genes have 97% amino acids in common and overall 41% amino acids encoded by these genes are same. The distinction lies in the daivergent amino acids encoded by the PR domain sequence and the number of zinc finger repeats of these genes. Conversely, PRDM9 carries 14 zinc finger repeats. The zinc finger sequence of PRDM7 demonstrates chief structural rearrangements that include modified gene splicing as well. It has been established that both *PRDM7* and *PRDM9* belong to the *PRDM* family and are expressed only in germ cells.

Feichtinger et al (2012) have discovered the PRDM9 protein in NTERA-2 cancerous cells though this protein was not found in healthy tissue for example, prostate tissues. It implies that PRDM9 can serve as a possible biomarker. In this research, the PRDM9 was successfully knocked down in HCT116 and SW480 cell lines, particularly when PRDM9 siRNA7 was utilized. mRNA level of *PRDM9* and the PRDM9 protein level were found to be decreased in these cell lines following three days treatment of siRNAs. Later, it was checked if the PRDM9 protein was needed for cancer cell proliferation. It involved culturing of SW480 cells followed by siRNA7 treatment for seven days. In case of this cell line, knockdown of PRDM9 resulted in substantial decrease in the proliferation of cells when growth curves were analysed which suggest PRDM9 might be required to activate proliferation promoting oncogenes.

3.3.2 Examine PRDM9 as transcriptional activator of some genes

It has been established that sites of meiotic recombination hotspots are determined by PRDM9 in mammals (Myers et al., 2010; Parvanov et al., 2010). Production of PRDM9 protein occurs during the initial phases of meiotic prophase (Sun et al., 2015). At this phase, binding between the PRDM9 C2H2 zinc finger (ZF) domain and particular motifs of DNA occurs. Indeed, the PR/SET domain of the protein causes trimethylation of the adjacent histone H3 proteins at 4^{th} lysine (H3K4me3) (Hayashi et al., 2005) and 36^{th} lysine (H3K36me3) (Eram et al., 2014). Trimethylation H3K4me3 has also been reported as an indicator found in promoters of genes which have been transcribed (Schubeler et al., 2004). In order to initiate DSBs, recruitment of SPO11, the DSB mediator, occurs at PRDM9-DNA binding site. Single-stranded DNA is formed when these DSBs are subjected to end resection. This ssDNA serves as a substrate for DMC1 which is a meiosis-specific recombinase protein (Baker et al 2015; Altemose et al., 2017).

It was suggested that PRDM9 trimethylase activity can be regulated expression of other genes during meiotic division (Hayashi et al., 2005). In mice, the Prdm9 protein (*Meisetz*) has been demonstrated to transcriptionally regulate the expression of

Morc2b (Rik) gene (Hayashi et al., 2005). This is in contrast to the finding made in current research that *PRDM9* overexpression was unable to effect the expression of human orthologues of *Rik* (*Morc2b)* including *MORC1, MORC2* and *MORC3* studied in the HeLa Tet-On 3G cells. It might therefore be stated that PRDM9 is not required for regulation of expression of *MORC* gene family in cancerous cells of humans.

It has recently been demonstrated by Altemose et al. (2017) that the PRDM9 protein in humans binds close to the promoter of certain genes and this binding causes activation of histone trimethylation resulting in activation of expression of relevant genes in HEK293T cells (Altemose et al., 2017). Several members of the PRDM family are capable of modifying the state of chromatin at certain promoters of gene. In this way they control the gene expression (Hohenauer et al., 2012). An Important question raised by this research is that whether PRDM9 protein is involved in regulating expression of other genes relating to meiotic division in tumour cells. This research involved analysis of expression of a number of genes in order to check if they are influenced by the PRDM9 protein in HeLa Tet-On 3G. For this purpose, RT-PCR was performed to evaluate expression of several genes that include the genes of *PRDM* family, meiosis-specific genes, CT genes and *MORC* family genes. Based on this work results, the RT-PCR analysis increased expression of *PRDM9* did not affect the expression of most of the evaluated genes in HeLaTet-on 3G cells. Still the possibility that only RT-PCR analysis is not enough of checking the role of PRDM9 in transcriptional activation of the gene expression. On the other hand, certain genes (*MAGEA1*, *GAGE1*, *PRDM7* and *PRDM11*) demonstrated considerable upregulation following over-expression of *PRDM9*.

MAGEA1 has been reported to be a member of the CT gene group (Feichtinger et al., 2012). During this research, uninduced cultures of clone A and B gave rise to extremely faint bands. However, when these clones were induced with doxycycline, upregulation of *MAGEA1* expression was noticed especially in clone B. *MAGEA1* was showed faint band in pTRE3G clone (negative control). Results were further verified through qRT-PCR which demonstrated high expression in transcripts of *MAGEA1* following overexpression of PRDM9. It can be suggested that *MAGEA1* expression affected by the overexpression of *PRDM9.*

High intensity band indicated that *PRDM7* was over-expressed in HeLaTet-On cell line following *PRDM9* overexpression. Co-expression of these two *PRDM* genes in cancerous cells is also anticipated. Co-expression of *PRDM7* and *PRDM9* has been reported by studies carried out in McFarlane laboratory in (K-562) cells and normal human testis (Almatrafi, PhD thesis 2014). It has been demonstrated through studies that certain *PRDM* genes get co-expressed and/or re-activated with other members of the *PRDM* family. Future studies should therefore involve western blotting and qRT-PCR to confirm co-expression or reactivation of *PRDM7* with expression of *PRDM9*. The fact that *PRDM7* and *MAGEA1* genes are activated upon expression of the *PRDM9* variant used here suggests that this version does have some transcriptional regulatory activity, which is not activate for other genes such as the *MORC* family.

During this research, we studied the methyl transferase activity of this PRDM9 variant in HeLa Tet-on 3G cells. We were unable to detect any correlate between PRDM9 with increase in either in H3K36me3 or in H3K4me3. Although, it has been reported by Eram et al., (2014) that expression of *PRDM9* is linked with significant increases in trimethylation of H3K4 and H3K36 in HEK293T cells. It was found during this research that the integrated *PRDM9* sequence form previous work carried two-exchange mutation. The template was made from cDNA taken from the sample collected from testis of adult male. This male was potentially carrying a natural *PRDM9* variant, the relative activity of this variant is unknown although the data reported here suggest some activity. It is unknown whether this individual was reproductively competent. It could be that this individual was infertile and the *PRDM9* used here does not reflect the activity of oncogenic *PRDM9*, as the sequence obtained from tumour cells does not carry these mutations.

Chapter 4

Cloning of *PRDM9*::*N-Flag* and *PRDM9*::*C-Myc* into Tet-On 3G inducible expression system

4. Cloning of *PRDM9::N-Flag* and *PRDM9*::*C-Myc* into Tet-On 3G inducible expression system

4.1 Introduction

As it described in the previous chapter the integrated *PRDM9* sequence was made from cDNA picked from the sample collected from adult testis male. It appears this male had a natural *PRDM9* variant. Also, the findings possibly indicated that PRDM9 might control transcription of certain genes in cancerous cells, even though the *PRDM9* gene used in that work contained what we assumed was a natural nucleotide variant. In order to find the role played by the accepted wild-type *PRDM9* gene in cancerous cells, a new wild-type clone is required. Moreover, a specific antibody is required to monitor levels of the recombinant protein, as it has been suggested that recombinant proteins can be utilized to investigate roles in cancerous cells (Terpe 2003; Waugh, 2005).

Generation of recombinant proteins has proven to be one of the most important tool devised in the field of molecular biology (Young et al., 2012). This research makes use of a recombinant DNA tool for tagging PRDM9. For this purpose, a small peptide comprising some amino acids is incorporated in the protein as a tag. When an extremely small peptide fragment is used as a tag, there are very small chances of alteration in the post-translational modification, transportation and biological function of the protein being tagged (Bucher et al., 2002; Young et al., 2012). An advantage is that the presence of the tag can be detected through a specific monoclonal antibody. Several assays can be conducted for such detection, including western blot. Western blot has proven to be an efficient technique for investigation of modification and levels of specific proteins. Several different epitope tags are available for use just like the Flag and Myc tags utilized in this research. As shown in Table 4.1, 8 amino acids constitute a Flag tag which can be inserted at the amino end of the protein to be tagged. Conversely, Myc tag is derived from a C-Myc protein and is made up of 10 amino acids.

Table 4.1 DNA and protein sequence of Myc and Flag tags.

Tags	DNA sequence (5'-3')	Protein sequence
Myc	GAACAAAAACTCATCTCAGAAGAGGATCTG	EQKLISEEDL
Flag	GATTACAAGGATGACGACGATAAG	DYKDDDDK

The aim of this work is to merge tags into the full sequence of PRDM9. Subsequently to clone the genes encoding the tagged proteins into pTRE3G plasmid and then transfected into HCT116 Tet-On 3G cells. Therefore, we will be able to examine the effectiveness of *PRDM9* overexpression in cancer cells gene.

4.2 Results

4.2.1 Prepare pTRE3G PRDM9::N-Flag and PRDM9::C-Myc

Regulation of the activities of mammalian genes can be carried out using the tetracycline controlled Tet-On expression system (Tetracycline-inducible), which is based on the constituents responsible for regulating the processes involved in resistance to tetracycline or its derivatives, like doxycycline (Dox). When cells are exposed to DOX treatment, the Tet-On 3G transactivator protein attaches to the tetracycline-responsive element promoters. This results in activation of the target gene (Loew et al., 2010). As shown in Figure 4.1, the Tet-On 3G system demonstrates sensitivity towards DOX and is optimized for target gene expression and transfection. HCT116 Tet-On 3G cells have transfected with pCMV-Tet3G plasmids previously obtained from the Clonetech kit in our lab. Figure 4.2 shows a map of the pTRE3G vector as well as restriction sites.

The clone pGEM-3ZF (+)::PRDM9 (called pAMO1; in our lab) was used for amplification of the complete length of human *PRDM9* gene (NCBI,Gene ID 56979), having a size of 2685 bp, in order to generate an inducible clone for *PRDM9*. Sequencing of the *PRDM9* inserted into the pAMO1 clone was conducted and it was ascertained that the sequence did not contain any mutations before the amplification process. Consequently, amplification of the complete length of *PRDM9* was carried out utilizing various primers and Phusion PCR Master Mix, including Phusion GC buffer Amplification primers contain a restriction enzyme site and two types of tags (C-MYC and N-FLAG) (Figure 4.3). Later, bands indicating the presence of *PRDM9* were taken out of the gel followed by purification steps and incubation with restriction enzymes (*Bam*HI and *Nhe*I). This process of digestion was carried out to ensure proper cloning. Restriction enzymes *Bam*HI and *Nhe*I were used for digestion of the vector pTRE3G followed by purification of the vector (Figure 4.4). The next step was ligation of the *PRDM9::N-Flag* and *PRDM9::C-Myc* fragments in the digested, purified vector pTRE3G with a ratio of 1:6. The presence of ligated plasmids in *E.coli* was detected using ampicillin antibiotic.

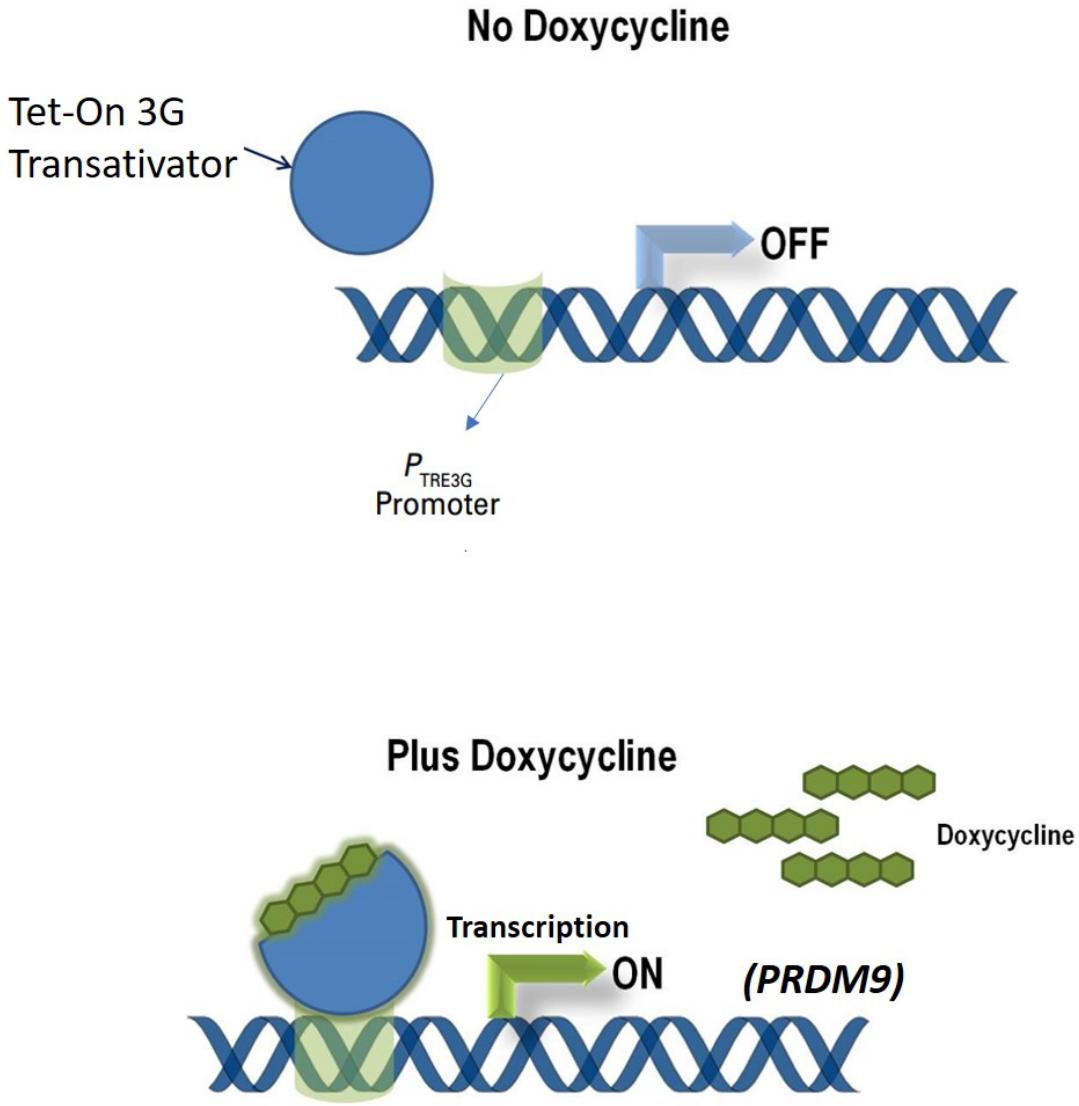

Figure 4.1 The (OFF/ON) inducible system can encourage *PRDM9* expression when doxycycline is added. The transactivator protein (blue) go through a conformational modification when doxycycline is used. This will help the protein to link to the tet-operator (tetO) (green) at the pTRE3G promoter which perfectly helps of the expression of PRDM9.

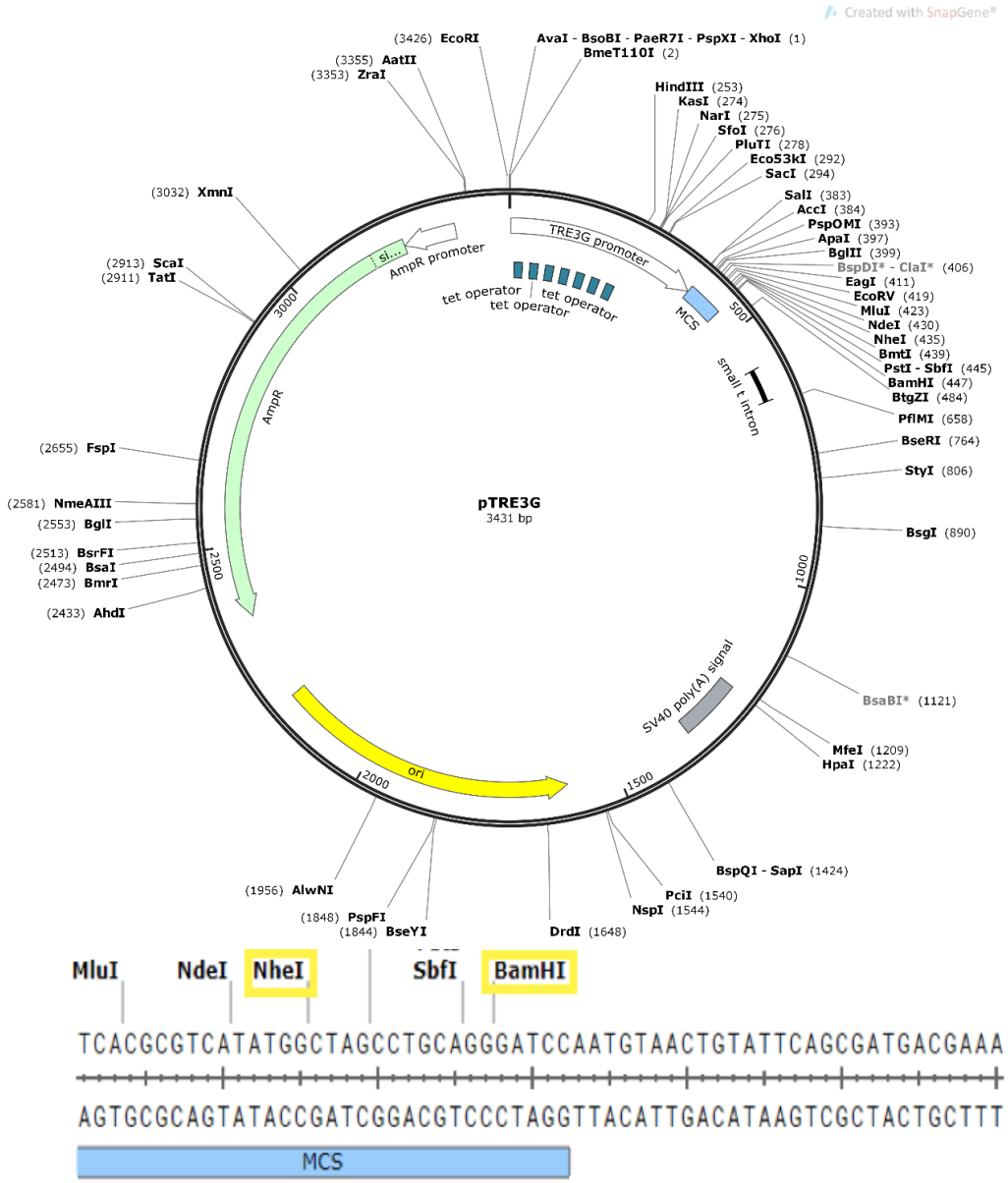

Figure 4.2 pTRE-3G plasmid map. PTRE3G vestor is 3431 bp Inducible Expression Plasmid System created for utilized with the Tet-On 3G system. pTRE3G consists of SV40V ploy A signal. Tet-responsive promoter (TRE-3G), Puc origin of replication, ampicillin resistance gene and different cloning site. Two restriction enzyme (*Bam*HI and *Nhe*I) were utilized. http://www.snapgene.com was utilized to adapt this figure.

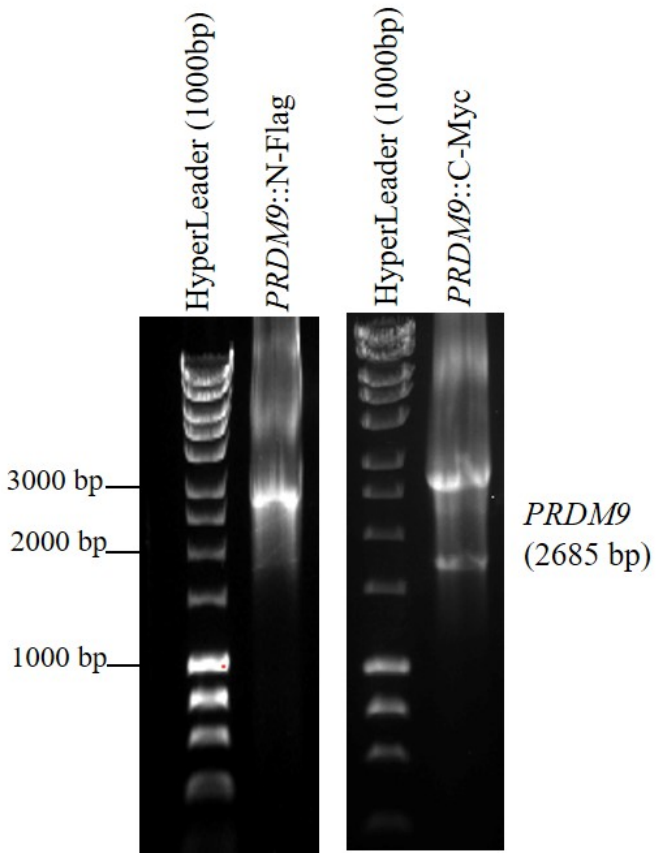

Figure 4.3 PCR amplification of *PRDM9* gene. RT-PCR was utilized to amplify the full open reading frame of *PRDM9.* 1% agarose gel prepared with a pic-green dye was used to detect the PCR products. Left gel displays the predict size of *PRDM9* fragment at 2685bp with N-Flag. Right gel displays *PRDM9* fragment with C-Myc on expected size. HyperLadder 1 Kb has been utilized as a marker.

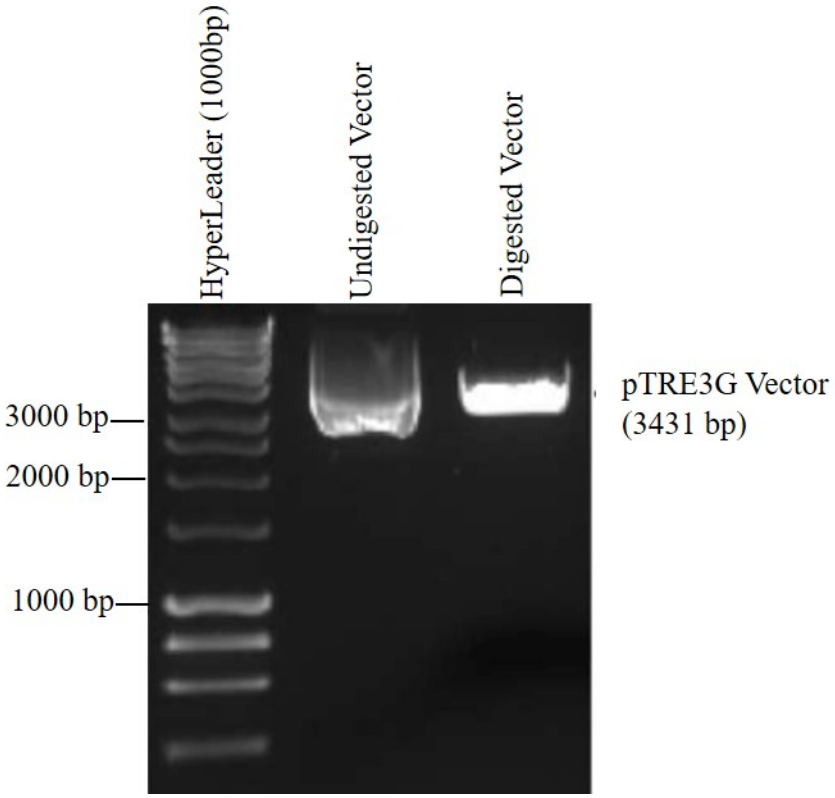

Figure 4.4 Cutting of pTRE3G plasmid. Lane 1 displays 1 Kb HyperLadder which utilized as a marker. Lane 2 displays an uncut pTRE3G as a negative control. Lane 3 shows restriction enzyme (*Bam*HI and *Nhe*I) cut pTRE3G then purified. 1% agarose gel prepared with pic green was utilized to detect the PCR products.

4.2.2 PCR Screening of colonies of *PRDM9::N-Flag and PRDM9::C-Myc* following transformation to *E. coli*.

We investigated whether the right colonies had been chosen after the transformation process by examining *E. coli* colonies. PCR took place to confirm that the successful insertion of *PRDM9* was carried on recombinant plasmids. A total of 12 plasmids containing *PRDM9::N-Flag* fragments and 11 plasmids containing *PRDM9::C-Myc* were selected from the *E. coli* (Figure 4.5).

Ten colonies with positive PCR results for *PRDM9::N-Flag* were selected for additional processes of confirmation, excluding colony 4, while for the *PRDM9::C-Myc* fragments, four colonies (13, 14, 15, 17) were selected for further confirmation.

4.2.3 Confirming the successfully cloned inserts utilizing *Bam*HI and *Nhe*I restriction enzymes

Validation of the insertion of *PRDM9::N-Flag* and *PRDM9::C-Myc* took place using two restriction enzymes. A digestion process of pTRE3G::PRDM9::N-Flag proved that colonies 2, 3, 6, 7, 8 and 9 were correct clones of the plasmids and had the desired fragment. Figure 4.6 shows two bands; the lower band is related to the insertion at 2685 bp while the upper band is related to the vector at 3431 bp. Colonies 1 and 10 showed lower bands of unexpected size and colony 5 showed only one band that was related to the vector.

Colonies 2 and 3 were subjected to a DNA sequencing to confirm that the fragments were subcloned successfully in the correct orientation and the insert had no mutations. The DNA sequencing data verified that the *PRDM9* sequence was 100% identical to the NCBI data and free from mutations.

A digestion restriction process of pTRE3G::PRDM9::C-Myc showed that colonies 13 14, 15 and17 displayed two bands with the upper band at 3431 bp, which is related to the vector,and the lower band being an unexpected size, which indicated unsuccessful cloning of pTRE3G::PRDM9::C-Myc, so we excluded the pTRE3G::PRDM9::C-Myc tag from further study.

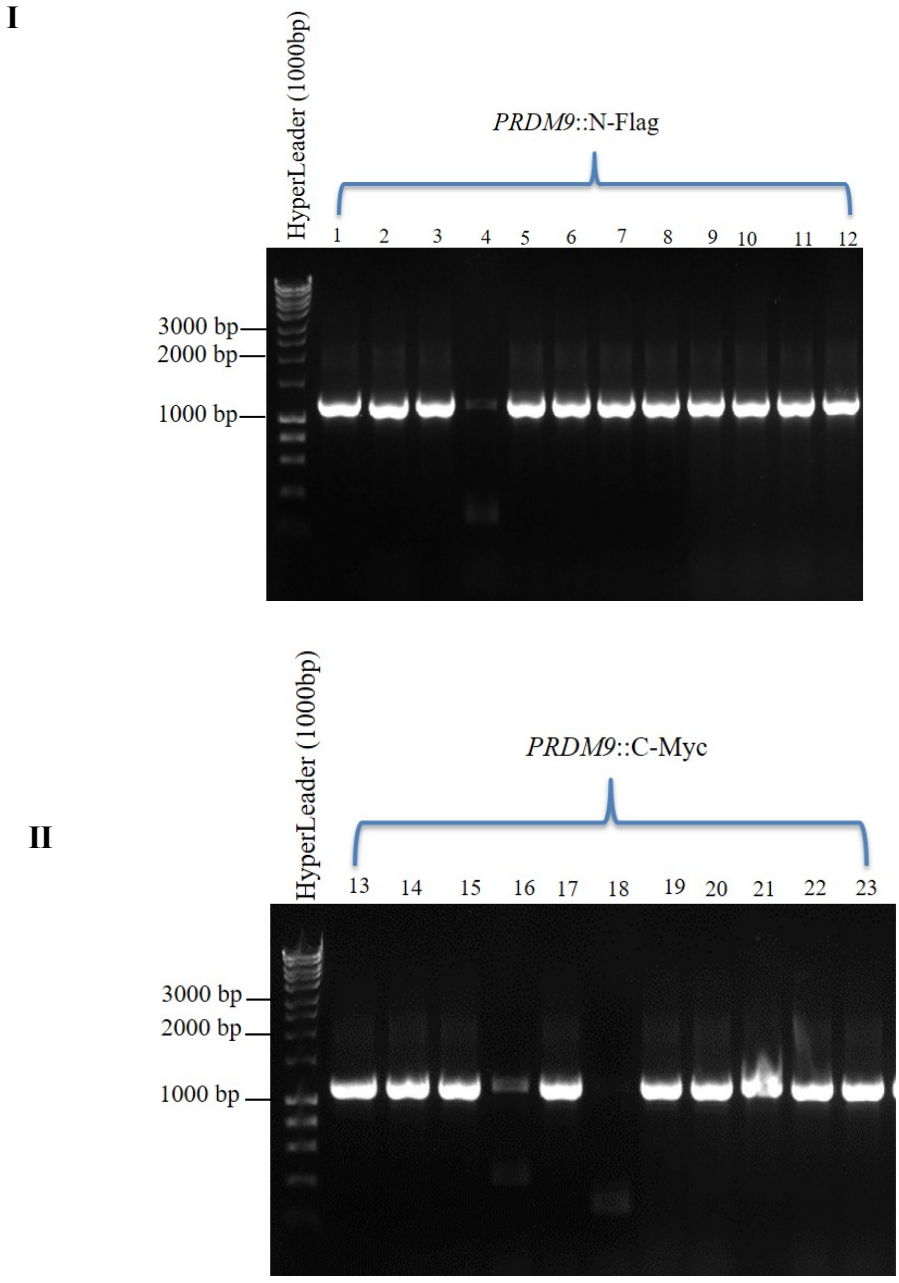

Figure 4.5 PCR profile analysis showing screening colonies after transformation stages. 1% agarose gel picture displays PCR screening data of *E.coli* colonies to find the recombinant plasmid via utilizing the *PRDM9* internal primers. I) Candidate colonies confirming the insert of (pTRE3G::*PRDM9*::N-Flag) and colonies number 1,2,3,5,6,7,8,9,10 have been detected for further study. II) Candidate colonies confirming the insert of (pTRE3G::*PRDM9*::C-Myc) and colonies number 13,14,15,17 have been detected for further study.

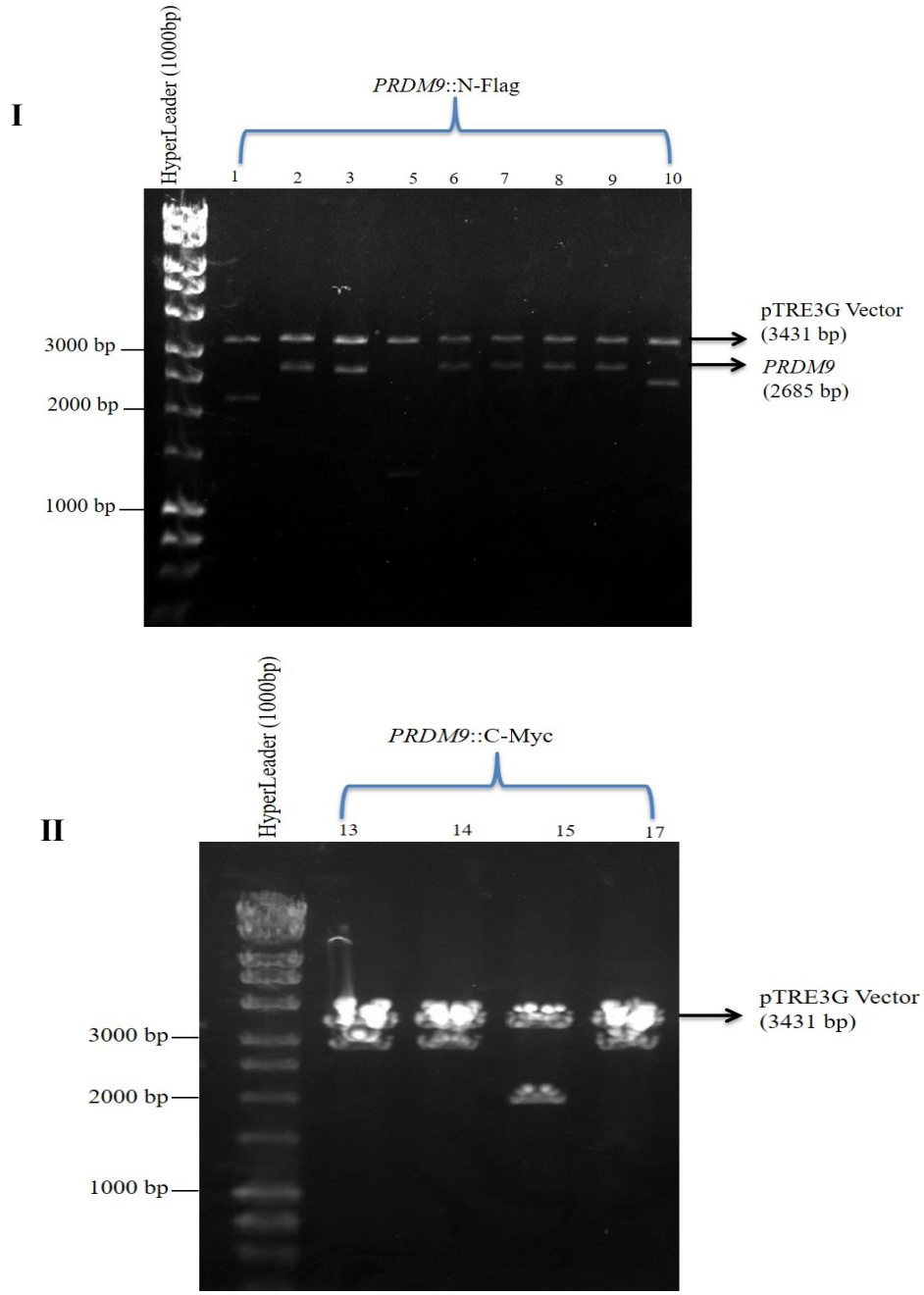

Figure 4.6 Cutting of recombinant plasmid with two restriction enzyme (*Bam*HI and *Nhe*I). I) Candidate colonies of (pTRE3G::*PRDM9*::N-Flag) colonies number (1 and 10) illustrating two bands and the fragments appeared in not predicted size of *PRDM9*. Colony number 5 shows only one band at 3431 bp. Colonies (2,3,4,6,7,8,9) were shown two bands the lower band at 2685 bp that is predicted size for *PRDM9* while the upper band at 3431 bp relates to pTRE3G vector. II) Candidate colonies of (pTRE3G:: *PRDM9*::C-Myc) colony (15) illustrating two bands and the fragments appeared in not predicted size of *PRDM9* as lower band appeared at approximately 2000 bp while the upper band at 3431 bp relate to pTRE3G vector. Colonies (13, 14, 17) illustrating two bands and the fragments appeared in not predicted size of *PRDM9*.

4.2.4 Generation of double-stable HCT116 Tet-on 3G cells

In this research, one of our goals was the production of a double – stable HCT116 Tet-On 3G cell line that would be able to induce *PRDM9* via controlling the pTRE3G promoter. Generation of this system for inducing overexpression of *PRDM9* in cancer cells is important to investigate *PRDM9* transcription activity. There are two important stages when creating a double-stable cell line to overexpress a target gene. In the first stage, cells should transfect a pCMV-Tet3G plasmid to allow expression of the transactivator protein via the G418 antibiotic. Previously in McFarlane lab, HCT116 cells transfected with pCMV-Tet3G plasmids have been made by Maryam Alahdal (Maryam Alahdal, phD thesis, 2017). The second stage involves generation of the double–stable cell line by co-transfecting HCT116 Tet-On 3G cells with established pTRE3G::*PRDM9*::N-Flag plasmids with a linear selection marker for puromycin. In the final step, double-stable transfected cells were chosen based on resistance to G418 and puromycin antibiotic (Figure 4.7).

4.2.5 Chosen of double-stable HCT116 Tet-On 3G cells

Various concentrations of puromycin were utilized to detect the lowest dose that was able to kill HCT116 Tet-On 3G cells before transfection. The HCT116 Tet-On 3G cells have been grown in media without any puromycin for 2 days. After that, the cells have been exposed to 0–10 μg/ml of puromycin for 5 days, as shown in Figure 4.8. The lowest puromycin concentration that suppressed the growth of HCT116 Tet-On 3G cells was 4 μg/ml. The HCT116 Tet-On 3G cell line has been cotransfected with pTRE3G::PRDM9::N-Flag or pTRE3G in addition to the puromycin linear selection marker. Cells were grown for 3 days in media without antibiotic, then 100 μg/ml of G418 and 4 μg/ml of puromycin have been added to the cultures. Following 4 days of antibiotic treatment, most cells did not survive, which may suggest a productive and efficient transfection process. After 2 weeks of utilizing 4 μg/ml of puromycin antibiotic, healthy and large colonies were transfected to grow individually in a 6-well plate (Figure 4.9), then transferred to 10 cm plates, then to T75 flasks. The harvested colonies were investigated to examine the overexpression of *PRDM9* in the presence or absence of 1 μg/ml doxycycline. The examined cells were cultured in high-quality Tet-system-approved foetal bovine serum because it contains no tetracycline.

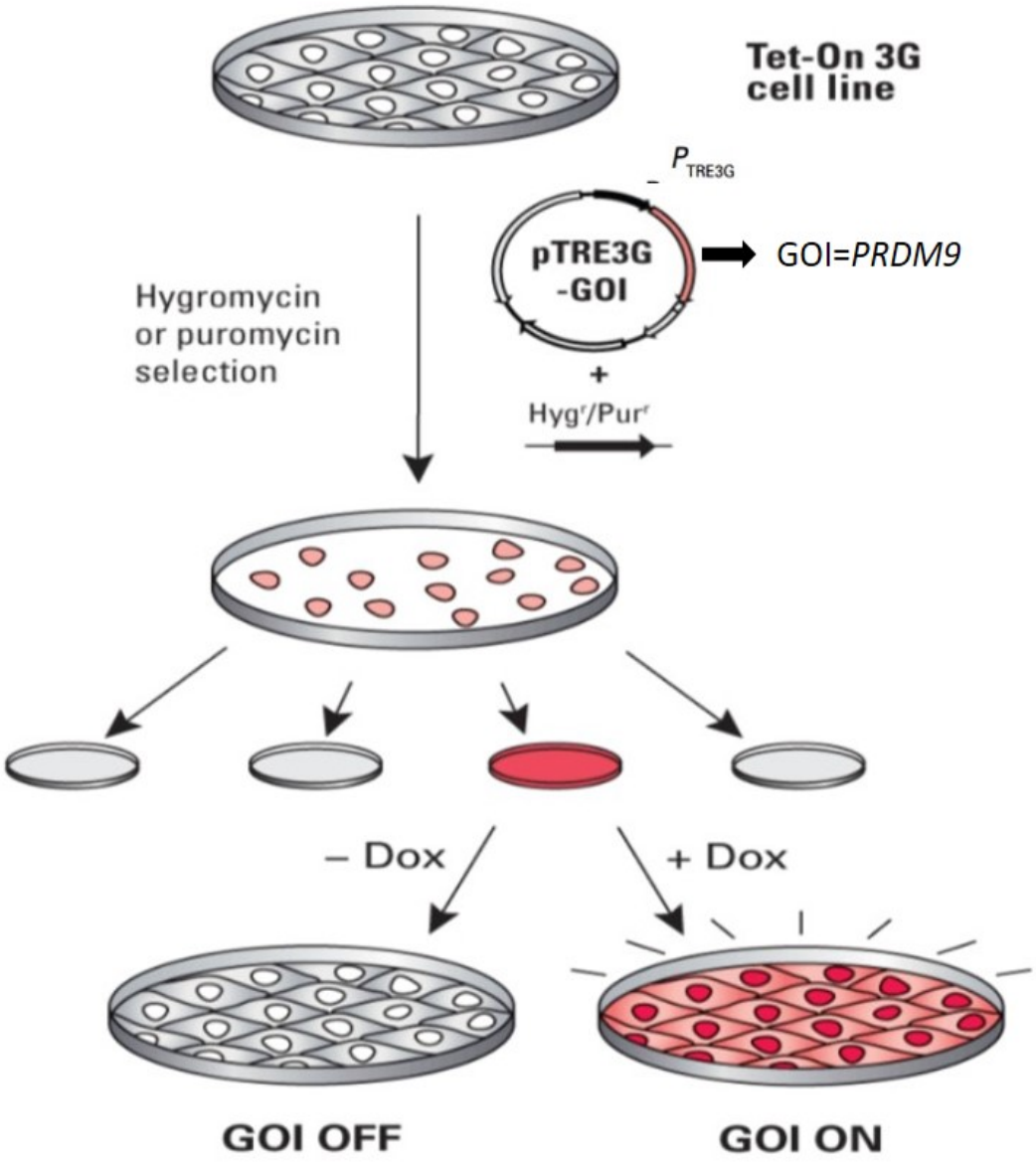

Figure 4.7 Diagram displaying the establishment double Tet-On 3G cells. The tetracycline-promoter controls the transactivator protein in HCT1116 Tet-On 3G cells. The establishment pTRE3G plasmids involving (*PRDM9*::N-Flag) have been transfected with a puromycin linear marker. Doxycycline (1 µL/ml) was utilized to examine overexpression of *PRDM9*.

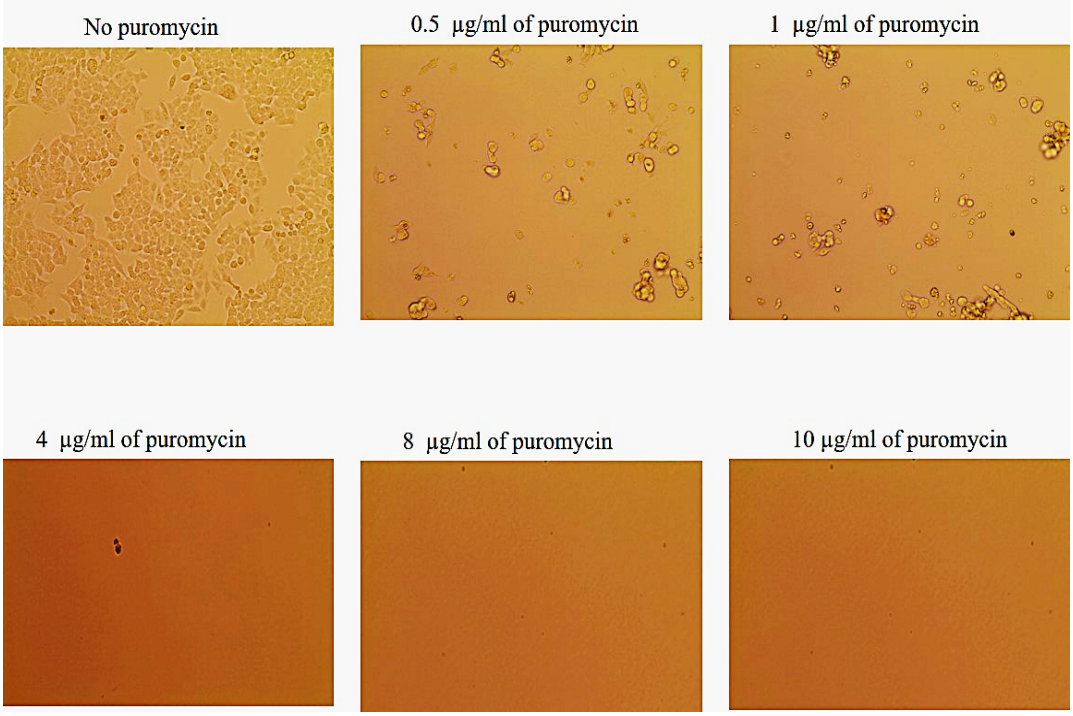

Figure 4.8 HCT116 Tet-On 3G cells have been exposed to several dosages of puromycin antibiotic. Untrasfected HCT116 Tet-On 3G cells were cultured for 2 days prior to using the various concentration of puromycin to detect the minimum amount that could stop growth of cells. The different doses (0–10 µg/ml) were utilized in each culture for 4–6 days. Untreated cells were utilized to contrast the effectiveness of puromycin on treated cells. A concentration of 4 µg/ml was enough to stop growth of HCT11 Tet-On 3 G cells.

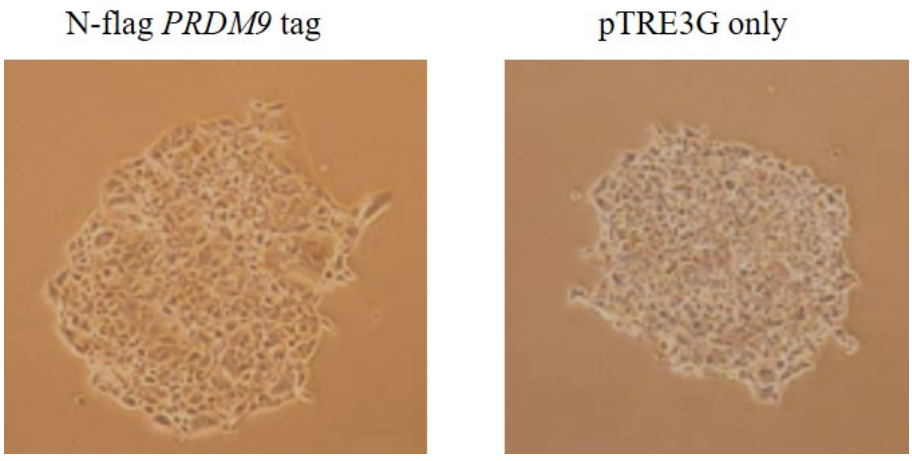

Figure 4.9 Samples of colonies of HCT116 cells resistant to puromycin. Picture displays healthy single colonies after 5 days of treatment with 4 µg/ml of puromycin. Cells were merged with PRDM9::N-Flag or pTRE3G alone.

4.2.6 Investigation of the overexpression level of *PRDM9* into HCT116 Tet-On 3G cells

Healthy colonies with possible tags have been investigated to validate the induction of *PRDM9* into HCT116 Tet-On 3G cells. Separately, each clone was cultured in the presence of 1 μg/ml doxycycline for 24 hours to examine the induction of PRDM9 in transfected cells with pTRE3G::*PRDM9*::N-Flag. The same number of cells were cultured in absence of doxycycline.

RT-PCR was used with 12 positive colonies appeared following the transfection of the recombinant vector pTRE3G::*PRDM9*::N-Flag to examine the induction of *PRDM9* in HCT116 Tet-On 3G cells after adding 1 μg/ml doxycycline treatment for 24 hours. *βACT* expression was used to test the quality of the synthesised cDNA (Figure 4.10.I) the data showed that clones (13/22) and (13/28) displayed high *PRDM9* expression while other examined clones did not show any expression. A colony that had pTRE3G (the vector) was considered a control (Figure 4.10.II) after storage the tow colonies (13/22 and 13/28) that shows successful integral of the recombinant plasmid, these colonies were re-investigated again for more affirmation. Each clone was cultured individually in the presence of 1 μg/ml doxycycline for 24 hours beside the cells cultured with no doxycycline treatment. Cells were harvested and the total RNA was isolated to synthesis cDNA to examine *PRDM9* expression. *βACT* expression was used to test the quality of the synthesised cDNA. cDNA from testis was utilized as a positive control for this experiment to examine the expression of *PRDM9*. The data confirmed high expression of *PRDM9* in examined colonies in presence of doxycycline when relevant to absence of doxycycline Figure (4.11).

qRT -PCR was carried out for further analysis to measure the expression of *PRDM9* in clones 13/22 and 13/28 following addition of doxycycline. qRT -PCR analysis illustrated an observed expression of *PRDM9* in both colonies after treatment of the cells with 1μg/ml doxycycline, while there was no expression of *PRDM9* in the untreated cultures. The *PRDM9* results were controlled to the qRT-PCR data of two reference genes GAPDH and *βACT*. qRT-PCR corresponded to the conventional RT-PCR data, and it showed significant induction of *PRDM9* after 24 hours of culture treatment; however, no expression of *PRDM9* was detected in the absence of doxycycline (Figure 4.12).

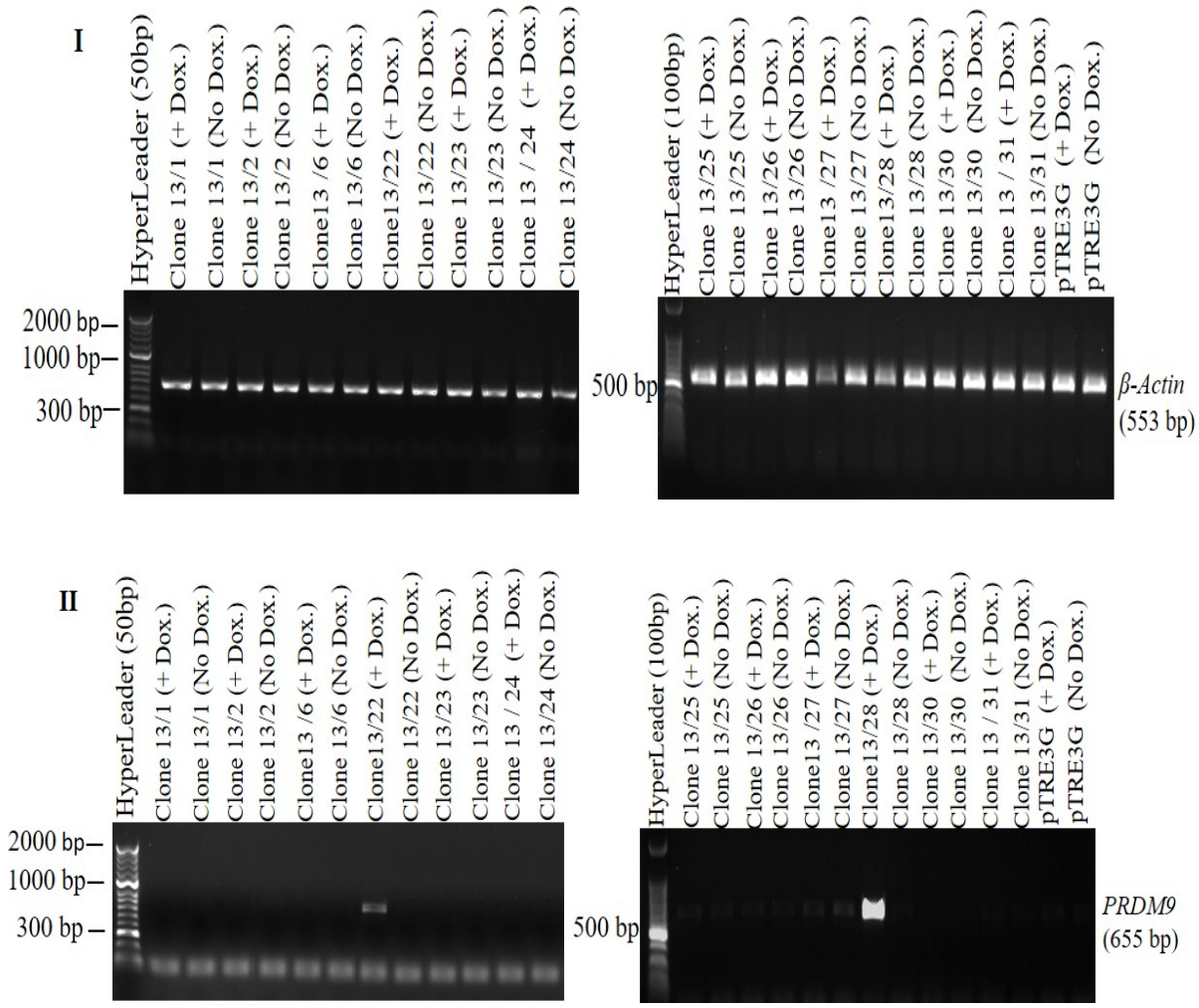

Figure 4.10 RT-PCR analysis displays *PRDM9* gene expression in HCT116 Tet-On 3G cell line following transfection. I) The quality of cDNA was examined by checking *βACT* mRNA. II) Various colonies were chosen to examine the induction of *PRDM9* after using doxycycline. Expression of PRDM9 in the presence of doxycycline were detected in two colonies (13/22 and 13/28).

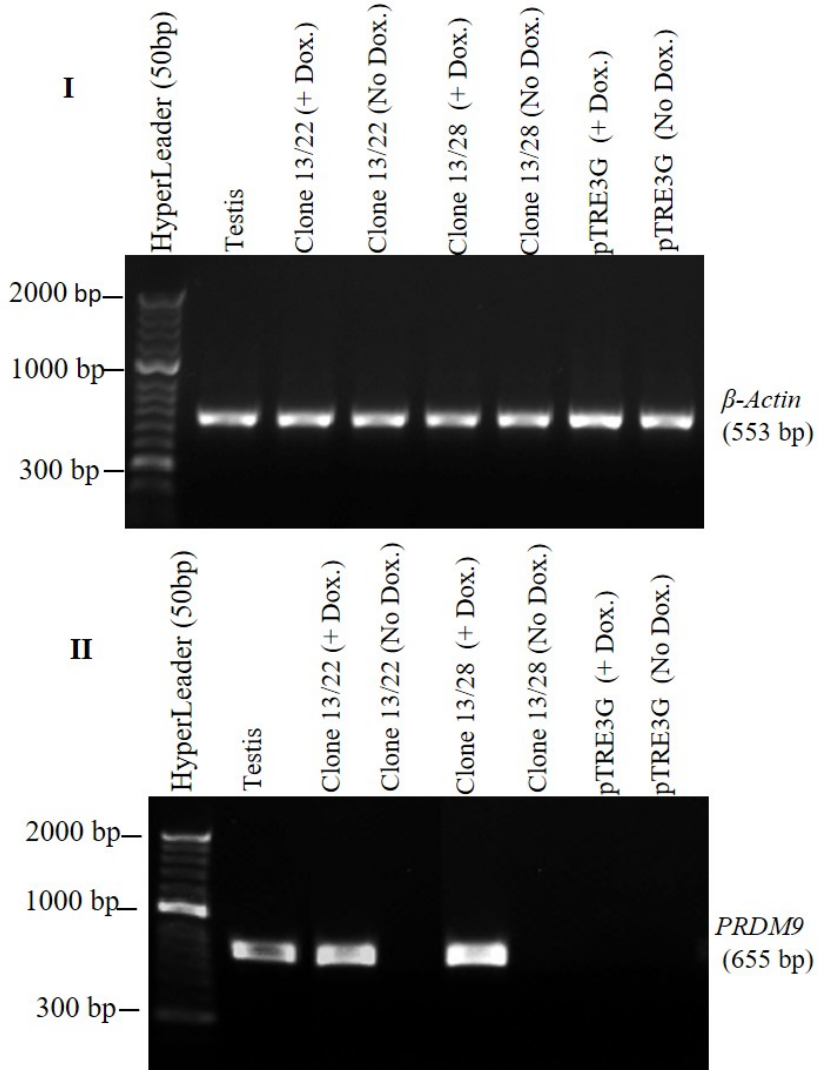

Figure 4.11 Analysis of proven expression of PRDM9 in 2 independent clones (13/22 and 13/28) in HCT116 Tet-On3G cells. I) The quality of the cDNA was examined by checking *βACT* mRNA. RT-PCR data illustrates the expression of PRDM9 after addition of doxycycline treatments. The testis is presented as a positive control for PRDM9 expression.

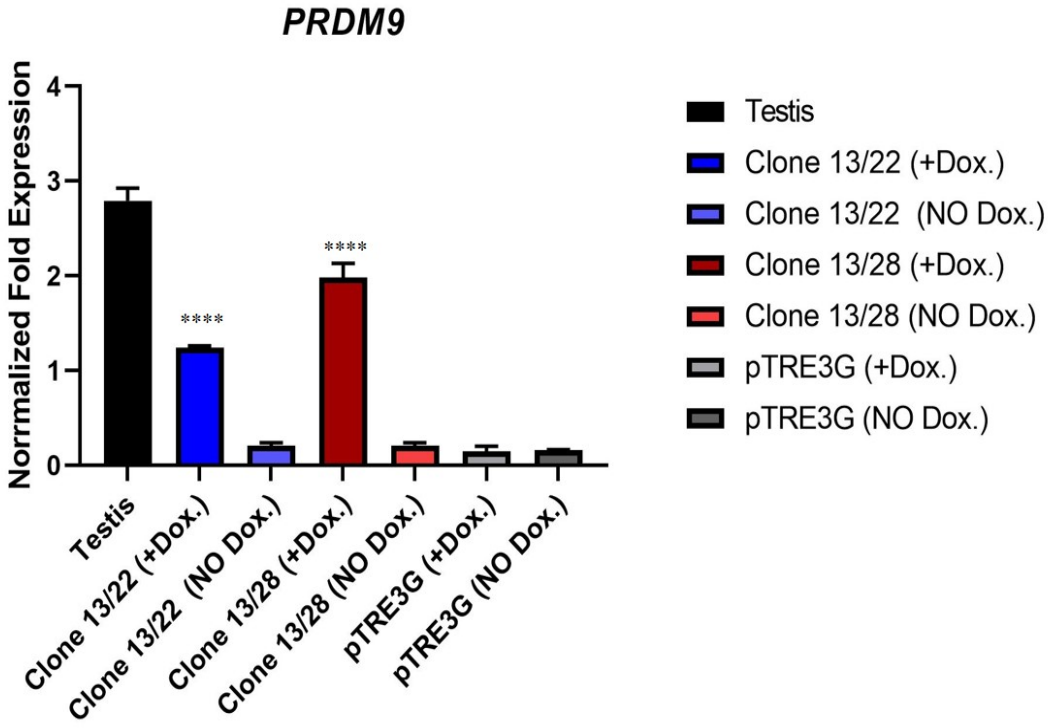

Figure 4.12 qRT-PCR analysis showing the mRNA levels of PRDM9 in two independent clones (13/22 and 13/28) in HCT116 Tet-On 3G cells. Clear expression of *PRDM9* was detected following doxycycline induction in both clones (13/22 as well as 13/28), while in the absence of doxycycline slight expression of *PRDM9* was detected. The testis is presented as a positive control for PRDM9 expression. The *PRDM9* data were relative to the qRT -PCR data of 2 references genes, *GAPDH* and *βACT*. P values presented significant changes in presence of doxycycline in clones (13/22 and 13/28), relative to the presence of doxycycline in (pTRE3G) (**** P value < 0.0001).

4.2.7 Investigation of PRDM9 protein in HCT116 Tet-On 3G cells

RT-PCR data showed that clones 13/22 and 13/28 displayed high *PRDM9* expression while other clones did not show any expression. Individual colonies 13/22 and 13/28 that had tags of potential interest were examined for the presence of N-flag when 1 μg/ml of doxycycline was utilized. In this study, commercial anti-flag antibodies (Cell Signalling antibody #8146 and Sigma #F1408) were utilized. Separately, each clone (13/22 and 13/28) was cultured in high-quality Tet-system foetal bovine serum medium that contained no tetracycline. Then 1 μg/ml was added to some cultures while other cultures were grown without any doxycycline. The cells grown in the absence of doxycycline were utilized as a control to examine the effects of doxycycline treatment. The cells were harvested, then lysate from each individual clone was extracted.

A western blot test was carried out to detect the N-Flag tag that was integrated with PRDM9 and the extracted lysates were checked against two different types of commercial anti-Flag antibodies. The PSNF5 cell line was transfected with an established clone of the *BLM* gene incorporated with a tagged sequence and utilized as a control to examine an anti-FLAG antibody. BLM::Flag appeared at an unexpected size of 160 kDa. The data from the western blot analysis displayed no induction signal of PRDM9::N-Flag at 104 kDa (Figure 4.13). This could be related to the fact that the N-Flag protein was not co-produced correctly with PRDM9. On the other hand, lysates of negative controls displayed signals of flag proteins that were not specified. BLM::Flag (positive control) showed a signal at an unexpected size of 160 kDa. This could be because the antibodies are not working effectively or these antibodies are nonspecific.

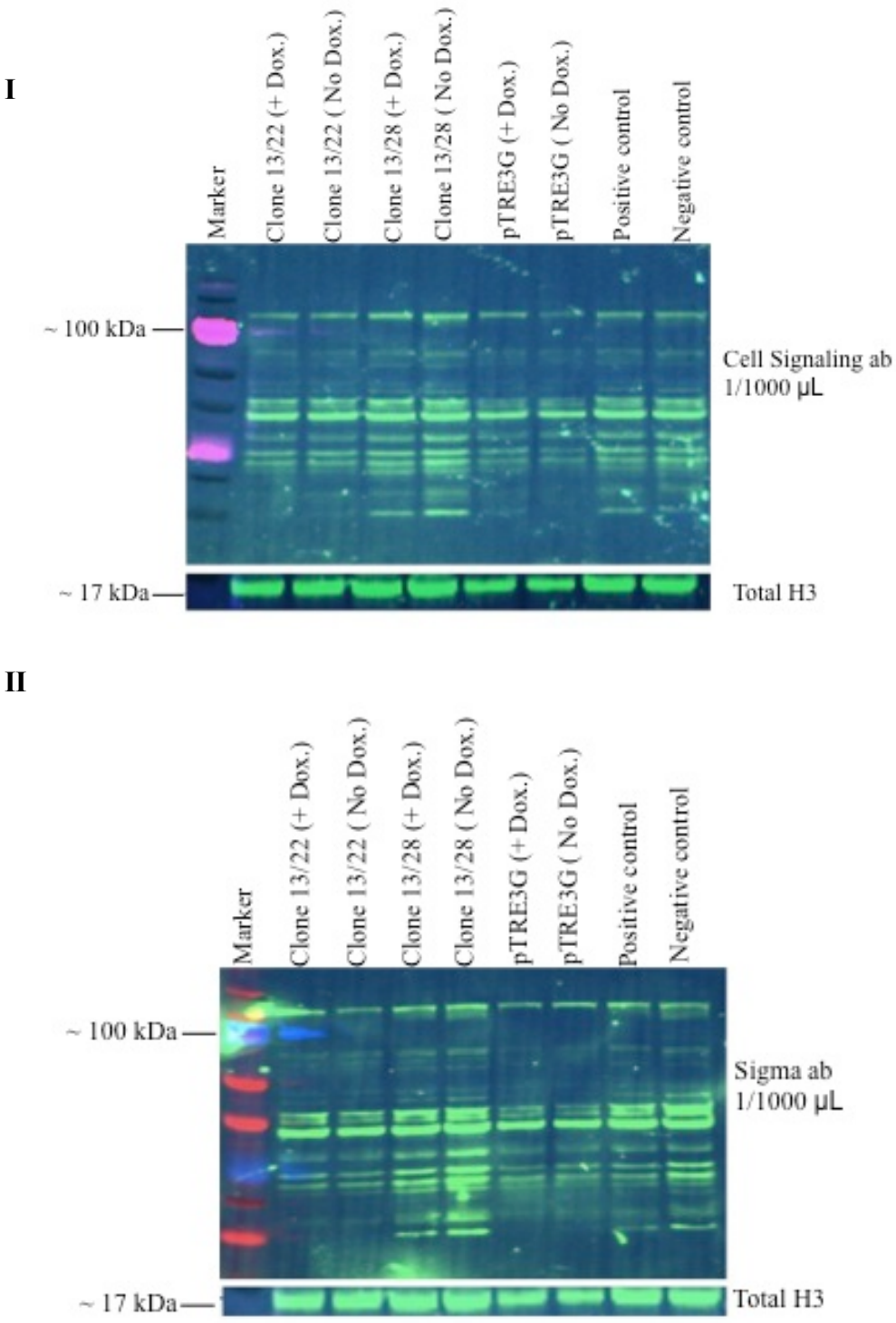

Figure 4.13 Western blot showing the N-Flag tag in two independent clones (13/22 and13/28) in HCT116 Tet-On 3G cells. Clones 13/22, 13/28 and pTRE3G that have the PRDM9::N-Flag have been treated with doxycycline for 24 hours. I) Lysates have been probed against anti-flag antibodies from a cell signalling company. II) Lysates have been probed against anti-flag antibodies from sigma company. No induction of PRDM9 at the expected size of 104kDa appeared. Indeed, the PSNF5 cell line with the BLM::FLAG showed a signal at nearly 100 kDa while the expected size for the BLM::FLAG is nearly 160 kDa.

4.3 Discussion

It has been established that *PRDM9* is a meiosis-specific gene. Its expression occurs in the initial phases of prophase I of meiosis (Baudat et al., 2010; Sun et al., 2015). In order to specify the sites of recombination or hotspots, the PRDM9 binds to DNA sequence (Baudat et al., 2010; Bilings et al., 2013; Baker et al., 2014). This binding to hotspot recruits other proteins, like SPO11, thereby allowing the process of recombination to initiate. It has recently been demonstrated that binding of PRDM9 to promoter sequences and adjacent transcription start sites (TSS) results in activation of some genes. It implies that PRDM9 can be involved in regulation of transcription (Altemose et al., 2017). It was proposed that PRDM9 might serve as a transcriptional activator in humans. Activation of two meiosis-specific genes namely *CTCFL* and *VCX* by PRDM9 has also been demonstrated (Altemose et al., 2017).

In addition to this, we aimed to throw more light on roles played by PRDM9. For this purpose, open-reading frame of *PRDM9* was merge with tags then transferred to the HCT116 Tet-On 3G system. This was done to investigate the influence of PRDM9 protein on gene regulation in cancer cells and for validating the antibody raised against PRDM9. Hence, the amino terminus (N-terminal) of the PRDM9 sequence was tagged with the Flag tag. These tags are made up of small sequences which in most of the cases do not affect the function of the protein.

In case of eukaryotes, the Tet-On 3G system has proven to be one of the most efficient systems for inducible gene expression. It allows expression of the gene of interest (GOI) to be controlled whether the DOX treatment is absent or present (Urlinger et al., 2000). Two clones of the double-stable HCT116 Tet-On 3G cells were generated in this research which carried a recombinant plasmid of pTRE3G::*PRDM9*::N-Flag. DNA sequencing was carried out to examine the *PRDM9* sequence and it was found that the inserted sequence has no mutations and was oriented correctly. RT-PCR and qRT-PCR assays were conducted to analyse the expression of integrated *PRDM9* into HCT116 Tet-On 3G cells. mRNA *PRDM9* levels were found to be increased after doxycycline induction. However, the non-induced HCT116 Tet-On 3G cell line showed slight expression of *PRDM9*.

The recombinant DNA technology allows insertion of small sequenced tags for detection of proteins with the help of antibodies against the tags. Two anti-FLAG antibodies (Sigma- F1408 and Cell Signaling-8146) were utilized in western blot analysis through this study. The PRDM9 protein signals were not overexpressed in presence of doxycycline this can be due to that the Tet On 3G system not act competently in translation level. Considering the protein signals of positive control which appeared in unexpected size, it can also be stated that the quality of anti-FLAG antibodies was not good enough to generate accurate results.

Chapter 5

Biological roles of TEX19 in human cancer cells

5. Biological roles of TEX19 in several human cancer cells

5.1 Introduction

The binding of PRDM9 to promoters of certain genes results in activation of histone trimethylation resulting in activation of expression of the relevant genes in HEK293T cells (Altemose et al., 2017). It may indicate that one meiotic regulator gene can affect transcriptional landscape in human (Altemose et al., 2017). This suggest meiotic regulators might control chromatin dynamics in cancer cells. *TEX19* is a mammalian-specific gene with expression restricted to the testis in healthy human adults, but is also expressed in cancer cells, so it is classified as a CTA gene (Feichtinger et al., 2012; Planells-Palop et al., 2017). Ongoing work in the McFarlane group had suggested TEX19 is required for cancer cells proliferation and might regulate gene expression (Planells-Palop et al., 2017).

In rodents, the *TEX19* orthologue has undergone a duplication to generate *Tex19.1* and *Tex19.2*, i.e. two gene paralogues (Kuntz et al., 2008). *Tex19.1* is expressed in adult testis, placenta and in the early embryo. Expression of *Tex19.2* has been found in adult testis and in the gonadal ridge. *Tex19.1* is likely involved in meiotic cell division, as *Tex19.1* deletion resulted in the disruption of meiotic synapses of chromosomes during spermatogenesis (Yang et al., 2010). It is proposed that *Tex19.1* is the murine functional orthoulouge of human *TEX19* as these genes have genomic positions (Kuntz et al., 2008). The pattern of expression of *Tex19.1* in embryonic stem cells (ESCs) is also almost the same as the pattern of expression of *Oct4* gene. This implies that *Tex19.1* has a function in regulating stemness, and Tex19.1 protein has been found to be linked with self-renewal of ESCs in mice (Kuntz et al., 2008; Tarabay et al., 2013). Human TEX19 protein is found to be crucial for cancer cell self-renewal as well as proliferation of cancerous cells. Accordingly, oncogenesis and human TEX19 have been suggested to be linked (Planells-Palop et al., 2017).

Expression of *TEX19* has previously been reported in several different cancerous cells and tissues and not in healthy and normal tissues with the exception of placenta and germ cells of adult testes. It implies that *TEX19* may serve as an oncogenic factor (Feichtinger et al., 2012). After this, it was reported that knockdown of *TEX19* in cancerous cells not only results in inhibition of proliferation, as well as a delay in progression of S-phase. But also causes transcriptional changes. It was proposed that *TEX19* may serve as a transcriptional regulator for several genes which are involved in promoting proliferation of cancerous cells. RNA collected from *TEX19* depleted cells and untreated cells were carried out for RNA sequencing analysis. Comparison of the results for the two groups indicated considerable changes in extent of transcription of 80 genes including potential oncogenes (Planells-Palop et al., 2017). Certain genes are involved in controlling growth and proliferation of cells. These genes are in turn regulated through chromatin modification of different forms (Cai et al., 2011). The transcriptional activation or inactivation generally involves the regulator function performed by specific post-translational modifications of histones within chromatin (Venkatesh et al., 2015).

Here, the influence of depletion of human *TEX19* on proliferation of cancerous cells has been investigated. Moreover, we wished to further validate the anti-TEX19 antibodies. This research therefore aims to validate the findings and further extend the investigation with the help of distinct cancer cell lines.

5.2 Results

5.2.1 Knockdown of TEX19 in several cancer cells

It was found that TEX19 is involved to control cancer cell proliferation (Planells-Palop et al., 2017). In this study we wanted to confirm the biological roles of TEX19 depletion in some cancer cells including SW480, H460, HCT116 and an HCT116 cell line derivative overexpressing N-HA:: TEX19,which had not previously been tested (This cell line was constructed previously in our lab).

5.2.1.1 Depletion of TEX19 in SW480 cancer cell line

TEX19 mRNA knockdown was performed in a SW480 cell line utilising small interfering RNA. siRNA number 7 was utilized to deplete the *TEX19* in all experiment because its ability to effects on protein coding region specifically in the exon number 2 of the TEX19 sequence. Previously siRNA 7 has been demonstrated to provide the optimum TEX19 depletion. siRNA 7 was transferred into cultures for 3 days. Untreated cells and non-interfering RNA were utilized as control for this experiment. RNA was extracted individually from each culture and cDNA were synthesised. RT-PCR analysis and qRT - PCR was used to detect the mRNA of *TEX19* and measure efficiency of depletion. The data in Figure 5.1 show that the cells cultured with siRNA7 have depletion in *TEX19* mRNA levels relative to the non-interfering RNA control.

Western blotting was utilized to assess alterations of TEX19 protein following the treatment of siRNA. siRNA was utilized for 3 days then cells were harvested and protein extracted. Newly purchased anti TEX19 antibody (R&D system; # AF6319) was used to identify TEX19 protein level. Untreated cells as well as non-interference presented an obvious band in nearly 23 kDa using the anti-TEX19 antibody. Notable depletion of TEX19 protein level occurred when siRNA7 was utilized (Figure 5.2). Western blot data show band at nearly ~23 kDa while the expected size of human TEX19 is 18.5 kDa, post-translational alterations of TEX19 could be proposed as a reason for migration at the higher than expected molecular weight, recombinant TEX19 purified in *Escherichia coli* also migrates at ~23 kDa (McFarlane lab), suggesting this is due to conformational changes.

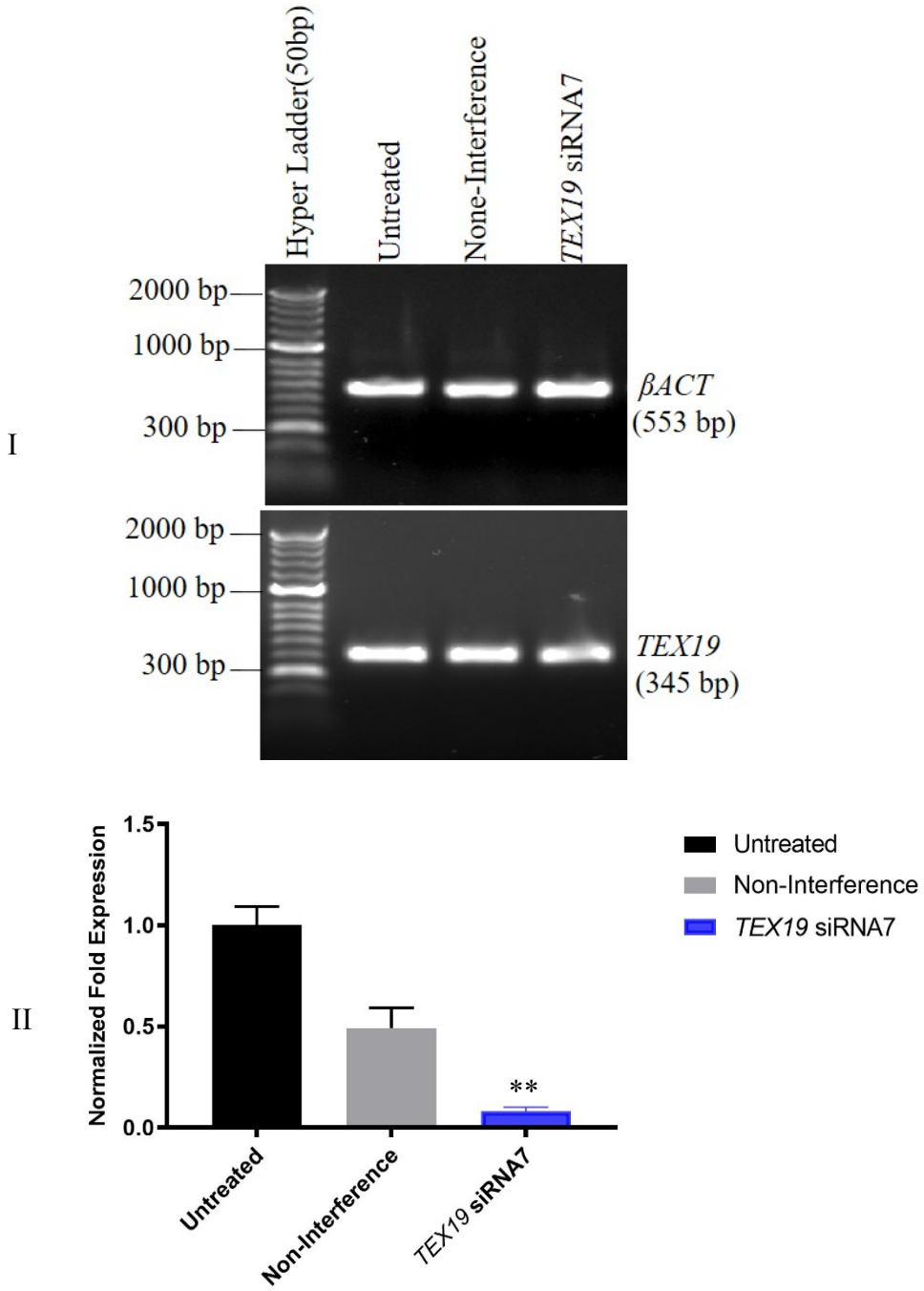

Figure 5.1 mRNA levels of *TEX19* after siRNA treatment in SW480 cells.
(I)The quality of the cDNA was examined by checking *βACT* mRNA. Clear expression of *TEX19* was detected in untreated and non-interference with slight expression in cells treated with siRNA7. (II) The bar chart displays the mRNA levels of *TEX19* in SW480. The *TEX19* mRNA data were normalised to the qRT-PCR data of two genes, *GAPDH* and *βACT*. P values presented significant changes when siRNA7 was utilised compared to the non-interference (** P value < 0.01).

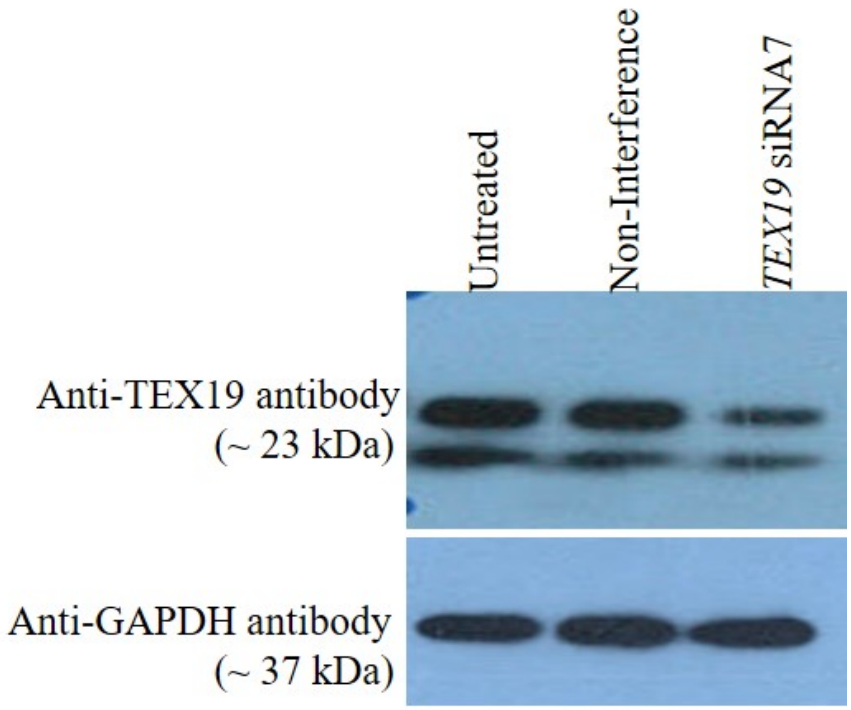

Figure 5.2 Western blot showing the amount of TEX19 protein following siRNA treatment in SW480 cells. siRNA number 7 was used to deplete TEX19 in SW480 cell line. Depleted was observed in cultures treated with siRNA7 at the size (roughly 23 kDa) compared to the positive control of untreated cells and non-interference RNA. GAPDH was carried out in this study as a loading control.

5.2.1.2 Depletion of TEX19 in H460 cancer cell line

siRNA number 7 was used to deplete the *TEX19* gene transcripts in lung cancer cell line H460. This cell line was cultured for 3 days with daily treating with siRNA7. Untreated cells and (non-interfering RNA) were utilized as control to detect *TEX19* knockdown. After the treatment, total RNA was extracted and cDNAs was synthesised. RT-PCR and qRT - PCR was used to detect the mRNA of *TEX19* and measure efficiency of depletion. The data in (Figure 5.3) shows that the cells cultured with siRNA7 presented significant depletion in *TEX19* mRNA level relative to the non-interfering RNA control (*** P value < 0.001).

The alterations of TEX19 protein following the treatment of siRNA7 was also examined using western blotting. Protein was extracted from all the samples after the treatment. Data showed significant depletion of TEX19 protein level when siRNA 7 was utilized (Figure 5.4). GAPDH was carried out in this experiment as a positive loading control.

5.2.1.3 Depletion of TEX19 in HCT116 cancer cell line

HCT116 cells were cultured and treated with siRNA 7 for 72 hours beside two different controls (the non-interference and untreated cells). The cells were then harvested and total RNA was extracted from each sample. RT-qPCR was carried out to detect *TEX19* mRNA levels after the treatment. The data showed that considerable knockdown of *TEX19* mRNA levels relative to the controls (Figure 5.5).

Western blot was also utilized to examine the TEX19 knockdown. Anti-TEX19 (R&D, #AF6319) was utilized and TEX19 migrated with a size of approximately 23kDa. Western blotting data showed dual bands, but the specificity of antibody has been confirmed via knockdown of siRNA 7. Cells treated with siRNA7 showed considerable reduce in the level of protein when relative to untreated cells as well as non-interference cells. Loading levels of the protein was validated via utilizing GAPDH antibody and the signal showed at the expected size of 37 KDa (Figure 5.6).

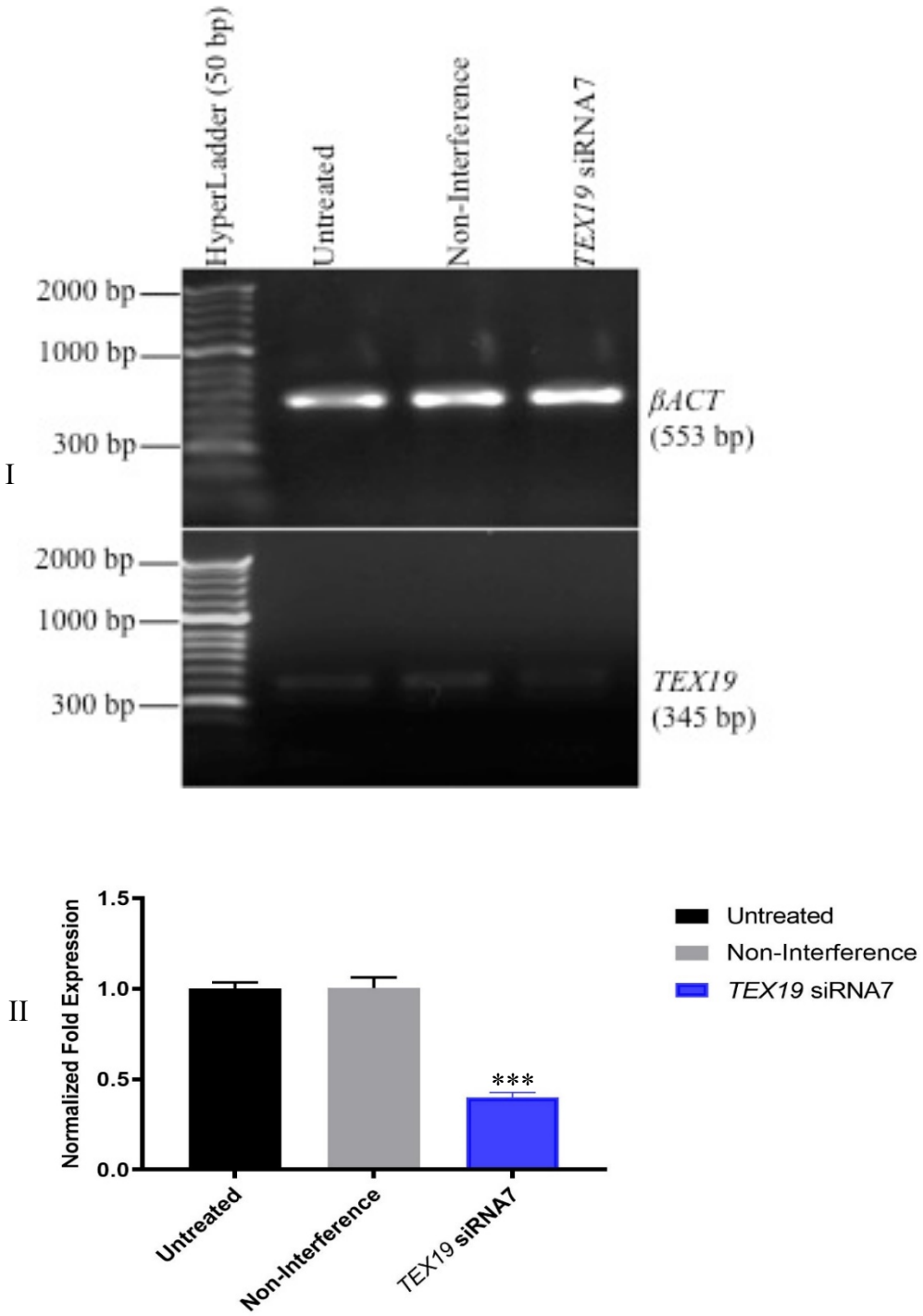

Figure 5.3 mRNA levels of *TEX19* after siRNA treatment in H460 cells.
(I)The quality of the cDNA was examined by checking *βACT* mRNA. Faint band of *TEX19* expression was observed when TEX19 primers were utilized. (II) The bar chart displays the mRNA levels of *TEX19* in H460. The *TEX19* mRNA data were normalised to the qRT-PCR data of two genes, *GAPDH* and *βACT*. P values presented significant changes when siRNA7 was utilised compared to the non-interference (*** P value < 0.001).

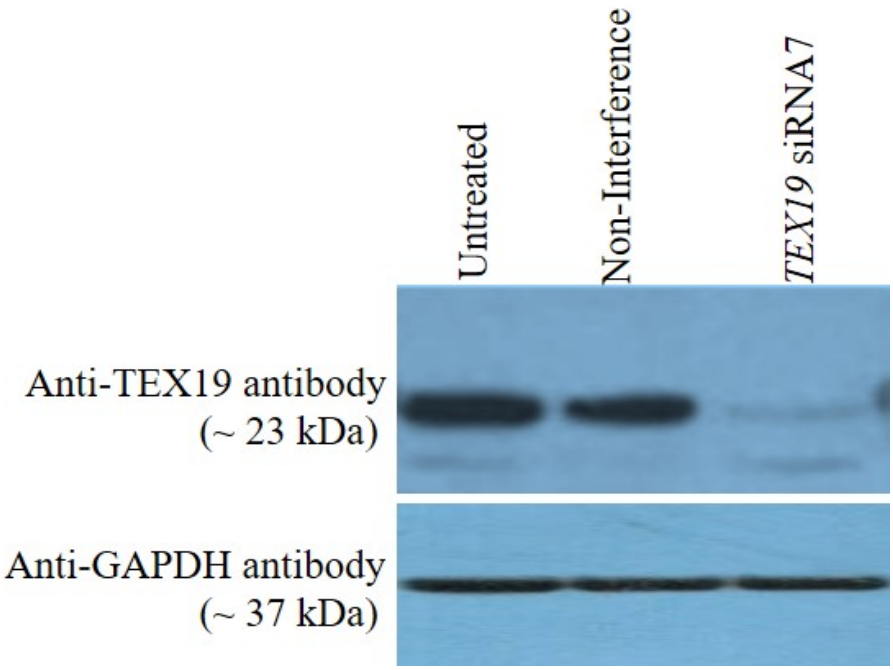

Figure 5.4 Western blot analysis of TEX19 protein following siRNA treatment in the H460 cells. siRNA number 7 was used to deplete TEX19 in H460 cell line. Depleted was observed in culture treated with siRNA7 compared to the controls untreated cells and non-interference. TEX19 migrates at approximately 23kDa. GAPDH was carried out in this study as a positive loading control.

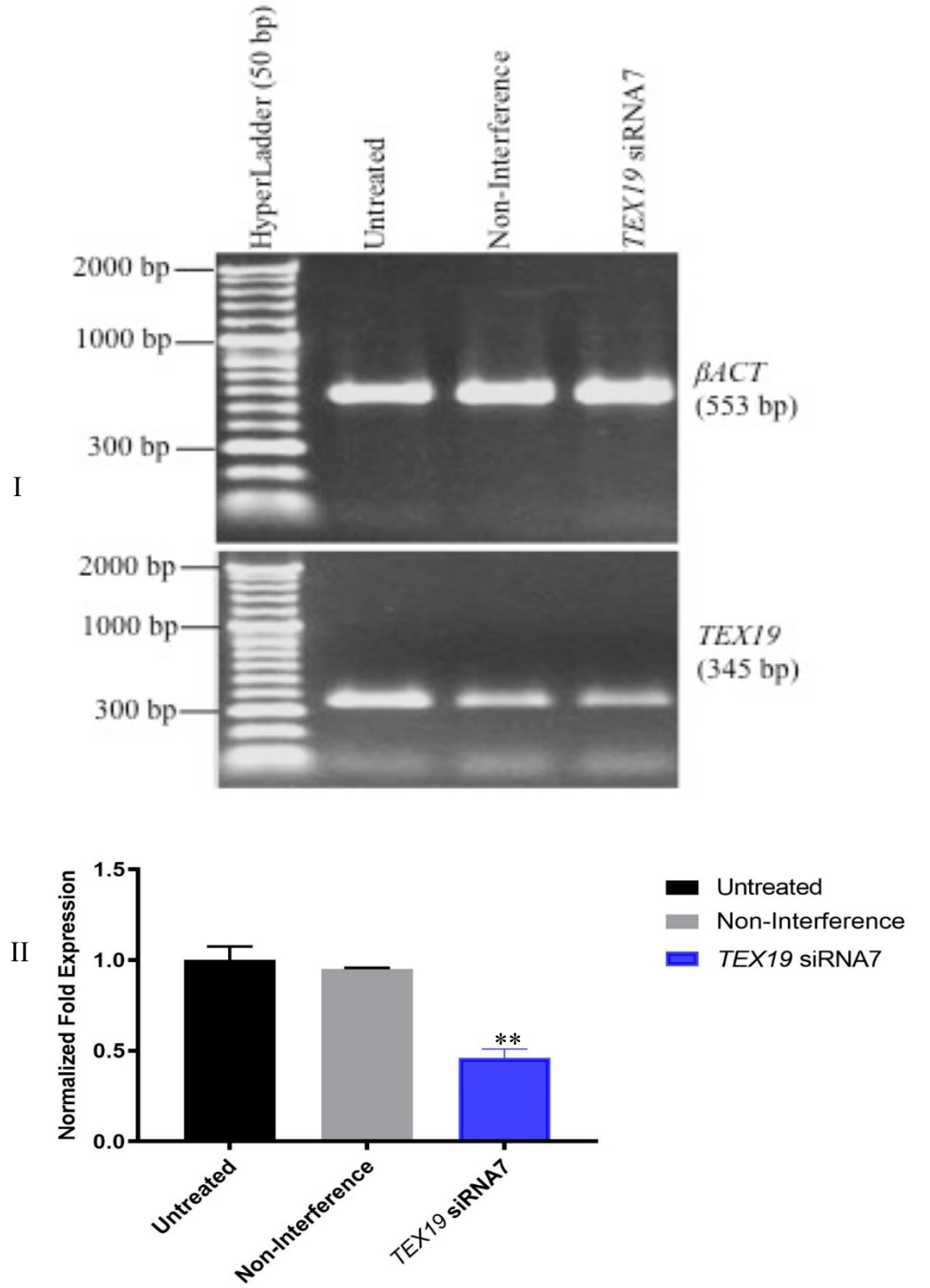

Figure 5.5 mRNA levels of *TEX19* after siRNA treatment in HCT116 cells.
(I)The quality of the cDNA was examined by checking *βACT* mRNA. Clear expression of *TEX19* was detected in expected size at 345 bp. (II) The bar chart displays the mRNA levels of *TEX19* in HCT116. The *TEX19* mRNA data were normalised to the qRT-PCR data of two genes, *GAPDH* and *βACT*. P values presented significant changes when siRNA7 was utilised compared to the non-interference (** P value < 0.01).

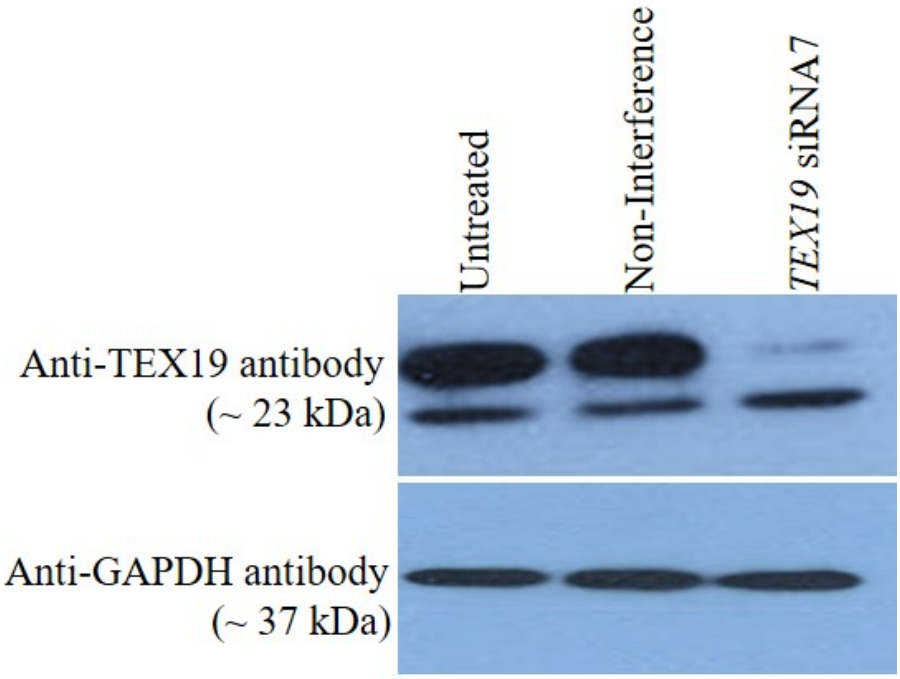

Figure 5.6 Western blot analysis of TEX19 protein following siRNA treatment in the HCT116 cells. siRNA number 7 was used to deplete TEX19 in HCT116 cell line. Depleted was observed in culture treated with siRNA7 compared to the controls untreated cells and non-interference. TEX19 migrates at approximately 23kDa. GAPDH was carried out in this study as a positive loading control.

5.2.1.4 Depletion of TEX19 in *TEX19*- HA HCT116 cancer cell line

In the McFarlane lab a constructed in which the amino terminus of *TEX19* was tagged with HA and cloned into a pCMV expression system. After that, it was transfected into the HCT116 cell line (*TEX19-HA* overexpression HCT116) (M. Hakami and E. Vernon/unpublished data). Here, the knockdown of *TEX19 HA::TEX19* was done by utilizing siRNA7 and compare the result with non-interfering RNA. After 72 hours of treatment, the knockdown of *TEX19* was evaluated at transcription and translation levels. RT-PCR data of *TEX19* gene expression showed that bright bands for *TEX19* in all samples (Figure 5.7.I). qRT - PCR was utilized to detect the mRNA of *TEX19* and measure efficiency of knockdown. The data in Figure 5.7.II show that the cells cultured with siRNA7 have a clear reduction in *TEX19* mRNA levels comparing with non-interfering RNA control.

The TEX19 protein depletion levels was examined by utilizing western blotting. The data shows two bands when the protein were utilized with anti-TEX19 antibody.
The strong signals appeared in upper band at nearly 25kDa with untreated and non-interfering RNA controls. Cells treated with siRNA7 showed reduced signal compare to the controls. Also, data showed lower band at nearly 23kDa with remarkable depletion of TEX19 protein after utilizing siRNA7 while strong signal appeared in both controls. This data indicate that the reduction signal is associated with TEX19 endogenous protein. Anti-HA tag antibody (Cell Signalling; #2367) was utilized with these lysates and data displayed one band at nearly ~25 kDa with significant inhibition of TEX19 when siRNA7 was utilized (Figure5.8).

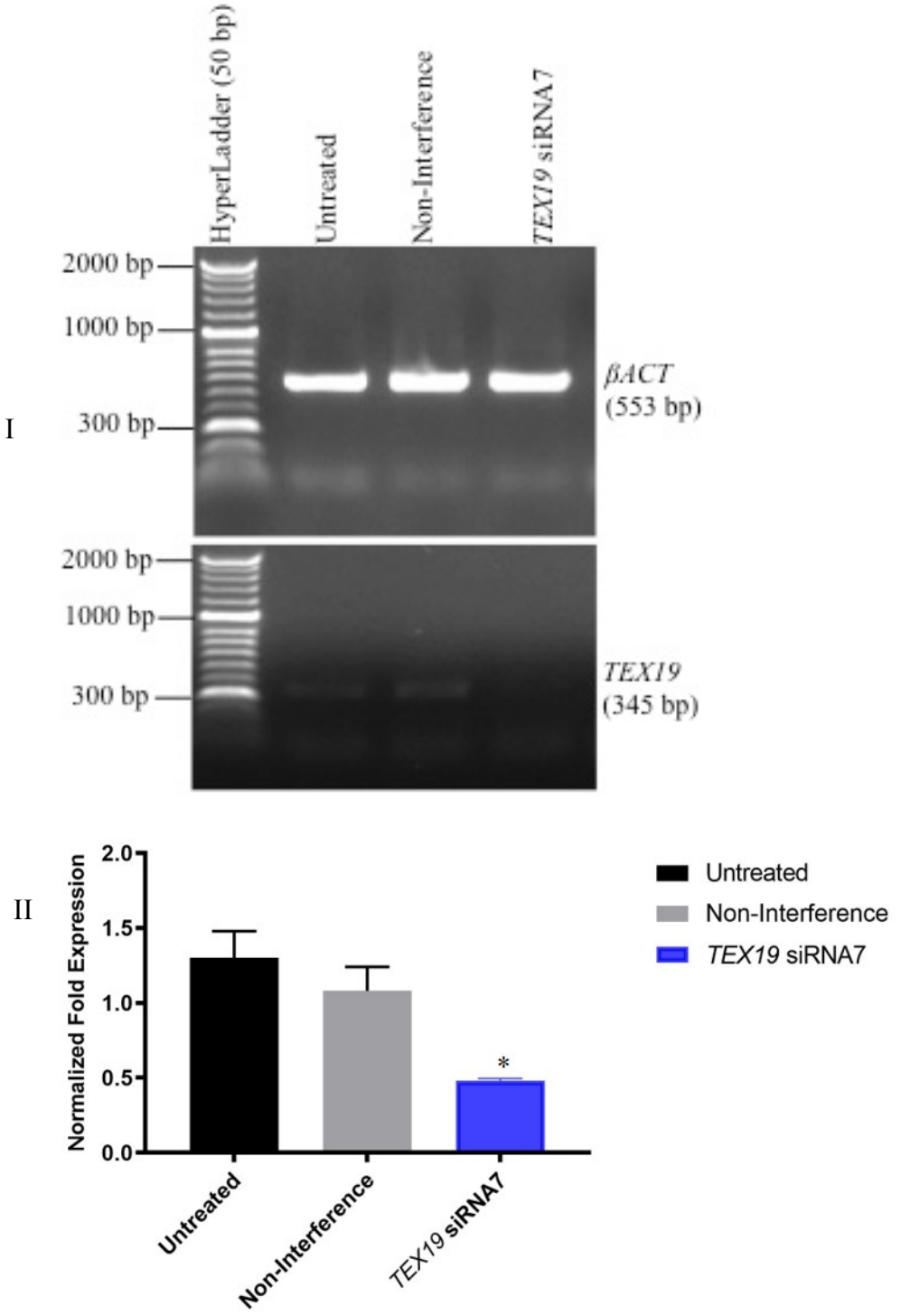

Figure 5.7 mRNA levels of *TEX19* after siRNA treatment in HA::*TEX19* - HCT116. (I)The quality of the cDNA was examined by checking *βACT* mRNA.Faint band of *TEX19* expression was observed when TEX19 primers were utilized. (II) The bar chart displays the mRNA levels of *TEX19* in SW480. The *TEX19* mRNA data were normalised to the qRT-PCR data of two genes, *GAPDH* and *βACT*. P values presented change when siRNA7 was utilised compared to the non-interference (* P value < 0.05).

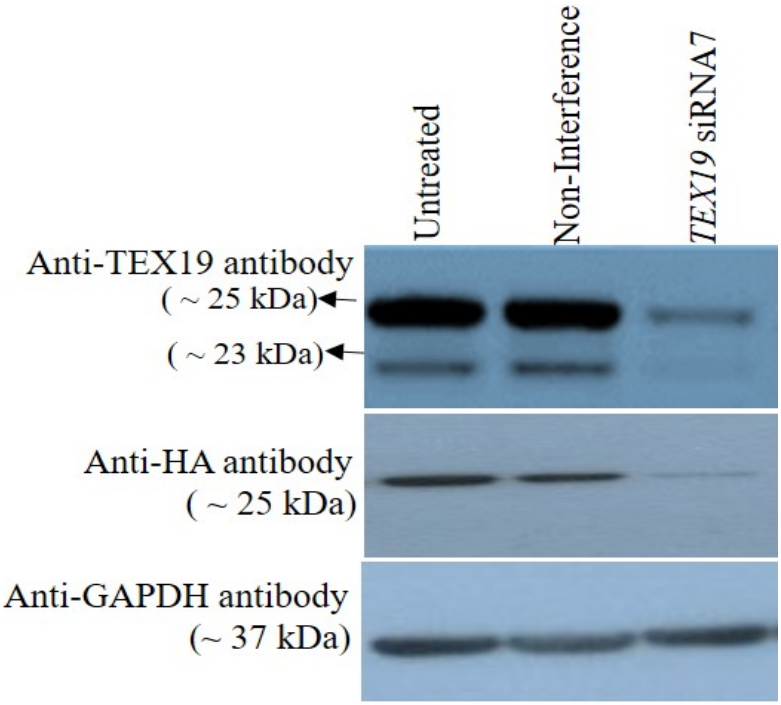

Figure 5.8 Western of TEX19 protein following siRNA treatment in the *HA::TEX19*- HCT116 cells. siRNA number 7 was used to deplete TEX19 *HA::TEX19*-HCT116 cell line. Lysates were blotted against anti-TEX19 antibody and depleted was detected in cultures treated with siRNA7 at the size roughly 23 kDa which is related to endogenous version of TEX19. Also, depleted was detected in cultures treated with siRNA7 at roughly 25 kDa which might relate to tagged version. The same lysates were also utilized with monoclonal anti-HA antibody and data displayed that significant knockdown of TEX19 in cultures treated with siRNA7. GAPDH was carried out in this study as a positive loading control.

5.2.2 Impact of TEX19 knockdown on cancer cell proliferation

The influential knockdown of TEX19 was utilized to examine/confirm whether TEX19 is important for cancerous cellular proliferation. Two cell lines were utilized in this experiment SW480 and HCT116 cells. siRNA 7 was utilized for 7 days beside untreated cells and non-interference (as negative control) to examine the impact of TEX19 depletion. In HCT116 cells, the cells treated with siRNA 7 displayed considerably decrease of cell numbers from the third day (* $P < 0.05$) relative to untreated cells and non-interference cultures. It was noticed from fourth to seventh days that the depletion of TEX19 corresponded to a clear reduction of proliferation (** $P < 0.01$ and *** $P < 0.001$) (Figure 5.9). In SW480 cells, it was noticed that the depletion of TEX19 also causes of noticeable reduction in cells proliferation from third until sixth day (Figure5.11).

Beside counting cells to detect the cell proliferation in SW480 and HCT116, the cells were harvested and RNA was extracted. qRT-PCR technique was carried out to examine the level of *TEX19* mRNA depletion in siRNA7 cultures at different days, as illustrated in Figure 5.10 and 5.12. siRNA treats caused a decrease in proliferation in compression of untreated cells and non-interference.

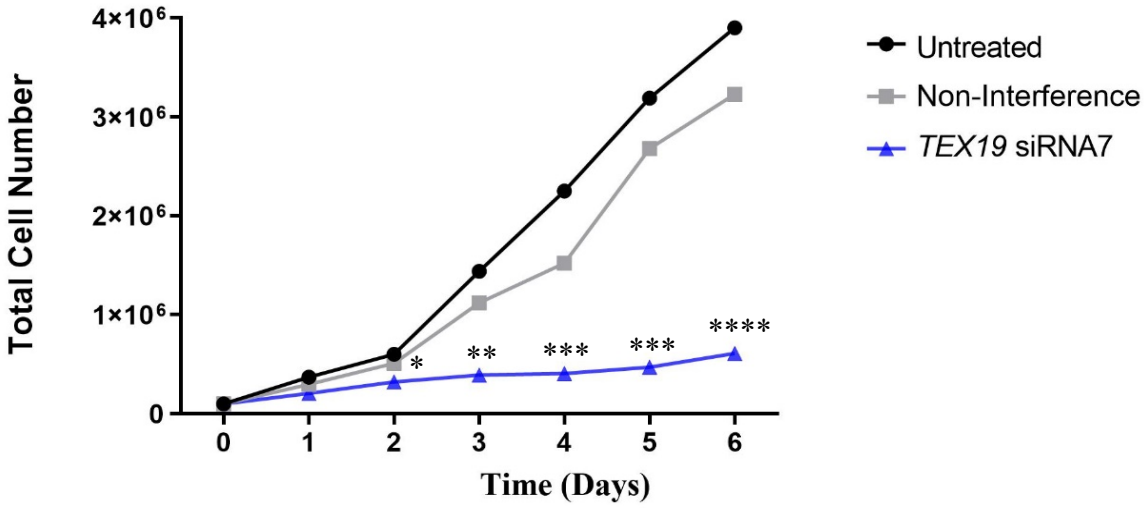

Figure 5.9 Cell proliferation analysis of SW480 cells constructed utilising *TEX19* siRNA7 for 6 days. I) The plot displays cell counts of treatment for 6 days. Significant proliferation inhibition was detected from the second day comparing untreated cells as well as non-interference siRNA which was utilized as negative control to examine the treatment. P values (*P < 0.05, **P<0.01 ,***P <0.001 and ****P < 0.0001).

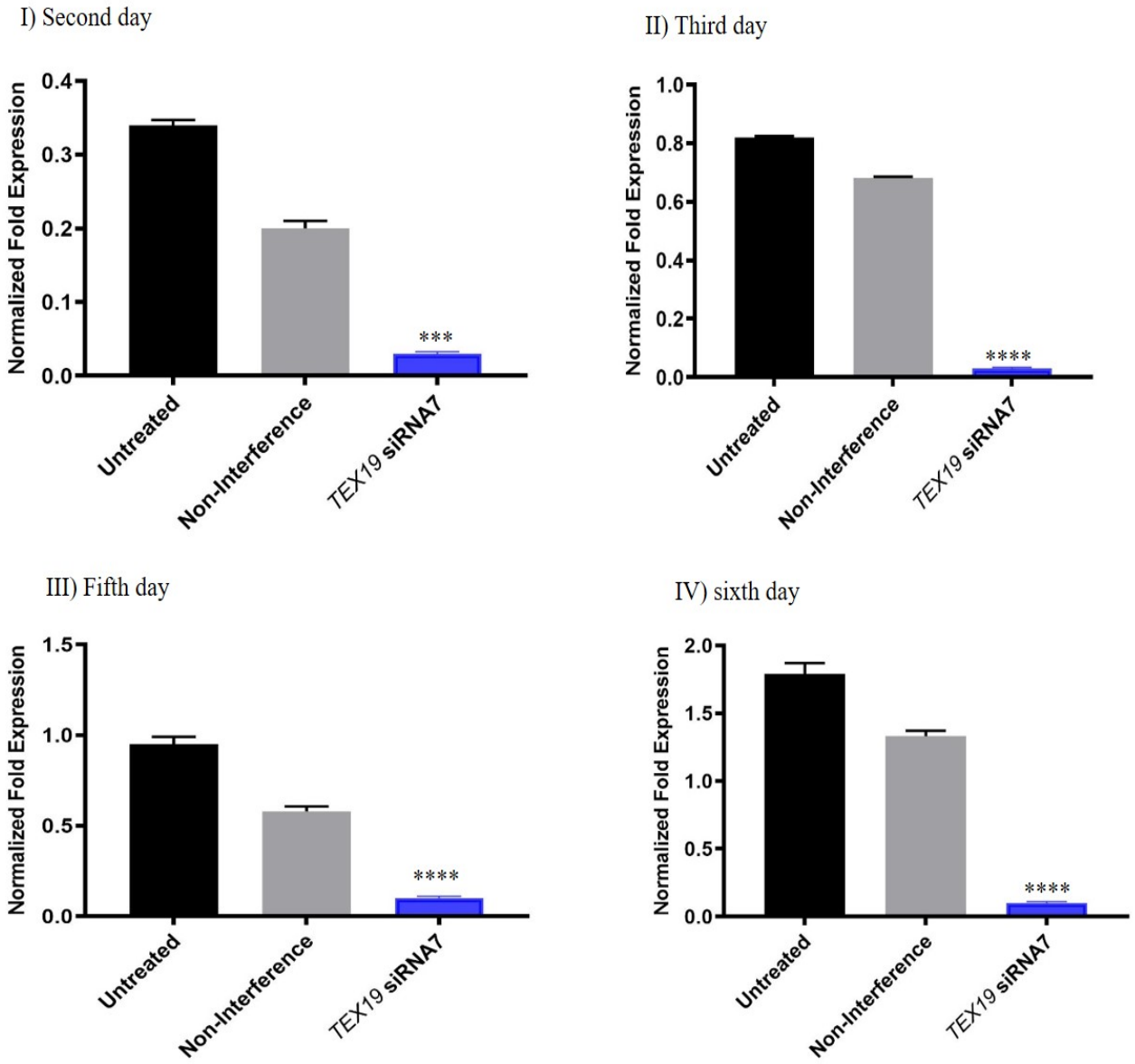

Figure 5.10 mRNA levels of *TEX19* after siRNA treatment in SW480 cells through the cellular proliferation analysis. The bar chart displays the mRNA levels of *TEX19* in SW480 for different days. The data displayed notable depletion of mRNA levels of *TEX19* in culture treated with siRNA7 in all examined days. The *TEX19* mRNA data were normalised to the qRT-PCR data of two genes, *GAPDH* and *βACT*. P values presented change when siRNA7 was utilised compared to the non-interference P values (***P <0.001 and ****P < 0.0001).

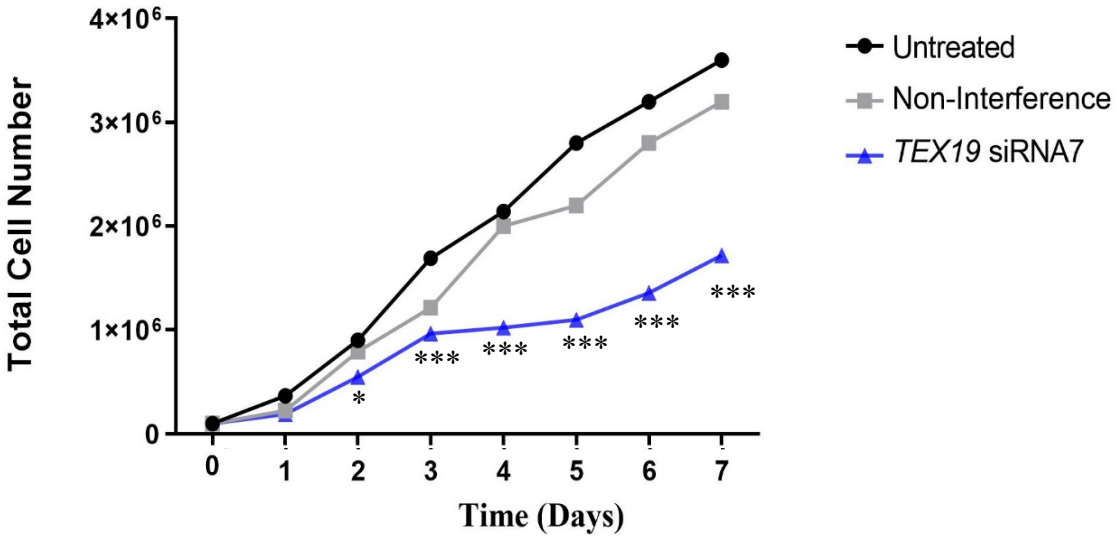

Figure 5.11 Cell proliferation analysis of HCT116 cells constructed utilising *TEX19* siRNA7 for 7 days. I) The plot displays cell counts of treatment for 7 days. Notable proliferation inhibition was detected comparing untreated cells as well as non-interference siRNA which was utilized as negative control to examine the treatment. P values (*P < 0.05 and ***P <0.001).

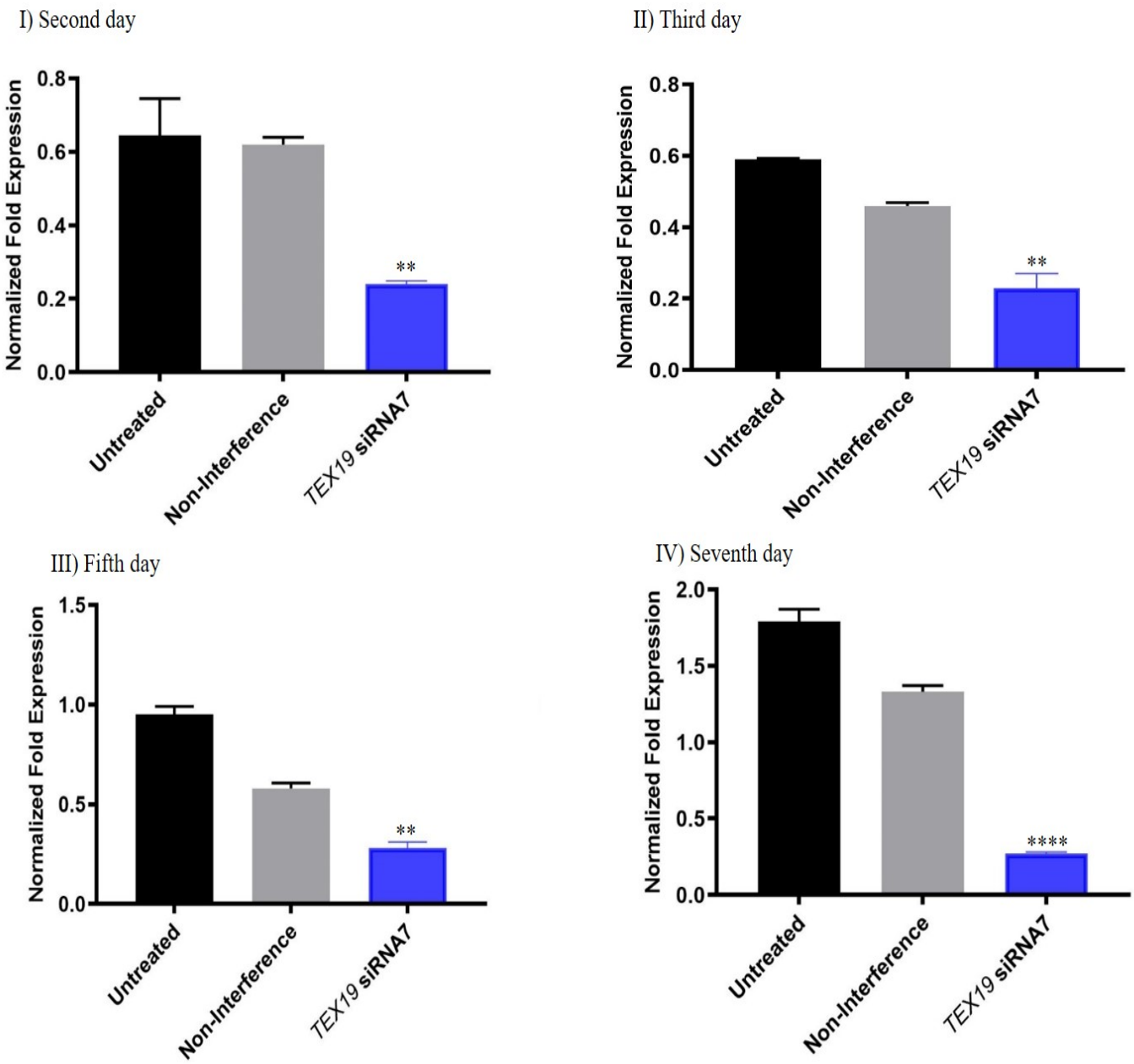

Figure 5.12 mRNA levels of *TEX19* after siRNA treatment in HCT116 cells through the cellular proliferation analysis. The bar chart displays the mRNA levels of *TEX19* in HCT116 for different days. The data displayed notable depletion of mRNA levels of *TEX19* in culture treated with siRNA7 in all examined days. The *TEX19* mRNA data were normalised to the qRT-PCR data of two genes, *GAPDH* and *βACT*. P values presented change when siRNA7 was utilised compared to the non-interference P values (**P <0.01 and ****P < 0.0001).

5.3 Discussion

Expression of human *TEX19* has been detected in several different cancers and in adult male testes and stem cells in humans (Feichtinger et al., 2012; Planells-Palop et al., 2017). Based on this expression profile, it has been proposed that TEX19 might be involved in driving oncogenesis. Planells-Palop et al. (2017) demonstrated that depletion of TEX19 in cancer cell lines reduces cancer cell proliferation and self-renewal. RNA sequencing was utilised on total RNA taken from SW480 cells treated with *TEX19* siRNA and untreated cells. It was indicated that at least of different gene transcripts were considerably altered (up-/down regulated) following treatment the cells of *TEX19* siRNA. Amongst the 80 affected genes, *RAD21L1* and *SEPT12* are recognised as CT genes suggesting TEX19 regulates at least some meiotic genes (Feichtinger et al., 2012). Additional analysis revealed that transcript levels of several genes linked to cancer cell proliferation were altered when TEX19 was depleted, suggesting an important role for *TEX19* in regulating oncogenic proliferation via a transcriptional regulation pathway (Planells-Palop et al., 2017).

Apoptosis of spermatogonia cells in mice is caused by a deletion of *Tex19.1*, an orthologue of human *TEX19* (Tarabay et al., 2013). Planells-Palop et al. (2017) reported a build-up of cells which were in the S-phase when TEX19-depleted human cancerous cells were analysed. Knockdown of TEX19 by using siRNA produce a few aberrant mitotic events suggesting the involvement of TEX19 in chromosome regulation. A role for mouse Tex19.1 in regulation of cohesion has been detected in oocytes of postnatal mice. Disturbance in sustenance of chiasmata has been observed in *Tex19.1* oocytes. Researchers have reconstituted various stages of this pathway in mitosis in order to show that Tex19.1 is capable of regulating an acetylated subset of SMC3 cohesin subunit by inhibiting the activity of E3 ubiquitin ligase UBR2, since UBR2 causes negative regulation of acetylated SMC3 (Reichmann et al., 2017). In oocytes, acetylated SMC3 has been shown to be linked with meiotic chromosome. It can be proposed that TEX19 has significant contribution in the regulation of acetylated SMC3 and cohesion of sister chromatids. However, considering the fact that human TEX19 is capable of affecting acetylated SMC3 (Reichmann et al., 2017), it can be suggested that TEX19 may take part in regulation of SMC3 acetylation in cancerous cells and for that reason, mitotic errors occur after loss of TEX19, and that

it is this feature which is linked to proliferative control. Interestingly, cohesion also controls transcription. So, this tow might feed into the altered transcriptional landscape observed following TEX19 depletion.

The data here demonstrate that the depletion of TEX19 in SW480, H460, HCT116 and *N-HA::TEX19* HCT116 appeared to significantly reduce *TEX19* mRNA and TEX19 protein. This emphasized the importance of utilizing TEX19 siRNA. The knockdown of TEX19 was affirmed via utilizing western blot analysis, which showed a single or double band. TEX19 is predicted to be nearly 18.5 KDa, but the antibody presented a signal at nearly 23 kDa. Post-translational alterations of TEX19 could be proposed as a reason for this related migration. The cause of the presence of a second band is not clear, and the results were not associated with the cancer cell types, passage number the confluence of the cells. However, when TEX19 was depleted in *N-HA::TEX19* HCT116 cells, the protein signals showed two bands; the lower one is at ~23 KDa, which we think is related to the endogenous version, while the upper band at ~25 KDa is related to the tagged version.

This research has also found that the depletion of TEX19 is associated with the inhibition of the proliferation of cancer cells. Proliferation was delayed or completely inhibited when SW480 and HCT116 cells were treated with anti-TEX19 siRNA7. These data seem to validate the fact that the proliferation of cancer cells essentially requires TEX19, and it leaves open the question about the relation between TEX19 and cancer cell proliferation. Planells-Palop and co-workers (2017) proposed that the function of TEX19 in encouraging cancer cell proliferation could be related to the transcriptional regulation of particular genes essential for cell proliferation or cell cycles (Planells-Palop et al., 2017). Histone modifications perform regulatory functions in modifying the activities of transcription (Tessarz & et al., 2014). Histone acetylation is a type of histone modification which is associated with "active" chromatin (Kouzarides, 2007; Dawson et al., 2012). Whilst conducting this work, a co-worker noted that histone H3K9 acetylation appeared to be reduced following TEX19 depletion. Given this, loss of H3K9 acetylation could cause proliferative inhibition. This observation will be explored further in the following chapter.

Chapter 6

The role of TEX19 in the regulation of epigenetic and LINE-1 programmes

6. The role of TEX19 in regulation of epigenetic and LINE-programmes

6.1 Introduction

Histones are the core nucleosome proteins which possess N-terminal tails which protrude from the core nucleosome. Post-translational modifications, like acetylation and methylation are responsible for modulating the role played by these proteins (Bannister et al., 2011). Histone modifications play important roles in various functions of the cell and also in regulating different cellular processes, for instance, histone modifications are involved in regulating processes like folding and assembly of nucleosomes, condensation of chromatin, heterochromatin silencing and gene transcription (Fuchs et al., 2006; Salmaninejad et al., 2016). Strong links have been identified between disturbance in histone modifications and the development of many kinds of cancers, such as cervical cancer (Liu et al., 2019). Promoters and enhancers of actively transcribed genes have been shown to be dependent on acetylation of H3K9 (H3K9-Ac) (Wang et al., 2008). When lysine of histones is acetylated, the positive charge of lysine is neutralized and in this way the chromatin relaxation is promoted, making DNA more accessible. Histone acetyltransferases (HATs) are responsible for adding an acetyl group to the lysine residue. Conversely, histone deacetylases (HDACs) are capable of removing the acetyl group resulting in deacetylation (Huang et al., 2011). Involvement of histone methylation in regulation of expression of genes has also been reported (Venkatesh & Workman, 2015). Histone methylation is linked to repression or activation of transcription, dependent on which histone residues get methylated (Bannister et al., 2011). Histone modifications make a significant contribution in epigenetic control of expression of CTA genes.

Retrotransposons are mobile genetic elements which constitute about 40% of the genome in mammals (Beck et al., 2011; Sotero-Caio, et al., 2017). These elements can bring about genetic variation, which is responsible for shaping genomic evolution as well as development of the living system. However, mobilization of these elements may result in mutation linked with several different cancers and genetic disorders (Beck et al., 2011; Burns, 2017). There are two main groups of retrotransposons and

this grouping is based on presence of long terminal repeat (LTR) sequences and genomic structure of retrotransposons. Short interspersed nuclear elements (SINEs) and long interspersed nuclear elements (LINEs) (Beck et al., 2011). LINE-1 (L1) elements catalyse all retrotransposition events occurring in humans. Two proteins are encoded by active L1s and these proteins are needed for the mobilization of these retrotransposons (Feng et al., 1996). These proteins are ORF1p and ORF2p. ORF1p refers to RNA binding protein which has the activity of a nucleic acid chaperon (Martin and Bushman, 2001). ORF2p refers to a multidomain protein possessing activities of endonuclease and reverse transcriptase (Feng et al., 1996).

Murine Tex19.1 may interact directly with L1-ORFp (MacLennan et al., 2017). Tex19.1 is capable of triggering polyubiquitylation of ORF1p as of well as degradation of ORF1p and may limit mobilization of LINE-1. It could be that there is relation between a function of Tex19.1, to some degree, through triggering the E3 ubiquitin ligase Ubr2 activity for L1-ORF1p protein. It can be postulated that Tex19.1 inhibits *de novo* retrotransposition during the pluripotent phase of germline cycle which LINE1-1 elements are transcribed. Post-translational modification of proteins encoded by L1 retrotransposons in mammals is capable of making significant contribution in sustenance of transgenerational genome stability and TEX19 is proposed to function in control of this process (MacLennan et al., 2017).

It has been established that TEX19 is associated with modulating cohesion of sister chromatids (Reichmann et al., 2017). Murine Tex19.1 protein regulates sister chromatid cohesion in postnatal oocytes. It has also been reported that human *TEX19* overexpression in transfected HEK239T cells is linked with regulating a subset of cohesion complex, a characteristic feature of which is that the SMC3 subunits of these complexes are acetylated. Cohesin complex containing acetylated SMC3 subunit are normally those which maintain the inter-sister cohesion. Considering these reports, it can be proposed that TEX19 is responsible for regulation of a chromatin-associated subset of cohesion which contains acetylated SMC3 (Reichmann et al., 2017). A co-worker noted that histone H3K9 acetylation appeared to be depleted after TEX19 knockdown (L.Alqhatani) if correct this observation would indicate an as yet unidentified function for TEX19. Therefore, in this chapter we aimed to examine this finding further ask whether TEX19 could have biological role associated to epigenetic

regulation in cancer cells. Additionally, we aim to establish whether TEX19 is related to control of L1 ORF1p in human cancer cells, thereby potentially influencing retroelement activity.

6.2 Results

6.2.1 The association between TEX19 and H3K9 acetylation in cancer cells.

It was proposed that a role of TEX19 in driving cancer cell proliferation could be related to the transcriptional regulation of particular genes essential for cell proliferation or cell cycles (Planells-Palop et al., 2017). Unpublished data from the McFarlane lab showed an association between TEX19 and H3K9 acetylation. H3K9 acetylation appeared to be reduced considerably following knockdown of TEX19. This finding requires verification and assessment in a number of cancer cell lines including *TEX19*- HA HCT116 cancer cell line expressing an epitope tagged gene.

TEX19 knockdown was performed in SW480, H460, HCT116 and *TEX19*-HA HCT116 cancer cell utilising small interfering RNA. siRNA 7 was utilised to deplete the *TEX19* gene transcripts. The negative control was non-interfering RNA. siRNA was transfected into cultures for 3 days, then RNA and protein were extracted from all the cultures.

The cells cultured with siRNA7 for 3 days had a clear reduction in TEX19 protein level relative to the non-interfering RNA control. SW480 cells exhibit no clear reduction of H3K9-Ac level compared to non-interfering RNAs treated cultures (Figure 6.1). While H3K9-Ac levels were decreased after the knockdown of TEX19 in H460 cancer cells (Figure 6.2). HCT116 cancer cells (Figure 6.3) and *TEX19*- HA HCT116 cancer cell (Figure 6.4). However, the data from the western blot analysis following knockdown of TEX19 showed that the level of total histone H3 have not been notably changed in all examined cancer cells. These data may suggest that extent of the TEX19 impact differently in each type of cancer cells.

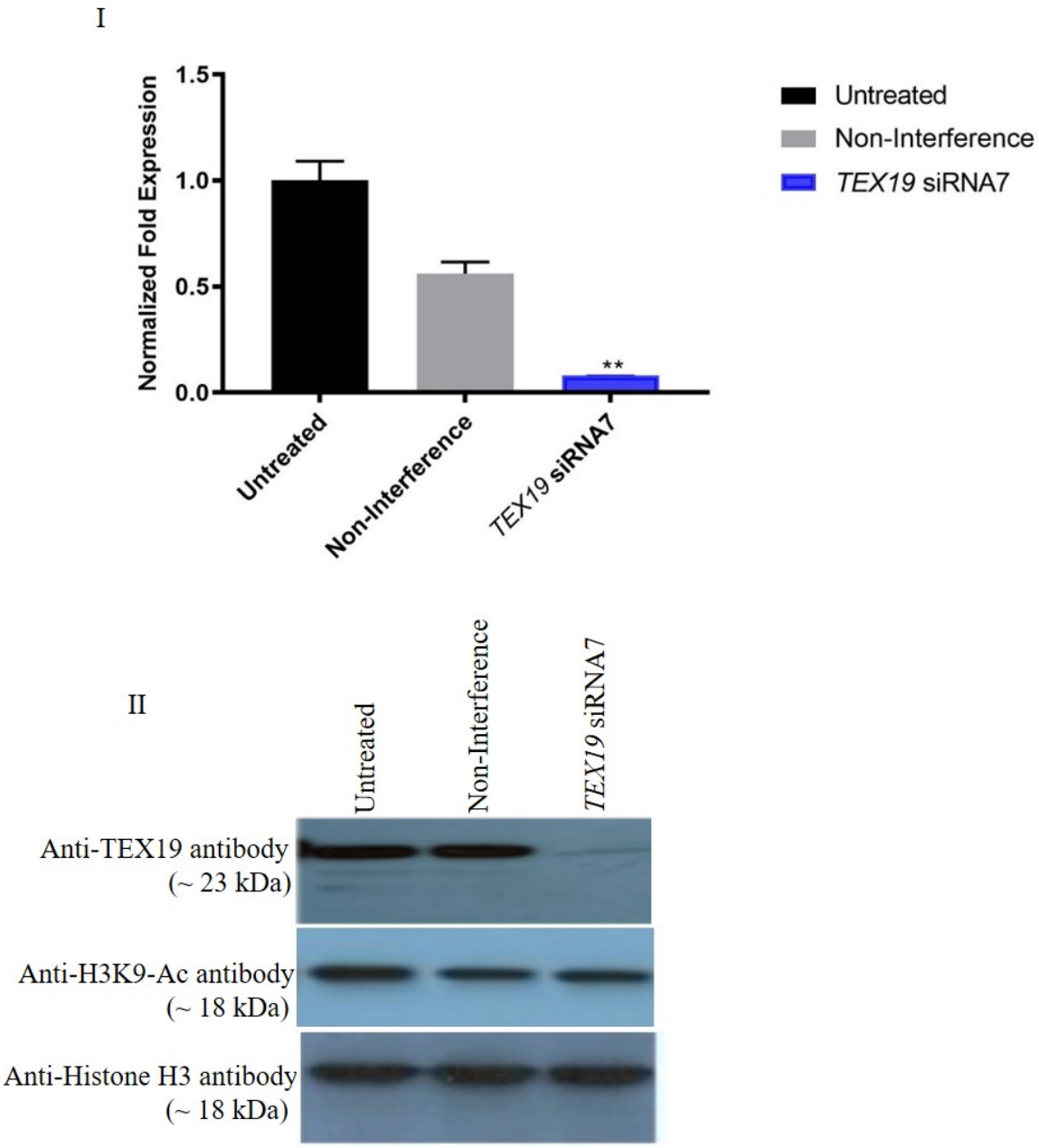

Figure 6.1 TEX19 depletion does not impacts H3K9 acetylation in SW480 cancer cells. (I) The bar chart displays the mRNA levels of *TEX19* in SW480 cancer cells following siRNA treatment. The *TEX19* mRNA data were normalised to the qRT-PCR data of two genes, *GAPDH* and *βACT*. P values presented significant changes when siRNA7 was utilised compared to the non-interference (** P value < 0.01). (II) Western blot analysis of TEX19 protein following siRNA treatment in the SW480 cancer cell line. siRNA7 was used to deplete TEX19 in SW480 cancer cell line. Blot has been probed to visualize the level of H3 K9 acetylation and total H3 protein. TEX19 depletion was observed in culture treated with siRNA7 compared to the controls untreated cells and non-interference. The blots display that knockdown of TEX19 not impacts on depletion of H3K9 acetylation levels, and no changed was notable in total H3 levels.

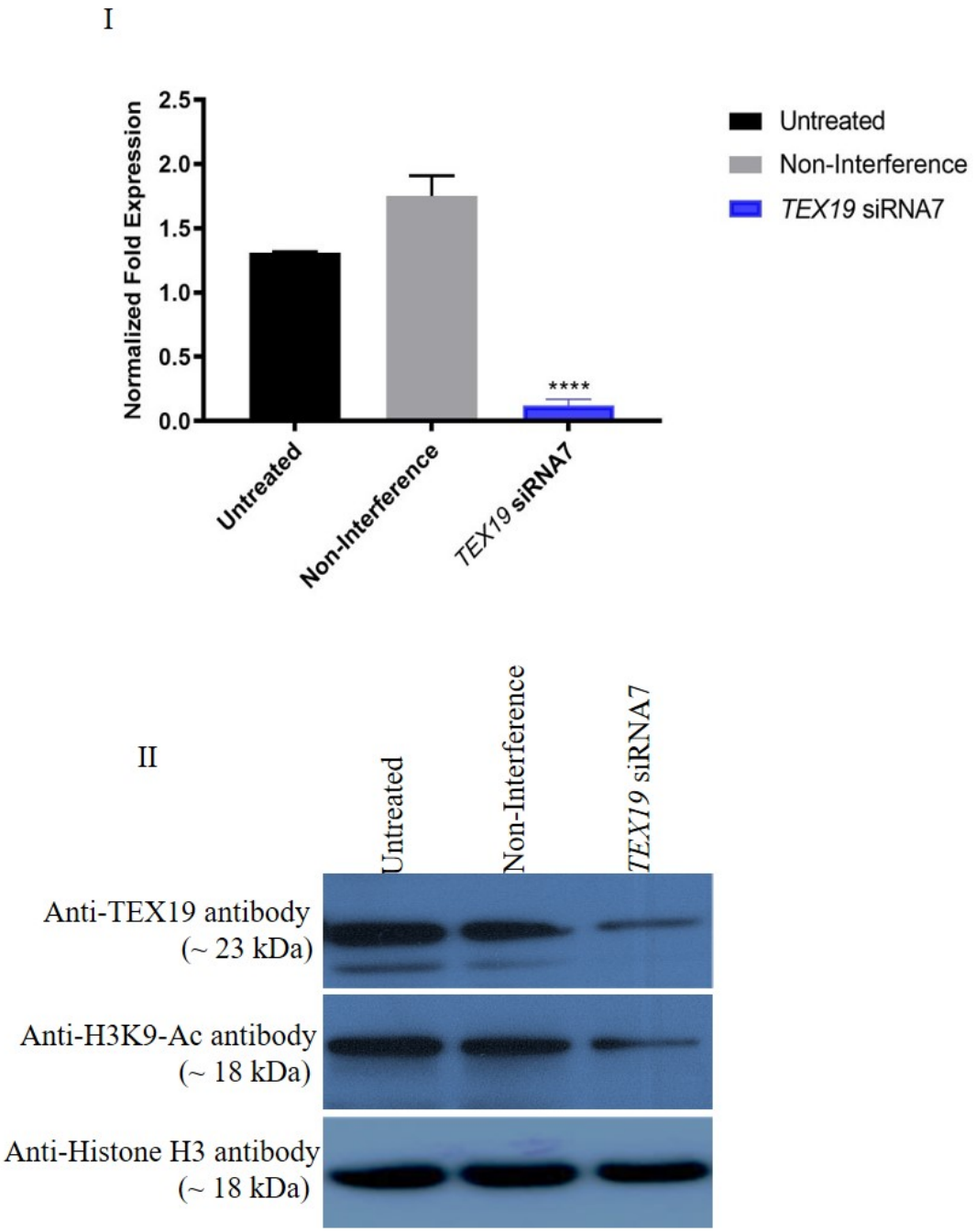

Figure 6.2 TEX19 depletion impacts on H3K9 acetylation in H460 cancer cells.
(I) The bar chart displays the mRNA levels of *TEX19* in H460 cancer cells following TEX19 depletion. The *TEX19* mRNA data were normalised to the qRT-PCR data of two genes, *GAPDH* and *βACT*. P values presented significant changes when siRNA7 was utilised compared to the non-interference (*** P value < 0.0001). (II) Western blot analysis of TEX19 protein following siRNA treatment in the H460 cancer cell line. siRNA7 was used to deplete TEX19. Blot has been probed to visualize the level of H3 K9 acetylation and total H3 protein. TEX19 depletion was observed in culture treated with siRNA7 compared to the controls untreated cells and non-interference. The blots display that knockdown of TEX19 impacts on depletion of H3K9 acetylation levels, and no changed was notable in total H3 levels.

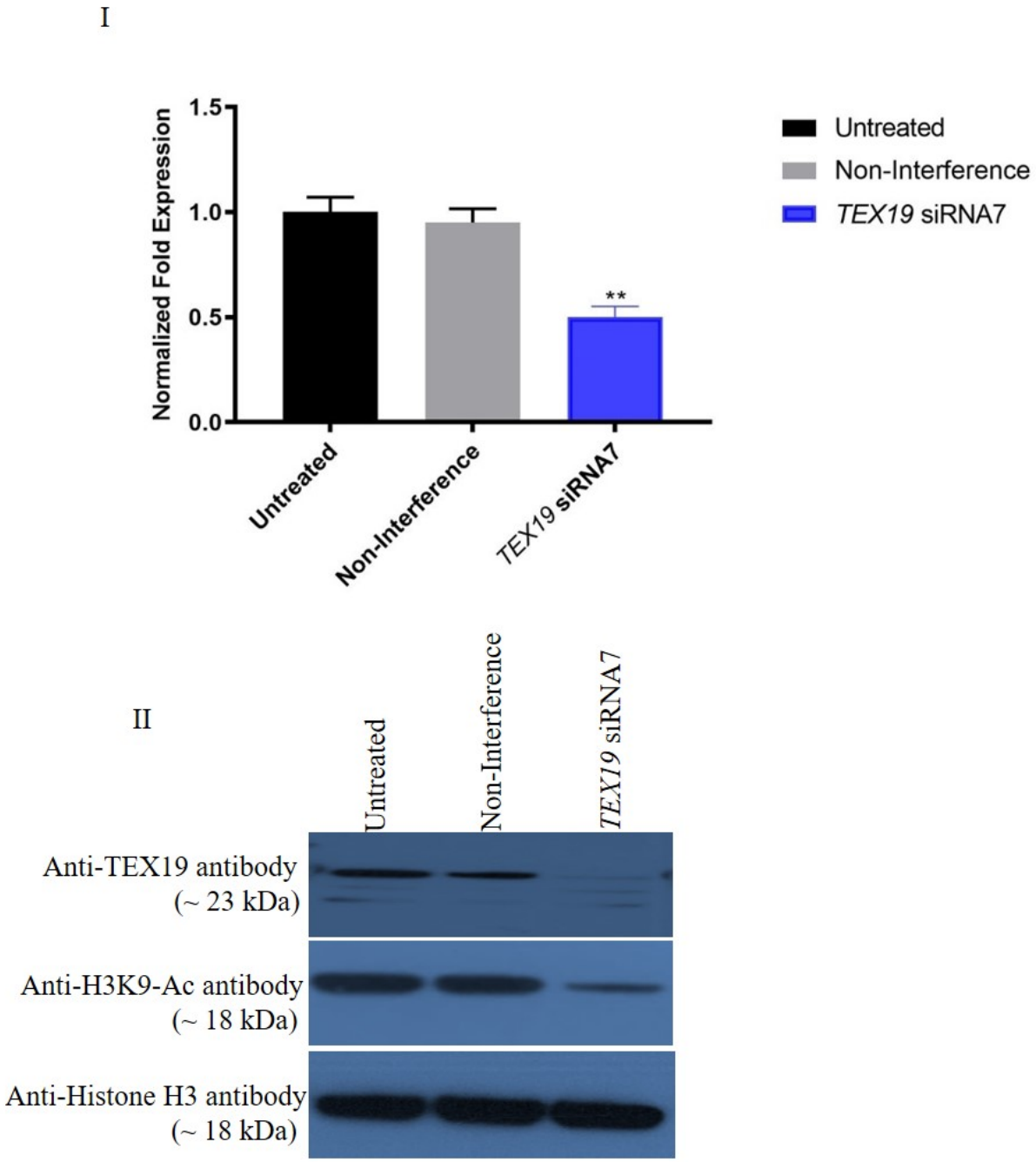

Figure 6.3 TEX19 depletion impacts on H3K9 acetylation in HCT116 cancer cells.
(I) The bar chart displays the mRNA levels of *TEX19* in HCT116 cancer cells following TEX19 depletion. The *TEX19* mRNA data were normalised to the qRT-PCR data of two genes, *GAPDH* and *βACT*. P values presented significant changes when siRNA7 was utilised compared to the non-interference (**P value < 0.01). (II) Western blot analysis of TEX19 protein following siRNA treatment in the HCT116 cancer cell line. siRNA7 was used to deplete TEX19. Blot has been probed to visualize the level of H3 K9 acetylation and total H3 protein. TEX19 depletion was observed in culture treated with siRNA7 compared to the controls untreated cells and non-interference. The blots display that knockdown of TEX19 impacts on depletion of H3K9 acetylation levels, and no changed was notable in total H3 levels.

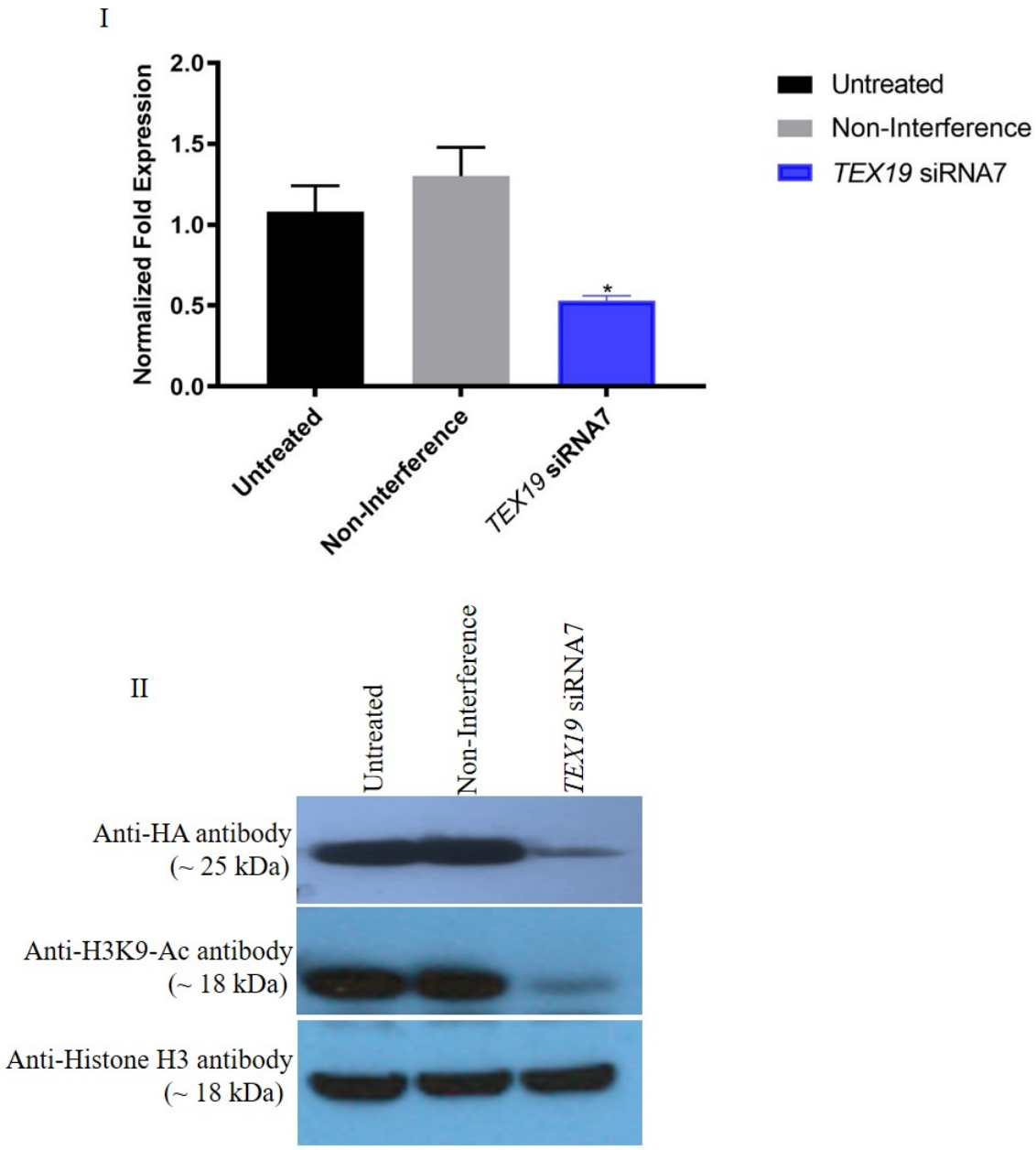

Figure 6.4 TEX19 depletion impacts on H3K9 acetylation in *TEX19*- HA HCT116 cancer cells. (I) The bar chart displays the mRNA levels of *TEX19* in *TEX19*- HA HCT116 cancer cells following TEX19 depletion. The *TEX19* mRNA data were normalised to the qRT-PCR data of two genes, *GAPDH* and *βACT*. P values presented significant changes when siRNA7 was utilised compared to the non-interference (*P value < 0.05). (II) Western blot analysis of TEX19 protein following siRNA treatment in the *TEX19*- HA HCT116 cancer cell line. siRNA7 was used to deplete TEX19. Blot has been probed to visualize the level of H3 K9 acetylation and total H3 protein. TEX19 depletion was observed in culture treated with siRNA7 compared to the controls untreated cells and non-interference. The blots display that knockdown of TEX19 impacts on depletion of H3K9 acetylation levels, and no changed was notable in total H3 levels.

6.2.2 TEX19 may control other histone modifications in H460 and HCT116 cancer cells

It was found that a biological role of TEX19 may impact on H3K9-Ac levels in H460 and HCT116 cancer cells. The change appeared in H3K9-Ac levels after knockdown of TEX19 encouraged us to look for different histone epigenetic marks. In this experiment, western blotting was utilized using several monoclonal antibodies to particular markers including H3K9-Ac, H3K4 mono-me, H3K4 di-me, H3K4 tri-me, H3K18-Ac, H3K9 tri-me and total histone (H3). siRNAs 7 was utilised to deplete TEX19 in H460 and HCT116 cancer cells for 3 days. The negative control was non-interfering RNA. TEX19 knockdown was proved via utilizing RT-qPCR analysis. *TEX19* mRNA level was significantly reduced relative to the non-interfering RNA control in H460 cancer cells (Figure 6.5.I) and also in the HCT116 cancer cells (Figure 6.6.I).

Western blot data showed that the levels of H3K9-Ac and H3K18-Ac were reduced following TEX19 depletion in H460 cancer cells Figure (6.5. II) and HCT116 cancer cells Figure (6.6.II). It was also noticed that the level of total H3 are not changed. This data leads to the proposal that TEX19 has an important role in regulation of distinct epigenetic marks. But the lack of change to other marks such as H3K4-me (Figure 6.5/6.6) indicate this is not a general epigenetic regulation role.

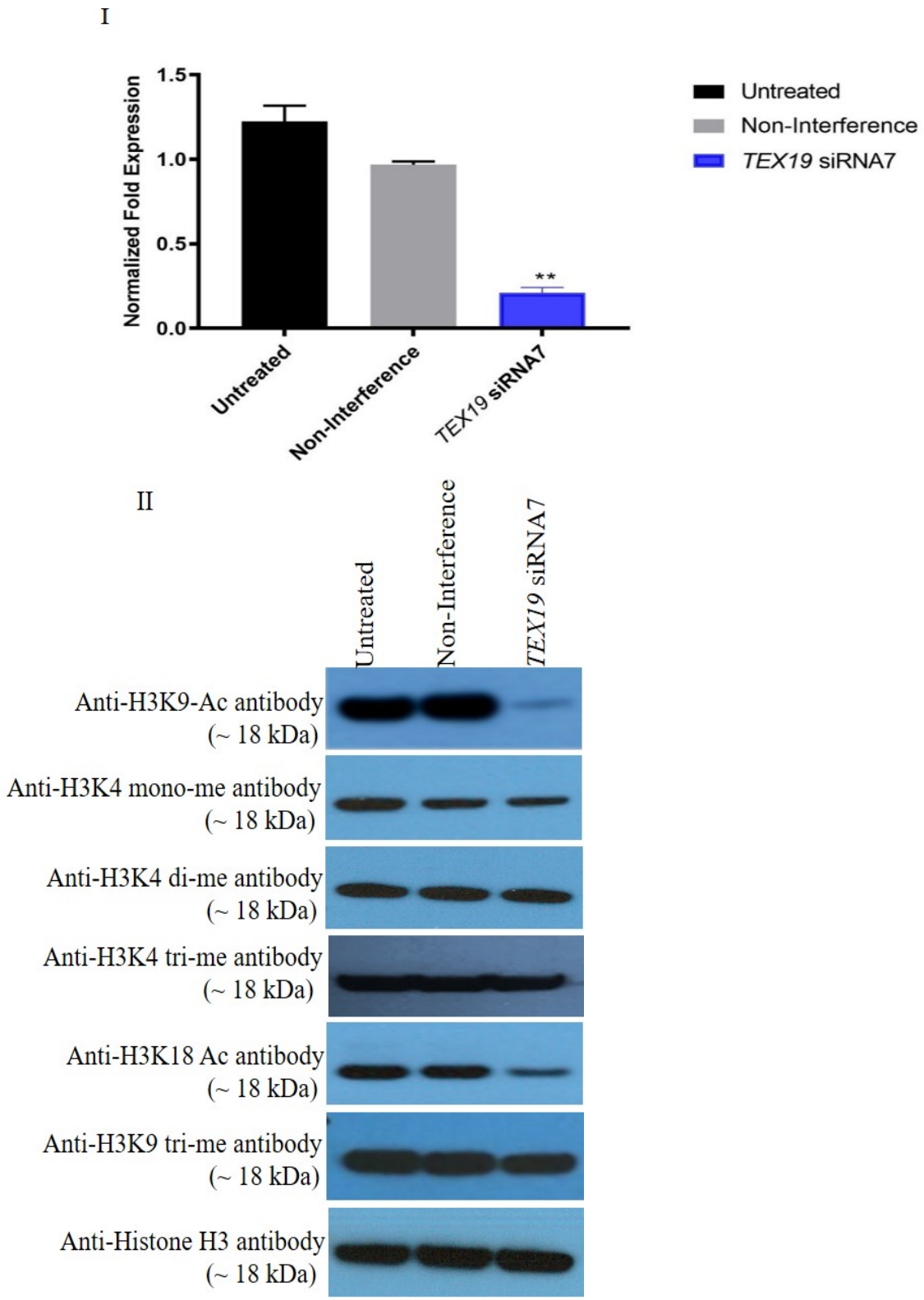

Figure 6.5 Examination of various histone H3 modification after knockdown of TEX19 in H460 cancer cells. (I) The bar chart displays the mRNA levels of *TEX19* in H460 cells. The *TEX19* mRNA data were normalised to the qRT-PCR data of two genes, *GAPDH* and *βACT*. P values presented significant changes when siRNA7 was utilised compared to the non-interference (** P value < 0.01). (II) Western blot analysis of histone extract of H460 cells following siRNA treatment. siRNA 7 was used to deplete TEX19 in H460 cells. Blots were probed to visualize the level of H3K9-Ac, H3K4 mono-me, H3K4 di-me, H3K4 tri-me, H3K18-Ac, H3K9 tri-me and total histone (H3) proteins. The blots display that knockdown of TEX19 impacts on depletion of H3K9-Ac and H3K18-Ac levels and no changed was notable in total H3 levels.

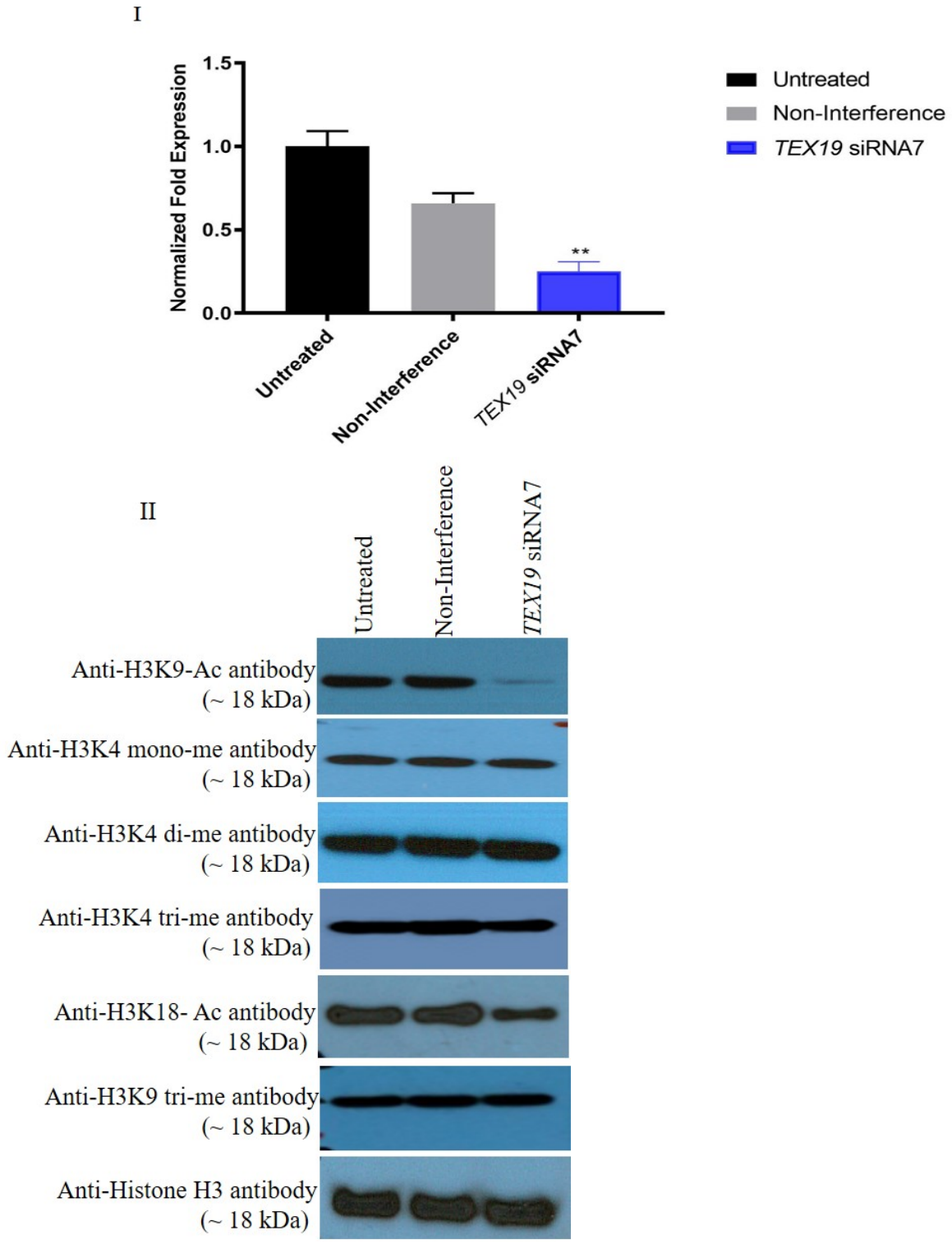

Figure 6.6 Examination of various histone H3 modification after knockdown of TEX19 in HCT116 cancer cells. (I) The bar chart displays the mRNA levels of *TEX19* in HCT116 cells. The *TEX19* mRNA data were normalised to the qRT-PCR data of two genes, *GAPDH* and *βACT*. P values presented significant changes when siRNA7 was utilised compared to the non-interference (** P value < 0.01). (II) Western blot analysis of histone extract of HCT116 cells following siRNA treatment. siRNA 7 was used to deplete TEX19 in HCT116 cells. Blots were probed to visualize the level of H3K9-Ac, H3K4 mono-me, H3K4 di-me, H3K4 tri-me, H3K18-Ac, H3K9 tri-me and total histone (H3) proteins. The blots display that knockdown of TEX19 impacts on depletion of H3K9-Ac and H3K18-Ac levels and no changed was notable in total H3 levels.

6.2.3 TEX19 regulates L1-ORF1p in some cancer cells

Tex19.1 in mice has been reported to regulate L1-orf1p levels. Moreover, other work in the Macfarlane group (unpublished) has indicated there might be a role for TEX19 in human cancer cells to regulate L1-ORF1. Here we wished to explore this further and address whether TEX19 does influence L1-ORF1 in cancer cells. *TEX19* knockdown was performed in SW480, H460 and HCT116 cancer cells utilising small interfering RNA. siRNA7 was utilised to deplete the *TEX19* gene transcripts. The negative control was non-interfering RNA. siRNA was transfected into cultures for 3 days, and then RNA and protein were extracted from all the cultures.

The successful knockdown of *TEX19* in SW480 resulted in no change of the *L1-ORF1* transcript levels (Figure 6.7.I). Furthermore, the Western blot data showed no change in L1-ORF1p following depletion of TEX19 relative to the untreated and non-interfering RNA controls (Figure 6.7.II). In HCT116 cancer cells, the *L1-ORF1* transcript level showed no change following significant knockdown of *TEX19.* Moreover, Western blot data of HCT116 cancer cells showed no L1-ORF1p, even in untreated and non-interfering cells (Figures 6.8. I and 6.8.II). H460 cancer cell data showed that the significant knockdown of *TEX19* resulted in a remarkable change of the *L1-ORF1* transcript levels (Figure 6.9.I). Western blot analyses also showed that successful knockdown of *TEX19* resulted in a clear depletion in L1-ORF1p compared with the untreated and non-interfering RNA controls (Figure 6.9.II).

For further confirmation of the results, L1-ORF1p protein levels were examined after depletion of *TEX19*. Western blot analysis was used with different protein lysates of HCT116, SW480 and H460. (The lysates were taken from a previous experiment; see Chapter 5). Intrestingly, ORF1 protein is not induced following TEX19 depletion. The data confirmed that L1-ORF1p did not appear in HCT116 cancer cells in any of the examined samples, including the untreated and non-interfering cells. The L1-ORF1p levels were not changed following TEX19 depletion in SW480 cancer cells, while in H460 cancer cells, the data confirmed that the L1-ORF1p level was reduced following TEX19 depletion (Figure 6.10).

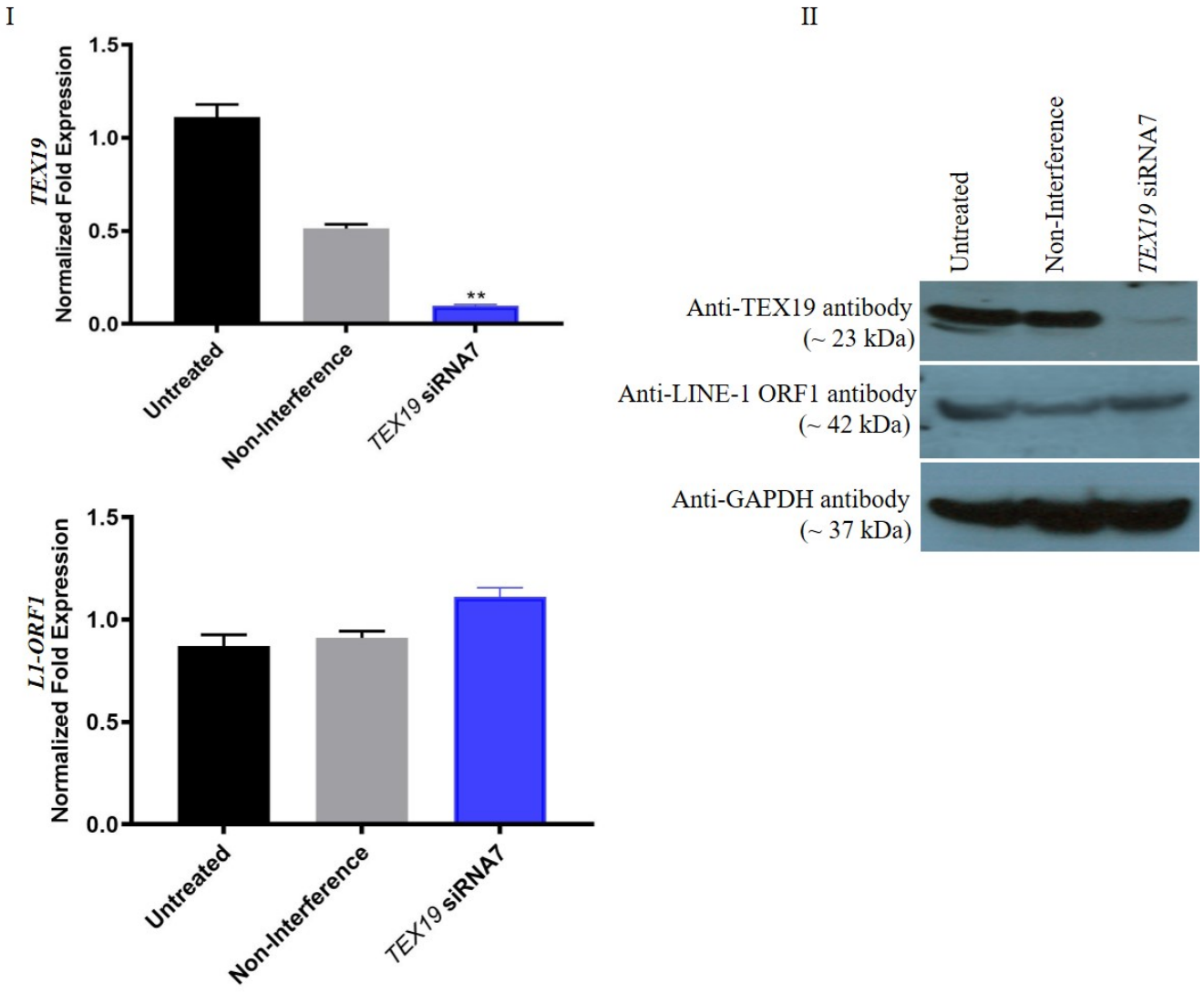

Figure 6.7 Examination of L1-ORF1 levels following *TEX19* knockdown in SW480 cells.
(I) The bar chart displays the mRNA levels of *TEX19* and *L1-ORF1* in SW480 following depletion of *TEX19*. The mRNA data were normalised to the qRT-PCR data of two genes, *GAPDH* and *βACT*. The *p*-values presented significant changes in the *TEX19* transcript level when siRNA7 was utilised compared with the non-interfering case (** *p*-value < 0.01), and no changes in *ORF1* transcript levels were detected. (II) Western blot analysis of SW480 cells following *TEX19* siRNA7 treatment. The data display that knockdown of TEX19 does not affect L1-ORF1 levels relative to the untreated and non-interfering RNA control. GAPDH was employed in this study as a positive loading control.

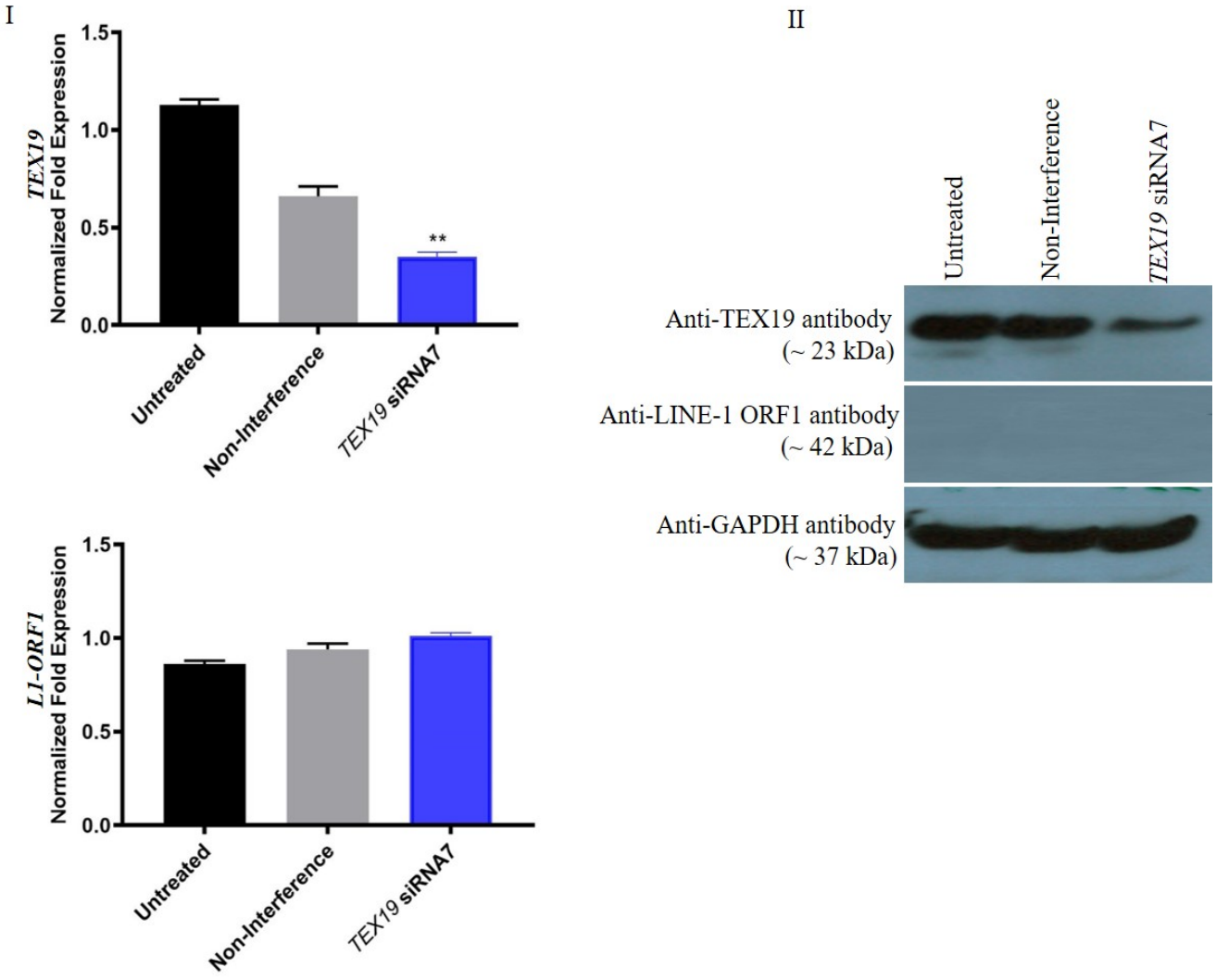

Figure 6.8 Examination of L1-ORF1 levels following *TEX19* knockdown in HCT116 cells.
(I) Bar chart displays the mRNA levels of *TEX19* and *L1-ORF1* in HCT116 following the depletion of *TEX19*. The mRNA data were normalised to the qRT-PCR data of two genes, *GAPDH* and *βACT*. The *p*-values presented significant changes in the *TEX19* transcript level when siRNA7 was utilised compared with the non-interfering case (** *p*-value < 0.01), and there were no changes in *ORF1* transcript levels. (II) Western blot analysis of HCT116 cells following *TEX19* siRNA7 treatment. The data display that no of L1-ORF1 protein was detected, even in the untreated and non-interfering RNA controls. GAPDH was employed in this study as a positive loading control.

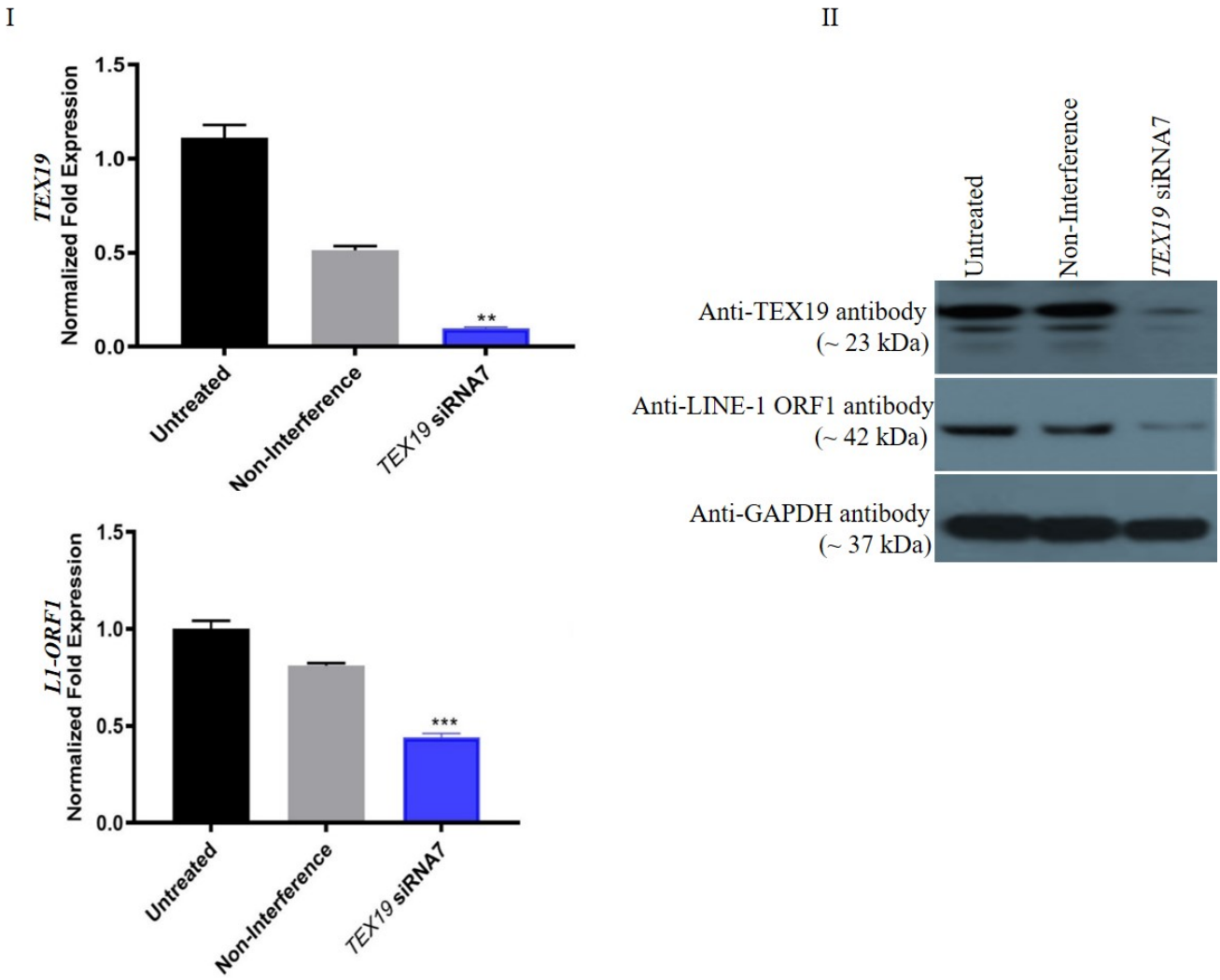

Figure 6.9 Examination of L1-ORF1 levels following *TEX19* knockdown in H460 cells.
(I) Bar chart displays the mRNA levels of *TEX19* and *L1-ORF1* in H460 following the depletion of *TEX19*. The mRNA data were normalised to the qRT-PCR data of two genes, *GAPDH* and *βACT*. The P values presented significant changes in the *TEX19* transcript level when siRNA7 was utilised compared to the non-interference case (** P value < 0.01) and significant changes in *ORF1* transcript levels were detected (***P value <0.001). (II) Western blot analysis of H460 cells following *TEX19* siRNA7 treatment. The data display that knockdown of TEX19 impacts on depletion of L1-ORF1p level relative to the untreated and the non-interfering RNA control. GAPDH was employed in this study as a positive loading control.

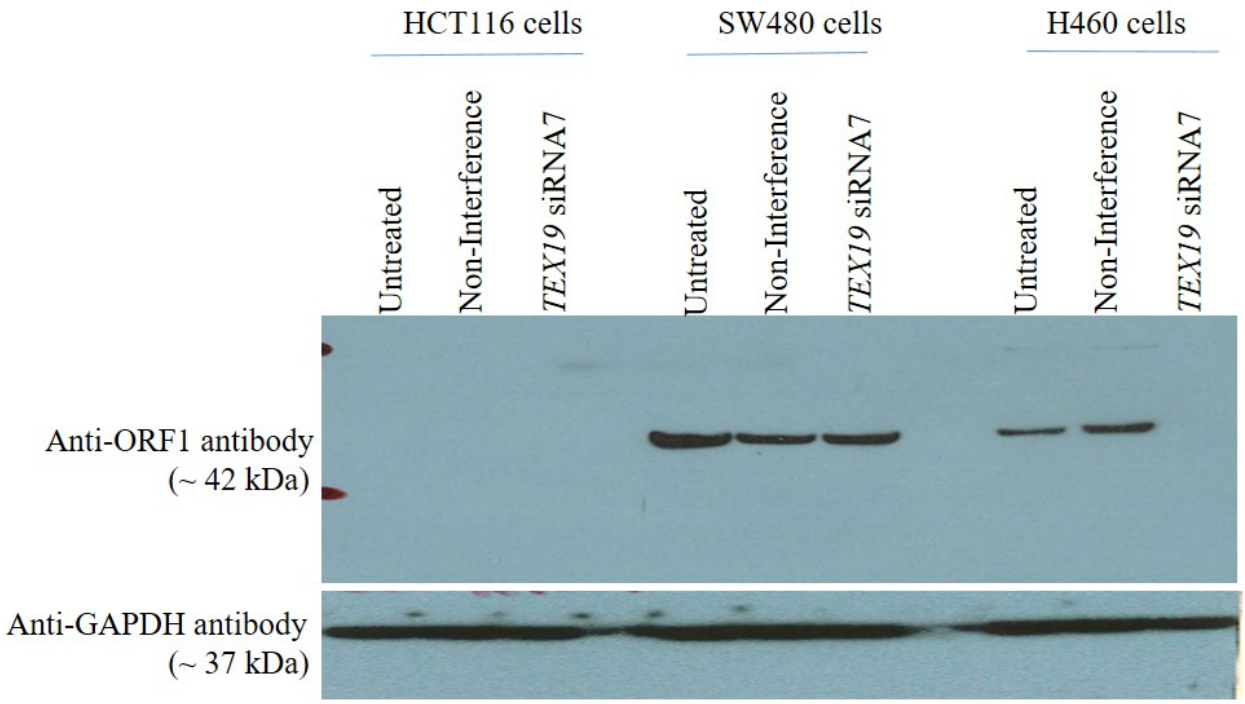

Figure 6.10 Confirmation of L1-ORF1 levels following *TEX19* knockdown in HCT116, SW480 and H460 cells. Western blot data of HCT116, SW480 and H460 cancer cells following *TEX19* siRNA7 treatment. The data verify that L1-ORF1p not appeared in HCT116 cancer cells in all examined samples including untreated and non-interference cells. L1-ORF1p levels were not changed following TEX19 depletion in SW480 cancer cells. In H460 cancer cells the data confirmed that L1-ORF1p level was reduced following TEX19 depletion. GAPDH was carried out in this study as a positive loading control.

6.3 Discussion

6.3.1 TEX19 can regulate histone acetylation in cancer cells

TEX19 has been shown to be associated with oncogenesis. Moreover, it has also been proven that TEX19 is required for self-renewal and proliferative potentials of different types of cancerous cells in humans (Planells-Palop et al., 2017). Considering these findings, it can be stated that TEX19 may serve as a promising cancer specific therapeutic target, possibly via small molecule inhibition.

The nucleus contains many acetylated proteins. These proteins affect transcription directly or indirectly through transcription factors, co-activators and nuclear receptors. SMC3 is a non-histone protein and acetylation of this protein is involved in regulating cohesion of sister chromatids as well as non-cohesion process (Kawasumi et al., 2017). Reichmann et al. (2017) have also demonstrated involvement TEX19 in regulation of acetylated SMC3. Certain post-translational modifications prove to be required for epigenetic pathways which may affect histone tails leading to remodelling of structure of chromatin thereby giving rise to changed transcriptional states (activated or inactivated) (Tessarz et al., 2012). Acetylation of H3 and H4 are key post-translational modifications which are linked with active chromatin marks (Dawson et al., 2012).

A preliminary study was carried out in the McFarlane group to check if depletion of TEX19 can cause changes in levels of histone and histone modifications. This investigation is importance since growth of cancerous cells is affected by epigenetic histone modification. Importantly, H3K9Ac is crucial for the regulation of chromosomes and control of gene expression. Unpublished data from the McFarlane lab showed an association between TEX19 and H3K9 acetylation. H3K9 acetylation appeared to be reduced considerably following knockdown of TEX19. The data here confirmed the preliminary results and clearly display a functional association between TEX19 and direct genome regulation in H460, HCT116 and *TEX19*- HA HCT116 cancer cells.

6.3.2 Involvement of TEX19 in regulation of distinct histone modifications in H460 and HCT116 cancer cells

TEX19 has been shown to impacts on regulating levels of H3K9-Ac and this effect was found to be variable in HCT116 and H460 cancer cells. Different histone modifications have been noticed to participate differently in regulation of genome functions and in controlling transcription of genes (activation or inactivation). Moreover, a number of these functions are connected to one another (Arnaudo et al., 2013). In general, H3K9-Ac has been found to be positively correlated with transcriptionally active chromatin. Accordingly, reduction in acetylation of H3K9 is expected to generate chromatin which is not much transcriptionally active.

Western blotting was utilized using several monoclonal antibodies to particular markers including H3K9-Ac, H3K4 mono-me, H3K4 di-me, H3K4 tri-me, H3K18-Ac, H3K9 tri-me and total histone (H3). It was noticed the levels of H3K9-Ac and H3K18-Ac were considerably decreased following TEX19 depletion. However, there was not any significant change in total H3 level. It has been demonstrated previously that H3K18-Ac is one of those histone modifications which indicate activation of transcription (Chervona &Costa, 2012). There is a correlation between certain histone modifications of specific chromatin domains and highly organized structure of chromatin as well as gene activity occurring at variable degrees. For example, de-condensation of chromatin together with development of chromatin loops is achieved through active chromatin marks that include H3K9-Ac. Such marks are responsible for making actively transcribed genes different from extremely condensed chromosome (Schones &Zhao, 2008). The results in this chapter may indicate involvement of TEX19 in positive regulation of transcriptionally active state of chromatin. One postulate relates to the fact TEX19 has many characteristics of a histone chaperone. This is explored in Chapter 7.

6.3.3 TEX19 can control L1-ORF1 in cancer cells

It has recently been found that mouse Tex19.1 actively contributes to the regulation of TEs. According to MacLennan et al. (2017), Tex19.1 may demonstrate direct interaction with L1-ORF1p, which is a protein encoded by L1 that is needed for retro-

transposition. Moreover, the polyubiquitylation and degradation of ORF1p and polyubiquitylation is triggered by Tex19.1, which is also responsible for limiting mobilisation of LINE-1. It was indicated that Tex19.1 may perform its function through stimulation of the activity of the enzyme E3 ubiquitin ligase Ubr2 to act on the L1-ORF1p protein (MacLennan et al., 2017).

Western blotting of proteins extracted from different cancer cells displayed that there is a functional relationship between TEX19 and L1-ORF1p in human cancer cells. However, there is fundamental intercellular heterogeneity, in that some cancer cells do not have detectable ORF1, some have ORF1 which is regulated by TEX19 and in some it is not.

The data in this study showed that *TEX19* depletion resulted in depletion of *L1-ORF1* in H460 cancer cells on the mRNA level, which may suggest that *L1-ORF1* gene expression or transcript is controlled by TEX19 in H460 cells. Importantly, a reduction of the transcript level of L1-ORFp in H460 cells appeared to result in a reduction of the protein level also after TEX19 knockdown.

In HCT116 cancer cells, data showed no effect of the transcription level of *L1-ORF1* and there is no detectable L1-ORF1. Furthermore, Western blotting results verified that there was no L1-ORFp protein in HCT116 cells. In SW480 cancer cells, the data showed no effect of the transcription level of *L1-ORF1*, while Western blotting showed that the level of L1-ORF1p did not change following TEX19 depletion. It was surmised that we did not detect the effect of TEX19 on L1-ORFp due to limited TEX19 depletion via siRNA, or alternatively, TEX19 may not be involved in controlling L1-ORF1p in this cell line. Indeed, more confirmation to deplete TEX19 in SW480 cancer cells is needed to verify this finding. This experiment was limited because of time limitations, and more verified analysis is required.

Interestingly, in mice Tex19.1 stimulates Orf1p degregation. If human and mouse mechanistic roles for TEX19/Tex19.1 were similar it might be postulates that TEX19 in human caused polyubiquitylation and degradation of ORF1, so that loss of TEX19 would result in increased levels of ORF1. This is clearly not the case. In cells lacking detectable ORF1, such as HCT116, we do not stimulate appearance of detectable

ORF1 by depleting TEX19. Moreover, in cells were TEX19 depletion does influence ORF1 levels, such as H460, it causes a reduction in ORF1, not an increase. This is likely due to reduction in *ORF1* transcripts, so TEX19 might stimulate transcription of LINE-1 mRNA. However, TEX19 might also directly stabilize ORF1 protein which in turn stabilize LINE-1 mRNA. Our current data can not distinguish between these two possibilities and further analysis is required.

So, it is clear TEX19 controls both ORF1 and histone H3K9-Ac. Both proteins have strong association with nucleic acids (ORF1 with LINE1 mRNA; H3K9-Ac with DNA). So, we speculate TEX19 could be a nucleic acid minics.

Chapter 7

Final discussion

7. Final discussion

A characteristic feature of stem cells and some cancerous cells is their capability of self-renewal. It has been postulated that some cancer cells may undergo a transition from soma to germline, or they may instigate programmes which are responsible for organizing the germ-like state (Feichtinger et al., 2014; McFarlane et al., 2014). The hallmarks of cancers, such as metastasis, invasiveness and uncontrolled proliferative potentials, are common biological features in both cancer cells and germ cells (Hanahan & Weinberg, 2011). Accordingly, it has been suggested that the reactivation of germline genes in cancer cells is involved in these phenomena. Similarly, the reactivation of several germline genes has been found to be involved in metastatic and aggressive traits of lung cancer. Accordingly, diagnostic and therapeutic approaches may consider utilizing these as targets (Rousseaux et al., 2013). Certain germline genes which have established roles in the regulation of meiosis have been demonstrated to bring about oncogenesis (Cho et al., 2014). Involvement of germline genes in the instigation, progression and sustenance of cancer is therefore clear.

Human *PRDM9* has proven to be a meiosis specific gene and the PRDM9 protein has methyltransferase activity. *PRDM9* is expressed in several different kinds of cancers (Feichtinger et al., 2014). The murine orthologue of human PRDM9, namely Meisetz, has been described as a meiotic recombination activator which is involved in regulation of transcription for other meiosis specific genes (Hayashi et al., 2005), and *PRDM9* overexpression play important roles in upregulation of a number of human genes in HEK293 cells (Altemose et al., 2017). This implies that expression of only one meiosis specific epigenetic regulator is capable of changing the transcriptional landscape of human cancer cells (Altemose et al., 2017).

Numerous studies have reported the role of PRDM9 in activating hotspot sites of meiotic recombination (Baudat et al., 2010; Myers et al., 2010; Parvanov et al., 2010). Still, research studies conducted in recent years have found that genomic stability is associated with meiotic recombination hotspot sequences (Houle et al., 2018). The PRDM9 protein contains zinc fingers which enable binding of this protein with particular genomic sequences (Paigen & Petkov, 2018; Grey et al., 2018). Analysis of binding sites of PRDM9 in human cancer cells points towards the fact that these

binding sites are linked with sites involved in genome rearrangements in different cancer cells (Houle et al., 2018). Considering this, it has been proposed that PRDM9 methyltransferase activity serves as hotspot activator as well as regulator of transcription of several meiosis specific proteins. It was confirmed by the idea that the expression of testis-specific *RIK* gene (Morc2b) has been controlled by Prdm9 in mice. During this study, HeLa Tet-On cells were transfected with *PRDM9* and overexpression of *PRDM9* caused upregulation of the CT genes *MAGEA1* and *GAGE* and *PRDM7*. It has therefore been proposed that PRDM9 may serve as regulator for transcription of other genes in cancerous cells.

PRDM9 has been found to comprise of a PR/SET domain demonstrating histone methyltransferase activity beside the KRAB (Kruppel-association box) protein-protein binding domain and multiple zinc finger arrays (Baudat et al., 2013). According to Hayashi et al., (2005), trimethylation of H3K4 is catalysed by the PR/SET domain of Prdm9. Transcription of genes is considerably affected by this trimethylation. Similarly, human *PRDM9*, when transfected in HEK293 cells, has been found to be capable of mediating trimethylation of H3K4 and H3K36 (Eram et al., 2014). In this research, trimethylated H3K4 and H3K36 activity was not significantly changed in this study following overexpression of transfected *PRDM9* in HCT116 Tet-On cells. This may because western blot analysis did not detect the signal of PRDM9 during this research, so in our hands the system did not appear to operate as we had hoped.

One more example of a meiosis-specific gene which has been described by researchers as a CT gene is human *TEX19*. TEX19 controls SPO11-mediated recombination and shows high impact in proliferation of cancer cells (Planells-Palop et al., 2017).
However, the exact function of TEX19 in human oncogenesis still needs to be found as disturbance in its activation was detected in different types of cancer (Feichtinger et al., 2012; Zhong et al., 2016).

The data of this research also found that TEX19 is very important for cancer cells and proliferation of cancer cells is substantially decreased following depletion of *TEX19*. It has been postulated that *TEX19* serve as gene that codes for a protein which works for regulation of transcription in cancer cells (Planells-Palop et al., 2017). Preliminary research conducted by a one of researcher in the McFarlane lab showed that TEX19 can be involved in regulating H3K9 acetylation as knockdown of TEX19 caused significant depletion of H3K9 acetylation in cancer cells. This research has confirmed that significant decrease in H3K9 acetylation level following knockdown of TEX19 in many cancer cells.

The data from this study strongly indicate that TEX19 is functionally involved in regulating chromatin network in cancer cells. Since H3K9 acytelation and H3K18 acetylation levels were reduced following TEX19 knockdown in cancer cells. It can be stated that acetylation of H3K9 acetylation is controlled by TEX19. In addition to this, depletion of TEX19 has also resulted in abnormal mitotic events (McFarlane group unpublished). This is further supported by the role of TEX19 in regulating chromatin network and chromatid cohesion. Researchers have also demonstrated the role of Tex19.1 in regulating cohesion in oocytes of postnatal mice (Reichmann et al., 2017).

So, how might TEX19 regulate chromatin?

It has been established that histone chaperones perform important functions in all cells of humans. In particular, these proteins are involved in loading, transport, storage and elimination of histones in human cells (Gurard-Levin et al., 2014; Warren &Shechter, 2017). Certain characteristic features of histone chaperones have been described by researchers, One of these characteristic is increasingly acidic nature since these proteins possess one acidic stretch at least. Studies indicate that TEX19 displays certain properties which have been used to characterize histone chaperones. Taking into account the finding that Tex19.1 participates in promotion of meiotic recombination required for chromatin remodelling (Crichton et al., 2017) and the finding that TEX19 displays properties which are characteristic features of histone

chaperones; one can postulate that TEX19 contributes in regulating histone dynamics by serving as a chaperone protein.

TEX19 protein has been found in embryo stem cells and germ cells of humans (Öllinger et al., 2008; Planells- Palop et al., 2017). Accordingly, investigating the possibility of regulation of histone acetylation by TEX19 in stem cells is crucial not only from a scientific perspective but also for comprehending the association between cancer cells and embryo stem cells. This investigation may involve depletion of TEX19 in hESCs followed by western blotting and genome-wide chromatin immune-precipitation (CHIP) by utilizing antibodies raised against H3K9-Ac.

References

Agalliu, I., Gapstur, S., Chen, Z., Wang, T., Anderson, R.L., Teras, L., Kreimer, A.R., Hayes, R.B., Freedman, N.D. & Burk, R.D. 2016. Associations of Oral alpha-, beta-, and gamma-Human Papillomavirus Types With Risk of Incident Head and Neck Cancer. *JAMA oncology,* 2 (5), pp. 599-606.

Akhavan-Niaki, H. & Samadani, A.A. 2013. DNA methylation and cancer development: molecular mechanism. *Cell biochemistry and biophysics,* 67 (2), pp. 501-513.

Ali, M., Hanif, M. & Farooqi, A.A. 2015. Epigenetic therapy for cancer. *Pak.J.Pharm.Sci,* 28 (3), pp. 1023-1032.

Almeida, L.G., Sakabe, N.J., Deoliveira, A.R., Silva, M.C.C., Mundstein, A.S., Cohen, T., Chen, Y., Chua, R., Gurung, S. & Gnjatic, S. 2008. CTdatabase: a knowledge base of high-throughput and curated data on cancer-testis antigens. *Nucleic acids research,* 37 (suppl_1), pp. D816-D819.

Altemose, N., Noor, N., Bitoun, E., Tumian, A., Imbeault, M., Chapman, J.R., Aricescu, A.R. & Myers, S.R. 2017a. A map of human PRDM9 binding provides evidence for novel behaviors of PRDM9 and other zinc-finger proteins in meiosis. *Elife,* 6 pp. e28383.

Aly, H.A. 2012. Cancer therapy and vaccination. *Journal of immunological methods,* 382 (1-2), pp. 1-23.

Aris, M. & Barrio, M.M. 2015. Combining immunotherapy with oncogene-targeted therapy: a new road for melanoma treatment. *Frontiers in immunology,* 6 pp. 46.

Arnaudo, A.M. & Garcia, B.A. 2013. Proteomic characterization of novel histone post-translational modifications. *Epigenetics & chromatin,* 6 (1), pp. 24.

Aung, P.P., Oue, N., Mitani, Y., Nakayama, H., Yoshida, K., Noguchi, T., Bosserhoff, A.K. & Yasui, W. 2006. Systematic search for gastric cancer-specific genes based on SAGE data: melanoma inhibitory activity and matrix metalloproteinase-10 are novel prognostic factors in patients with gastric cancer. *Oncogene,* 25 (17), pp. 2546.

Bagci, O. & Kurtgöz, S. 2015. Amplification of cellular oncogenes in solid tumors. *North American journal of medical sciences,* 7 (8), pp. 341.

Baker, C.L., Kajita, S., Walker, M., Saxl, R.L., Raghupathy, N., Choi, K., Petkov, P.M. & Paigen, K. 2015. PRDM9 drives evolutionary erosion of hotspots in Mus musculus through haplotype-specific initiation of meiotic recombination. *PLoS genetics,* 11 (1), pp. e1004916.

Baker, C.L., Walker, M., Kajita, S., Petkov, P.M. & Paigen, K. 2014. PRDM9 binding organizes hotspot nucleosomes and limits Holliday junction migration. *Genome research,* 24 (5), pp. 724-732.

Ballestar, E. 2011. An introduction to epigenetics. In: Anon*Epigenetic Contributions in Autoimmune Disease.* Springer. pp. 1-11.

Bannister, A.J. & Kouzarides, T. 2011. Regulation of chromatin by histone modifications. *Cell research,* 21 (3), pp. 381.

Barnes, J.L., Zubair, M., John, K., Poirier, M.C. & Martin, F.L. 2018. Carcinogens and DNA damage. *Biochemical Society transactions,* 46 (5), pp. 1213-1224.

Baudat, F., Buard, J., Grey, C., Fledel-Alon, A., Ober, C., Przeworski, M., Coop, G. & De Massy, B. 2010. PRDM9 is a major determinant of meiotic recombination hotspots in humans and mice. *Science,* 327 (5967), pp. 836-840.

Baudat, F., Imai, Y. & De Massy, B. 2013. Meiotic recombination in mammals: localization and regulation. *Nature Reviews Genetics,* 14 (11), pp. 794.

Baxter, D. 2014. Active and passive immunization for cancer. *Human vaccines & immunotherapeutics,* 10 (7), pp. 2123-2129.

Beck, C.R., Garcia-Perez, J.L., Badge, R.M. & Moran, J.V. 2011. LINE-1 elements in structural variation and disease. *Annual review of genomics and human genetics,* 12 pp. 187-215.

Behl, C. & Ziegler, C. 2014. Cell cycle: the life cycle of a cell. In: Anon*Cell Aging: Molecular Mechanisms and Implications for Disease.* Springer. pp. 9-19.

Bhushan, S., Wang, M., Kudipudi, P., Fijak, M. & Meinhardt, A. 2016. Testicular macrophages: Role in immune privilege and defense. *Journal of reproductive immunology,* (115), pp. 51.

Boddy, M.N., Gaillard, P.L., McDonald, W.H., Shanahan, P., Yates 3rd, J.R. & Russell, P. 2001. Mus81-Eme1 are essential components of a Holliday junction resolvase. *Cell,* 107 (4), pp. 537-548.

Bollschweiler, D., Radu, L., Plitzko, J.M., Henderson, R.M., Mela, I. & Pellegrini, L. 2018. Reconstitution of a flexible SYCP3-DNA fibre suggests a mechanism for SYCP3 coating of the meiotic chromosome axis. *BioRxiv,* pp. 369439.

Bonini, C. & Mondino, A. 2015. Adoptive T□cell therapy for cancer: The era of engineered T cells. *European journal of immunology,* 45 (9), pp. 2457-2469.

Bourque, G., Burns, K.H., Gehring, M., Gorbunova, V., Seluanov, A., Hammell, M., Imbeault, M., Izsvák, Z., Levin, H.L. & Macfarlan, T.S. 2018. Ten things you should know about transposable elements. *Genome biology,* 19 (1), pp. 199.

Boxer, L.M. & Dang, C.V. 2001. Translocations involving c-myc and c-myc function. *Oncogene,* 20 (40), pp. 5595.

Bray, F., Ferlay, J., Soerjomataram, I., Siegel, R.L., Torre, L.A. & Jemal, A. 2018. Global cancer statistics 2018: GLOBOCAN estimates of incidence and mortality worldwide for 36 cancers in 185 countries. *CA: a cancer journal for clinicians,* 68 (6), pp. 394-424.

Brown, M.S. & Bishop, D.K. 2015. DNA strand exchange and RecA homologs in meiosis. *Cold Spring Harbor perspectives in biology,* 7 (1), pp. a016659.

Brown, S., Kirkbride, P. & Marshall, E. 2015. Radiotherapy in the acute medical setting. *Clinical Medicine,* 15 (4), pp. 382-387.

Burns, K.H. 2017. Transposable elements in cancer. *Nature Reviews Cancer,* 17 (7), pp. 415.

Bzymek, M., Thayer, N.H., Oh, S.D., Kleckner, N. & Hunter, N. 2010. Double Holliday junctions are intermediates of DNA break repair. *Nature,* 464 (7290), pp. 937.

Caballero, O.L. & Chen, Y. 2009. Cancer/testis (CT) antigens: potential targets for immunotherapy. *Cancer science,* 100 (11), pp. 2014-2021.

Cai, L., Sutter, B.M., Li, B. & Tu, B.P. 2011. Acetyl-CoA induces cell growth and proliferation by promoting the acetylation of histones at growth genes. *Molecular cell,* 42 (4), pp. 426-437.

Cartegni, L., Chew, S.L. & Krainer, A.R. 2002. Listening to silence and understanding nonsense: exonic mutations that affect splicing. *Nature reviews genetics,* 3 (4), pp. 285.

Caspi, R.R. & Stein-Streilein, J. 2014. Immune privilege and the philosophy of immunology. *Frontiers in immunology,* 5 pp. 110.

Chan, Y.W. & West, S. 2015. GEN1 promotes Holliday junction resolution by a coordinated nick and counter-nick mechanism. *Nucleic acids research,* 43 (22), pp. 10882-10892.

Chen, H., Liu, H. & Qing, G. 2018. Targeting oncogenic Myc as a strategy for cancer treatment. *Signal transduction and targeted therapy,* 3 (1), pp. 5.

Chen, Q., Deng, T. & Han, D. 2016. Testicular immunoregulation and spermatogenesis. *Seminars in cell & developmental biology.* Elsevier. pp. 157.

Chen, Y., Venditti, C.A., Theiler, G., Stevenson, B.J., Iseli, C., Gure, A.O., Jongeneel, C.V., Old, L.J. & Simpson, A.J. 2005. Identification of CT46/HORMAD1, an immunogenic cancer/testis antigen encoding a putative meiosis-related protein. *Cancer Immun,* 5 (9), .

Chen, Y., Leng, C., Olivares, H., Lee, M., Chang, Y., Kung, W., Ti, S., Lo, Y., Wang, A.H. & Chang, C. 2004. Heterodimeric complexes of Hop2 and Mnd1 function with Dmc1 to promote meiotic homolog juxtaposition and strand assimilation. *Proceedings of the National Academy of Sciences,* 101 (29), pp. 10572-10577.

Chénais, B. 2013. Transposable elements and human cancer: a causal relationship? *Biochimica et Biophysica Acta (BBA)-Reviews on Cancer,* 1835 (1), pp. 28-35.

Cheng, Y., Wong, E.W. & Cheng, C.Y. 2011. Cancer/testis (CT) antigens, carcinogenesis and spermatogenesis. *Spermatogenesis,* 1 (3), pp. 209-220.

Chervona, Y. & Costa, M. 2012. Histone modifications and cancer: biomarkers of prognosis? *American journal of cancer research,* 2 (5), pp. 589.

Chiang, A., Jaju, P.D., Batra, P., Rezaee, M., Epstein Jr, E.H., Tang, J.Y. & Sarin, K.Y. 2018. Genomic stability in syndromic basal cell carcinoma. *Journal of Investigative Dermatology,* 138 (5), pp. 1044-1051.

Chicheportiche, A., Bernardino-Sgherri, J., de Massy, B. & Dutrillaux, B. 2007. Characterization of Spo11-dependent and independent phospho-H2AX foci during meiotic prophase I in the male mouse. *Journal of cell science,* 120 (10), pp. 1733-1742.

Chiriva, M., Yu, Y., Mirandola, L., Jenkins, M., Chapman, C., Cannon, M., Cobos, E. & Kast, W.M. 2010. No title. *Effective prevention and therapy of ovarian cancer with sperm protein 17 vaccination (95.7),* .

Cho, H., Noh, K.H., Chung, J., Takikita, M., Chung, E.J., Kim, B.W., Hewitt, S.M., Kim, T.W. & Kim, J. 2014. Synaptonemal complex protein 3 is a prognostic marker in cervical cancer. *PloS one,* 9 (6), pp. e98712.

Cho, N.W., Dilley, R.L., Lampson, M.A. & Greenberg, R.A. 2014. Interchromosomal homology searches drive directional ALT telomere movement and synapsis. *Cell,* 159 (1), pp. 108-121.

Choi, J.D. & Lee, J. 2013. Interplay between epigenetics and genetics in cancer. *Genomics & informatics,* 11 (4), pp. 164.

Chrun, E.S., Modolo, F. & Daniel, F.I. 2017. Histone modifications: A review about the presence of this epigenetic phenomenon in carcinogenesis. *Pathology-Research and Practice,* 213 (11), pp. 1329-1339.

Clift, D. & Marston, A.L. 2011. The role of shugoshin in meiotic chromosome segregation. *Cytogenetic and genome research,* 133 (2-4), pp. 234-242.

Constantinou, A., Chen, X., McGowan, C.H. & West, S.C. 2002. Holliday junction resolution in human cells: two junction endonucleases with distinct substrate specificities. *The EMBO journal,* 21 (20), pp. 5577-5585.

Crichton, J.H., Playfoot, C.J., MacLennan, M., Read, D., Cooke, H.J. & Adams, I.R. 2017. Tex19. 1 promotes Spo11-dependent meiotic recombination in mouse spermatocytes. *PLoS genetics,* 13 (7), pp. e1006904.

Croce, C.M. 2008. Oncogenes and cancer. *New England journal of medicine,* 358 (5), pp. 502-511.

Dawson, M.A. & Kouzarides, T. 2012. Cancer epigenetics: from mechanism to therapy. *Cell,* 150 (1), pp. 12-27.

De Massy, B. 2013. Initiation of meiotic recombination: how and where? Conservation and specificities among eukaryotes. *Annual Review of Genetics,* 47 pp. 563-599.

De Ryck, T., Duprez, F., Bracke, M., Van de Wiele, T. & Vanhoecke, B. 2015. Dynamic shifts in the oral microbiome during radiotherapy. *Clinical research infectious disease, 2 (1).*

de Carvalho, F., Vettore, A.L. and Colleoni, G.W., 2012. Cancer/Testis Antigen MAGE-C1/CT7: new target for multiple myeloma therapy. *Clinical and Developmental Immunology*, *2012*.

Dewannieux, M. & Heidmann, T. 2013. Endogenous retroviruses: acquisition, amplification and taming of genome invaders. *Current opinion in virology,* 3 (6), pp. 646-656.

Di Fagagna, F.d., Reaper, P.M., Clay-Farrace, L., Fiegler, H., Carr, P., Von Zglinicki, T., Saretzki, G., Carter, N.P. & Jackson, S.P. 2003. A DNA damage checkpoint response in telomere-initiated senescence. *Nature,* 426 (6963), pp. 194.

Di Zazzo, E., De Rosa, C., Abbondanza, C. & Moncharmont, B. 2013. PRDM proteins: molecular mechanisms in signal transduction and transcriptional regulation. *Biology,* 2 (1), pp. 107-141.

Dilley, R.L., Verma, P., Cho, N.W., Winters, H.D., Wondisford, A.R. & Greenberg, R.A. 2016. Break-induced telomere synthesis underlies alternative telomere maintenance. *Nature,* 539 (7627), pp. 54.

Dimitrova, E., Turberfield, A.H. & Klose, R.J. 2015. Histone demethylases in chromatin biology and beyond. *EMBO reports,* 16 (12), pp. 1620-1639.

Dray, E., Dunlop, M.H., Kauppi, L., San Filippo, J., Wiese, C., Tsai, M., Begovic, S., Schild, D., Jasin, M. & Keeney, S. 2011. Molecular basis for enhancement of the meiotic DMC1 recombinase by RAD51 associated protein 1 (RAD51AP1). *Proceedings of the National Academy of Sciences,* 108 (9), pp. 3560-3565.

Du, J., Johnson, L.M., Jacobsen, S.E. & Patel, D.J. 2015. DNA methylation pathways and their crosstalk with histone methylation. *Nature Reviews Molecular Cell Biology,* 16 (9), pp. 519.

Dubrova, Y.E., Plumb, M., Gutierrez, B., Boulton, E. & Jeffreys, A.J. 2000. Genome stability: transgenerational mutation by radiation. *Nature,* 405 (6782), pp. 37.

Dudas, A., Ahmad, S. & Gregan, J. 2011. Sgo1 is required for co-segregation of sister chromatids during achiasmate meiosis I. *Cell Cycle,* 10 (6), pp. 951-955.

Dvinge, H., Kim, E., Abdel-Wahab, O. & Bradley, R.K. 2016. RNA splicing factors as oncoproteins and tumour suppressors. *Nature reviews.Cancer,* 16 (7), pp. 413-430.

Eram, M.S., Bustos, S.P., Lima-Fernandes, E., Siarheyeva, A., Senisterra, G., Hajian, T., Chau, I., Duan, S., Wu, H. & Dombrovski, L. 2014. Trimethylation of histone H3 lysine 36 by human methyltransferase PRDM9 protein. *Journal of Biological Chemistry,* 289 (17), pp. 12177-12188.

Fabris, L., Ceder, Y., Chinnaiyan, A., Jenster, G., Sorensen, K., Tomlins, S., Visakorpi, T. and Calin, G., 2016. The Potential of MicroRNAs as Prostate Cancer Biomarkers. *European Urology*, 70(2), pp.312-322.

Feichtinger, J. & McFarlane, R.J. 2019. Meiotic gene activation in somatic and germ cell tumours. *Andrology,* .

Feichtinger, J., Aldeailej, I., Anderson, R., Almutairi, M., Almatrafi, A., Alsiwiehri, N., Griffiths, K., Stuart, N., Wakeman, J.A. & Larcombe, L. 2012. Meta-analysis of clinical data using human meiotic genes identifies a novel cohort of highly restricted cancer-specific marker genes. *Oncotarget,* 3 (8), pp. 843.

Feng, Q., Moran, J.V., Kazazian Jr, H.H. & Boeke, J.D. 1996. Human L1 retrotransposon encodes a conserved endonuclease required for retrotransposition. *Cell,* 87 (5), pp. 905-916.

Feng, W. Jasin, M. 2017. Homologous recombination and replication fork protection: BRCA2 and more! *Cold Spring Harbor symposia on quantitative biology.* Cold Spring Harbor Laboratory Press. pp. 329.

Ferguson, L.R., Chen, H., Collins, A.R., Connell, M., Damia, G., Dasgupta, S., Malhotra, M., Meeker, A.K., Amedei, A. & Amin, A. 2015. Genomic instability in human cancer: Molecular insights and opportunities for therapeutic attack and prevention through diet and nutrition. *Seminars in cancer biology.* Elsevier. pp. S5.

Florea, A. & Büsselberg, D. 2011. Cisplatin as an anti-tumor drug: cellular mechanisms of activity, drug resistance and induced side effects. *Cancers,* 3 (1), pp. 1351-1371.

Fog, C.K., Galli, G.G. & Lund, A.H. 2012. PRDM proteins: important players in differentiation and disease. *Bioessays,* 34 (1), pp. 50-60.

Fratta, E., Coral, S., Covre, A., Parisi, G., Colizzi, F., Danielli, R., Nicolay, H.J.M., Sigalotti, L. & Maio, M. 2011. The biology of cancer testis antigens: putative function, regulation and therapeutic potential. *Molecular oncology,* 5 (2), pp. 164-182.

Fuchs, J., Demidov, D., Houben, A. & Schubert, I. 2006. Chromosomal histone modification patterns–from conservation to diversity. *Trends in plant science,* 11 (4), pp. 199-208.

Gao, Y., Kardos, J., Yang, Y., Tamir, T.Y., Mutter-Rottmayer, E., Weissman, B., Major, M.B., Kim, W.Y. & Vaziri, C. 2018. The Cancer/Testes (CT) Antigen HORMAD1 promotes Homologous Recombinational DNA Repair and Radioresistance in Lung adenocarcinoma cells. *Scientific reports,* 8 (1), pp. 15304.

Garcia-Soto, A.E., Schreiber, T., Strbo, N., Ganjei-Azar, P., Miao, F., Koru-Sengul, T., Simpkins, F., Nieves-Neira, W., Lucci III, J. & Podack, E.R. 2017. Cancer-testis antigen expression is shared between epithelial ovarian cancer tumors. *Gynecologic oncology,* 145 (3), pp. 413-419.

Gedye, C., Quirk, J., Browning, J., Svobodová, S., John, T., Sluka, P., Dunbar, P.R., Corbeil, D., Cebon, J. & Davis, I.D. 2009. Cancer/testis antigens can be immunological targets in clonogenic CD133 melanoma cells. *Cancer immunology, immunotherapy,* 58 (10), pp. 1635-1646.

Gerton, J.L. & Hawley, R.S. 2005. Homologous chromosome interactions in meiosis: diversity amidst conservation. *Nature Reviews Genetics,* 6 (6), pp. 477.

Gibbs, Z.A. & Whitehurst, A.W. 2018. Emerging contributions of Cancer/Testis antigens to neoplastic behaviors. *Trends in cancer,* .

Girardot, M., Feil, R. & Llères, D. 2013. Epigenetic deregulation of genomic imprinting in humans: causal mechanisms and clinical implications. *Epigenomics,* 5 (6), pp. 715-728.

Gjerstorff, M.F., Andersen, M.H. & Ditzel, H.J. 2015. Oncogenic cancer/testis antigens: prime candidates for immunotherapy. *Oncotarget,* 6 (18), pp. 15772.

Gong, F. & Miller, K.M. 2017. Histone methylation and the DNA damage response. *Mutation Research/Reviews in Mutation Research,* .

Gordeeva, O. 2018. Cancer-testis antigens: unique cancer stem cell biomarkers and targets for cancer therapy. *Seminars in cancer biology.* Elsevier.

Graham, S., Jiang, J. & Mesnil, M. 2018. Connexins and Pannexins: Important Players in Tumorigenesis, Metastasis and Potential Therapeutics. *International journal of molecular sciences,* 19 (6), pp. 1645.

Greer, E.L. & Shi, Y. 2012. Histone methylation: a dynamic mark in health, disease and inheritance. *Nature Reviews Genetics,* 13 (5), pp. 343.

Grivennikov, S.I. & Karin, M. 2010. Inflammation and oncogenesis: a vicious connection. *Current opinion in genetics & development,* 20 (1), pp. 65-71.

Hammond, C.M., Strømme, C.B., Huang, H., Patel, D.J. & Groth, A. 2017. Histone chaperone networks shaping chromatin function. *Nature Reviews Molecular Cell Biology,* 18 (3), pp. 141.

Hanahan, D. & Weinberg, R.A. 2011. Hallmarks of cancer: the next generation. *Cell,* 144 (5), pp. 646-674.

Hanahan, D. & Weinberg, R.A. 2000. The hallmarks of cancer. *Cell,* 100 (1), pp. 57-70.

Handel, M.A. & Schimenti, J.C. 2010. Genetics of mammalian meiosis: regulation, dynamics and impact on fertility. *Nature Reviews Genetics,* 11 (2), pp. 124.

Hanks, L.M. & Millar, J.G. 2016. Sex and aggregation-sex pheromones of cerambycid beetles: basic science and practical applications. *Journal of chemical ecology,* 42 (7), pp. 631-654.

Harris, T.J. & Drake, C.G. 2013. Primer on tumor immunology and cancer immunotherapy. *Journal for immunotherapy of cancer,* 1 (1), pp. 12.

Hatzimichael, E. & Crook, T. 2013. Cancer epigenetics: new therapies and new challenges. *Journal of drug delivery,* 2013.

Hayashi, K., Yoshida, K. & Matsui, Y. 2005. A histone H3 methyltransferase controls epigenetic events required for meiotic prophase. *Nature,* 438 (7066), pp. 374.

He, Q., Au, B., Kulkarni, M., Shen, Y., Lim, K.J., Maimaiti, J., Wong, C.K., Luijten, M.N., Chong, H.C. & Lim, E.H. 2018. Chromosomal instability-induced senescence potentiates cell non-autonomous tumourigenic effects. *Oncogenesis,* 7 (8), pp. 62.

Henson, J.D., Neumann, A.A., Yeager, T.R. & Reddel, R.R. 2002. Alternative lengthening of telomeres in mammalian cells. *Oncogene,* 21 (4), pp. 598.

Heyer, W., Ehmsen, K.T. & Liu, J. 2010. Regulation of homologous recombination in eukaryotes. *Annual Review of Genetics,* 44 pp. 113-139.

Hirohashi, Y., Torigoe, T., Tsukahara, T., Kanaseki, T., Kochin, V. & Sato, N. 2016. Immune responses to human cancer stem□like cells/cancer□initiating cells. *Cancer science,* 107 (1), pp. 12-17.

Hirose, Y., Suzuki, R., Ohba, T., Hinohara, Y., Matsuhara, H., Yoshida, M., Itabashi, Y., Murakami, H. & Yamamoto, A. 2011. Chiasmata promote monopolar attachment of sister chromatids and their co-segregation toward the proper pole during meiosis I. *PLoS genetics,* 7 (3), pp. e1001329.

Ho, L. & Crabtree, G.R. 2010. Chromatin remodelling during development. *Nature,* 463 (7280), pp. 474.

Hofmann, O., Caballero, O.L., Stevenson, B.J., Chen, Y., Cohen, T., Chua, R., Maher, C.A., Panji, S., Schaefer, U. & Kruger, A. 2008. Genome-wide analysis of cancer/testis gene expression. *Proceedings of the National Academy of Sciences,* 105 (51), pp. 20422-20427.

Hohenauer, T. & Moore, A.W. 2012. The Prdm family: expanding roles in stem cells and development. *Development,* 139 (13), pp. 2267-2282.

Holthausen, J.T., Wyman, C. & Kanaar, R. 2010. Regulation of DNA strand exchange in homologous recombination. *DNA repair,* 9 (12), pp. 1264-1272.

Hosoya, N., Okajima, M., Kinomura, A., Fujii, Y., Hiyama, T., Sun, J., Tashiro, S. & Miyagawa, K. 2012. Synaptonemal complex protein SYCP3 impairs mitotic recombination by interfering with BRCA2. *EMBO reports,* 13 (1), pp. 44-51.

Huang, P., Chen, C., Chou, C., Sargeant, A.M., Kulp, S.K., Teng, C., Byrd, J.C. & Chen, C. 2011. Histone deacetylase inhibitors stimulate histone H3 lysine 4 methylation in part via transcriptional repression of histone H3 lysine 4 demethylases. *Molecular pharmacology,* 79 (1), pp. 197-206.

Hunder, N.N., Wallen, H., Cao, J., Hendricks, D.W., Reilly, J.Z., Rodmyre, R., Jungbluth, A., Gnjatic, S., Thompson, J.A. & Yee, C. 2008. Treatment of metastatic melanoma with autologous CD4 T cells against NY-ESO-1. *New England Journal of Medicine,* 358 (25), pp. 2698-2703.

Ianzini, F., Kosmacek, E.A., Nelson, E.S., Napoli, E., Erenpreisa, J., Kalejs, M. & Mackey, M.A. 2009. Activation of meiosis-specific genes is associated with depolyploidization of human tumor cells following radiation-induced mitotic catastrophe. *Cancer research,* 69 (6), pp. 2296-2304.

Janic, A., Mendizabal, L., Llamazares, S., Rossell, D. & Gonzalez, C. 2010. Ectopic expression of germline genes drives malignant brain tumor growth in Drosophila. *Science,* 330 (6012), pp. 1824-1827.

Janssen, A. & Medema, R.H. 2013. Genetic instability: tipping the balance. *Oncogene,* 32 (38), pp. 4459.

Janssen, A., Breuer, G.A., Brinkman, E.K., van der Meulen, Annelot I, Borden, S.V., van Steensel, B., Bindra, R.S., LaRocque, J.R. & Karpen, G.H. 2016. A single double-strand break system reveals repair dynamics and mechanisms in heterochromatin and euchromatin. *Genes & development,* 30 (14), pp. 1645-1657.

Jones, P.A. 2012. Functions of DNA methylation: islands, start sites, gene bodies and beyond. *Nature Reviews Genetics,* 13 (7), pp. 484.

Jungbluth, A.A., Ely, S., DiLiberto, M., Niesvizky, R., Williamson, B., Frosina, D., Chen, Y., Bhardwaj, N., Chen-Kiang, S. & Old, L.J. 2005. The cancer-testis antigens CT7 (MAGE-C1) and MAGE-A3/6 are commonly expressed in multiple myeloma and correlate with plasma-cell proliferation. *Blood,* 106 (1), pp. 167-174.

Kalejs, M. & Erenpreisa, J. 2005. Cancer/testis antigens and gametogenesis: a review and" brain-storming" session. *Cancer cell international,* 5 (1), pp. 4.

Kandoth, C., McLellan, M.D., Vandin, F., Ye, K., Niu, B., Lu, C., Xie, M., Zhang, Q., McMichael, J.F. & Wyczalkowski, M.A. 2013. Mutational landscape and significance across 12 major cancer types. *Nature,* 502 (7471), pp. 333.

Kang, M. & Kieff, E. 2015. Epstein–Barr virus latent genes. *Experimental & molecular medicine,* 47 (1), pp. e131.

Karow, J.K., Constantinou, A., Li, J., West, S.C. & Hickson, I.D. 2000. The Bloom's syndrome gene product promotes branch migration of holliday junctions. *Proceedings of the National Academy of Sciences,* 97 (12), pp. 6504-6508.

Katto, J. & Mahlknecht, U. 2011. Epigenetic regulation of cellular adhesion in cancer. *Carcinogenesis,* 32 (10), pp. 1414-1418.

Kazemi-Lomedasht, F., Behdani, M., Habibi-Anbouhi, M. & Shahbazzadeh, D. 2016. Production and characterization of novel camel single domain antibody targeting mouse vascular endothelial growth factor. *Monoclonal antibodies in immunodiagnosis and immunotherapy,* 35 (3), pp. 167-171.

Kitano, H., Chung, J., Noh, K.H., Lee, Y., Kim, T.W., Lee, S.H., Eo, S., Cho, H.J., Choi, C.H. & Inoue, S. 2017. Synaptonemal complex protein 3 is associated with lymphangiogenesis in non-small cell lung cancer patients with lymph node metastasis. *Journal of translational medicine,* 15 (1), pp. 138.

Klutstein, M. & Cooper, J.P. 2014. The chromosomal courtship dance—homolog pairing in early meiosis. *Current opinion in cell biology,* 26 pp. 123-131.

Kobayashi, W., Hosoya, N., Machida, S., Miyagawa, K. & Kurumizaka, H. 2017. SYCP 3 regulates strand invasion activities of RAD 51 and DMC 1. *Genes to Cells,* 22 (9), pp. 799-809.

Koh-Stenta, X., Joy, J., Poulsen, A., Li, R., Tan, Y., Shim, Y., Min, J., Wu, L., Ngo, A. & Peng, J. 2014. Characterization of the histone methyltransferase PRDM9 using biochemical, biophysical and chemical biology techniques. *Biochemical Journal,* 461 (2), pp. 323-334.

Koprinarova, M., Schnekenburger, M. & Diederich, M. 2016. Role of histone acetylation in cell cycle regulation. *Current topics in medicinal chemistry,* 16 (7), pp. 732-744.

Koslowski, M., Türeci, Ö, Bell, C., Krause, P., Lehr, H., Brunner, J., Seitz, G., Nestle, F.O., Huber, C. & Sahin, U. 2002a. Multiple splice variants of lactate dehydrogenase C selectively expressed in human cancer. *Cancer research,* 62 (22), pp. 6750-6755.

Koslowski, M., Türeci, Ö, Bell, C., Krause, P., Lehr, H., Brunner, J., Seitz, G., Nestle, F.O., Huber, C. & Sahin, U. 2002b. Multiple splice variants of lactate dehydrogenase C selectively expressed in human cancer. *Cancer research,* 62 (22), pp. 6750-6755.

Kouraklis, G. & Theocharis, S. 2002. Histone deacetylase inhibitors and anticancer therapy. *Current Medicinal Chemistry-Anti-Cancer Agents,* 2 (4), pp. 477-484.

Kouzarides, T. 2007. Chromatin modifications and their function. *Cell,* 128 (4), pp. 693-705.

Kowalczykowski, S.C. 2015. An overview of the molecular mechanisms of recombinational DNA repair. *Cold Spring Harbor Perspectives in Biology,* 7 (11), pp. a016410.

Kreamer, K.M. 2014. Immune checkpoint blockade: a new paradigm in treating advanced cancer. *Journal of the advanced practitioner in oncology,* 5 (6), pp. 418.

Kronja, I. & Orr-Weaver, T.L. 2011. Translational regulation of the cell cycle: when, where, how and why? *Philosophical Transactions of the Royal Society B: Biological Sciences,* 366 (1584), pp. 3638-3652.

Kular, R.K., Yehiely, F., Kotlo, K.U., Cilensek, Z.M., Bedi, R. & Deiss, L.P. 2009. GAGE, an antiapoptotic protein binds and modulates the expression of nucleophosmin/B23 and interferon regulatory factor 1. *Journal of Interferon & Cytokine Research,* 29 (10), pp. 645-656.

Kulkarni, P., Dunker, A.K., Weninger, K. & Orban, J. 2016. Prostate-associated gene 4 (PAGE4), an intrinsically disordered cancer/testis antigen, is a novel therapeutic target for prostate cancer. *Asian Journal of Andrology,* 18 (5), pp. 695.

Kuntz, S., Kieffer, E., Bianchetti, L., Lamoureux, N., Fuhrmann, G. & Viville, S. 2008. Tex19, a mammalian□specific protein with a restricted expression in pluripotent stem cells and germ line. *Stem cells,* 26 (3), pp. 734-744.

Lai, Q., Melandro, F., Pinheiro, R.S., Donfrancesco, A., Fadel, B.A., Levi Sandri, G.B., Rossi, M., Berloco, P.B. & Frattaroli, F.M. 2012. Alpha-fetoprotein and novel tumor biomarkers as predictors of hepatocellular carcinoma recurrence after surgery: a brilliant star raises again. *International journal of hepatology,* 2012 pp. 893103.

Lajmi, N., Luetkens, T., Yousef, S., Templin, J., Cao, Y., Hildebrandt, Y., Bartels, K., Kröger, N. & Atanackovic, D. 2015. Cancer□testis antigen MAGEC 2 promotes proliferation and resistance to apoptosis in Multiple Myeloma. *British journal of haematology,* 171 (5), pp. 752-762.

Lam, I. & Keeney, S. 2015. Mechanism and regulation of meiotic recombination initiation. *Cold Spring Harbor perspectives in biology,* 7 (1), pp. a016634.

Lawrence, M.S., Stojanov, P., Mermel, C.H., Robinson, J.T., Garraway, L.A., Golub, T.R., Meyerson, M., Gabriel, S.B., Lander, E.S. & Getz, G. 2014. Discovery and saturation analysis of cancer genes across 21 tumour types. *Nature,* 505 (7484), pp. 495.

Lee, B. & Amon, A. 2001. Meiosis: how to create a specialized cell cycle. *Current opinion in cell biology,* 13 (6), pp. 770-777.

Lee, J.T. & Bartolomei, M.S. 2013. X-inactivation, imprinting, and long noncoding RNAs in health and disease. *Cell,* 152 (6), pp. 1308-1323.

Leroy, B., Fournier, J.L., Ishioka, C., Monti, P., Inga, A., Fronza, G. & Soussi, T. 2012. The TP53 website: an integrative resource centre for the TP53 mutation database and TP53 mutant analysis. *Nucleic acids research,* 41 (D1), pp. D962-D969.

Li, Q. & Zhang, Z. 2012. Linking DNA replication to heterochromatin silencing and epigenetic inheritance. *Acta Biochim Biophys Sin,* 44 (1), pp. 3-13.

Li, S. & Shogren-Knaak, M.A. 2008. Cross-talk between histone H3 tails produces cooperative nucleosome acetylation. *Proceedings of the National Academy of Sciences,* 105 (47), pp. 18243-18248.

Li, X. & Heyer, W. 2008. Homologous recombination in DNA repair and DNA damage tolerance. *Cell research,* 18 (1), pp. 99.

Li, Y., Li, J., Wang, Y., Zhang, Y., Chu, J., Sun, C., Fu, Z., Huang, Y., Zhang, H. & Yuan, H. 2017. Roles of cancer/testis antigens (CTAs) in breast cancer. *Cancer letters,* 399 pp. 64-73.

Lichten, M. & de Massy, B. 2011. The impressionistic landscape of meiotic recombination. *Cell,* 147 (2), pp. 267-270.

Liu, S., Chang, W., Jin, Y., Feng, C., Wu, S., He, J. & Xu, T. 2019. The function of histone acetylation in cervical cancer development. *Bioscience reports,* 39 (4), pp. BSR20190527.

Llano, E., Herrán, Y., García-Tuñón, I., Gutiérrez-Caballero, C., de Álava, E., Barbero, J.L., Schimenti, J., de Rooij, D.G., Sánchez-Martín, M. and Pendás, A.M., 2012. Meiotic cohesin complexes are essential for the formation of the axial element in mice. *J Cell Biol*, 197(7), pp.877-885.

Llinas-Arias, P. & Esteller, M. 2017. Epigenetic inactivation of tumour suppressor coding and non-coding genes in human cancer: an update. *Open biology,* 7 (9), pp. 170152.

Lok, B.H. & Powell, S.N. 2012. Molecular pathways: understanding the role of Rad52 in homologous recombination for therapeutic advancement. *Clinical cancer research,* 18 (23), pp. 6400-6406.

Lynch, D. & Murphy, A. 2016. The emerging role of immunotherapy in colorectal cancer. *Annals of translational medicine,* 4 (16), .

Machida, S., Takizawa, Y., Ishimaru, M., Sugita, Y., Sekine, S., Nakayama, J., Wolf, M. & Kurumizaka, H. 2018. Structural basis of heterochromatin formation by human HP1. *Molecular cell,* 69 (3), pp. 385-397. e8.

Mack, S.C., Suzuki, H. & Taylor, M.D. 2017. Transposase-driven rearrangements in human tumors. *Nature genetics,* 49 (7), pp. 975.

MacLennan, M., García-Cañadas, M., Reichmann, J., Khazina, E., Wagner, G., Playfoot, C.J., Salvador-Palomeque, C., Mann, A.R., Peressini, P. & Sanchez, L. 2017. Mobilization of LINE-1 retrotransposons is restricted by Tex19. 1 in mouse embryonic stem cells. *Elife,* 6 pp. e26152.

Mantere, T., Tervasmäki, A., Nurmi, A., Rapakko, K., Kauppila, S., Tang, J., Schleutker, J., Kallioniemi, A., Hartikainen, J.M. & Mannermaa, A. 2017. Case-control analysis of truncating mutations in DNA damage response genes connects TEX15 and FANCD2 with hereditary breast cancer susceptibility. *Scientific reports,* 7 (1), pp. 681.

Maquat, L.E. 2001. The power of point mutations. *Nature genetics,* 27 (1), pp. 5.

Marcar, L., Ihrig, B., Hourihan, J., Bray, S.E., Quinlan, P.R., Jordan, L.B., Thompson, A.M., Hupp, T.R. & Meek, D.W. 2015. MAGE-A cancer/testis antigens inhibit MDM2 ubiquitylation function and promote increased levels of MDM4. *PloS one,* 10 (5), pp. e0127713.

Margueron, R. & Reinberg, D. 2010. Chromatin structure and the inheritance of epigenetic information. *Nature Reviews Genetics,* 11 (4), pp. 285.

Martini, E., Borde, V., Legendre, M., Audic, S., Regnault, B., Soubigou, G., Dujon, B. & Llorente, B. 2011. Genome-wide analysis of heteroduplex DNA in mismatch repair–deficient yeast cells reveals novel properties of meiotic recombination pathways. *PLoS genetics,* 7 (9), pp. e1002305.

Martin-Moreno, J.M., Soerjomataram, I. & Magnusson, G. 2008. Cancer causes and prevention: a condensed appraisal in Europe in 2008. *European journal of cancer,* 44 (10), pp. 1390-1403.

Maxfield, K.E., Taus, P.J., Corcoran, K., Wooten, J., Macion, J., Zhou, Y., Borromeo, M., Kollipara, R.K., Yan, J. & Xie, Y. 2015. Comprehensive functional characterization of cancer–testis antigens defines obligate participation in multiple hallmarks of cancer. *Nature communications,* 6 pp. 8840.

Mazin, A.V., Mazina, O.M., Bugreev, D.V. & Rossi, M.J. 2010. Rad54, the motor of homologous recombination. *DNA repair,* 9 (3), pp. 286-302.

McFarlane, R.J., Feichtinger, J. & Larcombe, L. 2015. Germline/meiotic genes in cancer: new dimensions. *Cell Cycle,* 14 (6), pp. 791.

McFarlane, R.J. & Wakeman, J.A. 2017. Meiosis-like functions in oncogenesis: a new view of cancer. *Cancer research,* 77 (21), pp. 5712-5716.

Medina, P.J. & Adams, V.R. 2016. PD□1 Pathway Inhibitors: Immuno□Oncology Agents for Restoring Antitumor Immune Responses. *Pharmacotherapy: The Journal of Human Pharmacology and Drug Therapy,* 36 (3), pp. 317-334.

Meikar, O., Da Ros, M. & Kotaja, N. 2013. Epigenetic regulation of male germ cell differentiation. In: Anon*Epigenetics: Development and Disease.* Springer. pp. 119-138.

Mellman, I., Coukos, G. & Dranoff, G. 2011. Cancer immunotherapy comes of age. *Nature,* 480 (7378), pp. 480.

Meretoja, T.J., Andersen, K.G., Bruce, J., Haasio, L., Sipilä, R., Scott, N.W., Ripatti, S., Kehlet, H. & Kalso, E. 2017. Clinical prediction model and tool for assessing risk of persistent pain after breast cancer surgery. *Journal of Clinical Oncology,* 35 (15), pp. 1660-1667.

Miller, M.P., Amon, A. & Ünal, E. 2013. Meiosis I: when chromosomes undergo extreme makeover. *Current opinion in cell biology,* 25 (6), pp. 687-696.

Mirandola, L., Pedretti, E., Figueroa, J.A., Chiaramonte, R., Colombo, M., Chapman, C., Grizzi, F., Patrinicola, F., Kast, W.M. & Nguyen, D.D. 2017. Cancer testis antigen Sperm Protein 17 as a new target for triple negative breast cancer immunotherapy. *Oncotarget,* 8 (43), pp. 74378.

Miyamoto, T., Minase, G., Shin, T., Ueda, H., Okada, H. & Sengoku, K. 2017. Human male infertility and its genetic causes. *Reproductive medicine and biology,* 16 (2), pp. 81-88.

Modarressi, M.H., Behnam, B., Cheng, M., Taylor, K.E., Wolfe, J. & van der Hoorn, Frans A 2004. Tsga 10 encodes a 65-kilodalton protein that is processed to the 27-Kilodalton fibrous sheath protein. *Biology of reproduction,* 70 (3), pp. 608-615.

Morgan, R.A., Chinnasamy, N., Abate-Daga, D.D., Gros, A., Robbins, P.F., Zheng, Z., Feldman, S.A., Yang, J.C., Sherry, R.M. & Phan, G.Q. 2013. Cancer regression and neurologic toxicity following anti-MAGE-A3 TCR gene therapy. *Journal of immunotherapy (Hagerstown, Md.: 1997),* 36 (2), pp. 133.

Muller, P.A. & Vousden, K.H. 2013. P53 mutations in cancer. *Nature cell biology,* 15 (1), pp. 2.

Myers, S., Bowden, R., Tumian, A., Bontrop, R.E., Freeman, C., MacFie, T.S., McVean, G. & Donnelly, P. 2010. Drive against hotspot motifs in primates implicates the PRDM9 gene in meiotic recombination. *Science,* 327 (5967), pp. 876-879.

Mzoughi, S., Tan, Y.X., Low, D. & Guccione, E. 2016. The role of PRDMs in cancer: one family, two sides. *Current opinion in genetics & development,* 36 pp. 83-91.

Narita, T., Weinert, B.T. & Choudhary, C. 2019. Functions and mechanisms of non-histone protein acetylation. *Nature Reviews Molecular Cell Biology,* 20 (3), pp. 156-174.

Negrini, S., Gorgoulis, V.G. & Halazonetis, T.D. 2010. Genomic instability—an evolving hallmark of cancer. *Nature reviews Molecular cell biology,* 11 (3), pp. 220.

Nelson, P.T., Zhang, P.J., Spagnoli, G.C., Tomaszewski, J.E., Pasha, T.L., Frosina, D., Caballero, O.L., Simpson, A.J., Old, L.J. & Jungbluth, A.A. 2007. Cancer/testis (CT) antigens are expressed in fetal ovary. *Cancer Immunity Archive,* 7 (1), pp. 1.

Nielsen, A. & Gjerstorff, M. 2016. Ectopic expression of testis germ cell proteins in cancer and its potential role in genomic instability. *International journal of molecular sciences,* 17 (6), pp. 890.

Nikolov, I. & Taddei, A. 2016. Linking replication stress with heterochromatin formation. *Chromosoma,* 125 (3), pp. 523-533.

O'Donovan, P.J. & Livingston, D.M. 2010. BRCA1 and BRCA2: breast/ovarian cancer susceptibility gene products and participants in DNA double-strand break repair. *Carcinogenesis,* 31 (6), pp. 961-967.

Öllinger, R., Childs, A.J., Burgess, H.M., Speed, R.M., Lundegaard, P.R., Reynolds, N., Gray, N.K., Cooke, H.J. & Adams, I.R. 2008. Deletion of the pluripotency-associated Tex19. 1 gene causes activation of endogenous retroviruses and defective spermatogenesis in mice. *PLoS genetics,* 4 (9), pp. e1000199.

Page, S.L. & Hawley, R.S. 2004. The genetics and molecular biology of the synaptonemal complex. *Annu.Rev.Cell Dev.Biol.,* 20 pp. 525-558.

Page, S.L. & Hawley, R.S. 2003. Chromosome choreography: the meiotic ballet. *Science,* 301 (5634), pp. 785-789.

Paigen, K. & Petkov, P.M. 2018. PRDM9 and its role in genetic recombination. *Trends in Genetics,* 34 (4), pp. 291-300.

Parrales, A. & Iwakuma, T. 2015. Targeting oncogenic mutant p53 for cancer therapy. *Frontiers in oncology,* 5 pp. 288.

Parvanov, E.D., Petkov, P.M. & Paigen, K. 2010. Prdm9 controls activation of mammalian recombination hotspots. *Science,* 327 (5967), pp. 835.

Petronczki, M., Siomos, M.F. & Nasmyth, K. 2003. Un menage a quatre: the molecular biology of chromosome segregation in meiosis. *Cell,* 112 (4), pp. 423-440.

Planells-Palop, V., Hazazi, A., Feichtinger, J., Jezkova, J., Thallinger, G., Alsiwiehri, N.O., Almutairi, M., Parry, L., Wakeman, J.A. & McFarlane, R.J. 2017. Human germ/stem cell-specific gene TEX19 influences cancer cell proliferation and cancer prognosis. *Molecular cancer,* 16 (1), pp. 84.

Powers, N.R., Parvanov, E.D., Baker, C.L., Walker, M., Petkov, P.M. & Paigen, K. 2016. The meiotic recombination activator PRDM9 trimethylates both H3K36

and H3K4 at recombination hotspots in vivo. *PLoS genetics,* 12 (6), pp. e1006146.

Pylayeva-Gupta, Y., Grabocka, E. & Bar-Sagi, D. 2011. RAS oncogenes: weaving a tumorigenic web. *Nature Reviews Cancer,* 11 (11), pp. 761.

Rajagopalan, K., Mooney, S.M., Parekh, N., Getzenberg, R.H. & Kulkarni, P. 2011. A majority of the cancer/testis antigens are intrinsically disordered proteins. *Journal of cellular biochemistry,* 112 (11), pp. 3256-3267.

Ranjha, L., Howard, S.M. & Cejka, P. 2018. Main steps in DNA double-strand break repair: an introduction to homologous recombination and related processes. *Chromosoma,* 127 (2), pp. 187-214.

Ranzani, M., Annunziato, S., Adams, D.J. & Montini, E. 2013. Cancer gene discovery: exploiting insertional mutagenesis. *Molecular Cancer Research,* 11 (10), pp. 1141-1158.

Raynard, S., Bussen, W. & Sung, P. 2006. A double Holliday junction dissolvasome comprising BLM, topoisomerase IIIα, and BLAP75. *Journal of Biological Chemistry,* 281 (20), pp. 13861-13864.

Reichmann, J., Reddington, J.P., Best, D., Read, D., Öllinger, R., Meehan, R.R. & Adams, I.R. 2013. The genome-defence gene Tex19. 1 suppresses LINE-1 retrotransposons in the placenta and prevents intra-uterine growth retardation in mice. *Human molecular genetics,* 22 (9), pp. 1791-1806.

Richards, R., McNoe, B., Iosua, E., Reeder, A.I., Egan, R., Marsh, L., Robertson, L., Maclennan, B., Latu, A.T.F. & Quigg, R. 2017. Cancer Mortality, Early Detection and Treatment among Adult New Zealanders: Changes in Perceptions between 2001 and 2014/5. *Asian Pacific journal of cancer prevention: APJCP,* 18 (12), pp. 3401.

Rifkin, S.A., Houle, D., Kim, J. & White, K.P. 2005. A mutation accumulation assay reveals a broad capacity for rapid evolution of gene expression. *Nature,* 438 (7065), pp. 220.

Rivera, M., Wu, Q., Hamerlik, P., Hjelmeland, A.B., Bao, S. & Rich, J.N. 2015. Acquisition of meiotic DNA repair regulators maintain genome stability in glioblastoma. *Cell death & disease,* 6 (4), pp. e1732.

Robert, T., Vrielynck, N., Mézard, C., de Massy, B. & Grelon, M. 2016. A new light on the meiotic DSB catalytic complex. *Seminars in cell & developmental biology.* Elsevier. pp. 165.

Rödel, F., Martin, D., Balermpas, P., Wieland, U., Winkelmann, R., Riekmann, T., Falk, S., Rödel, C. & Fokas, E. 2018. Modulation of radiation sensitivity and antitumor immunity by viral pathogenic factors: Implications for radio-immunotherapy. *Biochimica et Biophysica Acta (BBA)-Reviews on Cancer,* .

Rossi, F., Molnar, C., Hashiyama, K., Heinen, J.P., Pampalona, J., Llamazares, S., Reina, J., Hashiyama, T., Rai, M. & Pollarolo, G. 2017. An in vivo genetic screen in Drosophila identifies the orthologue of human cancer/testis gene SPO11 among a network of targets to inhibit lethal (3) malignant brain tumour growth. *Open biology,* 7 (8), pp. 170156.

Rousseaux, S., Debernardi, A., Jacquiau, B., Vitte, A., Vesin, A., Nagy-Mignotte, H., Moro-Sibilot, D., Brichon, P., Lantuejoul, S. & Hainaut, P. 2013. Ectopic activation of germline and placental genes identifies aggressive metastasis-prone lung cancers. *Science translational medicine,* 5 (186), pp. 186ra66.

Rousseaux, S., Wang, J. & Khochbin, S. 2013. Cancer hallmarks sustained by ectopic activations of placenta/male germline genes. *Cell Cycle,* 12 (15), pp. 2331-2332.

Roy, N.K., Bordoloi, D., Monisha, J., Anip, A., Padmavathi, G. & Kunnumakkara, A.B. 2017. Cancer—An Overview and Molecular Alterations in Cancer. In: Anon*Fusion Genes And Cancer.* World Scientific. pp. 1-15.

Salmaninejad, A., Zamani, M.R., Pourvahedi, M., Golchehre, Z., Hosseini Bereshneh, A. & Rezaei, N. 2016. Cancer/testis antigens: expression, regulation, tumor invasion, and use in immunotherapy of cancers. *Immunological investigations,* 45 (7), pp. 619-640.

San Filippo, J., Sung, P. & Klein, H. 2008. Mechanism of eukaryotic homologous recombination. *Annu.Rev.Biochem.,* 77 pp. 229-257.

Sang, M., Gu, L., Yin, D., Liu, F., Lian, Y., Zhang, X., Liu, S., Huang, W., Wu, Y. & Shan, B. 2017. MAGE-A family expression is correlated with poor survival of patients with lung adenocarcinoma: a retrospective clinical study based on tissue microarray. *Journal of clinical pathology,* 70 (6), pp. 533-540.

Santiago-Ortiz, J.L. & Schaffer, D.V. 2016. Adeno-associated virus (AAV) vectors in cancer gene therapy. *Journal of Controlled Release,* 240 pp. 287-301.

Schneider, R., Bannister, A.J., Myers, F.A., Thorne, A.W., Crane-Robinson, C. & Kouzarides, T. 2004. Histone H3 lysine 4 methylation patterns in higher eukaryotic genes. *Nature cell biology,* 6 (1), pp. 73.

Schon, S.B., Luense, L.J., Wang, X., Bartolomei, M.S., Coutifaris, C., Garcia, B.A. & Berger, S.L. 2019. Histone modification signatures in human sperm distinguish clinical abnormalities. *Journal of assisted reproduction and genetics,* 36 (2), pp. 267-275.

Schones, D.E. & Zhao, K. 2008. Genome-wide approaches to studying chromatin modifications. *Nature Reviews Genetics,* 9 (3), pp. 179.

Schooten, E., Di Maggio, A., en Henegouwen, Paul MP van Bergen & Kijanka, M.M. 2018. MAGE-A antigens as targets for cancer immunotherapy. *Cancer treatment reviews,* 67 pp. 54-62.

Schramm, S., Fraune, J., Naumann, R., Hernandez-Hernandez, A., Höög, C., Cooke, H.J., Alsheimer, M. and Benavente, R., 2011. A novel mouse synaptonemal complex protein is essential for loading of central element proteins, recombination, and fertility. *PLoS genetics*, *7*(5).

Schübeler, D., MacAlpine, D.M., Scalzo, D., Wirbelauer, C., Kooperberg, C., van Leeuwen, F., Gottschling, D.E., O'Neill, L.P., Turner, B.M. & Delrow, J. 2004. The histone modification pattern of active genes revealed through genome-wide chromatin analysis of a higher eukaryote. *Genes & development,* 18 (11), pp. 1263-1271.

Sehorn, M.G., Sigurdsson, S., Bussen, W., Unger, V.M. & Sung, P. 2004. Human meiotic recombinase Dmc1 promotes ATP-dependent homologous DNA strand exchange. *Nature,* 429 (6990), pp. 433.

Shamsi, M. & Islamian, J.P. 2017. Breast cancer: Early diagnosis and effective treatment by drug delivery tracing. *Nuclear Medicine Review,* 20 (1), pp. 45-48.

Shanmugam, M.K., Arfuso, F., Arumugam, S., Chinnathambi, A., Jinsong, B., Warrier, S., Wang, L.Z., Kumar, A.P., Ahn, K.S. & Sethi, G. 2018. Role of novel histone modifications in cancer. *Oncotarget,* 9 (13), pp. 11414.

Sharma, S., Kelly, T.K. & Jones, P.A. 2010. Epigenetics in cancer. *Carcinogenesis,* 31 (1), pp. 27-36.

Shen, H., Xu, W. & Lan, F. 2017. Histone lysine demethylases in mammalian embryonic development. *Experimental & molecular medicine,* 49 (4), pp. e325.

Shibata, A., Moiani, D., Arvai, A.S., Perry, J., Harding, S.M., Genois, M., Maity, R., van Rossum-Fikkert, S., Kertokalio, A. & Romoli, F. 2014. DNA double-strand break repair pathway choice is directed by distinct MRE11 nuclease activities. *Molecular cell,* 53 (1), pp. 7-18.

Silkworth, W.T. & Cimini, D. 2012. Transient defects of mitotic spindle geometry and chromosome segregation errors. *Cell division,* 7 (1), pp. 19.

Simon, J.A. & Kingston, R.E. 2009. Mechanisms of polycomb gene silencing: knowns and unknowns. *Nature reviews Molecular cell biology,* 10 (10), pp. 697.

Simpson, A.J., Caballero, O.L., Jungbluth, A., Chen, Y. & Old, L.J. 2005. Cancer/testis antigens, gametogenesis and cancer. *Nature Reviews Cancer,* 5 (8), pp. 615.

Sims Iii, R.J. & Reinberg, D. 2009. Processing the H3K36me3 signature. *Nature genetics,* 41 (3), pp. 270.

Singhavi, H., Ahluwalia, J.S., Stepanov, I., Gupta, P.C., Gota, V., Chaturvedi, P. & Khariwala, S.S. 2018. Tobacco carcinogen research to aid understanding of cancer risk and influence policy. *Laryngoscope investigative otolaryngology,* 3 (5), pp. 372-376.

So, A., Le Guen, T., Lopez, B.S. & Guirouilh□Barbat, J. 2017. Genomic rearrangements induced by unscheduled DNA double strand breaks in somatic mammalian cells. *The FEBS journal,* 284 (15), pp. 2324-2344.

Son, K.A., Lee, D.Y. & Choi, D. 2019. Association of BRCA Mutations and Anti-mullerian Hormone Level in Young Breast Cancer Patients. *Frontiers in endocrinology,* 10 pp. 235.

Sonnenschein, C. & Soto, A.M. 2013. The aging of the 2000 and 2011 Hallmarks of Cancer reviews: a critique. *Journal of Biosciences,* 38 (3), pp. 651-663.

Sorrentino, A., Federico, A., Rienzo, M., Gazzerro, P., Bifulco, M., Ciccodicola, A., Casamassimi, A. & Abbondanza, C. 2018. PR/SET domain family and cancer: novel insights from The Cancer Genome Atlas. *International journal of molecular sciences,* 19 (10), pp. 3250.

Sotero-Caio, C.G., Platt, R.N., Suh, A. & Ray, D.A. 2017. Evolution and diversity of transposable elements in vertebrate genomes. *Genome biology and evolution,* 9 (1), pp. 161-177.

Soto, M., Raaijmakers, J.A., Bakker, B., Spierings, D.C.J., Lansdorp, P.M., Foijer, F. & Medema, R.H. 2017. p53 Prohibits Propagation of Chromosome Segregation Errors that Produce Structural Aneuploidies. *Cell reports,* 19 (12), pp. 2423-2431.

Souquet, B., Abby, E., Hervé, R., Finsterbusch, F., Tourpin, S., Le Bouffant, R., Duquenne, C., Messiaen, S., Martini, E. & Bernardino-Sgherri, J. 2013. MEIOB targets single-strand DNA and is necessary for meiotic recombination. *PLoS genetics,* 9 (9), pp. e1003784.

Speranzini, V., Pilotto, S., Sixma, T.K. & Mattevi, A. 2016. Touch, act and go: landing and operating on nucleosomes. *The EMBO journal,* 35 (4), pp. 376-388.

Steele, C.B., Thomas, C.C., Henley, S.J., Massetti, G.M., Galuska, D.A., Agurs-Collins, T., Puckett, M. & Richardson, L.C. 2017. Vital Signs: Trends in Incidence of Cancers Associated with Overweight and Obesity - United States, 2005-2014. *MMWR.Morbidity and mortality weekly report,* 66 (39), pp. 1052-1058.

Stevenson, B.J., Iseli, C., Panji, S., Zahn-Zabal, M., Hide, W., Old, L.J., Simpson, A.J. & Jongeneel, C.V. 2007. Rapid evolution of cancer/testis genes on the X chromosome. *Bmc Genomics,* 8 (1), pp. 129.

Stoye, J.P. 2012. Studies of endogenous retroviruses reveal a continuing evolutionary saga. *Nature Reviews Microbiology,* 10 (6), pp. 395.

Stracquadanio, G., Wang, X., Wallace, M.D., Grawenda, A.M., Zhang, P., Hewitt, J., Zeron-Medina, J., Castro-Giner, F., Tomlinson, I.P. & Goding, C.R. 2016. The importance of p53 pathway genetics in inherited and somatic cancer genomes. *Nature reviews Cancer,* 16 (4), pp. 251.

Strahm, B. & Capra, M. 2005. Insights into the molecular basis of cancer development. *Current Paediatrics,* 15 (4), pp. 333-338.

Strunnikov, A. 2013. Cohesin complexes with a potential to link mammalian meiosis to cancer. *Cell Regeneration,* 2 (1), pp. 4.

Sumiyoshi, T., Sato, K., Yamamoto, H., Iwasaki, Y.W., Siomi, H. & Siomi, M.C. 2016a. Loss of l (3) mbt leads to acquisition of the ping-pong cycle in Drosophila ovarian somatic cells. *Genes & development,* 30 (14), pp. 1617-1622.

Sumiyoshi, T., Sato, K., Yamamoto, H., Iwasaki, Y.W., Siomi, H. & Siomi, M.C. 2016b. Loss of l (3) mbt leads to acquisition of the ping-pong cycle in Drosophila ovarian somatic cells. *Genes & development,* 30 (14), pp. 1617-1622.

Sun, F., Fujiwara, Y., Reinholdt, L.G., Hu, J., Saxl, R.L., Baker, C.L., Petkov, P.M., Paigen, K. & Handel, M.A. 2015. Nuclear localization of PRDM9 and its role in meiotic chromatin modifications and homologous synapsis. *Chromosoma,* 124 (3), pp. 397-415.

Suri, A., Jagadish, N., Saini, S. & Gupta, N. 2015. Targeting cancer testis antigens for biomarkers and immunotherapy in colorectal cancer: Current status and challenges. *World journal of gastrointestinal oncology,* 7 (12), pp. 492.

Szostak, J.W., Orr-Weaver, T.L., Rothstein, R.J. & Stahl, F.W. 1983. The double-strand-break repair model for recombination. *Cell,* 33 (1), pp. 25-35.

Tarabay, Y., Kieffer, E., Teletin, M., Celebi, C., Van Montfoort, A., Zamudio, N., Achour, M., El Ramy, R., Gazdag, E. & Tropel, P. 2013. The mammalian-specific Tex19. 1 gene plays an essential role in spermatogenesis and placenta-supported development. *Human reproduction,* 28 (8), pp. 2201-2214.

Tessarz, P. & Kouzarides, T. 2014. Histone core modifications regulating nucleosome structure and dynamics. *Nature reviews Molecular cell biology,* 15 (11), pp. 703.

Thor Straten, P. & Garrido, F. 2016. Targetless T cells in cancer immunotherapy. *Journal for immunotherapy of cancer,* 4 (1), pp. 23.

Toiyama, Y., Okugawa, Y. & Goel, A. 2014. DNA methylation and microRNA biomarkers for noninvasive detection of gastric and colorectal cancer. *Biochemical and biophysical research communications,* 455 (1-2), pp. 43-57.

Trego, K.S., Groesser, T., Davalos, A.R., Parplys, A.C., Zhao, W., Nelson, M.R., Hlaing, A., Shih, B., Rydberg, B. & Pluth, J.M. 2016. Non-catalytic Roles for XPG with BRCA1 and BRCA2 in Homologous Recombination and Genome Stability. *Molecular cell,* 61 (4), pp. 535-546.

Tsai, J. & McKee, B.D. 2011. Homologous pairing and the role of pairing centers in meiosis. *J Cell Sci,* 124 (12), pp. 1955-1963.

Tsubouchi, H. & Roeder, G.S. 2002. The Mnd1 protein forms a complex with hop2 to promote homologous chromosome pairing and meiotic double-strand break repair. *Molecular and cellular biology,* 22 (9), pp. 3078-3088.

Türeci, Ö, Sahin, U., Zwick, C., Koslowski, M., Seitz, G. & Pfreundschuh, M. 1998. Identification of a meiosis-specific protein as a member of the class of cancer/testis antigens. *Proceedings of the National Academy of Sciences,* 95 (9), pp. 5211-5216.

Turner, S.J., Russ, B.E., Denton, A.E., Hatton, L., Croom, H. & Olson, M.R. 2012. Defining the molecular blueprint that drives CD8 T cell differentiation in response to infection. *Frontiers in immunology,* 3 pp. 371.

Urbanski, L.M., Leclair, N. & Anczukow, O. 2018. Alternative-splicing defects in cancer: Splicing regulators and their downstream targets, guiding the way to novel cancer therapeutics. *Wiley interdisciplinary reviews.RNA,* 9 (4), pp. e1476.

van der Bruggen, P., Traversari, C., Chomez, P., Lurquin, C., De Plaen, E., Van den Eynde, B., Knuth, A. & Boon, T. 1991. A gene encoding an antigen recognized by cytolytic T lymphocytes on a human melanoma. *Science,* 254 (5038), pp. 1643-1647.

van Duin, M., Broyl, A., de Knegt, Y., Goldschmidt, H., Richardson, P.G., Hop, W.C., van der Holt, B., Joseph-Pietras, D., Mulligan, G. & Neuwirth, R. 2011.

Cancer testis antigens in newly diagnosed and relapse multiple myeloma: prognostic markers and potential targets for immunotherapy. *Haematologica,* 96 (11), pp. 1662-1669.

Venkatesan, S., Birkbak, N.J. & Swanton, C. 2017. Constraints in cancer evolution. *Biochemical Society transactions,* 45 (1), pp. 1-13.

Venkatesh, S. & Workman, J.L. 2015. Histone exchange, chromatin structure and the regulation of transcription. *Nature reviews Molecular cell biology,* 16 (3), pp. 178-189.

Videtic Paska, A. & Hudler, P. 2015. Aberrant methylation patterns in cancer: a clinical view. *Biochemia medica: Biochemia medica,* 25 (2), pp. 161-176.

Villeneuve, A.M. & Hillers, K.J. 2001. Whence meiosis? *Cell,* 106 (6), pp. 647-650.

Wahid, B., Ali, A., Rafique, S. & Idrees, M. 2017. New insights into the epigenetics of hepatocellular carcinoma. *BioMed research international,* 2017.

Walczak, C.E., Cai, S. & Khodjakov, A. 2010. Mechanisms of chromosome behaviour during mitosis. *Nature reviews Molecular cell biology,* 11 (2), pp. 91.

Wang, C., Gu, Y., Zhang, K., Xie, K., Zhu, M., Dai, N., Jiang, Y., Guo, X., Liu, M. & Dai, J. 2016. Systematic identification of genes with a cancer-testis expression pattern in 19 cancer types. *Nature communications,* 7 pp. 10499.

Wang, E., Zaman, N., Mcgee, S., Milanese, J.S., Masoudi-Nejad, A. & O'Connor-McCourt, M. 2015. Predictive genomics: a cancer hallmark network framework for predicting tumor clinical phenotypes using genome sequencing data. *Seminars in cancer biology,* 30 pp. 4-12.

Wang, G.G., Allis, C.D. & Chi, P. 2007. Chromatin remodeling and cancer, Part I: Covalent histone modifications. *Trends in molecular medicine,* 13 (9), pp. 363-372.

Wang, Z., Tang, Y., Tan, Y., Wei, Q. & Yu, W. 2019. Cancer-associated fibroblasts in radiotherapy: challenges and new opportunities. *Cell Communication and Signaling,* 17 (1), pp. 47.

Wang, Z., Zang, C., Rosenfeld, J.A., Schones, D.E., Barski, A., Cuddapah, S., Cui, K., Roh, T., Peng, W. & Zhang, M.Q. 2008. Combinatorial patterns of histone acetylations and methylations in the human genome. *Nature genetics,* 40 (7), pp. 897.

Ward, A., Hopkins, J., Mckay, M., Murray, S. & Jordan, P.W. 2016. Genetic interactions between the meiosis-specific cohesin components, STAG3, REC8, and RAD21L. *G3: Genes, Genomes, Genetics,* 6 (6), pp. 1713-1724.

Wardle, J., Robb, K., Vernon, S. & Waller, J. 2015. Screening for prevention and early diagnosis of cancer. *American psychologist,* 70 (2), pp. 119.

Wassmann, K. 2013. Sister chromatid segregation in meiosis II: deprotection through phosphorylation. *Cell Cycle,* 12 (9), pp. 1352-1359.

Watkins, J., Weekes, D., Shah, V., Gazinska, P., Joshi, S., Sidhu, B., Gillett, C., Pinder, S., Vanoli, F. & Jasin, M. 2015. Genomic complexity profiling reveals

that HORMAD1 overexpression contributes to homologous recombination deficiency in triple-negative breast cancers. *Cancer discovery,* 5 (5), pp. 488-505.

Weinberg, R. 2013. The Biology of Cancer, Second. *Garland Science,* .

Whitehurst, A.W. 2014. Cause and consequence of cancer/testis antigen activation in cancer. *Annual Review of Pharmacology and Toxicology,* 54 pp. 251-272.

Wicker, T., Sabot, F., Hua-Van, A., Bennetzen, J.L., Capy, P., Chalhoub, B., Flavell, A., Leroy, P., Morgante, M. & Panaud, O. 2007. A unified classification system for eukaryotic transposable elements. *Nature Reviews Genetics,* 8 (12), pp. 973.

Wodarz, D. & Zauber, A.G. 2015. Cancer: Risk factors and random chances. *Nature,* 517 (7536), pp. 563-564.

Wu, C. & Bekaii-Saab, T. 2012. CpG island methylation, microsatellite instability, and BRAF mutations and their clinical application in the treatment of colon cancer. *Chemotherapy research and practice,* 2012.

Wu, H., Mathioudakis, N., Diagouraga, B., Dong, A., Dombrovski, L., Baudat, F., Cusack, S., de Massy, B. & Kadlec, J. 2013. Molecular basis for the regulation of the H3K4 methyltransferase activity of PRDM9. *Cell reports,* 5 (1), pp. 13-20.

Wu, L. & Qu, X. 2015. Cancer biomarker detection: recent achievements and challenges. *Chemical Society Reviews,* 44 (10), pp. 2963-2997.

Wu, S., Zhu, W., Thompson, P. & Hannun, Y.A. 2018. Evaluating intrinsic and non-intrinsic cancer risk factors. *Nature communications,* 9 (1), pp. 3490-z.

Wurtele, H. & Verreault, A. 2006. Histone post-translational modifications and the response to DNA double-strand breaks. *Current opinion in cell biology,* 18 (2), pp. 137-144.

Xu, C. 2018. A review of somatic single nucleotide variant calling algorithms for next-generation sequencing data. *Computational and structural biotechnology journal,* 16 pp. 15-24.

Yadav, T., Quivy, J. & Almouzni, G. 2018. Chromatin plasticity: A versatile landscape that underlies cell fate and identity. *Science,* 361 (6409), pp. 1332-1336.

Yamada, S., Kim, S., Tischfield, S.E., Jasin, M., Lange, J. & Keeney, S. 2017. Genomic and chromatin features shaping meiotic double-strand break formation and repair in mice. *Cell Cycle,* 16 (20), pp. 1870-1884.

Yamada, T. & Ohta, K. 2013. Initiation of meiotic recombination in chromatin structure. *The Journal of Biochemistry,* 154 (2), pp. 107-114.

Yan, J., Jiang, J., Lim, C.A., Wu, Q., Ng, H. & Chin, K. 2007. BLIMP1 regulates cell growth through repression of p53 transcription. *Proceedings of the National Academy of Sciences,* 104 (6), pp. 1841-1846.

Yang, F., Cheng, Y., An, J.Y., Kwon, Y.T., Eckardt, S., Leu, N.A., McLaughlin, K.J. & Wang, P.J. 2010. The ubiquitin ligase Ubr2, a recognition E3 component of the N-end rule pathway, stabilizes Tex19. 1 during spermatogenesis. *PloS one,* 5 (11), pp. e14017.

Yang, F., Eckardt, S., Leu, N.A., McLaughlin, K.J. & Wang, P.J. 2008. Mouse TEX15 is essential for DNA double-strand break repair and chromosomal synapsis during male meiosis. *J Cell Biol,* 180 (4), pp. 673-679.

Yang, J.C. & Rosenberg, S.A. 2016. Adoptive T-cell therapy for cancer. In: Anon*Advances in immunology.* Elsevier. pp. 279-294.

Yang, P., Huo, Z., Liao, H. & Zhou, Q. 2015. Cancer/testis antigens trigger epithelial-mesenchymal transition and genesis of cancer stem-like cells. *Current pharmaceutical design,* 21 (10), pp. 1292-1300.

Yao, Y. & Dai, W. 2014. Genomic instability and cancer. *Journal of carcinogenesis & mutagenesis,* 5.

Youds, J.L. & Boulton, S.J. 2011. The choice in meiosis–defining the factors that influence crossover or non-crossover formation. *J Cell Sci,* 124 (4), pp. 501-513.

Young, C.L., Britton, Z.T. & Robinson, A.S. 2012. Recombinant protein expression and purification: a comprehensive review of affinity tags and microbial applications. *Biotechnology journal,* 7 (5), pp. 620-634.

Zajac, P., Schultz-Thater, E., Tornillo, L., Sadowski, C., Trella, E., Mengus, C., Iezzi, G. & Spagnoli, G.C. 2017. MAGE-A antigens and cancer immunotherapy. *Frontiers in medicine,* 4 pp. 18.

Zhang, Y., Zhang, Y. & Zhang, L. 2019. Expression of cancer–testis antigens in esophageal cancer and their progress in immunotherapy. *Journal of cancer research and clinical oncology,* 145 (2), pp. 281-291.

Zhao, X., Wei, C., Li, J., Xing, P., Li, J., Zheng, S. & Chen, X. 2017. Cell cycle-dependent control of homologous recombination. *Acta biochimica et biophysica Sinica,* 49 (8), pp. 655-668.

Zhong, J., Chen, Y., Liao, X., Li, J., Wang, H., Wu, C., Zou, X., Yang, G., Shi, J. & Luo, L. 2016. Testis expressed 19 is a novel cancer-testis antigen expressed in bladder cancer. *Tumor Biology,* 37 (6), pp. 7757-7765.

Zickler, D. & Kleckner, N. 2015. Recombination, pairing, and synapsis of homologs during meiosis. *Cold Spring Harbor perspectives in biology,* 7 (6), pp. a016626.

Zickler, D. & Kleckner, N. 1999. Meiotic chromosomes: integrating structure and function. *Annual Review of Genetics,* 33 (1), pp. 603-754.